









Université du Québec  
à Rimouski

**MÉCANISMES CELLULAIRES ET PHYSIOLOGIQUES DES  
STADES DE DÉVELOPPEMENT DE L'OURSIN VERT EN  
RÉPONSE AUX NANOPARTICULES D'ARGENT**

Thèse présentée  
dans le cadre du programme de doctorat en Océanographie  
en vue de l'obtention du grade de *Philosophiæ doctor*

PAR

© Adriano da Silva Magesky

Août 2016



**Composition du jury :**

**Réjean Tremblay, président du jury, Université du Québec à Rimouski**

**Émilien Pelletier, directeur de recherche, Université du Québec à Rimouski**

**Christopher Wood, examinateur externe, University of British Columbia**

Dépôt initial le 03 mai 2016

Dépôt final le 1 août 2016



UNIVERSITÉ DU QUÉBEC À RIMOUSKI  
Service de la bibliothèque

Avertissement

La diffusion de ce mémoire ou de cette thèse se fait dans le respect des droits de son auteur, qui a signé le formulaire « *Autorisation de reproduire et de diffuser un rapport, un mémoire ou une thèse* ». En signant ce formulaire, l'auteur concède à l'Université du Québec à Rimouski une licence non exclusive d'utilisation et de publication de la totalité ou d'une partie importante de son travail de recherche pour des fins pédagogiques et non commerciales. Plus précisément, l'auteur autorise l'Université du Québec à Rimouski à reproduire, diffuser, prêter, distribuer ou vendre des copies de son travail de recherche à des fins non commerciales sur quelque support que ce soit, y compris l'Internet. Cette licence et cette autorisation n'entraînent pas une renonciation de la part de l'auteur à ses droits moraux ni à ses droits de propriété intellectuelle. Sauf entente contraire, l'auteur conserve la liberté de diffuser et de commercialiser ou non ce travail dont il possède un exemplaire.



*À ma grande famille (ma belle  
famille et mes précieux amis)*



## **REMERCIEMENTS**

D'abord, je tiens à remercier mon directeur de thèse, Émilien Pelletier, pour la confiance qu'il m'a accordée en acceptant d'encadrer ce travail doctoral, mais aussi pour sa patience, son appui, sa positivité, son investissement dans ma formation, son encouragement et pour m'avoir beaucoup appris au long de cette grande expérience scientifique.

Je remercie également à tout le personnel de l'ISMER (administration, techniciens, agents de recherche) d'avoir été là tout le temps pour m'aider en cas de besoin.

Au personnel du Bureau des étudiants de l'UQAR, et spécialement à Annie Duchenne et à Étienne Michou.

À mes amis qui sont au Brésil, au Canada et ailleurs dans le monde, toujours présents dans ma vie même à grande distance.

À ma famille qui a su comprendre ma décision de quitter mon pays pour faire vivre ce projet.

À prof. Carlos Renato R. Ventura et à prof. Nadia Améziane de m'avoir tellement appris sur la biologie des échinodermes.

Au Conseil de recherche en sciences naturelles et génie (CRSNG) et au réseau de recherche Québec-Océan (FQRNT) pour leur appui financier.



## **AVANT-PROPOS**

L'idée de concilier la biologie des stades de développement à l'étude des mécanismes de toxicité des contaminants est née au début de l'an 2010 quand j'étais encore au Brésil et s'est concrétisée en 2011 quand je suis arrivé au Canada pour mon doctorat. L'approche principale (mécanistique) visait à travailler à l'interface de l'embryologie et de la toxicologie animale pour comprendre la réponse biologique des invertébrés en développement à la contamination de leur milieu. D'emblée, la compréhension de la biologie du développement chez les organismes marins d'eau froide et la mise en place d'une technique d'obtention des différents stades de développement en laboratoire ont été les étapes les plus difficiles et donc les plus importantes pour le début de ce projet. J'ai ensuite commencé les expériences en 2012 avec des contaminants organiques, les organostanniques (TBT) et les nanomatériaux. L'originalité de mon travail est particulièrement basée sur l'explication des mécanismes de toxicité des nanoparticules d'argent, de l'argent ionique et leur interaction avec les nanotubes de carbone, en rapport avec l'ontogénie des stades de développement de l'oursin vert. En outre, le projet a avancé et une vaste base de données concernant les oursins verts ainsi que les étoiles de mer polaires a été obtenue et reste encore en partie à être analysée. Ceci confirmera les idées présentées dans ma thèse et peut-être élargira notre compréhension quant à l'objet de cette thèse. L'approche utilisée dans mon travail ouvre une nouvelle perspective d'étude sur la biologie du développement d'autres espèces d'invertébrés en toxicologie environnementale.



## RÉSUMÉ

Les nanoparticules d'argent (AgNPs) sont de plus en plus incorporées à des produits d'usage quotidien compte tenu de leurs propriétés physico-chimiques et antimicrobiennes. Il est déjà établi que l'argent relâché par ces produits se retrouve dans les eaux usées. Ainsi, la possibilité qu'une combinaison massive d'utilisation des produits de consommation puisse augmenter la concentration de l'argent dans les écosystèmes marins est nettement présente. Ceci demande donc des efforts pour comprendre la toxicité des AgNPs chez les invertébrés marins, plus spécifiquement au cours de leurs stades de développement. Les étapes de l'embryogénèse, de la métamorphose des larves échinoplutei et le développement juvénile de l'oursin vert *Strongylocentrotus droebachiensis* ont été utilisées comme modèles biologiques. Les objectifs du projet reposent sur les hypothèses suivantes : (1) la sensibilité aux contaminants existe en fonction des transformations morphologiques subies par les trois feuillets tissulaires de base (l'ectoderme, le mésoderme et l'endoderme), ses dérivés et les cavités coelomiques (l'axocœle, l'hydrocœle et la somatocœle); (2) les voies d'entrée des contaminants et l'augmentation de l'espace interne des cavités coelomiques optimisent respectivement l'assimilation, la distribution et l'accumulation des xénobiotiques; (3) lors de l'exposition à des concentrations sous-létales, les organismes réagissent par des mécanismes cellulaires précis à chaque contaminant en un temps relativement court. Nous avons utilisé diverses méthodes comme la microscopie confocale, la microscopie électronique à transmission, l'analyse chimique par ICP-MS, les essais fluorimétriques, l'*immunoblotting* et une grande série de biotests pour arriver à nos résultats. Au cours du développement, les processus de transformation subis par les organismes expliquent le changement de toxicité des ions Ag et des AgNPs. L'ectoderme perméable de l'embryon, le tractus gastrointestinal et les cavités coelomiques secondaires des larves et des juvéniles ont montré que les contaminants peuvent arriver par différentes voies. Lorsque combiné aux nanotubes de carbone, l'argent ionique a perturbé de façon significative le développement. La cavité periviscérale et les peritoneocytes semblent être essentiels à la nano-translocation interne chez les larves et les juvéniles. En plus, le nanoAg semble être lié à l'activité phagocytaire et cytoprotective des coelomocytes. L'argent libre conduit à un processus d'oncrosis suivi par la nécrose, alors que le nano-argent est relié à des processus apoptotiques. Pendant que les ions Ag<sup>+</sup> (et ses complexes solubles) mobilisent davantage la coopération des spherulocytes et des amoebocytes avec l'expression des hsp70 dans les réactions de coagulation et réparation chez les juvéniles, les AgNPs mènent à une plus forte expression des hsp 60 et 70, du type protectif. La réponse au stress est aussi adaptée aux cohorts juvéniles : les organismes les plus petits contaminés avec l'argent libre ont exprimé les hsp70 à 24h tandis que les plus grands l'ont fait à 48h. Les mécanismes de toxicité de chaque forme chimique de l'argent sont discutés en fonction des différents groupes cellulaires et des spécificités morphologiques de chaque stade.

Mots clés : Oursins verts, nanoparticules d'argent, mécanismes, toxicité, stress physiologique et cellulaire, microscopie confocale, MET, développement.



## ABSTRACT

Silver nanoparticles (AgNPs) are increasingly incorporated into daily use products given their antimicrobial and physicochemical properties. It has already been proven that silver released from these products will be found in wastewaters. Thus, the possibility that a combination of a massive use of products related to silver can increase its concentration in the marine ecosystems is clear. Thus, new efforts to understand the AgNP toxicity in marine invertebrates and specifically in their development stages are highly needed. The stages of embryogenesis, metamorphosis of echinoplutei larvae and juvenile development of the sea urchin *Strongylocentrotus droebachiensis* were used as biological models. The project was based on the following assumptions: (1) sensitivity to contaminants is based on morphological transformations of the three basic tissue layers (ectoderm, mesoderm and endoderm), its derivatives and the coelomic cavities (the axocœl, the hydrocœl and somatocoel); (2) new routes for contaminants and increasing inner space of coelomic cavities maximize assimilation, respectively, distribution and accumulation of xenobiotics; (3) exposed to sub-lethal concentrations, organisms react with specific cellular mechanisms to each contaminant in a relatively short time. We have been using a number of techniques such as confocal microscopy, transmission electron microscopy, chemical analysis by ICP-MS, fluorimetric assays, immunoblotting and several bioassays to achieve our objectives. Many transformation processes experienced by organisms explained how toxicity of  $\text{Ag}^+$  ions and AgNPs could shift during development. The permeable ectoderm of embryos, the gastrointestinal tract and secondary coelomic cavities of larvae and juveniles showed that contaminants can be uptake in different ways. When combined with carbon nanotubes, free silver significantly disturbed the development. The perivisceral cavity and peritoneocytes seem to be essential to the internal nano-translocation in larvae and juveniles. In addition, the nanoAg modulated phagocytic activity and cytoprotective mechanisms in coelomocytes. Ionic silver (and soluble complexes) seemed to lead to an oncosis process followed by necrosis, while nanosilver was associated to an apoptotic-like process. While free Ag further mobilized the cooperation of spherulocytes and amoebocytes with hsp70 expression for coagulation and repair in juveniles, AgNPs led to a stronger protective expression of both hsp 60 and 70. The timing for stress response followed juvenile cohorts: smaller individuals contaminated with  $\text{Ag}^+$  ions expressed hsp 70 at 24h while the larger ones did so at 48h. Overall, mechanisms of toxicity of each silver chemical form are discussed in terms of different cell groups and morphological features of each stage.

**Keywords:** Sea urchins, silver nanoparticles, mechanisms, cellular toxicity, physiological mechanisms, heat shock proteins, confocal microscopy, transmission electron microscopy, development.



## TABLE DES MATIÈRES

REMERCIEMENTS.....	v
AVANT-PROPOS.....	vi
RÉSUMÉ.....	vii
ABSTRACT.....	viii
TABLE DES MATIÈRES.....	ix
LISTE DES TABLEAUX.....	xvi
LISTE DES FIGURES.....	xvii
LISTE DES ABRÉVIATIONS, DES SIGLES ET DES ACRONYMES.....	xx
INTRODUCTION GÉNÉRALE.....	1
LA BIODIVERSITÉ, LE DEVELOPPEMENT INITIAL DES INVERTÉBRÉS MARINS ET LES CONTRAINTES ENVIRONNEMENTALES.....	1
LES ÉCHINODERMES COMME MODÈLES D'ÉTUDE EN ÉCOTOXICOLOGIE.....	6
LES EFFETS DE LA CONTAMINATION CHEZ LES ORGANISMES AQUATIQUES EN DEVELOPPEMENT.....	9
LES SYSTEMES DE DEFENSE CHEZ LES ECHINODERMES.....	11
LA CONTAMINATION PAR L'ARGENT LIBRE.....	13
LES NANOPARTICULES D'ARGENT.....	15

LE COMPORTEMENT DES NANOParticules METALLIQUES ET LES MECANISMES DE TOXICITE CELLULAIRE	19
LA MISE EN CONTEXTE DU TRAVAIL.....	22
OBJECTIFS DE LA THESE.....	23
CHAPITRE 1 : LES MÉCANISMES DE TOXICITÉ DE L'ARGENT IONIQUE ET DES NANOParticules D'ARGENT PAAM ET LEURS INTERACTIONS AVEC LES NANOTUBES DE CARBONE PENDANT LE DEVELOPPEMENT EMBRYONNAIRE DES OURSINS VERTS	27
1.1    RÉSUMÉ EN FRANÇAIS DU PREMIER ARTICLE.....	27
1.2    TOXICITY MECHANISMS OF IONIC SILVER AND POLYMER-COATED SILVER NANOPARTICLES WITH INTERACTIONS OF FUNCTIONALIZED CARBON NANOTUBES ON EARLY DEVELOPMENT STAGES OF SEA URCHIN	29
1.3    ABSTRACT.....	29
1.4    INTRODUCTION.....	30
1.5    MATERIAL AND METHODS.....	33
1.5.1    Collection and spawning.....	33
1.5.2    Embryos handling and blastulae hatching.....	33
1.5.3    Preparation and characterization of PAAm-AgNPs.....	34
1.5.4    Surface treatment and characterization of functionalized SWCNTs.....	35
1.5.5    Stock solutions and nominal concentrations.....	36
1.5.6    Experimental design.....	37

1.5.7 Confocal microscopy.....	41
1.5.8 Measurement of dissolved and adsorbed silver.....	42
1.5.9 Statistical analysis.....	42
1.6 RESULTS.....	43
1.6.1 Dissolved and adsorbed silver in exposure wells.....	43
1.6.2 Preliminary acute tests.....	44
1.6.3 Effects on body shape and swimming behavior.....	44
1.6.4 First treatment (T1).....	47
1.6.5 Second treatment (T2).....	48
1.6.6 Third treatment (T3).....	51
1.6.7 Fourth treatment (T4).....	53
1.6.8 Fifth and sixth treatments (T5 and T6).....	56
1.6.9 Disturbed congregation of spiculogenic cells by silver forms.....	57
1.6.10 The fate of f-SWCNTs.....	59
1.6.11 Recovery period.....	59
1.6.12 Analysis of mortality among contaminated stages.....	62
1.6.13 Analysis of mortality as a function of contaminants.....	63
1.7 DISCUSSION.....	64
1.7.1 Embryogenic impairments during chemical stress.....	64

1.7.2 Ag <sup>+</sup> toxicity mechanism.....	67
1.7.3 PAAm-AgNPs toxicity mechanism.....	69
1.7.4 Influence of f-SWCNTs on mechanisms of toxicity of Ag <sup>+</sup> and PAAm-AgNPs.....	71
1.7.5 Recovery period after acute exposures.....	73
1.8 SUMMARY AND CONCLUSION.....	74
CHAPITRE 2 : EFFETS PHYSIOLOGIQUES ET RÉPONSES CELLULAIRES DES LARVES MÉTAMORPHIQUES ET JUVENILES D'OURSIN APRÈS L'EXPOSITION À L'ARGENT IONIQUE ET AUX NANOPARTICULES D'ARGENT	75
2.1 RÉSUMÉ EN FRANÇAIS DU DEUXIÈME ARTICLE.....	75
2.2 PHYSIOLOGICAL EFFECTS AND CELLULAR RESPONSES OF METAMORPHIC LARVAE AND JUVENILES OF SEA URCHIN EXPOSED TO IONIC AND NANOPARTICULATE SILVER	77
2.3 ABSTRACT.....	77
2.4 INTRODUCTION.....	78
2.5 MATERIAL AND METHODS.....	81
2.5.1 Preparation and characterization of silver solutions and PAAm-AgNPs suspensions.....	81
2.5.2 Fluorescent dyes.....	82

2.5.3 Sea urchin collection, spawning and larvae handling.....	83
2.5.4 Experimental design.....	84
2.5.5 Observations in confocal microscopy.....	87
2.5.6 Sample preparation for Transmission electronic microscopy (TEM)....	87
2.5.7 Statistical analysis.....	88
2.6 RESULTS.....	89
2.6.1 Distribution of dissolved, particulate and adsorbed silver in exposure wells.....	89
2.6.2 Toxicity tests.....	91
2.6.3 Uptake of nanoAg-FITC and Qdots 525 by larvae (L <sub>8</sub> <sub>1</sub> , L <sub>8</sub> <sub>2</sub> ), postlarvae and juveniles.....	103
2.6.4 Internalization of PAAm-AgNPs by echinopluteus larvae and juveniles after chronic exposure.....	108
2.7 DISCUSSION.....	116
2.7.1 Juvenile stage.....	116
2.7.2 Postlarva stage.....	120
2.7.3 Larval stage (eight-arm echinopluteus stage).....	121
2.7.4 PAAm-AgNPs cytotoxic effects.....	123
2.7.5 Cellular responses and likelihood of detoxification process related to	

PAAm-AgNPs.....	125
2.8 SUMMARY AND CONCLUSION.....	127
CHAPITRE 3: SILVER NANOPARTICLES AND DISSOLVED SILVER ACTIVATE CONTRASTING IMMUNE RESPONSES AND STRESS-INDUCED HSP EXPRESSION IN SEA URCHIN	129
3.1 RESUME EN FRANÇAIS DU TROISIEME ARTICLE.....	129
3.2 SILVER NANOPARTICLES AND DISSOLVED SILVER ACTIVATE CONTRASTING IMMUNE RESPONSES AND STRESS-INDUCED Hsp EXPRESSION IN SEA URCHIN	131
3.3 ABSTRACT.....	131
3.4 INTRODUCTION.....	132
3.5 MATERIAL AND METHODS.....	134
3.5.1 Test organism conditions.....	134
3.5.2 Preparation of PAAm-AgNPs and characterization.....	135
3.5.3 Measurement of dissolved silver in exposure media and sea urchins.....	135
3.5.4 Stock solutions and test concentrations.....	135
3.5.5 Experimental set-up for stress proteins, bioaccumulation, oxygen reactive species detection, pigment production and migration of immune cells	136
3.5.6 Oxygen reactive assessment.....	137
3.5.7 Pigment extraction and quantification.....	137
3.5.8 Immune cell migrations detection.....	138
3.5.9 Proteins extraction, SDS-Page and Immunoblotting for Hsp analysis....	138

3.5.10 Sample preparation for Transmission electronic microscopy (TEM).....	139
3.5.11 Statistical design.....	139
3.6 RESULTS.....	139
3.6.1 Silver distribution in exposure media, sea urchins and phytoplankton...	139
3.6.2 Cellular mechanisms against Ag <sup>+</sup> and PAAm-AgNPs.....	141
3.7 DISCUSSION.....	161
3.7.1 Effects of Ag concentrations in sea urchins.....	161
3.7.2 Immune cell cooperation after dissolved silver and nanosilver contamination.....	163
3.7.3 Silver effects and anti-stress hsp60 and 70 expressions.....	165
3.7.4 Silver nanoparticles route mechanisms in sea urchin.....	168
3.7.5 Mechanisms of cellular internalization and elimination of AgNPs.....	169
3.7.6 Intracellular effects of AgNps in coelomocytes.....	171
3.8 SUMMARY AND CONCLUSION.....	173
CONCLUSION GENERALE.....	175
APPENDICE.....	212
RÉFÉRENCES BIBLIOGRAPHIQUES.....	247



## **LISTE DES TABLEAUX**

Tableau 1 : Concentration nominale des contaminants .....	36
Tableau 2: Les temps de traitement des stades successifs de l'embryogénèse.....	38
Tableau 3: Distribution des formes chimiques de l'argent pendant l'exposition (larves).....	89
Tableau 4: Distribution des formes chimiques de l'argent pendant l'exposition (juvéniles).....	90
Tableau 5: L'argent dissous dans le milieu d'exposition, adsorbé par les parois des puits, pris comme matière particulée et accumulé.....	140



## LISTE DES FIGURES

Figure 1 : Cycle de vie initial de l'oursin <i>Strongylocentrotus droebachiensis</i> .....	5
Figure 2: Clivages de l'oeuf et formation des dérivés des feuillets primordiaux.....	8
Figure 3: Stade de midgastrule en microscopie confocale.....	13
Figure 4: Propriétés physico-chimiques des nanoparticules d'argent.....	16
Figure 5: Modèle comparatif de taille des nanoparticules et les protéines.....	18
Figure 6: Représentation schématique des objectifs de thèse.....	26
Figure 7: Image MEV des nanoparticules d'argent PAAm et des nanotubes.....	35
Figure 8: Représentation des événements principaux de l'embryogénèse.....	40
Figure 9: Proportion relative d'argent ionique en milieu d'exposition.....	43
Figure 10: Stades de développement contaminés pendant l'embryogénèse.....	46
Figure 11: Analyse morphologique <i>in vivo</i> des embryons contaminés.....	49
Figure 12: Migration des cellules pigmentaires chez les embryons et les larves.....	52
Figure 13: Le stress cellulaire causé par l'argent chez les larves et les blancs.....	54
Figure 14: Le syncytium spiculogénique et la contamination par l'argent.....	58
Figure 15: Les groupes de larves et embryons formés après la récupération.....	61
Figure 16: Analyse de la mortalité par stade de développement après la récupération.....	62
Figure 17: Analyse de la mortalité totale par contaminant.....	63
Figure 18: Analyse de la métamorphose pendant la contamination avec l'argent.....	93
Figure 19: Analyse des conditions physiologiques des postlarves et des juvéniles non-nourris contaminés avec l'argent	97

Figure 20: Analyse MDS des conditions physiologiques des juvéniles nourris et non-nourris contaminés avec l'argent	100
Figure 21: Analyse MDS des conditions physiologiques des juvéniles nourris.....	102
Figure 22: Profile des niveaux de fluorescence du marqueur nanoAg-FITC chez les larves.....	103
Figure 23: Transfert du marqueur nanoAg-FITC pendant la période perimétamorphique.....	105
Figure 24: Micrographie MEV de l'intestin larvaire exposé aux AgNPs.....	109
Figure 25: Micrographie MEV du cœlome larvaire exposé aux AgNPs.....	111
Figure 26: Micrographie MEV du cœlome periviscéral et épigastrique des juvéniles contaminés avec les AgNPs	113
Figure 27: Micrographie MEV du mésothélium de larves contaminées avec les AgNPs.....	114
Figure 28: Micrographie MEV du mésothélium de juvéniles contaminées avec les AgNPs.....	115
Figure 29: Coopération des spherulocytes et des amoebocytes pendant l'exposition à l'argent....	144
Figure 30: Courbe d'absorbance d'expression des pigments pendant l'exposition à l'argent.....	147
Figure 31: Micrographie MEV du cœlome intra-péritonéal des juvéniles contaminés avec les AgNPs	148
Figure 32: Micrographie MEV d'un coelomocyte du cœlome intra-péritonéal des juvéniles contaminés avec les AgNPs	149
Figure 33: Micrographie MEV d'un coelomocyte contaminé avec les AgNPs.....	150
Figure 34: Micrographie MEV des sinus coelomiques, vaisseau hémal et tissu digestif d'un juvénile exposé aux AgNPs	151
Figure 35: Quantification des Hsp70 chez les juvéniles exposés à l'argent.....	154
Figure 36: Quantification des Hsp60 chez les juvéniles exposés à l'argent.....	159
Figure 37: Modèle d'interaction avec les contaminants chez les embryons.....	177
Figure 38: Modèle d'interaction argent-cellules minéralisatrices.....	178

Figure 39: Modèle d'assimilation des ions Ag <sup>+</sup> chez les larves d'oursin nourries.....	179
Figure 40: Modèle d'interaction contaminant-épiderme/contaminant-épithélium digestif proposé pour les larves échinoplutei	180
Figure 41: Modèle d'interaction des AgNPs avec l'épiderme, l'épithélium digestif et le mésoderme chez les échinoplutei	182
Figure 42: Modèle d'interaction des Ag <sup>+</sup> avec l'épiderme, l'épithélium digestif et le mésoderme chez les échinoplutei	183
Figure 43: Modèle des mécanismes d'agrégation et d'internalisation des AgNPs après l'assimilation par voie orale chez les juvéniles	185
Figure 44: Modèle des mécanismes d'assimilation, agrégation et internalisation des AgNPs chez les échinoplutei en métamorphose	187
Figure 45: Modèle d'interaction de l'argent dissous et des PAAm-AgNPs avec les f-SWCNTs	193
Figure 46: Modèle d'interaction contaminant-tissus dérivés du mésoderme proposé pour les juvéniles d'oursin vert après l'exposition aux nanoAg	195
Figure 47: Modèle des voies d'entrée et de nano-translocation chez les oursins en développement	197
Figure 48: Réseau du système hémal lié au tractus digestif.....	198
Figure 49: Modèle d'interaction des AgNPs avec la membrane cellulaire des coelomocytes.....	201
Figure 50: Différences entre les mécanismes de toxicité cellulaires des AgNPs et des ions Ag <sup>+</sup> chez l'oursin vert en stade juvénile	203
Figure 51: Schéma de la structure des nanoparticules d'argent PAAm.....	206
Figure 52: Modèle d'action des PAAm-AgNPs dans un milieu aqueux.....	207

## **LISTE DES ABRÉVIATIONS, DES SIGLES ET DES ACRONYMES**

**Ac:** abnormal or deformed cluster      **Ec:** ectoderm, **ec:** euchromatin

**AgNPs:** silver nanoparticles      **eHv:** external haemal vessel

**Ap:** animal pole      **En:** enterocyte

**Apo:** apical organ      **er:** endoplasmatic reticulum

**Aq:** archenteron      **Es:** endocytic vesicle

**Bc:** blastocoel      **Esp:** oesophagus

**Blc:** blastocoelar cells      **Fp:** filopodia

**c:** coelomocyte      **f-SWCNTs:** single walled carbon nanotubes functionalized

**C:** trunk coelom (somatocoel)      **g:** Golgi apparatus

**cb:** cell breb      **Git:** gastrointestinal tract

**Cec:** coelomic epithelial cells      **hc:** heterochromatin

**Ci:** cilium      **Hv:** haemal vessel

**Cœ:** coelomocyte      **Int:** intestine

**Cp:** coelomic pouches      **L:** lumen

<b>m:</b> mesentery	<b>Psp:</b> intra-peritoneal space (coelom)
<b>mb:</b> cell membrane	<b>Pv:</b> perivisceral coelom
<b>Mc:</b> mesenchyme cells	<b>s:</b> septate junctions
<b>Me:</b> contractile process of myoepithelial cell	<b>Sc:</b> secretory cell
<b>mu:</b> mucus	<b>sg:</b> secretion granule
<b>Mv:</b> microvilli	<b>SMCs:</b> secondary mesenchyme cells
<b>Nc:</b> cell nucleus	<b>Sp:</b> spicule
<b>ne:</b> nuclear envelope	<b>Sph:</b> spherule cell
<b>n-vs:</b> nano-dense vesicle	<b>Sphc:</b> cardiac sphincter
<b>Pa:</b> phagocyte	<b>Sr:</b> striated rootlet
<b>Pc:</b> peritoneal cell/peritoneocyte	<b>sRE:</b> smooth endoplasmic reticulum
<b>pci:</b> perinuclear cisternae	<b>Stc:</b> stomach
<b>Pgc:</b> pigment cells	<b>Stm:</b> stomodeum (opening mouth)
<b>Ph:</b> phagosome	<b>V:</b> vacuole
<b>Phs:</b> phagolysosome	<b>Vp:</b> vegetal pole
<b>Plc:</b> petaloid cell	<b>vs:</b> vesicle
<b>PMCs:</b> primary mesenchyme cells	<b>Vtlc:</b> ventro-lateral clusters
<b>pn:</b> perinuclear space	
<b>pp:</b> parietal peritoneum	







## **INTRODUCTION GÉNÉRALE**

Aujourd’hui les activités humaines semblent influencer chacun des grands écosystèmes aquatiques de la planète. Parfois, cette altération mène à l’augmentation de l’apport des nutriments essentiels comme l’azote et le phosphore, ce qui a une conséquence directe sur l’utilisation des fertilisants ou des pesticides. D’un autre côté, des sources variées comme le dépôt atmosphérique, l’activité minière, les effluents industriels et l’apport des eaux usées peuvent mener à la contamination métallique dans les régions côtières et océaniques. Ce genre de contamination est devenu problématique dans l’environnement marin et même des éléments chimiques considérés rares (comme l’argent) commencent à susciter des questions de sécurité environnementale.

Depuis longtemps, les sociétés humaines se sont servies des cours d’eau comme site principal de décharge et de dilution des résidus toxiques dont la composition est variée. Les eaux de rejet, issues des agglomérations urbaines à la proximité du littoral, atteignent facilement l’environnement marin sous forme traitée, partiellement traitée ou non-traitée. Ainsi, elles peuvent périodiquement apporter des contaminants en état mélangé et nuire, à court ou à long terme, à la faune et la flore. Or, la compréhension de la toxicité mécanistique des contaminants chez les organismes marins devient une étape primordiale pour connaître les effets toxiques isolés ou en combinaison avec d’autres facteurs (le manque de nourriture, d’autres contaminants, etc) ainsi que les réponses biologiques face au stress chimique.

## **LA BIODIVERSITE, LE DEVELOPPEMENT INITIAL DES INVERTEBRES MARINS ET LES CONTRAINTES ENVIRONNEMENTALES**

Les océans abritent une énorme biodiversité d’espèces connues et inconnues certainement dû à la grande variabilité d’habitats disponibles dans les milieux aquatiques et en particulier dans le milieu benthique (May, 1994). En effet, la plus grande partie de la biodiversité marine est constituée d’invertébrés habitant les sédiments (l’épifaune et

l’ifaune) et représentant 98% de toutes les espèces (Widdicombe et Spicer, 2008). L’immensité de l’espace marin permet l’existence d’une phase planctonique du cycle de vie pour environ 70% des espèces marines. En général, les invertébrés marins benthoniques ont une phase planctonique de durée variable suivie d’une courte phase de fixation au substrat, le moment où larve se métamorphose en juvénile et acquiert un mode de vie proche à celui des adultes. Cependant, des variations extrêmes à ce modèle classique de développement existent aussi, comme dans le cas de l’étoile de mer *Pteraster tesselatus* dont le développement est strictement pélagique sans stade larvaire ou métamorphose (McEdward and Miner, 2001). Une larve planctonique peut passer plusieurs semaines ou même des mois dans la colonne d’eau avant la sédimentarisation et le début de la métamorphose. Il est bien établi que la température et la disponibilité de nourriture sont des variables très importantes qui définissent la durée du développement chez les larves d’invertébrés. Dans les environnements froids, par exemple, la durée du développement est plus longue.

La microcouche de surface des océans (MS) est une interface (1-1000 µm) métaboliquement très productive où une grande partie de la matière organique particulée et dissoute est transportée après avoir été abondamment produite par le phytoplancton (Soloviev et Lukas, 2014). Or, les bactéries, le phytoplancton et les invertébrés y sont aussi enrichis par des facteurs de  $10^2$ - $10^4$ ,  $1\text{-}10^2$  et  $1\text{-}10$ , respectivement (Cunliffe et al., 2013). Dans cette microcouche, plusieurs contaminants organiques et métalliques, comme l’argent, sont également présents parfois dans l’ordre du  $\mu\text{g.L}^{-1}$  (Cunliffe et al., 2013; Wurl et Obbard, 2004). Ainsi, on s’attend à ce que l’accumulation des polluants puisse mener à un développement aberrant, à la diminution du rythme de développement, à la prolongation du temps d’éclosion et même à la mort chez les larves de poissons, échinodermes et autres métazoaires qui y demeurent (Wurl et Obbard, 2004). Dans la colonne d’eau, les stades de développement des invertébrés peuvent être trouvés dans différents compartiments au cours du temps. Dans les zones pélagiques, les larves subissent une forte influence du mélange turbulent (Mann et Lazier, 2006). Ainsi, elles peuvent se limiter à des zones précises, mais éventuellement migrer d’une couche à l’autre en fonction des besoins alimentaires comme

dans les cas des échinoplutei qui éventuellement traversent l'halocline (Metaxas et Young, 1998). En fait, la densité de la plupart des larves d'invertébrés benthiques excède celle de l'eau de mer et les organismes doivent donc nager pour assurer leur flottabilité. Pourtant, à la fin du développement, la larve a une tendance plus grande à s'enfoncer que la capacité de nager à cause de sa taille et son volume, ce qui coïncide avec l'étape de fixation et de métamorphose.

La métamorphose est une période sensible du développement des invertébrés marins. Les larves compétentes doivent se fixer à un substrat dont les stimuli chimiques sont souvent spécifiques et essentiels à cette étape. Lorsque la larve ne trouve pas ces stimuli ou pendant une contamination chimique dans l'eau, la métamorphose est alors retardée (Weiss, 2014). Les larves planctotrophiques qui ne sont pas exposées se maintiennent donc dans le plancton en activité d'alimentation; pouvant même avoir une croissance modérée (Pechenik et al., 1998). N'importe quel stress subi durant la vie larvaire (température, manque de ressources alimentaires, pollution, par exemple), influencera le développement post-métamorphique en termes de taux de croissance et de performance juvénile (Pechenik et al., 1998). L'effet de la métamorphose retardée en soi peut augmenter la mortalité après la sédimentarisation ou la compétence des juvéniles à s'établir sur l'habitat et d'explorer les ressources alimentaires nécessaires dans son nouvel environnement. Ce processus de changement de forme au développement requiert la mise en place d'un complexe réseau métabolique génétiquement programmé, mais facilement perturbé par les variables environnementales comme des variations de température, la présence des contaminants organiques ou inorganiques et, dans le cas des larves planctotrophiques, le manque ou la qualité de la nourriture.

Pendant la métamorphose, l'épithélium qui forme la bande ciliaire subit des processus de mort cellulaire (apoptose et autophagie) et les cellules blastocoelaires contribuent à l'élimination des cellules épithéliales mortes, mais l'intégrité du tissu épithelial est préservée (Sato et al., 2006). Il est connu que des neurotransmetteurs du système nerveux des larves d'oursins, comme le la dopamine, la L-DOPA, la glutamine et l'acide

glutamique induisent la sédimentarisation larvaire alors que l’oxyde nitrique et l’histamine agissent comme des modulateurs de la compétence métamorphique (Bishop et Brandhorst, 2007; Sutherby et al., 2012). Pourtant, il est encore difficile à préciser par quels mécanismes moléculaires les xénobiotiques perturbent l’ontogénie dans cette période. Gosselin et Jangoux (1998) ont décrit la période perimétamorphique comme un moment de courte durée lorsque les larves planctotrophiques acquièrent la compétence à la sédimentarisation, passent par le changement de forme (métamorphose) de façon à devenir des postlarves, aussi considérées comme des juvéniles recrutés endotrophiques. Cette période finit quand les postlarves acquièrent un tube digestif relativement bien formé et sont capables de manger (juvéniles exotrophiques). Les facteurs biotiques responsables de la mortalité juvéniles sont : la préation, la compétition, les complications lors du développement et les maladies (Gosselin et Qian, 1997). Les facteurs abiotiques sont similaires à ceux qui normalement posent des problèmes aux organismes qui habitent les zones intertidales : la dessiccation, la température, le stress physique et la radiation solaire. Chez l’oursin vert *Strongylocentrotus droebachiensis*, le cycle de vie de l’œuf jusqu’à la sédimentarisation dure 1 mois et 7 jours à 8°C, suivi d’à peu près 15 jours pour la période perimétamorphique (Figure 1).

Considérant l’importance de l’environnement benthique et de son réservoir de biodiversité, tout impact qui modifie les conditions abiotiques de l’eau et du fond océanique peut donc avoir un grand potentiel d’affecter les cycles de vie des organismes marins. À court terme, plusieurs activités anthropiques dans les milieux marins, telles que leutrophisation, le changement physique de l’habitat et l’hyper-sédimentation démontrent un impact aussi fort que les produits chimiques déversés (Hylland, 2006). Cependant, la seule différence reste au niveau du temps d’exposition et du type de processus impliqué. Plusieurs espèces démontrent un rapport complexe avec l’environnement des sédiments, ce qui peut effectivement influencer leurs répartitions. Ce rapport prend en compte la température, la salinité, la profondeur, la productivité de la superficie, la dynamique des sédiments, la géochimie, les interactions biologiques et même les polluants (Snelgrove, 1999). Le comportement d’évitement des endroits contaminés dans le fond océanique

semble exister chez certaines espèces d'invertébrés benthiques, surtout en ce qui concerne la contamination par les hydrocarbures aromatiques polycycliques. Les étoiles de mer tropicales de l'espèce *Patiriella exigua* détectent des sédiments avec du pétrole brut et les évitent directement en fonction de la dose appliquée (Ryder et al., 2004).

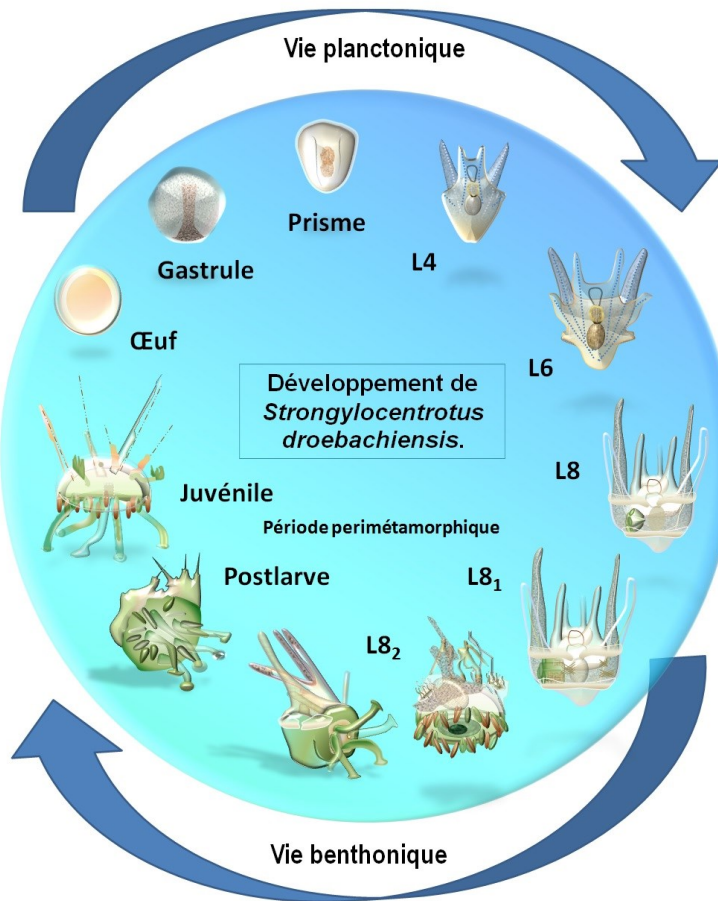


Figure 1: Représentation du cycle de vie initial de l'oursin *Strongylocentrotus droebachiensis*. La formation de la gastrule se produit entre 2-3 jours à 8°C, puis chaque stade larvaire prend au moins 2 semaines de développement avant la sédimentarisation. La larve L8 comprend deux périodes de formation : L8<sub>1</sub> (planctonique) et L8<sub>2</sub> (épibenthique). La L8<sub>2</sub> est considérée comme L8<sub>2</sub> compétente, au début de la période perimétamorphique; et L8<sub>2</sub> métamorphique plus vers la fin quand la larve devient essentiellement une postlarve.

Actuellement, plus de la moitié de la population mondiale humaine habite à moins de 60 km de la côte, cette proportion pourra atteindre 75% vers l'an 2026 (Roberts et Hawkins, 1999). Donc, il n'y a pas de doute que l'ampleur des impacts anthropiques sur les océans s'est accru et que les régions côtières reçoivent une gamme de polluants chimiques et biologiques de plus en plus large (Suchanek, 1993). En milieu marin, les régions toutes proches des sources émettrices des contaminants peuvent voir, par conséquent, leur biodiversité modifiée et parfois réduite. De plus, certaines substances ont une nature persistante et peuvent donc demeurer dans le milieu à long terme par des processus d'échanges entre les compartiments biotiques et abiotiques, pouvant engendrer des modifications importantes dans les chaînes trophiques des communautés (Hylland, 2006; Turner, 2010).

## **LES ECHINODERMES COMME MODELES D'ETUDE EN ECOTOXICOLOGIE**

Les échinodermes constituent un ancien clade d'invertébrés marins benthiques dont le registre fossile date de 600 à 570 millions d'années. Le phylum est un groupe-frère des Hémichordés, ce qui les place dans le clade des métazoaires deutérostomiens (Superphylum Deuterostomia). Dans tous les océans et à toutes les profondeurs, les échinodermes (Phylum Echinodermata) sont considérés comme des composants-clés des systèmes marins, où ils contribuent à plus de 90% de la biomasse benthique (Ventura et al., 2006). Le phylum est formé de 6500 à 7000 espèces, parmi lesquelles on compte 2000 ophiuroïdes, 1800 étoiles de mer, 1400 concombres de mer, 900 oursins et 700 crinoïdes (Brusca et al., 2016). Tous les membres du groupe garantissent la diversité environnementale, soit en tant que consommateurs primaires, ce qui maintient l'équilibre des espèces de macroalgues ; soit comme prédateurs, ce qui maintient la diversité des autres groupes d'invertébrés marins (Ventura et al., 2006).

Pendant l'embryogénèse de l'oursin *Strongylocentrotus purpuratus*, environ 12 000 à 13 000 gènes ont été répertoriés au début du développement de l'embryon (Sodergren et al., 2006). Étant donné que l'organisme en développement doit gérer le stress causé par des

variations physiques, chimiques et biologiques dans l'environnement, une partie des familles de gènes et des voies métaboliques s'est développée de manière à les protéger. Une partie de ces mécanismes est reliée au système immunologique, qui répond aux pathogènes marins; l'autre groupe de gènes contrôle le complexe protéomique contre le stress chimique. On sait que le génome des oursins est le quart de la taille de celui de l'humain, mais possède approximativement le même nombre de gènes que ce dernier (Ghosh et al., 2010). Cette proximité phylogénétique fait en sorte qu'une série de voies métaboliques ainsi que des éléments du système immunitaire présentent des similarités surprenantes.

Le phylum a quelques caractéristiques morpho-physiologiques exceptionnelles qui ouvrent un vaste potentiel d'investigation sur la sensibilité biologique aux contaminants, lesquels sont d'ailleurs de plus en plus complexes dans leurs combinaisons et interactions chimiques. La première caractéristique est basée sur l'épithélium et le tissu connectif collagénique dont les propriétés mécaniques mutables permettent l'entrée des substances dissoutes présentes dans le milieu. Durant une contamination environnementale, les échinodermes sont perçus en tant que des « organismes-cible », principalement en ce qui concerne le stockage des micropolluants dans les sédiments. Puisqu'ils occupent souvent le plus haut niveau trophique dans certains milieux, leur susceptibilité aux processus de biomagnification des substances toxiques peut se produire davantage. En ce qui concerne la biologie du développement, toute la complexité des processus de transformation des stades (dans l'eau et sur l'interface l'eau-substrat) devient un précieux outil d'investigation pour comprendre les mécanismes de toxicité des contaminants (Figure 2). Finalement, comme mentionné auparavant, le status phylogénétique de l'embranchement, deutérostomiens comme les vertébrés, est un autre avantage qui prend en compte les similarités physiologiques et des voies hormonales avec les chordés. Or, même la capacité régénérative des échinodermes peut être considérée comme un aspect biologique d'intérêt en ce qui concerne l'effet déstabilisateur de certains contaminants sur les voies hormonales.

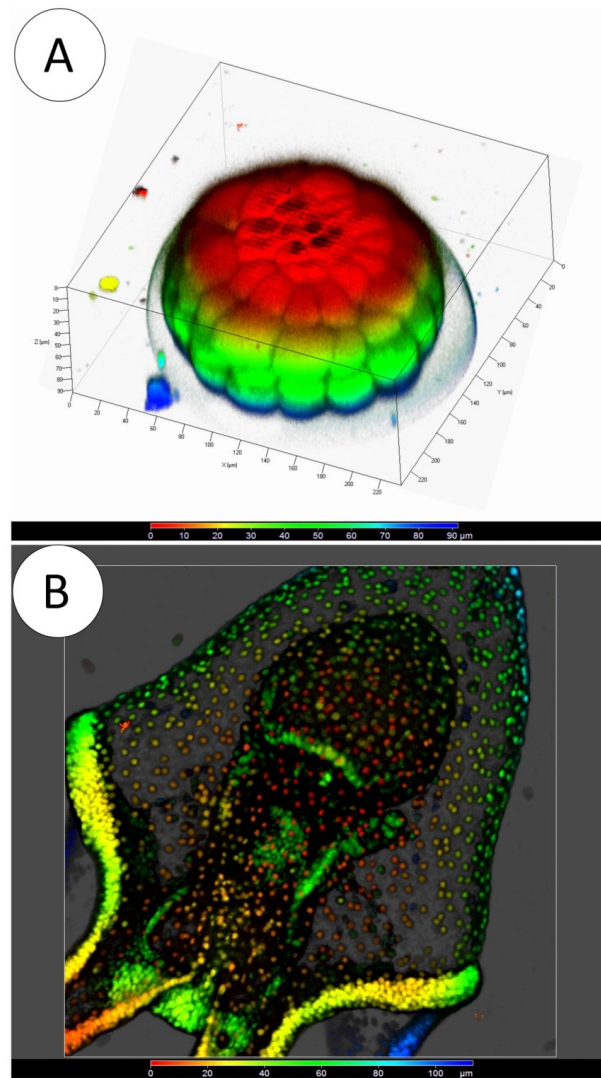


Figure 2: A- Images des clivages de l'oeuf et formation des macromères (jaune, bleue, vert) et des micromères (rouge) au pôle végétal: ils formeront les mésenchymes primaires et secondaires, le tractus gastrointestinal et une partie de l'ectoderme de *S.droebachiensis*. B- Image de la formation des dérivés des feuillets primordiaux chez la larve (l'épiderme, le tractus digestif). Le mésoderme serait représenté les cellules minéralisatrices et spherulocytes rouges. (En microscopie confocale, A : du rouge au bleu foncé, 0-90 μm ; B : du rouge au bleu foncé, 0-100 μm ; ISMER).

## **LES EFFETS DE LA CONTAMINATION CHEZ LES ORGANISMES AQUATIQUES EN DEVELOPPEMENT**

Chez tous les organismes et à n'importe quel stade du cycle de vie, la dynamique des effets toxiques des contaminants est très complexe. Quand les substances toxiques disponibles dans l'environnement pénètrent dans le système biologique, des effets létaux et/ou sous-létaux surgissent. C'est un processus directement lié à la quantité dissoute du contaminant dans le milieu mais aussi à la capacité du système de dépurateur d'opérer de façon optimale. Newman (2015) mentionne que les effets directs de la contamination sont souvent la mort, mais aussi des changements physiologiques, des aberrations cytogénétiques et la carcinogénèse. Quand le matériel génétique est endommagé, les altérations métaboliques peuvent aussi contribuer à l'intoxication des organismes (Depledge, 1998).

L'assimilation (ou efficience d'absorption) d'un xénobiotique est la fraction de sa quantité totale disponible dans un milieu qui est transférée à un organisme et dont la quantification équivaut à la différence entre l'entrée et l'élimination. La plus grande partie de ces substances est assimilée par le corps via la diffusion passive à travers des membranes semi-perméables comme le revêtement de la bouche, les branchies et le tissu gastro-intestinal, mais également par endocytose. Les espèces du zooplancton se trouvent normalement en phase d'équilibre chimique avec la fraction dissoute du xénobiotique, non seulement à cause de leur petite taille, mais aussi dû aux mouvements natatoires et de ventilation qui accentuent le taux d'entrée des substances en solution (Rand et al., 1995). D'un autre côté, les phénomènes d'adsorption jouent aussi un rôle important quant aux processus d'accumulation sur le tégument des animaux par des forces covalentes, électrostatiques ou moléculaires, affectant les fonctions de l'épithélium (García-Alonso et al., 2011).

Chez les embryons et les larves des invertébrés, quelques mécanismes d'assimilation des contaminants sont proposés. Il existe l'hypothèse concernant la protection des embryons en développement par la membrane de fertilisation et il semble que ceci pourrait plutôt être

un mécanisme important chez les invertébrés d'eau froide compte tenu du temps plus long d'éclosion des blastules ou des larves. Néanmoins, Zhu et al. (2011) ont démontré que des agrégats de nanoparticules d'oxyde de titane ( $TiO_2$ NPs) augmentent la toxicité du tributylétain de 20% comparativement à son exposition simple chez les embryons de l'abalone *Haliotis diversicolor supertexta* encore protégés par la membrane de fertilisation. L'hypothèse des auteurs est basée sur la capacité des  $TiO_2$ NPs (562 nm à 22.7 $\mu$ m) de s'associer à la surface des membranes et de libérer le tributylétain vers les embryons. Nous avons observé que les larves de l'étoile de mer *Leptasterias polaris* exposées aux marqueurs nanoAg-FITC et aux Quantum dots 525 sont fortement marquées sur la surface de la membrane de fertilisation jusqu'à l'éclosion quand les tissus larvaires deviennent plus fluorescents (Magesky and Pelletier, 2015). Šiller et al. (2012) ont démontré que les nanoparticules d'argent (5-35 nm-AgNPs), assimilées par les larves échinoplutei de *Paracentrotus lividus*, se trouvent dispersées sous forme de complexes chimiques ( $Ag_2O$ ,  $AgO^-$ ,  $Ag_2S$ ,  $AgNO_3$ ,  $AgCl$ ), mais aucun mécanisme d'internalisation n'a été développé. En général, la voie orale est fréquemment mentionnée comme la principale porte d'entrée des contaminants métalliques associés avec la nourriture chez les larves d'invertébrés, mais les mécanismes impliqués sont rarement décrits.

Chez les invertébrés dont les larves minéralisent un squelette interne, la perméabilité épithéliale et le passage des ions dissous de l'eau de mer vers les cavités corporelles sont essentiels. La possibilité que cette voie soit aussi utilisée par les contaminants métalliques avant le début du développement du système digestif pourrait expliquer les malformations du squelette aux premiers stades. Chez les oursins, l'activité des cellules mésenchymateuses pendant l'arrangement final de l'œsophage et de la bouche est facilement perturbée par les métaux. Quelques études menées avec les embryons d'oursin montrent le potentiel des métaux cationiques (comme le lithium et le nickel) à perturber les différentes étapes de l'embryogénèse en produisant des larves aberrantes (Hardin et al., 1992; Emily-Fenouil et al., 1998). Chez les embryons du céphalopode *Loligo pealeii* l'organogénèse est profondément endommagée par le lithium après 6 jours d'exposition (Crawford, 2003).

Dans ce cas, les structures normalement associées aux tissus ectodermiques comme les tentacules, les yeux, le manteau, les nageoires et le siphon deviennent difformes.

### **LES SYSTEMES DE DEFENSE CHEZ LES EQUINODERMES**

Une gamme de contaminants environnementaux peut induire une réponse immunitaire chez les invertébrés benthiques. Leur système immunitaire est caractérisé par l'absence de défenses spécifiquement contrôlées par des anticorps, un système dit non-spécifique ou inné. Pourtant, la phagocytose, la cytotoxicité et l'encapsulation représentent les plus importants mécanismes de réponse immunologique contre les infections (Silva, 2013).

Chez les échinodermes, l'immunité cellulaire (cœlomocytes, amoebocytes, phagocytes, spherulocytes, etc) et humorale (système du complément, hémagglutinines, peptides, lectines, hémolysines, système phélonoxidase, les espèces réactives oxygénées - ROS) ont un rôle important de protection contre les pathogènes, mais aussi contre les contaminants de toute nature (Silva, 2013). La manière dont le système immunitaire est élaboré varie selon l'espèce considérée. Les cœlomocytes, par exemple, sont diversifiés en structures et fonctions physiologiques; souvent très sensibles aux perturbations physiologiques du milieu interne. Ces cellules sont rapidement mobilisées dans les processus de chimiotaxie, de phagocytose, d'encapsulation, de l'agglutination et du rejet de greffes (Gross et al., 2000). En fait, Pinsino et Matranga (2015) mentionnent que les phagocytes ont deux types morphologiques avec des fonctions différentes : les cellules pétaloïdes qui phagocytent et les cellules filopodiales qui démarrent la formation des coagules. Chez les embryons et coelomocytes de l'oursin *Lytechinus variegatus*, les protéines hsp70 (constitutives hsc70 et inducibles hsp70) participent aux réactions de coagulation des cellules d'oursin en condition hypotonique menant probablement à la division cellulaire et l'inhibition de la dispersion cellulaire (Brown et al., 2007). Il est aussi possible que chez les oursins, les hsp70s libérées par des cellules puissent activer des facteurs NF- $\kappa$ B qui régulent l'expression des molécules cytokines en déclenchant un processus d'inflammation (Pinsino et Matranga, 2015).

Dès la sédimentation des larves vers l'environnement benthique, un système immunitaire efficace doit se mettre en place pour les protéger contre des nouveaux pathogènes et s'adapter à de nouvelles conditions. Chez les embryons d'oursins en gastrulation, les cellules mésenchymateuses qui migrent de l'archentéron vers la blastocoele démontrent déjà une activité phagocytaire qui ne diffère pas de celle des adultes (Silva, 2000) (Figure 3). Dans le cas des larves échinoïdes, l'action antioxydante des cellules pigmentaires (spherulocytes) est liée à des réactions cytotoxiques et antibactériennes (Silva, 2013). Comparativement, le système immunitaire des larve bipinnaria de l'étoile de mer *Asterina pectinifera* répond à la présence des bactéries gram-positives et négatives, à des grains de polystyrène et de l'huile de silicone avec les cellules mésenchymateuses formant un syncytium qui engloutit toutes ces particules (Furukawa et al., 2009).

Depuis peu de temps, le décryptage du génome de l'oursin *Strongylocentrotus purpuratus* a révélé un complexe système de gènes (*Sp185/333*) responsable du contrôle d'un système immunitaire sophistiqué dont les protéines répondent à une panoplie de pathogènes (Silva, 2013; Pinsino et Matranga, 2015). Chez l'oursin *S. purpuratus*, le système *Sp185/333* gère la réponse immunologique dans le fluide axial, l'organe axial, les gonades, le pharynx, l'œsophage et l'intestin des adultes de façon à activer les cœlomocytes. Par ailleurs, le même système se met en place assez tôt dans les cellules de la blastocoele de 60% des larves quand il y a une forte concentration de microorganismes dans l'eau (Ghosh et al., 2010). Le système immunitaire des oursins devient de plus en plus connu à l'aide des modèles d'étude basés sur la biologie des embryons, des cellules directement récupérées des cavités coelomiques ou en culture. En contrepartie, il n'y a pas d'information concernant le système immunitaire des juvéniles en développement et/ou en exposition aux xénobiotiques. Comment le système immunitaire des invertébrés marins se comportent face au stress causé par des nouveaux contaminants (comme les nanoparticules) demeure un vaste terrain à explorer.

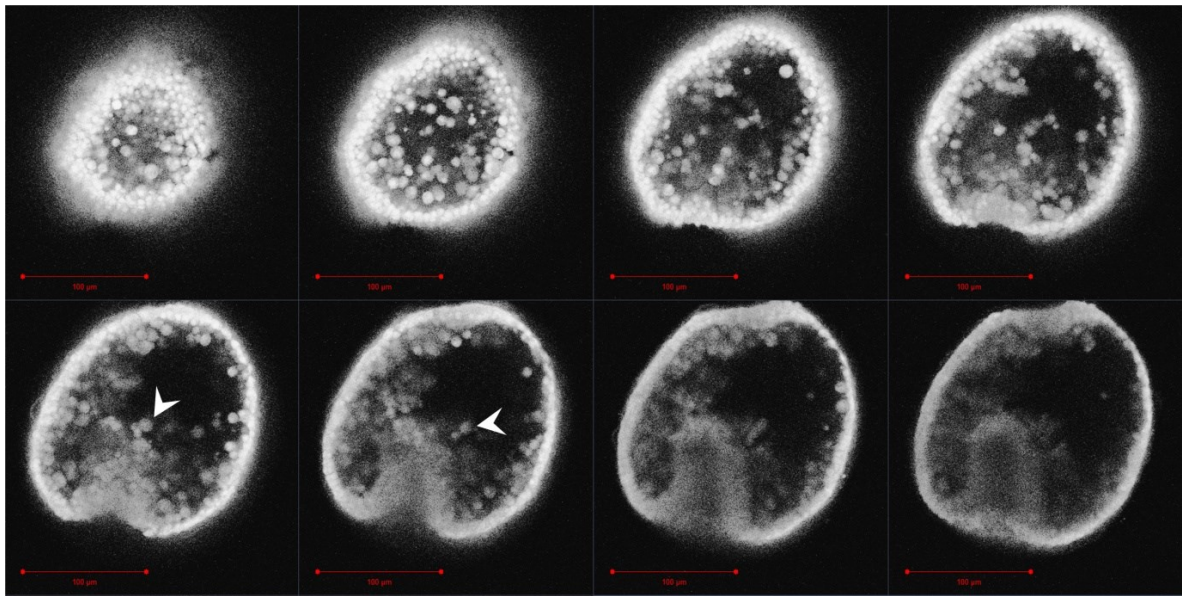


Figure 3: Images séquentielles d'une midgastrule de *S. droebachiensis* obtenues en microscopie confocale (ISMER). Les cellules mésenchymateuses secondaires qui quittent l'archentéron de la midgastrule sont indiquées par les flèches blanches. (Barre rouge: 100 µm).

#### LA CONTAMINATION PAR L'ARGENT LIBRE

L'argent est un métal rare trouvé dans la nature sous des formes natives, des oxydes, des sulfites et des sels (Purcell and Peters, 1998). Cependant, l'addition d'une petite fraction d'argent par des sources anthropiques dans l'eau mène à d'importants changements hors des conditions naturelles (Howe et Dobson, 2002; Luoma, 2008). Pour atteindre son stabilité chimique dans l'eau, l'argent cationique s'associe rapidement à des ligands négativement chargés. Donc, près de régions urbanisées, dans les eaux fortement contaminées ou à forte concentration de matière organique, l'argent peut être présent sous forme de complexes organiques à groupements thiolates (Adams et Kramer, 1999; Howe et Dobson, 2002). Cette affinité chimique de l'argent pour les groupements thiols ( $-C-SH$  or  $R-SH$ ) permet des échanges dynamiques des ions  $Ag^+$  entre les thiolates de la matière organique, mais aussi entre les thiolates et les groupes thiols des cellules d'un organisme quelconque (Bell et Kramer, 1999).

Dans les estuaires, le comportement de l'argent est non-conservatif. Ainsi, les concentrations des ions  $\text{Ag}^+$  tendent à diminuer avec la salinité, grâce à son affinité pour les particules organiques en suspension. À faible salinité, les effets toxiques de l'argent peuvent être optimisés après la formation des complexes neutres potentiellement lipophiles  $\text{AgCl}$  (aq) et  $\text{AgHS}$  (aq) (Tappin et al., 2010). À forte salinité en milieu océanique, les fractions macromoléculaires diminuent et des  $\text{Ag}^0$ -complexes avec les chlorures sont plutôt formés ( $\text{AgCl}^0$ ,  $\text{AgCl}^{2-}$ ,  $\text{AgCl}_3^{2-}$  and  $\text{AgCl}_4^{3-}$ ), mais une certaine portion des ions  $\text{Ag}^+$  reste disponible et s'associe aux matières organiques réfractaires dans l'eau (Ndungu et al., 2006). Les plus faibles concentrations d'argent sont trouvées dans l'océan (0.03 à 0.1  $\text{ng}\cdot\text{L}^{-1}$ ), quoique récemment une augmentation de 50% a été reportée dans les eaux de surface (1.3 à 12  $\text{pmol}\cdot\text{kg}^{-1}$ ), probablement dû à des nouvelles sources anthropiques (Ranville et Flegal, 2005; Gallon et Flegal, 2015). Lanceleur et al. (2011) ont aussi registrado une augmentation de la bioaccumulation de l'argent chez les huîtres (de 39 à 116  $\text{mg}\cdot\text{kg}^{-1}$ ) à partir de sources inconnues dans un système estuaire. En général, les plus fortes concentrations d'argent registrées ces dernières années ont varié de 64 à 327  $\text{ng}\cdot\text{L}^{-1}$  pour les eaux usées et de 6 à 189  $\text{ng}\cdot\text{L}^{-1}$  pour les eaux côtières (Luoma et Phillips, 1988; Smith et Flegal, 1993; Ranville et Flegal, 2005).

Depuis longtemps, l'argent a été utilisé dans le milieu médical et industriel, ainsi que dans la vie courante avec les électroménagers (Siripattanakul-Ratpukdi and Fürhacker, 2014). Par conséquent, la remobilisation des ions  $\text{Ag}^+$  à partir des sédiments historiquement contaminés par le drainage acide des mines ou le déversement des eaux usées urbaines et industrielles est probablement une bonne explication dans les cas où les concentrations d'argent sont relativement élevées (Tappin et al., 2010). Dans ce genre de situation, l'association éventuelle de l'argent avec les sédiments ou les particules en suspension n'élimine pas sa biodisponibilité, cela le rend potentiellement plus disponible aux organismes (Luoma, 2008). Pour rentrer dans les cellules, l'argent agit comme un métal essentiel (dont les constantes de stabilité avec les ligands sont élevées) permettant un passage relativement facile via les protéines transmembranaires (Bury and Wood, 1999; Campbell

and Couillard, 2004). En plus, la vitesse d'accumulation de l'argent comparée aux autres métaux traces chez les invertébrés marins est considérée comme très élevée (Wang, 2001).

### **LES NANOPARTICULES D'ARGENT (AgNPs)**

Au delà des problèmes causés par les polluants qui sont déjà déversés dans les milieux naturels depuis des années, l'émergence des nouvelles substances à effets potentiellement nuisibles est de plus en plus sujet à débat (Sutherland et al., 2010; Sharma et al., 2014). Aujourd'hui, le développement exponentiel des nanotechnologies et des nanomatériaux est considéré comme l'étape ultime de la miniaturisation intégrant une technologie d'avant-garde. Mis à part les bénéfices et applications multiples en pleine expansion des nanotechnologies dans plusieurs domaines, il se pose de nombreuses questions en toxicologie humaine et en écotoxicologie quant à la biodégradabilité et aux effets aigus et secondaires à long terme des nanomatériaux dans les milieux de travail et les environnements aquatiques.

En quoi consistent les nanoparticules? Une nanoparticule (NP) peut être définie comme étant une particule dont au moins une dimension spatiale est inférieure à 100 nm. Ces nanoparticules peuvent avoir des origines aussi bien naturelles qu'anthropiques. Les sources naturelles sont de nature biologique (dont l'ADN, l'ATP, l'ARN, plusieurs bactéries et virus, etc.) et minérale (les fumées et cendres volcaniques ou de feux de forêts, de certaines poussières atmosphériques, etc.). L'origine humaine comprend les nanoparticules manufacturées et les émissions polluantes de diesel et les fumées de soudure, etc. (Handy et al., 2008; Prosie et al., 2008; Lanone et Boczkowski, 2010). Les nanoparticules manufacturées comptent une grande variété de matériaux avec des compositions chimiques, de tailles, de formes et des propriétés chimiques et physiques différentes. Le comportement de ces NPs dans les systèmes aquatiques estuariens montre qu'elles peuvent être présentes dans les eaux de surface, la colonne d'eau et l'environnement benthique, en fonction de la salinité et d'autres paramètres chimiques. Leur comportement peut se révéler extrêmement

complexe si nous considérons plusieurs processus physicochimiques qui influencent aussi leur toxicité. Prenons l'exemple des AgNPs dans la Figure 4.

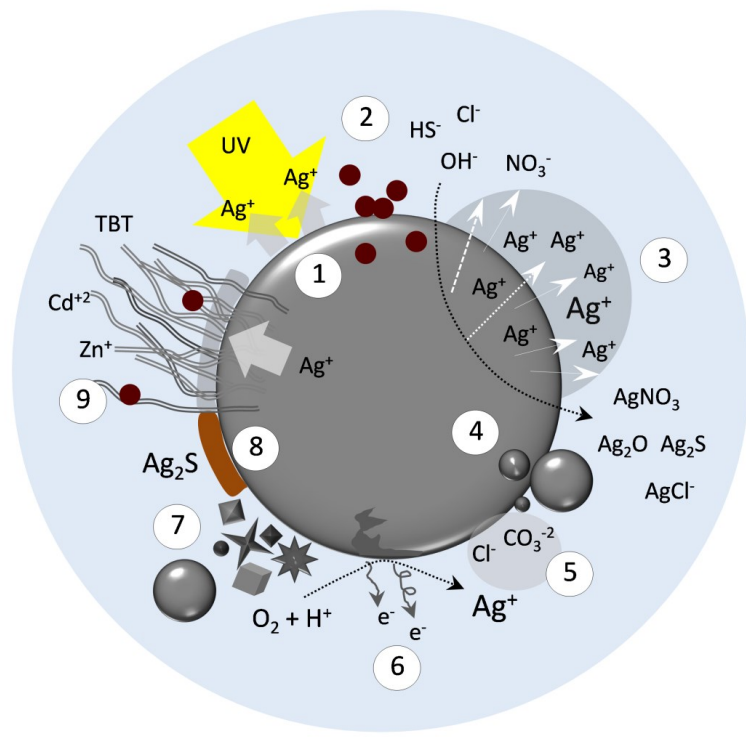


Figure 4: Modèle explicatif des caractéristiques des nanoparticules d'argent (AgNPs) ainsi que les processus physico-chimiques qui influencent leur toxicité dans les milieux aquatiques. (1) Photo-oxydation. (2) Interaction avec la matière organique. (3) Dissolution de la particule par attaque anionique avec la libération des ions  $\text{Ag}^+$ , par des processus d'oxydation. (4) Agrégation avec d'autres nanoparticules. (5) Adsorption ionique sur la surface. (6) Oxydation et libération des  $\text{Ag}^+$  à la surface irrégulière des particules où il y a des défauts cristallographiques; la charge est un élément important pour la compréhension de la toxicité. (7) Différentes formes de nanoparticules qui peuvent influencer l'assimilation cellulaire et donc la toxicité. (8) La sulfuration des AgNPs peuvent ralentir ou empêcher la libération des ions. (9) L'enveloppe organique donne la stabilité, mais agit aussi comme un endroit de capture-relâche d'autres contaminants ou même des ions  $\text{Ag}^+$ . Les divers mécanismes sont tirés de Lapresta-Fernández et al. (2012).

Les NPs ont des formes et une très petite taille qui leur donnent une grande surface de contact par unité de masse. Leur réactivité est en fonction du rapport taille/surface : le nombre de particules par gramme croît considérablement ainsi que la capacité de réaction de la nanoparticule quand on décroît leur taille. Les phénomènes d'agrégation des NPs rendent possible une dispersion colloïdale stable en solution (pour les particules possédant un diamètre de 1nm à 1µm), une interaction électrostatique avec d'autres structures colloïdales et enfin leur capture par le sédiment. Quand les NPs entrent dans les systèmes biologiques, elles sont immédiatement exposées à une panoplie de protéines à diverses concentrations (Huang et al., 2014) (Figure 5). Les interactions physico-chimiques entre protéines et nanoparticules sont influencées par leurs propriétés de surface. D'après Lynch et Dawson (2008), les irrégularités de surface des NPs peuvent aussi produire des effets sur la structure secondaire des peptides. Les NPs de grande taille ont une surface de contact plus importante lorsque les peptides y sont adsorbés, ce qui résulte en des perturbations de leurs conformations. Bien que les protéines puissent garder une partie de leur structure dans ces conditions, leur stabilité thermodynamique diminue, ce qui les rend plus sensibles à des agents dénaturants comme l'urée (Fei et Perrett, 2009).

Les nanoparticules d'argent préparées en industrie (1-100 nm) peuvent s'intégrer à un large éventail d'applications. Les nanoparticules d'argent (AgNPs) ont des propriétés antimicrobiennes, thermiques, électriques et optiques remarquables. Ainsi, elles sont de plus en plus incorporées à une grande variété de produits comme des cellules photo-électriques solaires, des écrans tactiles, des batteries électriques, des systèmes de purification de l'eau et de l'air, des sondes pour délivrer des médicaments et des gènes, des cosmétiques, des dentifrices, des vêtements, des électroménagers, des emballages alimentaires, des produits pour les enfants, etc. (Reidy et al., 2013). Plusieurs auteurs ont déjà démontré que la majorité des AgNPs issues des produits commerciaux sont éventuellement relâchées dans le réseau d'égouts municipaux et devront atteindre les systèmes de traitement des eaux usées (Geranio et al., 2009; Kaegi et al., 2011; Quadros et al., 2013; Angel et al., 2013; Kaegi et al., 2013).

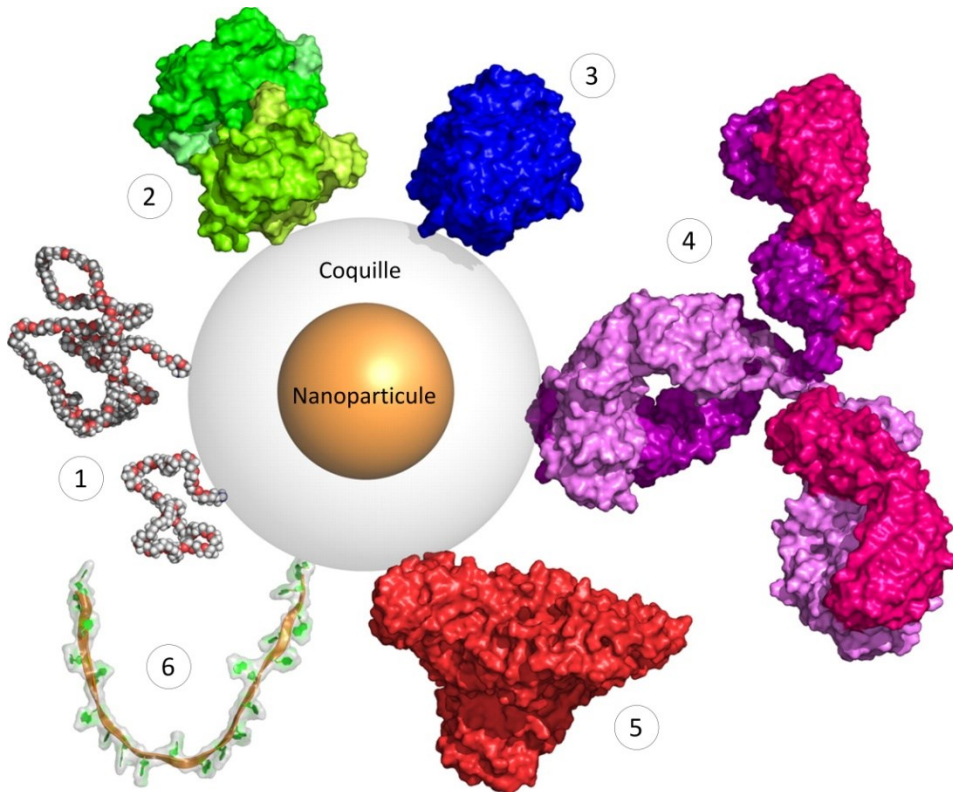


Figure 5: Modèle comparatif de la taille d'une nanoparticule et de quelques biomolécules (d'après Sperling et al., 2010). La nanoparticule dans le schéma aurait 5 nm, et la coquille 10 nm. (1) Polymère de poly(éthylène-glycol). (2) Streptavidine (52800 kDa). (3) Transferrine (76 kDa), protéine du foie humain. (4) Anticorps IgG (150.000 kDa). (5) Albumine (66.5 kDa). (6) Simple brin d'ADN (20 mer, oligonucléotide de 20 subunités). Les schémas des protéines ont été tirés de la base de données Protein Data bank.

En général, les formes chimiques libérées dans les eaux de lessive sont en fonction des caractéristiques originellement incorporées dans le textile, la composition du détergent au lavage et de la procédure (e.g. la vitesse de rotation de la machine à laver) (Yetisen et al., 2015). Pendant la lessive, les textiles contenant l' $\text{Ag}^0$  libèrent une quantité relativement élevée d'argent ionique et particulaire dans le liquide de lavage. L'utilisation de l'eau de javel ( $\text{NaClO}^-$ ) lors du lavage peut aussi contribuer à une oxydation rapide des AgNPs, avec la libération des  $\text{OCl}^-$  et formation des  $\text{AgCl}$  (Garg et al., 2016). Une couverture de lit, par exemple, qui contient 110 mg  $\text{Ag kg}^{-1}$  libère 4.8 mg  $\text{Ag kg}^{-1}$  dans la sueur pendant 1h. Les

chaussettes constituent un autre bon exemple : celles qui normalement contiennent 1360 µg nanoAg g<sup>-1</sup> libèrent 650 µg d'argent dans l'eau distillée (500 mL) pendant 24h (Yetisen et al., 2015). Donc, il est de plus en plus accepté qu'une combinaison de plusieurs produits qui ont de l'argent dans leur composition a le potentiel d'augmenter significativement les concentrations de ce métal dans l'environnement. Ceci pourrait bien être le cas dans les régions où le déversement d'égouts se fait sans traitement ou lorsque les systèmes de dépurations ne fonctionnent pas de façon à efficacement pour enlever les nanoAg des effluents. Or, l'argent est fortement attaché à la boue d'épuration et elle peut directement augmenter sa concentration dans les sédiments des écosystèmes à la proximité des exutoires d'eaux usées (Howe and Dobson, 2002). Selon Kaegi et al. (2013), après être passée par les installations de traitement, une certaine fraction de l'argent peut encore être relâchée dans les eaux de surface.

#### **LE COMPORTEMENT DES NANOPARTICULES METALLIQUES ET LES MECANISMES DE TOXICITE CELLULAIRE**

La toxicité des AgNPs est principalement marquée par un mécanisme dit «cheval de Troie», quand les particules se dissolvent en libérant les ions Ag<sup>+</sup> réactifs à l'intérieur des cellules. Ces ions peuvent interagir avec la couche bi-lipidique des membranes de façon à les déstabiliser et augmenter la perméabilité membranaire. Les effets physiques des nanoparticules sur des membranes cellulaires sont aussi considérés. L'argent ionique est capable d'établir des liaisons covalentes avec l'ADN en inhibant sa synthèse et aussi agir de façon catalytique avec l'oxygène moléculaire de façon à produire des radicaux libres (Hossain et Huq, 2002). En fait, la production d'espèces réactives (ROS) est considérée comme l'un des mécanismes responsables de l'expression des facteurs d'inflammation et d'initiation de l'apoptose chez les cellules humaines, probablement par déstabilisation des membranes mitochondrielles en premier lieu. Par un effet de boucle, les espèces réactives semblent aussi participer à l'oxydation des AgNPs mêmes dans le cytosol (Hsiao et al., 2015). La toxicité des nanoparticules d'argent (AgNPs) est encore très peu étudiée chez les

invertébrés marins (Canesi et Corsi, 2016). Par conséquent, tous les mécanismes cellulaires causés par les AgNPs doivent encore être décrits.

Il existe un certain nombre de nanoparticules métalliques dont les mécanismes de toxicité sont relativement bien connus et qui peuvent servir à éclairer le mécanisme d'action des AgNPs. Les nanoparticules de d'oxyde de zinc (ZnONPs) sont connues pour se dissoudre rapidement dans l'eau de mer (Garner et Keller, 2014). Le pH joue un rôle critique dans la dissolution des ZnONPs. Ainsi, les environnements dont les conditions sont plus acidiques (e.g.  $\text{Cl}^-$ ,  $\text{SO}_4^{2-}$ ) favorisent la libération des ions  $\text{Zn}^{2+}$ . Un deuxième élément d'importance écotoxicologique est l'influence naturelle de la matière organique (MO) sur le devenir des ZnONPs. En fournissant des agents chélateurs, la MO peut accélérer la dissolution des ZnONPs par capture des ions  $\text{Zn}^{2+}$  ou l'inhiber par adsorption avec les nanoparticules, ce qui empêche des interactions plus directes avec l'eau. La toxicité des ZnONPs est aussi attribuée à leur capacité photocatalytique à 368 nm (3.37 eV), notamment par les rayons solaires (Ma et al., 2013). Ceci favorise la génération de ROS et induit de la phototoxicité. La dissolution intracellulaire des ZnONPs semble augmenter les niveaux d'ions  $\text{Zn}^{2+}$  qui se trouvent déjà dans le milieu intracellulaire, un fait qui est associé avec une hausse de production de ROS, le disfonctionnement des mitochondries, des lysosomes, de l'activité enzymatique et des niveaux d'ATP (Pandurangan et Kim, 2015).

Les nanoparticules d'or (AuNPs) dans un milieu biologique sont capables de catalyser l'oxyde nitrique (NO) à partir des groupements thiols-S-nitrosés, ce qui mène à des réactions oxydatives en chaîne dans les cellules (Lapresta-Fernández et al., 2012). Schaeublin et al. (2011) ont reporté que la charge (neutre, positive et négative) des particules 1.5 nm-AuNPs ( $10\text{-}100 \mu\text{g mL}^{-1}$ ) peut induire différents effets toxiques qui mènent à un mécanisme de mort cellulaire spécifique (nécrose ou apoptose). Lorsque les cellules sont exposées aux 1.5 nm-AuNPs, la toxicité des nanoparticules électriquement chargés apparaît à  $10 \mu\text{g mL}^{-1}$  alors que les neutres sont toxiques à  $25 \mu\text{g mL}^{-1}$ . Le principal mécanisme lié au stress cellulaire provoqué par les petites AuNPs semble être associé au

disfonctionnement des mitochondries. Normalement, ces organites produisent de l'ATP, stockent du Ca<sup>2+</sup> et des activateurs de l'apoptose. Les mitochondries sont essentiellement constituées d'une membrane externe, un espace inter-membranaire, une membrane interne avec une petite région de bord interne et une matrice. La membrane externe est très sensible et légèrement négative du côté cytosolique dû à la charge positive formée par la pompe à protons de l'espace inter-membrane. Tandis que les AgNPs chargées (+) ou (-) agissent de façon à activer la perméabilisation de la membrane des mitochondries (MMP : mitochondrial membrane permeability) et à induire le début de l'apoptose, les nanoparticules neutres diminuent l'expression des gènes apoptotiques et induisent à la nécrose (Schaeublin et al., 2011).

La perméabilisation (MMP) peut être considérée comme un événement cellulaire décisif qui établit les limites entre la viabilité et la mort cellulaire (Kroemer et al., 2007). Une fois qu'une batterie de facteurs de transcription incluant lipides, métabolites, gradients ioniques, enzymes apoptotiques (e.g. caspases) sont déstabilisés par un stress d'ordre biologique (des maladies, des infections) ou chimique (xénobiotiques), le MMP est activé. Les AuNPs-(+) sont attirées par la membrane mitochondriale externe négativement chargée et s'y accumulent en causant sa dépolarisation. Ces effets perturbent l'homéostasie des molécules liées au MMP, ce qui induit l'apoptose. D'un autre côté, les AuNPs(-) accumulées à l'extérieur des mitochondries augmenteraient la charge négative de la membrane. Ce déséquilibre demanderait un ajustement du potentiel de membrane mitochondriale par libération des Ca<sup>2+</sup> à partir de la matrice, ce qui induirait les voies de signalisation de l'apoptose (Schaeublin et al., 2011).

Les mécanismes de mort cellulaire déclenchés pendant la nano-contamination sont fonction des caractéristiques physiques et chimiques des nanoparticules (surface, charge, taille, comportement chimique dans la cellule) mais sont aussi étroitement associé au métabolisme cellulaire (spécifique au type cellulaire) qui doit répondre à l'internalisation.

**LA MISE EN CONTEXTE DU TRAVAIL :**

Jusqu'à 2007, peu de produits contenant des nanoparticules avaient été décrits dans les travaux scientifiques (Nowack et Bucheli, 2007). Actuellement, les nanoparticules d'argent (AgNPs) sont les plus utilisées dans au moins 32 pays et plus de 435 produits, de composition chimique connue, sont rapportés par le site [www.nanotechproject.org](http://www.nanotechproject.org), du *The Project on Emerging Nanotechnologies* (Vance et al., 2015). Depuis la fin des années 2000, avec les progrès de la recherche et l'application des nanomatériaux dans plusieurs domaines de la technologie et de la vie quotidienne, des questions sur le devenir et la toxicité des nanoparticules métalliques dans l'environnement ont commencé à se poser (Nowack et Bucheli, 2007; Handy et al., 2008; Klaine et al., 2008; Baun et al., 2008; Fabrega et al., 2011; Holden et al., 2012; Schultz et al., 2014).

Selon Canesi et Corsi (2015), les publications ayant les invertébrés marins comme modèles se sont accrues de 20%, mais plusieurs groupes zoologiques restent ignorés notamment les échinodermes et leurs stades de développement. Les aspects morphologiques des organismes aquatiques directement impliqués dans l'assimilation, le transport interne, la toxicité ainsi que la transformation du nanoAg dans les organismes sont très peu connus. Pour les nanoparticules d'argent enveloppées avec les polyallylamines (PAAm-AgNPs) et l'argent dissous, la série de données présentée ici révèle les mécanismes de toxicité qui incluent : l'assimilation, la bioaccumulation, l'internalisation (cellulaire et acellulaire), la nano-translocation entre tissus, l'interaction avec des nanotubes de carbone, la réponse immunitaire et la récupération post-exposition. Les aspects morphologiques des stades embryonnaires, des larves et des juvéniles en développement liés aux mécanismes de toxicité de l'Ag<sup>0</sup> ont été particulièrement étudiés de façon à mieux comprendre les mécanismes de toxicité.

Dans le contexte d'une étude sur l'argent nanoparticulaire et dissous, les estuaires deviennent un environnement d'un grand intérêt, puisqu'ils constituent des zones écologiquement riches et en même temps proches des sources de pollution. La salinité

variable, l'apport de matière organique, la production primaire, et même les marées constituent des variables importantes à considérer sur le terrain dans le but de comprendre la toxicité, le comportement des contaminants, leur persistance et remobilisation à partir des sédiments. Selon Garner et Keller (2014), les AgNPs peuvent se maintenir agrégées dans l'eau de mer et sédimenter en quelques jours, mais leur temps de dissolution dépasse généralement plusieurs semaines. Ceci mène vraisemblablement à quatre scénarios dont les conséquences sont importantes : (a) l'exposition directe des larves aux nanoparticules en période de basse production primaire ou manque total de nourriture; (b) l'ingestion de phytoplankton contaminé soit avec les ions  $\text{Ag}^+$  ou/et les AgNPs lors des floraisons, (c) l'exportation des pellets contaminés vers le benthos, (d) l'exposition des larves métamorphiques, les postlarves et les juvéniles vers l'environnement benthique. Alternativement, en considérant uniquement une pré-exposition dans la colonne d'eau, les larves contaminées ainsi que les postlarves pourraient subir les effets toxiques tardifs pendant la période perimétamorphique sur le substrat.

## **OBJECTIFS DE LA THESE**

### **Objectif général**

Compte tenu des propriétés de l'argent (ionique et particulé) qui optimisent la pénétration, le transport, la bioaccumulation et la réactivité avec d'autres structures exogènes, ces contaminants semblent engendrer des perturbations assez importantes tant au niveau cellulaire qu'au niveau des individus. Spécialement chez les échinodermes, tout le développement est accompagné d'une grande modification des espaces internes par la métamérisation et la dérivation des cavités coelomiques et l'organogénèse, deux phénomènes d'ordre cœnogénétique. Évaluer comment ces transformations morphologiques dans chaque stade sont importantes pour comprendre la toxicité des xénobiotiques devient essentiel.

Donc l'objectif général de cette thèse est de développer un modèle biologique avec une espèce d'invertébré marin en développement (l'oursin *S. droebachiensis*) pour comprendre les mécanismes de toxicité de l'argent libre et des nanoparticules d'argent, l'importance des aspects morphologiques et cellulaires pour expliquer l'assimilation, la distribution et les effets du contaminant, puis élucider les mécanismes de défense qui émergent en réponse à l'agression toxique.

**Objectifs spécifiques (voir figure 6):**

- 1- Déterminer et caractériser les stades les plus sensibles à l'argent en fonction des transformations morphogéniques subies par l'organisme en établissant un rapport entre l'assimilation, l'apparition des malformations morphologiques (effets sous-létaux), le niveau de contamination dans le milieu d'exposition et la mortalité.
- 2- Démontrer (*in vivo*) et analyser (en microscopie électronique à transmission) les voies d'entrées principales, le trajet et la distribution interne (cavités et tissus) des contaminants lorsque les organismes en développement sont exposés pour de courtes ou longues périodes.
- 3- Investiguer les mécanismes cellulaires de défense qui se mettent en place pendant une exposition sous-létale avec l'argent (dissous et nanoparticulaire) en fonction de la forme chimique du contaminant et du temps d'exposition.

Ainsi, le chapitre 1 de la thèse vise à répondre à la question sur la sensibilité aux contaminants ( $\text{Ag}^+$ , AgNps et nanotubes de carbone) en rapport avec les processus morphogéniques d'un stade de développement. L'hypothèse de départ est que la sensibilité aux contaminants devient optimale en fonction des transformations morphologiques subies par les trois feuillets tissulaires de base (l'ectoderme, le mésoderme et l'endoderme) dès les stades initiaux et les cavités cœlomiques (l'axocœle, l'hydrocœle et la somatocœle). Pendant l'organogénèse, sous la production des nouveaux feuillets et le surgissement de la bouche, de l'hydropore et de la plaque madréporite, l'assimilation des xénobiotiques et la

contamination intracorporelle augmentent davantage. Ainsi, les mécanismes de toxicité des contaminants ont été étudiés au cours de l'embryogénèse de l'oursin vert jusqu'au premier stade larvaire.

Le chapitre 2 porte sur les processus d'assimilation (voies d'entrées) et distribution des contaminants dans les larves et les juvéniles en rapport avec la toxicité des ions Ag<sup>+</sup> et AgNPs. Les voies d'entrées formées (bouche, plaque madréporite) et les modifications des espaces internes (cavités coelomiques) optimisent, respectivement, l'assimilation et la translocation des stresseurs ainsi que l'accumulation dans les sites importants à la morphogénèse. Dans cette étude, nous avons utilisé les échinoplutei (en compétence larvaire et en métamorphose), les postlarves et les juvéniles d'oursin pour comprendre l'assimilation de l'argent sans ou avec nourriture, le processus d'intoxication et la nano-internalisation tissulaire et non-cellulaire (des cavités coelomiques).

Le chapitre 3 porte sur les mécanismes cellulaires de défense contre les Ag<sup>+</sup> et les AgNPs. Nous avons étudié les conditions de bioaccumulation, la production de ROS, la mobilisation des spherulocytes et amoebocytes sur les tissus chimiquement endommagés, l'expression des protéines de stress hsp60 et hsp70 contre les contaminants et les mécanismes d'internalisation cellulaire des nanoparticules. Les différences de toxicité des formes chimiques de l'argent (ionique et particulé) ont été évaluées au niveau cellulaire prenant les coortes de juvéniles d'oursin comme modèles biologiques.

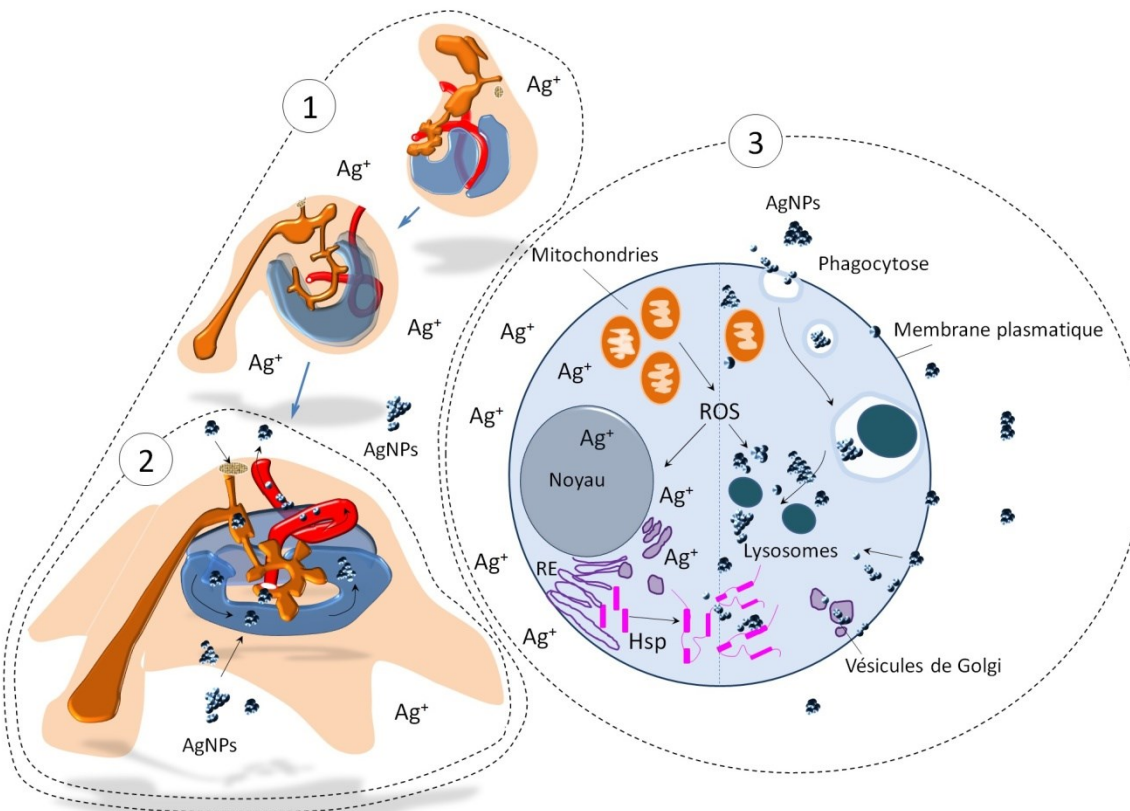


Figure 6: Représentation schématique des objectifs de la thèse (en rouge : tractus digestif, en orange : axocœles et hydrocœles, en bleu : somatocœles). (1) L'étude des mécanismes de toxicité des ions  $\text{Ag}^+$  et des AgNPs en considérant les transformations morphologiques pour expliquer les effets toxiques. (2) L'étude des voies de contamination, transport et distribution interne. (3) L'étude des mécanismes cellulaires de protection contre les ions  $\text{Ag}^+$  et les AgNPs.

# CHAPITRE 1

## LES MÉCANISMES DE TOXICITÉ DE L'ARGENT IONIQUE ET DES NANOPARTICULES D'ARGENT ET LEURS INTERACTIONS AVEC LES NANOTUBES DE CARBONE PENDANT LE DEVELOPPEMENT EMBRYONNAIRE DES OURSINS VERTS

### 1.1 RESUME EN FRANÇAIS DU PREMIER ARTICLE

L'exposition des organismes aquatiques à des mélanges de contaminants est susceptible d'avoir lieu dans les estuaires et les zones côtières. Ainsi, des effets toxiques combinés doivent être examinés particulièrement sur les stades de développement. Parmi les contaminants émergents, l'argent ionique ( $\text{Ag}^+$ ) et les nanoparticules d'argent (AgNPs) ont démontré des effets contrastants sur les invertébrés marins. Pourtant, leurs effets avec les nanotubes de carbone (f-SWCNTs) n'ont pas été investigués jusqu'à présent. Donc, dans l'objectif d'analyser les impacts et de comprendre les mécanismes de toxicité des  $\text{Ag}^+$  et des AgNPs ainsi que leurs effets combinés avec les f-SWCNTs, les stades successifs de développement de l'oursin vert *Strongylocentrotus droebachiensis* ont été exposés aux  $\text{Ag}^+$ , AgNPs et f-SWCNTs, séparément ou en mélange à des concentrations nominales modérées et réalistes. Nous avons aussi évalué les conséquences des effets toxiques à long terme avec les organismes en conditions de récupération. Les caractéristiques morphologiques telles que l'allongement de l'archentéron, le devenir des cellules mésenchymateuses primaires et secondaires, la migration des cellules pigmentaires, l'activité des cellules minéralisatrices et le développement de l'intestin ont montré différents effets des  $\text{Ag}^+$  et du nanoAg pendant les étapes de développement de l'embryon et du premier stade larvaire (prisma). Pendant que les  $\text{Ag}^+$  ont conduit à la végétalisation et l'extrusion des cellules mésenchymateuses primaires chez les embryons, le mélange f-SWCNTs- $\text{Ag}^+$  a fortement perturbé la régionalisation du tractus gastrointestinal des échinoplutei. Les cellules blastocoeliaires se sont vacuolisées et ont perdu leur forme originale avec les AgNPs, mais se sont

normalement développées lorsque exposées aux mélanges avec les f-SWCNTs. Les fortes concentrations des  $\text{Ag}^+$  et des f-SWCNTs- $\text{Ag}^+$  ont causé la plus forte mortalité durant la récupération, par la capacité des f-SWCNTs de rendre l'argent plus disponible pendant l'exposition et des effets toxiques à long terme.

Ce premier article, intitulé « *Toxicity mechanisms of ionic silver and polymer-coated silver nanoparticles with interactions of functionalized carbon nanotubes on early development stages of sea urchin* », fut corédigé par moi-même ainsi que par le professeur Émilien Pelletier. Il fut accepté pour publication dans sa version finale en 2015 par les éditeurs de la revue *Aquatic Toxicology*. En tant que premier auteur, ma contribution à ce travail fut l'essentiel de la recherche sur l'état de l'art, le développement de la méthode, l'exécution des tests de performance et la rédaction de l'article. Le professeur Émilien Pelletier, second auteur, a fourni l'idée originale. Il a aidé à la recherche sur l'état de l'art, au développement de la méthode ainsi qu'à la révision de l'article.

## **1.2 TOXICITY MECHANISMS OF IONIC SILVER AND POLYMER-COATED SILVER NANOPARTICLES WITH INTERACTIONS OF FUNCTIONALIZED CARBON NANOTUBES ON EARLY DEVELOPMENT STAGES OF SEA URCHIN**

### **1.3 ABSTRACT**

Exposures of aquatic organisms to multiple contaminants are likely to take place in estuarine and coastal areas and combined effects on early life stages have to be examined. Among emerging contaminants, ionic silver ( $\text{Ag}^+$ ) and silver nanoparticles (AgNPs) have demonstrated contrasting effects on marine invertebrates, but their interactions with functionalized carbon nanotubes (f-SWCNTs) have not yet been investigated in details. In order to observe the impacts and understand the toxicity mechanism of  $\text{Ag}^+$  and polymer-coated AgNPs, and their combined effects with f-SWCNTs, successive development stages of embryos of sea urchin, *Strongylocentrotus droebachiensis*, were exposed to  $\text{Ag}^+$ , AgNPs and f-SWCNTs, separately and in mixtures using moderate environmental concentrations. We also assessed long-term effects of treatments under recovery conditions. Morphological endpoints such as archenteron elongation, primary and secondary mesenchyme cells fate, pigment cells migration, spiculogenic cells and gut development indicated different effects of silver and nanosilver forms during successive development stages. Whereas  $\text{Ag}^+$  induced vegetalization and extrusion of mesenchyme cells in early embryos; f-SWCNTs+ $\text{Ag}^+$  strongly interfered with gut regionalization in late larvae. Sensitive blastocoelar cells got vacuolized and shapeless with AgNPs, but not with mixtures with f-SWCNTs. Increased concentrations of  $\text{Ag}^+$  and f-SWCNTs+ $\text{Ag}^+$  led to the most disruptive effects during development, but f-SWCNTs+ $\text{Ag}^+$  caused the highest mortality rate during the recovery period, which indicated far-reaching effects driven by f-SWCNTs and their ability to keep silver more available during exposure period.

## 1.4 INTRODUCTION

Metal contamination levels in aquatic ecosystems are considered higher in estuaries than in open sea (Dauvin, 2008), mainly because coastal areas are often densely populated with highly industrialized zones nearby. Hence, coastal areas and particularly estuary ecosystems are considered as complex and sensitive receiving environments impacted by effluents with mixtures of pollutants including engineering nanomaterials (Novack et al., 2012). Wastes from electrical and electronic equipment, municipal solid sewer inflow, industrial, medical and domestic sewage are the main anthropic sources for trace metals released in solution and in suspension (Eckelman and Graedel, 2007). Nowadays, raising concerns about silver release in natural waters are related to the growing use of silver nanoparticles (AgNPs) in consumer products (Been et al., 2010). Owing to biocide and thermo-electrical properties, AgNPs are massively used in consumer products ranging from cosmetics, clothing, health and fitness products, disinfecting sprays and household appliances. As a result, continuous discharges of nanosilver into sewer systems and receiving aquatic environments are likely to occur (Reidy et al., 2013; Kaegi et al., 2015). In coastal and estuarine areas, chemical behavior of silver is mainly governed by salinity of marine waters and even small inputs from human activities can trigger high enrichment and dispersion in seawater (Luoma et al., 1995). Given the high concentration of chloride ions in seawater, chloro-complexation with silver enhances ionic complexation, reduces precipitation and increases silver bioavailability to organisms (Levard et al., 2012).

Ionic silver ( $\text{Ag}^+$ ) is known to be highly toxic to marine fauna and especially to very early stages of development of invertebrates. Short pulses of one hour with low concentrations of  $\text{Ag}^+$  at 20°C rapidly affected embryogenesis and early life development of surf clam *Spisula solidissima* (Zoto and Robinson, 1985). Authors showed that under raising concentrations of  $\text{Ag}^+$ , mineralization of bivalve larvae shells was progressively disturbed as well. Lower  $\text{Ag}^+$  concentrations also interfered with normal early development of sea urchin *Diadema antillarum* and biomimetic mineralization in larvae (Bielmyer et al., 2005). On another hand, AgNPs showed contrasting toxicity effects on early life stages of marine

invertebrates, with  $\text{Ag}^+$  being less responsible for toxicity. As an example, citrate-coated AgNPs were much more disruptive than  $\text{Ag}^+$  on skeleton formation and embryogenesis of echinoplutei of *Paracentrotus lividus* during 24h exposures at 19°C (Šiller et al., 2013). Likewise, early life stages of the polychaete *Platynereis dumerilii* were highly sensitive to waterborne exposure to  $\text{Ag}^+$  and citrate-coated AgNPs (48h exposure at 18°C), but both humic acid-coated AgNPs and citrate-coated AgNPs were more toxic than  $\text{Ag}^+$  and mostly affected late larvae and juveniles (García-Alonso et al., 2014).

Environmental fate of silver nanoparticles has been addressed these past few years particularly for marine ecosystems in realistic case scenarios (Buffet et al., 2014). Silver nanoparticles seem to be trapped at the mixed layer of saline halocline in stratified waters from estuaries and coastal areas (Klaine et al., 2008). Despite the fact that less than 5% of nanosilver goes to seawater layer, bioavailability may last for a longer time in surface layer as well (Pelletier et al., 2014). It is well established in marine ecology that many small estuarine invertebrates (pelagic phase of larvae and zooplankton species) can migrate inside or through the halocline to find rich feeding ground. Echinopluteus larvae in starvation also have the ability to actively cross halocline to feed and increase probability of survival even though they would rather stay in the high salinity layer (Metaxas and Young, 1998). All these findings lead us to put into perspective how different early life stages of marine invertebrates would be exposed to silver contamination in such conditions.

In addition to AgNPs, carbon nanotubes represent another example of newly produced nanostructures exhibiting electronic, mechanical, thermal, optical, and transport properties (Niyogi et al., 2002). Among carbonaceous nanomaterials, single-walled carbon nanotubes (SWCNTs) have a unique tubular graphitic one-dimensional structure with exterior walls of one atom thickness characterized by strong covalent bonding, high tensile strength and resilience (Niyogi et al., 2002). Due to intense van der Walls forces along their length axis, SWCNTs display high hydrophobic behavior and tend to aggregation in aqueous solution. Of particular interest is the ability of carbon nanotubes to interact and penetrate cell membranes, delivering therapeutic agents (Liu, 2013). To do so,

functionalization process was taken as a crucial process in order to enhance solubility of carbon nanotubes in physiological systems and get rid of their metallic impurities, reducing their toxicity. After oxidation, functionalized single-walled carbon nanotubes (f-SWCNTs) become potential nanovehicles with -COOH and -OH functionalities, which improves dispersion and their capacity to bond with other small and polymeric molecules (Sun et al., 2002). Therefore, major concerns about transport, mobilization and bioavailability of other contaminants especially adsorbed by f-SWCNTs have been raised. Interactions of f-SWCNTs with organic matter after releasing also make them more dispersed and optimizes metal adsorption (Adeleye and Keller, 2014). By now, only a few studies have demonstrated that f-SWCNTs increased metal and hydrophobic organic contaminants accumulation in freshwater crustacean and fish, respectively (Yu and Wang, 2013; Su et al., 2013), but how f-SWCNTs interfere with toxicity of other contaminants in early life stages of marine/estuarine animals is still largely unknown.

Following the above considerations, it can be hypothesized that Ag<sup>+</sup>, AgNPs and f-SWCNTs can be found together in estuarine and coastal waters and do interact individually and together with early life stages of marine organisms. This hypothesis would particularly apply to highly industrialized and populated areas where wastewater treatment plants are not properly operated or absent. In this work, our first aim was to observe and understand toxicity mechanism of ionic silver (Ag<sup>+</sup>) and polymer-coated silver nanoparticles (PAAm-AgNPs) as well as the interactions of f-SWCNTs with both silver chemical forms. More particularly, we aimed to describe in detail how six successive early life stages of an estuarine invertebrate could respond to different toxic treatments at low temperature. Finally, we investigated long-term effects of these exposures during a recovery period of three weeks.

To do so, we have been using embryos of sea urchin *Strongylocentrotus droebachiensis* (O. F. Müller, 1976) as a biological model. Because of their sensitivity to toxicants, the embryonic development of sea urchins has been extensively used as a classic tool to assess toxicity of chemicals (Weis, 2014). Moreover, being deuterostomes,

echinoderms are known to share some metabolic and physiological pathways with vertebrates. We report and compare detailed observation of morphogenic changes occurring during the normal development of embryos and early larvae; and the effects induced by the presence of all three chemicals mentioned above.

## 1.5 MATERIAL AND METHODS

### 1.5.1 Collection and spawning

Young adults ( $6.0 \pm 1.5$  cm average diameter) of green sea urchin *Strongylocentrotus droebachiensis* were collected in a rocky intertidal zone during their natural breeding season from April to August near Canuel Island ( $48^{\circ}26'48.47''N$ :  $68^{\circ}34'53.06''W$ ), on the south shore of the Lower St. Laurent Estuary, eastern Canada. Immediately after collection, sea urchins were acclimatized in large aquariums supplied with a flow-through system (unfiltered natural seawater at  $5^{\circ}C \pm 2^{\circ}C$  and salinity 28-30 PSU), and a 12h photoperiod. All physical and chemical parameters were very similar to the natural environment and the specimens in captivity fed *Laminaria* sp *ad libitum*. Fertilization was obtained by inducing males and females to spawn after injecting 3.5 mL of KCl 0.5M through their perioral membrane. The sea urchins were then inverted oral side up in petri dishes in order to collect the gametes by extrusion. The oocytes from three females were transferred to a beaker containing 800 mL of filtered seawater, fertilized with 400  $\mu$ L of diluted sperm from one male (200  $\mu$ L of concentrated sperm in 100 mL of seawater) and then gently mixed. After 15 min, fertilized eggs with a raised fertilization membrane (95% to 100%) were washed three times.

### 1.5.2 Embryos handling and blastulae hatching

The egg suspension was transferred to three Erlenmeyer flasks with 1600 mL of seawater filtered on 0.45 $\mu$ m cellulose nitrate membrane filters and acclimated into temperature controlled chambers at  $8^{\circ}C$  and  $15^{\circ}C$  to achieve the blastulae hatching from 24 to 30h. When blastulae were seen swimming at the water surface, they were transferred to

12-well tissue culture plates (Falcon-353043 polystyrene made). Each well was filled with 5.5 mL of filtered seawater and 70 blastulae were added. Immediately, because our main experiments were taken at 5°C all the plates were placed in a refrigerator at 5°C for 3h for acclimation before the exposure to contaminants.

### 1.5.3 Preparation and characterization of PAAm-AgNPs

Poly(allylamine)-coated silver nanoparticles (PAAm-AgNPs) were prepared in our laboratory by adapting a protocol from Al-Sid-Cheikh et al. (2011). Silver nitrate powder ( $\text{AgNO}_3$ , >99%) and polyallylamine (PAAm) as a viscous liquid (molecular weight ~65,000 Da) were purchased from Sigma Aldrich. After synthesis, the PAAm-AgNPs were resuspended in nanopure water for an additional cleaning procedure by ultrafiltration (Ultracel® 30 KDa) to remove most of unreacted ionic silver and PAAm. The primary PAAm-AgNPs size and dispersion were assessed by transmission electron microscopy (TEM Delong Instruments LVEM 5, precision  $\pm$  2 nm). In addition, their size and shape were analyzed by scanning electron microscopy (SEM) JEOL 6460LV. The coated silver nanoparticles used in our study had an average diameter of 15 nm ( $\pm$  5 nm) (Figure 7 A). PAAm-AgNP stock suspension had a total silver concentration of 2.8 mM with 2.6% free silver ions.

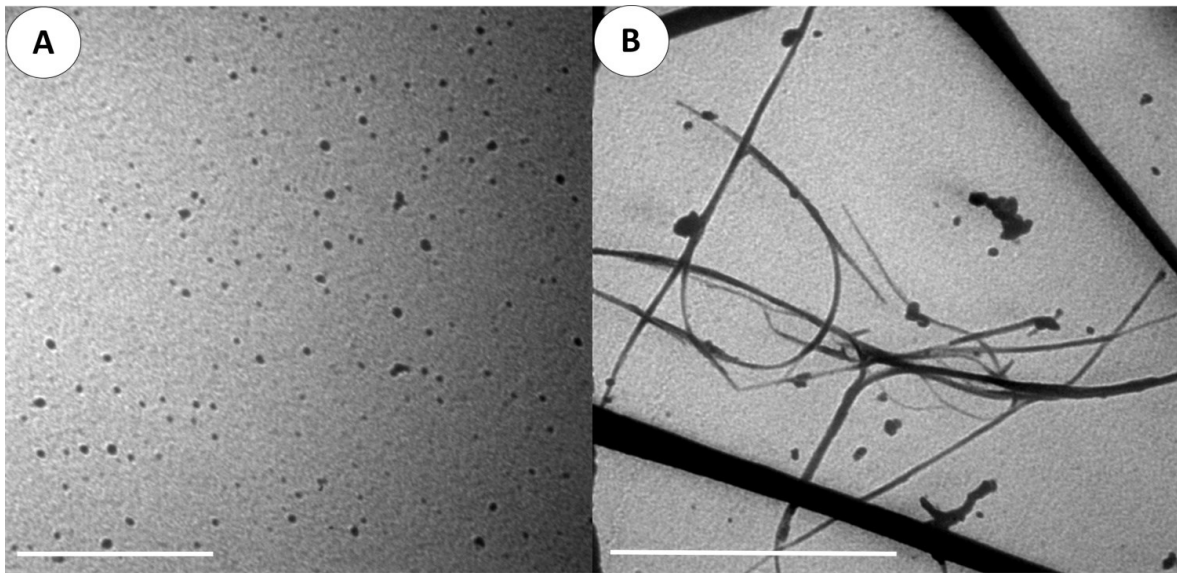


Figure 7: A- TEM image (x500 nm) of organic-coated silver nanoparticles dispersed in nanopure water. B- TEM image (x1 $\mu$ m) of functionalized single-walled carbon nanotubes suspended in nanopure water after sonication procedure.

#### 1.5.4 Surface treatment and characterization of functionalized SWCNTs

In brief, high-purity carboxylated ( $-COOH$ ) single-walled carbon nanotubes (COOH-SWCNTs) were purchased from NanoAmor Inc. (Houston, TX, USA). As the purchased material had a low level of substituted carboxyl groups (about 2.6%), a raw sample of SWCNTs was heated to 60°C with a mixture of concentrated nitric and sulfuric acids following a method described by Berjeb et al. (2013). Functionalized-SWCNTs (f-SWCNTs) were washed repetitively with nanopure water to remove any trace of acids and metals. The substitution level ( $-COOH$ ) on f-SWCNTs surface was 7.5% and a stable suspension of f-SWCNTs was easily obtained in nanopure water. An aliquot of the suspension was added to 100% ethanol for observation by electron microscopy (Figure 7B). Full characterization of f-SWCNTs is given in Berjeb et al. (2013).

### 1.5.5 Stock solutions and nominal concentrations

Stock solutions of AgNO<sub>3</sub> (75 mg·100mL) and PAAm-AgNPs (4.768 mg PAAm-AgNPs·100mL) were prepared in nanopure water for dilution to nominal exposure concentrations. An amount of 0.1486 g f-SWCNTs was dispersed in 40 mL of nanopure water for the stock suspension. Before dilution of solution stock of f-SWCNTs and at the beginning of the toxicity tests, the suspensions were sonicated for 1 h to ensure their homogeneity. All solutions and suspensions were stored in the dark at 5°C to minimize photodegradation. For the first series of toxicity tests, embryos were exposed to a control and four nominal concentrations chosen according to pre-screening results and named hereafter as NC1 (highest), NC2 and NC3 (intermediate) and NC4 (lowest). For f-SWCNTs, the concentrations were 50, 10, 5; and 2 mg·L for NC1, NC2, NC3 and NC4, respectively. Concentrations of Ag<sup>+</sup> and PAAm-AgNPs as well as the mixtures of f-SWCNTs+Ag<sup>+</sup> or +PAAm-AgNPs are given in Table 1. After the first acute tests were completed, only two sublethal nominal concentrations (NC2 and NC3) were kept for morphologic study using confocal microscopy.

Table 1: Nominal concentrations of contaminants

<b>Nominal concentrations</b>	<b>Contaminants</b>		
	<b>f-SWCNTs</b>	<b>Ag<sup>+</sup> or PAAm-AgNPs</b>	<b>f-SWCNTs+Ag<sup>+</sup> or f-SWCNTs+PAAm-AgNPs</b>
NC1 (strongest)	50 mg·L	500 µg·L	50 mg·L + 500 µg·L
NC2	10 mg·L	100 µg·L	10 mg·L + 100 µg·L
NC3	5 mg·L	50 µg·L	5 mg·L + 50 µg·L
NC4 (weakest)	2 mg·L	20 µg·L	2 mg·L + 20 µg·L

### 1.5.6 Experimental design

#### a) Exposure periods

Acute 96h toxicity tests were performed successively at 10°C, 8°C and finally at 5°C in order to observe sublethal and lethal effects of Ag<sup>+</sup>, PAAm-AgNPs and f-SWCNTs separately, and in a wide range of temperature. Then, we tested f-SWCNTs combined with either Ag<sup>+</sup> or PAAm-AgNPs. For all these tests, exposures were conducted in 48-well cell culture cluster flat bottom plates (Corning Costar 3548, polystyrene made) filled with 1.5 mL of 0.45 µm filtered seawater. These preliminary tests consisted in four nominal concentrations and a control plate, with six replicate wells for each concentration and the control. A 10-µL aliquot of either Ag<sup>+</sup> or PAAm-AgNPs test solutions was added to each well with 5 embryos already transferred into it. For f-SWCNTs tests, four different volumes were used as following: 100µL (NC1), 20µL (NC2), 10µL (NC3) and 4µL (NC4). Organisms were not fed during these experiments. Toxicity tests were performed according to the Standard guide for conducting static acute toxicity tests with echinoids embryos E1563-98 (ASTM, 2004). All experiments were done under 12h light/12h dark cycles, but the plates were always protected against direct light exposure to minimize photoreaction with contaminants.

Once preliminary experiments completed, a new set of acute exposures were performed at 5°C to better observe morphologic abnormalities appearing in embryos and in early echinopluteus (prisma) after 48h and at the end of the tests (96h). The relatively slow developmental events due to low temperature allowed us to study in details the effects of toxic conditions on six important development stages hereafter described as six treatments (T1-T6) conducted independently from each other. Two sublethal nominal concentrations (NC2 and NC3) were used as described above. Working from a large batch of embryos kept in constantly renewed clean seawater, 70 hatched blastulae (at the required development stage) were selected for each well and added to 12-well tissue culture plates with flat bottom (Falcon 353043, polystyrene made), each well being filled up with 5.5 mL of 0.45 µm filtered seawater. Five toxic conditions were tested in addition to the control for

each condition: (1) f-SWCNTs, (2) Ag<sup>+</sup> and (3) PAAm-AgNPs in separate treatments; and the combined exposures of (4) Ag<sup>+</sup> with f-SWCNTs, and (5) PAAm-AgNPs with f-SWCNTs. After a 96h exposure period, the ability of larvae to feed on phytoplankton cells (filtration and pellet production) was observed over 24h by adding 200 µL of *Dunaliella tertiolecta* culture ( $7.8 \times 10^6$  cells per mL) in each well. All tests were independently repeated three times. We rigorously determined six important development stages considering the major events in embryogenesis and prisma formation. The timetable of developmental events in *S. droebachiensis* embryos maintained at 8°C and for contamination events at 5°C is presented in Table 2. As development proceeded for all contaminated stages, a large set of morphological features was obtained for each time and nominal concentrations used (see morphological database in Supplementary material, Aquatic toxicology 167:106-23). Toxicity was determined by considering a feature as: (0) when absent or very weak trait; (1) as weak or not well developed; (2) as intermediate condition; and (3) as a strong trait or well developed.

Table 2: Timetable for treatments of successive development stages and summary of major events of development and endpoints

T°C	Pulse	Timing	Major event	Stages exposed	Endpoints
8°C	none	24h after fertilization	Cilia formation	Blastula	—
		30 h after cilia formed	Hatching	Swimming blastula	—
		46 h after hatching	All blastula hatched		—
5°C	T1	50 h after hatching	PMCs ingestion	Early mesenchyme blastula	PMCs ring, biominerilization, archenteron elongation.
	T2	23 h after T1	Invagination	Invaginating blastula	Primary invagination completion, PMCs ring, biominerilization.
	T3	24 h after T2	1st invagination ends	Early gastrula (midgastrula)	Secondary invagination completion, spiculogenic cells activities, pigment cells differentiation and migration.
	T4	30 h after T3	2nd invagination ends	Mid-to-late gastrula	SMCs connection to animal pole, spiculogenic cells activities, blastocoelar cells organization.
	T5	22 h after T4	Pigment cells differentiation	Late gastrula to very early prism	Stomodeum formation, gut regionalization, skeletogenic cells activities.
	T6	25 h after T5	Gut regionalization	Mid-to-late prisma	Skeletogenic cells activities, gut development.

Embryo and prisma development followed classification of Kominami and Takata (2004) and schematic drawings in Figure 8 represent a general description of exposed stages (adapted from Kominami and Takata, 2004; Duboc et al., 2010). Abbreviations used in figures are given as follows: Ac= abnormal or deformed cluster, Ap= animal pole, Apo= apical organ. Aq= archenteron, Bc= blastocoel, Blc= blastocoelar cells, Cp= coelomic pouches, Ec= ectoderm, Esp= oesophagus, Fp= filopodia, Git= gastrointestinal tract, Int= intestine, Mc= mesenchyme cells, Pgc= pigment cells, PMCs= primary mesenchyme cells, SMCs= secondary mesenchyme cells, Stm= stomodeum (opening mouth), Sc= spiculogenic or skeletogenic cells, Sp= spicule, Sphc= cardiac sphincter, Stc= stomach, Vp= vegetal pole, Vtlc= ventro-lateral clusters. The successive development stages were described in details in Supplementary material, Appendix 1.

Figure 8: Schematic representation of major events in embryogenesis and early prisma formation for chemical treatments. A- No toxic treatment: hatching blastula stage. After several rounds of cleavages, the blastula develops cilia and hatches from fertilization membrane; B- First treatment (T1): early mesenchyme blastula exposed. Epithelium at the vegetal pole of the blastula flattens and thickens to form later the vegetal plate; primary mesenchyme cells move from vegetal plate into blastocoel and give rise to the larval skeleton later; C- Second treatment (T2): invaginating blastula exposed. Primary invagination starts and a squat archenteron is later formed, primary mesenchyme cells tend to form a ring with two ventro-lateral clusters; D- Third treatment (T3): early gastrula stage exposed. The primary mesenchyme cells ring is formed and a spiculogenic syncytium builds the first spicules of skeleton; E- Fourth treatment (T4): mid-to-late gastrula stage exposed. A short stub-like gut rudiment was formed (end of primary invagination), but continues to be stretched towards animal pole (secondary invagination); F- Fifth treatment (T5): late gastrula to very early prism stage exposed. Gastrulation finishes, some secondary mesenchyme cells begin to differentiate into non-skeletogenic mesodermal cells: pigment cells, blastocoelar cells, coelomic pouch cells and circum-esophageal muscles; G- Sixth and last treatment (T6): mid-to-last prism stage exposed. Organogenesis begins. Abbreviations: Ac= abnormal or deformed cluster, Ap= animal pole, Apo= apical organ, Aq= archenteron, Bc= blastocoel, Cp= coelomic pouches, Ec= ectoderm, Esp= oesophagus, Fp= filopodia, Int= intestine, Pgc= pigment cells, PMCs= primary mesenchyme cells,

SMCs= secondary mesenchyme cells, Stm= stomodeum, Sp= spicule, Sphc= cardiac sphincter, Stc= stomach, Vp= vegetal pole, Vtlc= ventro-lateral clusters.

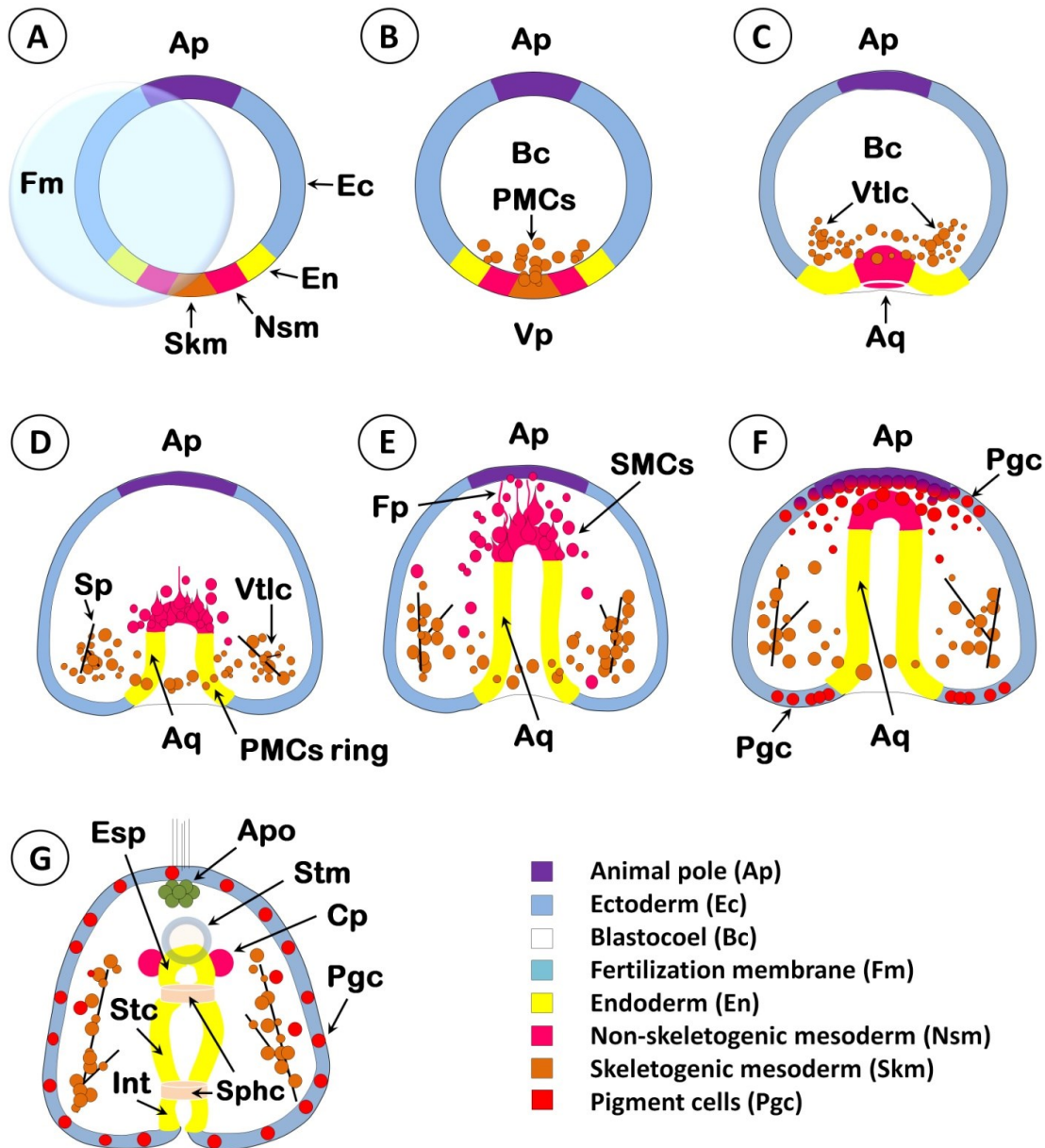


(Figure 8, see legend on previous page)

b) Recovery periods

Exposure assays as described above were repeated under identical conditions to conduct a recovery experiment. Immediately at the end of 96h acute toxicity tests, 30 embryos/larvae were transferred into small petri dishes with clean seawater and then transferred again in 12-well tissue culture plates (Falcon 353043) filled up with 5.5 mL of 0.45 µm filtered seawater. Also, their capacity to feed over three weeks was checked by adding 200 µL of *Dunaliella tertiolecta* culture ( $7.8 \times 10^6$  cells per mL) every time we renewed seawater in wells, which was strictly done at 96h interval for three times to reach a total of 288h (3 x 96h). Finally, embryos and larvae were fixed and the frequency of developmental malformations was determined according to following morphological criteria: skeleton malformed, development blockage at gastrula stage, functional gastrointestinal tract, atrophied/delayed larvae, and dead embryos. This experience was repeated two times.

### 1.5.7 Confocal microscopy

Morphological impairments at 48h and 96h were assessed for each treatment and all five contaminant conditions at concentrations NC2 and NC3. Images of embryos exposed to the contaminants were always taken *in vivo* with Inverted microscope Axio Cam Observer Z1 and Laser scanning microscope in Confocal microscopy (LSM700 Carl Zeiss) under 10X (0.34 µm/pixel), 20X (0.17 µm/pixel), 40X (0.085 µm/pixel) and 63X (0.05397 µm/pixel) magnifications. For each observation, we randomly took 10 embryos/larvae, which were immobilized with 6 µL 100% ethanol injected into 300 µL of seawater on the glass bottom dishes. A database containing 3184 pictures was used to analyze in details all the tracked endpoints during tests. The SYBR® Green (Molecular probes) dye allowed us to investigate cellular clusters inside the organisms. We considered a specific impairment representing an abnormal trait when present in equal or more than 90% of the individuals analyzed compared to the controls. After the time recovery (3 x 96h), all the

embryos/larvae were fixed with glutaraldehyde 2.5% and 0.1 M sodium cacodylate buffer for final assessment.

### **1.5.8 Measurement of dissolved and adsorbed silver**

Dissolved silver concentrations in exposure media and silver adsorbed on the surface of wells were determined by inductively coupled plasma mass spectroscopy (ICP-MS) at 0h, 48h and 96h. Supernatants in cells were centrifuged at 7400 rpm for 10 min at 4°C using centrifugal filters Ultracel-10K (Amicon Ultra-4) to separate particulate silver (agglomerated PAAm-AgNPs and adsorbed silver on particulate organic matter) from dissolved silver forms. Filtrated seawater samples were then later diluted in concentrated HNO<sub>3</sub> (1.2 mL), digested with 0.5 mL of hydrogen peroxide at 60°C for 45 min before the analysis. To better assess the amount of free silver (chloro-silver complexes and dissolved organic-silver complexes) in the medium with the organisms, the residual silver that could have been adsorbed by inner-surface of wells was quantified. After the removal of the exposure medium, the empty wells were rinsed with 1.5mL of concentrated HNO<sub>3</sub> and the same volume of nanopure water. Digestion and analysis were performed as described above. The detection limit was 0.015 µg·L<sup>-1</sup> and the quantification limit was 0.120 µg·L<sup>-1</sup>.

### **1.5.9 Statistical analysis**

Data were analyzed using permutational analysis of variance (PERMANOVA) ( $p < 0.05$ ) with Primer 6.1.1.12 and Permanova+ 1.0.2 to better understand the overall tendencies in our data. After the factors were chosen, we square root-transformed the data before resemblance analysis based on Bray-Curtis similarity matrices. Then, we visualized our groups and their relationships respectively by Cluster and MDS (non-metric multidimensional scaling) analysis. To test the homogeneity of multivariate dispersions, we performed PERMDISP and finally to determine the significant effects, the Permanova two-way crossed pairwise tests with unrestricted permutation of raw data (for one factor) and permutation of residuals under a reduced model (for two or more factors) were used.

## 1.6 RESULTS

### 1.6.1 Dissolved and adsorbed silver in exposure wells

The analysis of dissolved silver in exposure media and total silver adsorbed to inner surface of wells was performed for the first intermediate nominal concentration only (NC2, 100  $\mu\text{g}\cdot\text{L}$ ) for all 4-exposure conditions involving silver and nanosilver with or without f-SWCNTs (Figure 9).

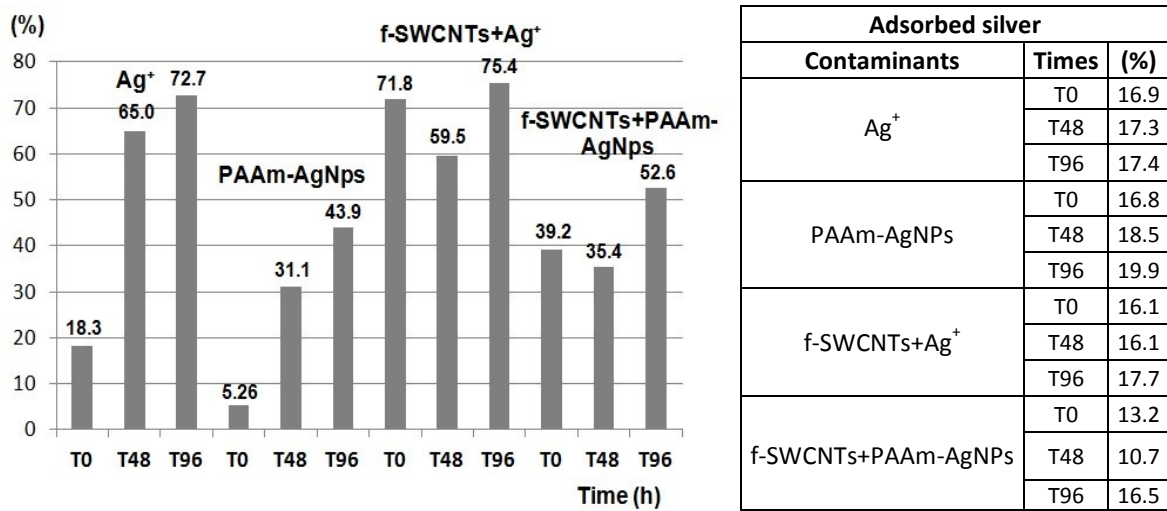


Figure 9: Relative proportion (%) of dissolved silver in exposure media (left) and total silver adsorbed to surface of wells (right) as a function of elapsed time determined by ICP-MS for the exposure concentration NC2 with a nominal concentration of 100  $\mu\text{g}\cdot\text{L}$  (corresponding to 100% in the graph) of silver in all cases.

Chemical analysis showed that the proportion of dissolved silver (chloro-complexes and/or soluble organic-complexes of silver) was the highest when Ag<sup>+</sup> was added in presence of f-SWCNTs at t0 and 96h with a small apparent decrease at 48h. Although the Ag<sup>+</sup> single exposure showed only 18.3% free silver at t0, dissolved silver concentrations increased to 65% at 48h and 72.4% after 96h which could be related to a desorption process occurring in the wells. Interestingly, the addition of PAAm-AgNPs alone generated a constant increase of soluble silver with time, ranging from 5.2% at t0 to 43.9% after 96h. It should be noted that the stock solution of PAAm-AgNPs already contained 2.6% free

silver. The simultaneous presence of f-SWCNTs with PAAm-AgNPs strongly raised the amount of dissolved silver to values ranging from 39.2% at t0 to 52.6% at 96h. It seems f-SWCNTs rapidly contributed to dissolution of Ag<sub>2</sub>O layer recovering AgNPs following the model described by Li et al (2012). The proportion of silver adsorbed to the wall of wells was rather constant between 16 to 20%, but appeared slightly lower with the mixture f-SWCNTs+PAAm-AgNPs (13.2 to 16.4%). We assumed that the behavior of dissolved silver in the medium and its adsorption to the inner surface of wells observed here for the nominal concentration NC2 was similar for other nominal concentrations with similar proportional values.

### **1.6.2 Preliminary acute tests**

When *S. droebachiensis* hatched blastulae were treated with 500 µg·L (NC1); 100 µg·L (NC2), 50 µg·L (NC3) and 20 µg·L (NC4) of Ag<sup>+</sup> or PAAm-AgNPs at 5°C, only the intermediate nominal concentrations NC2 and NC3 caused sublethal effects over embryogenesis. Under NC1 exposure, embryos died within 12h whereas NC4 showed no visible effects. The same result was obtained when considering the mixtures f-SWCNTs+Ag<sup>+</sup> and f-SWCNTs+PAAm-AgNPs. Single exposures to f-SWCNTs did not induce any visible effects on early development stages because of its low concentration (from 2 to 50 mg·L). When T1 to T6 treatments were first performed at 8°C and 10°C with NC2 and NC3 concentrations, early echinopluteus (prisma) struggled to survive at T5 and T6 possibly due to starvation. However, when treatments were conducted at 5°C, no mortality for any contaminant was observed.

### **1.6.3 Effects on body shape and swimming behavior**

Body shape clearly indicated distinct effects of contaminants and concentrations over embryos and early larvae. Embryos and larvae conditions at 48h are described in Supplementary data, Appendix 1. During T1, Ag<sup>+</sup>-treated blastulae atrophied early at 48h and even more at 96h in contrast to the controls (Figure 10 A1-A2). The mixture f-SWCNTs+Ag<sup>+</sup> had strong effects on final larval shape as well (Figure 10 A4). On the

contrary, PAAm-AgNPs and f-SWCNTs+PAAm-AgNPs did not prevent mesenchyme blastulae undergoing to mid-gastrula at 48h and to early prisma and late gastrula stages at 96h (Figure 10 A3 and A5). For T2 treatment, differences of size are less evident among contaminated embryos at 48h, but were different to the controls (Appendix 1). At 96h, Ag<sup>+</sup>-treated embryos became atrophied arrested gastrula, while controls reached to prisma stage (Figure 10 B1 and B2). Embryos in f-SWCNTs+Ag<sup>+</sup> conditions had small size compared to PAAm-AgNPs and f-SWCNTs+PAAm-AgNPs exposures (Figure 10 B3, B4 and B5). Under f-SWCNTs+PAAm-AgNPs condition, embryos showed an expanded blastocoel at mid-to-late prisma stage.

After 96h of T3, while Ag<sup>+</sup> and f-SWCNTs+Ag<sup>+</sup> gastrulas failed to fully develop into prisma stage, their PAAm-AgNPs and f-SWCNTs+PAAm-AgNPs-treated siblings were similar to the controls (Figure 10 C1-C5). T4 larvae in controls showed a progressive mineralization and developed arm buds (Figure 10 D1). At 48h, we found late gastrula to early-to-mid prisma stages delayed by Ag<sup>+</sup>, f-SWCNTs+Ag<sup>+</sup> and f-SWCNTs+PAAm-AgNPs, contrarily to PAAm-AgNPs (See Appendix 1). At T4 with contaminants, it seems Ag<sup>+</sup> harmed embryos instantaneously whereas f-SWCNTs+Ag<sup>+</sup> took more time to induce the same strong effects observed at 96h (Figure 10 D2, D4). Only PAAm-AgNPs conditions gave rise to a regular midprisma shape. However, prisms from both nanosilver conditions did not get a sharp triangular shape found in late prisms to early 2 arms-echinopluteus stage from the controls at 96h (Figure 10 D1, D3 and D5). Moreover, from 48h to 96h at T5, late prisms under Ag<sup>+</sup> contamination were rather shapeless than under nanosilver forms and controls (Figure 10 E1-E5). f-SWCNTs+Ag<sup>+</sup>-treated larvae were also affected (Figure 10 E4). When reaching T6 treatment, f-SWCNTs+Ag<sup>+</sup> progressively altered larval shape, which was severely deformed comparing to controls and contaminated siblings at 96h (Figure 10 F1-F5).

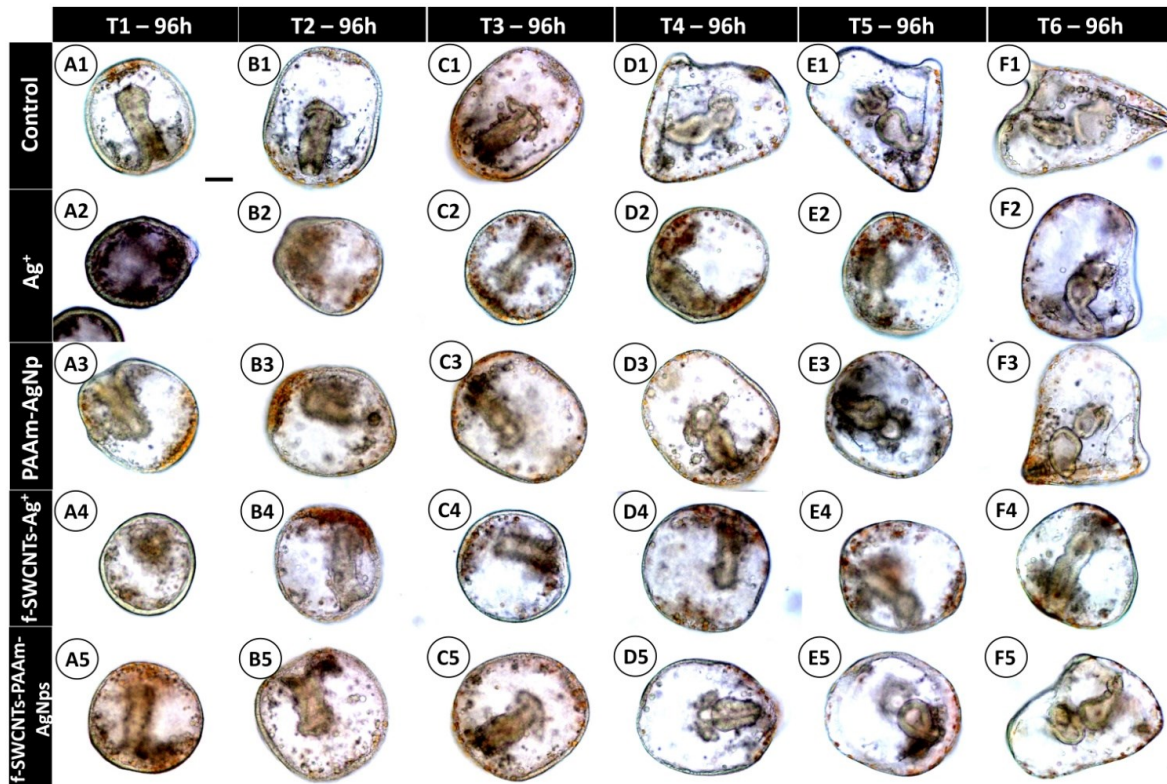


Figure 10: General view of development stages of embryos and larvae in controls and under treatment using NC2 concentrations of  $\text{Ag}^+$ , PAAm- $\text{AgNPs}$ , f-SWCNTs+ $\text{Ag}^+$  and f-SWCNTs+PAAm- $\text{AgNPs}$  after 96h (20X, scale bar: 200 $\mu\text{m}$ ). Timing for treatments appears on the top line, and contaminants are given on the left axis. Description of controls (A1-F1): A1: early-to-mid prisma, B1: mid-to-late prisma, C1: late prisma, D1: late prisma to early 2 arms-echinopluteus, E1: early 2 arms-echinopluteus, F1: late 2 arms-echinopluteus. Main observations in presence of contaminants at T1-96h: (A2: arrested blastula, A3: early-to-mid prisma, A4: arrested midgastrula, A5: mid-to-late gastrula); T2-96h (B2: arrested midgastrula, B3: mid-to-late prisma, B4: late gastrula to early prisma, B5: mid-to-late prisma); T3-96h (C2, C4: late gastrula to early prisma, C3, C5 : late prisma); T4-96h (D2: atrophied midprisma, D3: late prisma, D4: late gastrula to early prisma, D5: late prisma); T5-96h (E2, E4: atrophied late prisma to early pluteus, E3, E5: delayed late prisma to early 2 arms-echinopluteus) and T6-96h (F2: delayed early 2 arms-echinopluteus, F3: delayed 2 arms-echinopluteus, F4: atrophied late prisma to early 2 arms-echinopluteus, F5: delayed early 2 arms-echinopluteus).

Because embryos had different sensitivities along embryogenesis and prisma development, swimming behavior was useful to rapidly assess contaminant effects over time. Abnormal gastrulas either had short and slow movements or rotated around their own body axis at the bottom of the wells. Primas were mostly lethargic and unable to swim through water when strongly intoxicated by contaminants. At T1 and T2 stages, while Ag<sup>+</sup> and f-SWCNTs+Ag<sup>+</sup>-exposed embryos were highly lethargic at 48h and 96h, larvae treated with PAAm-AgNPs were only slightly affected compared to controls at 96h. During T1, f-SWCNTs+PAAm-AgNPs had minor visible effects on prisms behavior at 48h, but they quickly recovered at 96h when normal behavior arose again. Low lethargy was detected in both 48h and 96h of T3 and T5 treatments with ionic silver forms. At 96h of T4, prisms behavior was also strongly affected by Ag<sup>+</sup> forms. Again, when Ag<sup>+</sup> was added alone to medium, it seemed to cause a rapid immobilization with organisms slower than those exposed to f-SWCNTs+Ag<sup>+</sup>. Finally, during T6, early 2-arms pluteus had equally slow movements under silver forms in both times, and PAAm-AgNPs led to lethargy only at 96h.

#### **1.6.4 First treatment (T1)**

At 48h, PMCs (primary mesenchyme cells) in control already began to organize as a ring surrounding archenteron, holding triradiate spicules (Figure 11 A). Among contaminated embryos, Ag<sup>+</sup> (NC2) interfered with archenteron elongation, SMCs (secondary mesenchyme cells) delamination was inhibited and PMCs were poorly arranged around the rudiment of invaginating archenteron (Figure 11 B). Cable-like syncytium formation was though observed at 48h under PAAm-AgNPs (NC2) alone and f-SWCNTs+PAAm-AgNPs (NC2) conditions. Likewise, embryos exposed to a lower concentration of Ag<sup>+</sup>, PAAm-AgNPs and f-SWCNTs+Ag<sup>+</sup> had the syncytium ring formed. Cells at the tip of the archenteron became detached in uncontaminated embryos as well as in those exposed to Ag<sup>+</sup> (NC3), PAAm-AgNPs (NC2) (Figure 11 C), f-SWCNTs+Ag<sup>+</sup> (NC2) and f-SWCNTs+PAAm-AgNPs (NC2). None of the exposed embryos showed any sign of mineral deposition.

Following 96h exposure, early prisma emerged in the controls showing initial pigment cell migration, stomodeum formation, archenteron elongation completed, and advanced spicule mineralization inside a well-organized syncytium ring (Figure 11 D). Meanwhile, contamination with Ag<sup>+</sup> (NC2) gave rise to vegetalized blastulae in which vegetal plate appeared thickened, with indistinctive mesenchyme cells inside blastocoel (Figure 11 E). Early prisms from f-SWCNTs+PAAm-AgNPs and PAAm-AgNPs (Figure 11 F) exposures were similar to those from uncontaminated water, but without spiculogenic cells syncytium and spicules. Deformed ventro-lateral clusters were formed, pigment cells migration began and SMCs started to mold coelomic pouches at the tip of gastrointestinal tract. Abnormal gastrulas from f-SWCNTs+Ag<sup>+</sup> (NC2) medium did not complete the secondary invagination; archenteron remained a stub-like gut rudiment and free mesenchyme cells stayed near vegetal plate (Figure 11 G). No mineral deposition occurred and few pigment cells appeared at animal pole. Some mineral deposition activity occurred at the lower NC3 concentrations of all contaminants, and small rhombohedral granules with triradiate extension appeared among cell bodies. Mesenchyme ring with long filopodial extensions organized by spiculogenic cells sometimes were present. Archenteron elongation also occurred for all contaminants in lower concentrations.

### 1.6.5 Second treatment (T2)

Under normal conditions at 48h, PMCs formed a ring surrounding the invaginating archenteron (Figure 11 H) and some congregations of cell bodies occupied two loci in the ring. These cells fused their filopodia and formed a spiculogenic syncytium where mineral deposition took place about midway through gastrulation. When invaginating mesenchyme blastulae were contaminated with NC2 concentrations of Ag<sup>+</sup> or f-SWCNTs+Ag<sup>+</sup>, a massive agglomeration of mesenchyme cells appeared around the archenteron (Figure 11 I), mineral deposition did not occur and a stub-like gut rudiment became more retracted than before at time 0h.

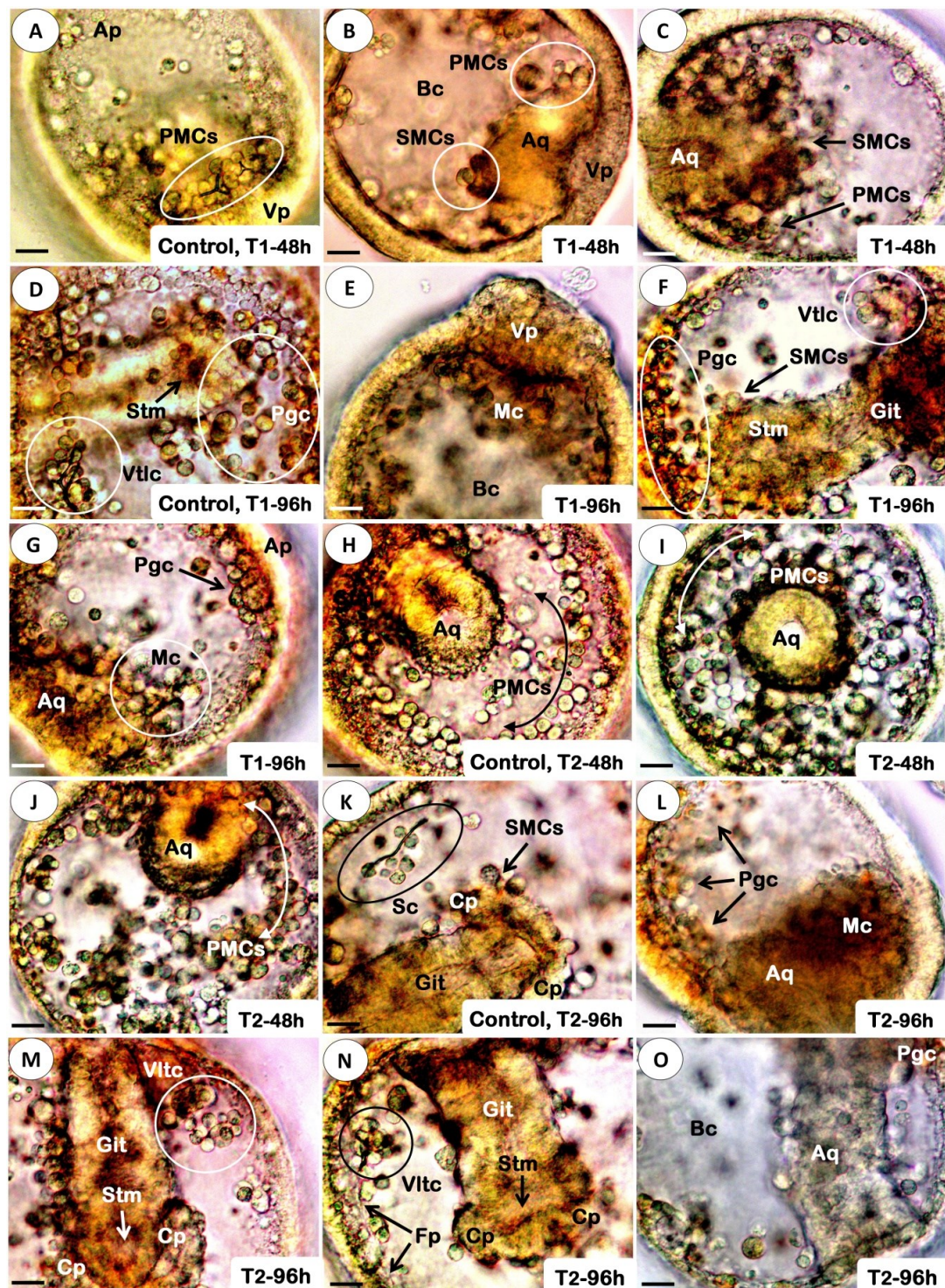


(Figure 11, see legend on next page)

Figure 11: *In vivo* morphological analysis of embryonic stages and prisma development of *S. droebachiensis* contaminated with NC2 concentrations of Ag<sup>+</sup>, PAAm-AgNPs, f-SWCNTs+Ag<sup>+</sup> and f-SWCNTs+PAAm-AgNPs at T1 and T2 (40X, scale bar: 25μm). A- Midgastrulas from controls showing PMCs ring with triradiate spicules. B- Blastulae exposed to Ag<sup>+</sup> developed into a delayed invaginating blastula with disturbed PMCs, few SMCs delaminated from archenteron. C- PAAm-AgNPs-treated embryos become midgastrulas, SMCs got delaminated; but PMCs were not organized. D- PMCs ring got organized as much as ventro-lateral clusters in the controls; stomodeum formation and pigment cells scattering began. E- Vegetalizing embryos with thickened vegetal plate after Ag<sup>+</sup> stress. F- Embryos exposed to PAAm-AgNPs became prisma, but without skeleton. G- f-SWCNTs+Ag<sup>+</sup> interfered with archenteron elongation; some pigment cells appeared at animal pole and unorganized mesenchyme cells occupied blastocoel. H- Larvae from T2 controls showed a well-organized PMCs ring. I- Under Ag<sup>+</sup> treatment, PMCs were unable to form the syncytium ring around the archenteron. J- Under PAAm-AgNPs conditions, PMCs seemed to be barely organized and void of visible mineral deposition. K- Controls showed advanced skeleton deposition and gut formation. L- Arrested gastrulas contaminated by Ag<sup>+</sup> had the archenteron collapsed and mesenchyme cells dispersed at vegetal plate. M- PAAm-AgNPs disrupted spiculogenesis and abnormal ventro-lateral clusters appeared; gastrointestinal tract, stomodeum and coelomic pouches were developed. N- Delayed spiculogenesis under f-SWCNTs+PAAm-AgNPs, with small triradiate spicules inside ventro-lateral clusters; filopodia got extended and gastrointestinal tract was developed. O- Embryos contaminated with f-SWCNTs+Ag<sup>+</sup> had archenteron extended, no spiculogenic cells, and differentiated pigment cells did not migrate. Abbreviations- Ap: animal pole, Aq: archenteron, Bc: blastocoel, Cp: coelomic pouches, Git: gastrointestinal tract, Fp: filopodia, Mc: mesenchyme cells, PMCs: primary mesenchyme cells, Pgc: pigment cells, SMCs: secondary mesenchyme cells, Stm: stomodeum, Vlct: ventro-lateral clusters, Vp: vegetal pole.

SMCs were visible at the tip of the gut rudiment in all exposures, especially for PAAm-AgNPs and f-SWCNTs+PAAm-AgNPs (not shown). Although embryos exposed to these both contaminants had a spiculogenic syncytium surrounding archenteron as a cable-like structure, they were void of visible mineralization (Figure 11 J). In this case, we suggest that metabolic stress caused by nanosilver forms may compromise first mineral deposition rather than PMCs organization. Under NC3 concentrations, no embryo treated

with f-SWCNTs+Ag<sup>+</sup> had PMCs organized in contrast to those treated with only Ag<sup>+</sup>, PAAm-AgNPs or f-SWCNTs+PAAm-AgNPs. As such, biominerization occurred, but was delayed when compared to controls.

At 96h exposure, mid-to-late prisms from controls had long spicules; coelomic pouches more organized by SMCs, stomodeum invagination progressing and gastrointestinal tract developed (Figure 11 K). Subsequent observations of gut development confirmed that only Ag<sup>+</sup> (NC2)-treated embryos had their archenteron collapsed over the vegetal plate (Figure 11 L). Conversely, embryos exposed to PAAm-AgNPs (NC2) and f-SWCNTs+PAAm-AgNPs (NC2) had gastrointestinal tract very similar to the controls (Figure 11 M and 5N). Late gastrulas exposed to f-SWCNTs+Ag<sup>+</sup> had archenteron stretched towards the inner surface of the apical pole, but differentiation into gastrointestinal tract did not appear (Figure 11 O). Embryos did not exhibit visible mineralization under NC2 concentrations of any contaminant. Ventro-lateral clusters agglomerations were exclusively observed in gastrulas contaminated with PAAm-AgNPs and f-SWCNTs+PAAm-AgNPs (Figure 11 M and N), but clusters were only deformed under PAAm-AgNPs. Small calcite composites particularly appeared inside clusters of f-SWCNTs+PAAm-AgNPs-treated embryos (Figure 11 N). Among embryos contaminated with f-SWCNTs+Ag<sup>+</sup> (NC2), spiculogenic cells were not even detected (Figure 11 O).

### **1.6.6 Third treatment (T3)**

As a rule, a subpopulation of SMCs released from the tip of archenteron made contact with inner surface of animal pole and moved inside by means of pseudopods. The fact that pseudopods remained attached to animal pole pulling the invaginating archenteron also indicated that SMCs contact with ectoderm was accomplished by all embryos exposed to all contaminants for NC2 and NC3 concentrations. Thus, pigment granules usually red, but occasionally yellow, began to accumulate in some cells in animal and vegetal regions at 48h, for all exposures. After 96h, pigment cells of uncontaminated embryos that have accumulated red pigments ingressed into blastocoel from the animal pole. Concomitantly, another subpopulation of these cells got scattered over the ectoderm, migrating towards the

vegetal pole. After migration, pigment cells occupied regular positions at the outer ectoderm of normal larvae (Figure 12 A). On the contrary, cells of late gastrula to early prisma stage under NC2 concentrations of  $\text{Ag}^+$  and f-SWCNTs+ $\text{Ag}^+$  did not migrate into lateral ectoderm from the animal pole (Figures 12 B and C). Under lower NC3 concentrations, both  $\text{Ag}^+$  and f-SWCNTs+ $\text{Ag}^+$  delayed scattering and it was almost similar to embryos exposed to NC2 concentrations of PAAm-AgNPs (Figure 12 D) and f-SWCNTs+PAAm-AgNPs. The ability of a large number of pigment cells to shift and migrate was delayed, but not suppressed, by nanosilver forms. These mitotic cells were red-orange and held small mineral granules in their cytoplasm during migration in the ectoderm (Figure 12 E).

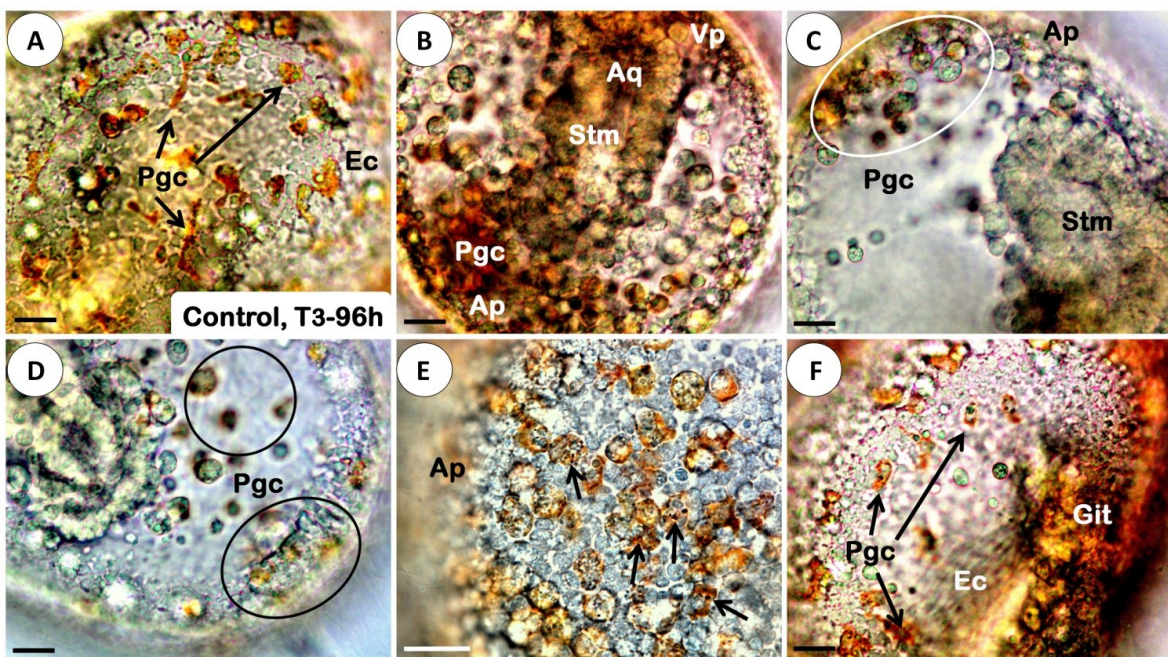


Figure 12: Pigment cells scattering at 96h of T3. A- Pigment cells from controls were well distributed over ectoderm. B- Abnormal larvae under NC2 concentrations of  $\text{Ag}^+$  had pigment cells restricted to animal pole. C- f-SWCNTs+ $\text{Ag}^+$  (NC2) prevented pigment cells migration; they also appeared less differentiated. D- After PAAm-AgNPs (NC2) exposure, pigment cells scattered and shifted into blastocoel and ectoderm subpopulations. E- Delayed scattering over epidermis from PAAm-AgNPs (NC3)-treated larvae; small mineral granules are indicated by black arrows. F- NC3

concentrations of f-SWCNTs+PAAm-AgNPs did not interfere with pigment cells scattering. Abbreviations- Ap: animal pole, Aq: archenteron, Ec: ectoderm, Git: gastrointestinal tract, Pgc: pigment cells, Stm: stomodeum, Vp: vegetal pole. (A-D, F: 40X, scale bar: 25 $\mu$ m; E: 63X, scale bar 15 $\mu$ m).

There were little differences in pigment cells distribution between the two concentrations of PAAm-AgNPs mostly due to mismatched timing for scattering among contaminated larvae. Their scattering in f-SWCNTs+PAAm-AgNPs conditions was similar to the controls in both concentrations (Figure 12 F). Therefore, pigment cells motility seems to have been affected in a concentration-dependent manner, but also as a function of contaminant tested. Ag<sup>+</sup> and f-SWCNTs+Ag<sup>+</sup> at higher CN2 concentrations were the strongest scattering inhibitors, while f-SWCNTs+PAAm-AgNPs lowest concentration was the weakest. Spiculogenic cells looked like an unorganized group of cells in Ag<sup>+</sup> and f-SWCNTs+Ag<sup>+</sup> (NC2) conditions. Some abnormal clusters had seldom small granules of calcite inside or even minuscule triradiate spicules. This strong inhibition of spiculogenesis by silver forms can be expected to indicate a perturbation of mineral influx and precipitation carried out by PMCs. In summary, we observed that PAAm-AgNPs and f-SWCNTs+PAAm-AgNPs delayed biomineralization because triradiate spicules were bigger and frequently laid inside small groups of ventral clusters relatively well aggregated. With NC3 low concentrations, spiculogenic process was less impacted and major differences among all the contaminated embryos were not observed.

### **1.6.7 Fourth treatment (T4)**

As opposed to controls, embryos from NC2 concentrations of Ag<sup>+</sup>, f-SWCNTs+Ag<sup>+</sup> and f-SWCNTs+PAAm-AgNPs failed to acquire skeleton elongation at 48h. Abnormal clusters were distinguished enclosing very small triradiate spicules under Ag<sup>+</sup> and f-SWCNTs+Ag<sup>+</sup> conditions. NC3 concentrations also confirmed Ag<sup>+</sup> and f-SWCNTs+Ag<sup>+</sup> as main mineral deposition stressors. Strikingly, gastrulas exposed to PAAm-AgNPs (NC2) seemed to be more resilient to nanosilver. In fact, two types of abnormal development forms emerged from PAAm-AgNPs conditions: early prisma and atrophied late gastrulas.

Both showed ongoing mineralization process, well organized ventral-lateral clusters holding triradiated spicules and gut without coelomic pouches. Atrophied late gastrulas found in PAAm-AgNPs conditions were quite similar to those from Ag<sup>+</sup> and f-SWCNTs+Ag<sup>+</sup> media, but with well organized spiculogenic cells. At 96h, larvae from the controls showed advanced skeleton mineralization and gut regionalization (Figure 13 A). Spiculogenic cells aspect confirmed that organisms exposed to Ag<sup>+</sup> (NC2), f-SWCNTs+Ag<sup>+</sup> (NC2) and f-SWCNTs+PAAm-AgNPs (NC2) had abnormal clusters and spiculogenesis inhibition at 96h. PAAm-AgNPs exposure alone sometimes gave rise to larvae having the same mineralization disturbance, but some of them had cluster organized with individualized cells around few amorphous cellular aggregations (Figure 13 B).

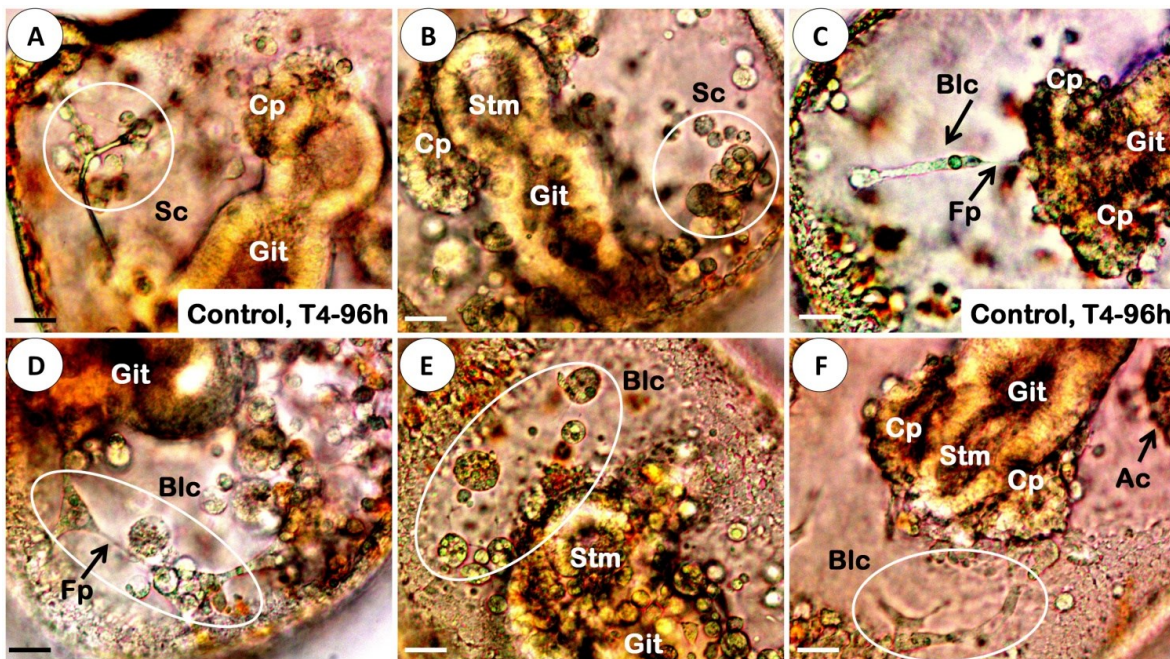


Figure 13: Cellular stress at 96h of T4 (40X, scale bar: 25μm). A- Larvae from controls had gastrointestinal tract well shaped while skeleton was built by skeletogenic cells inside growing bud arms. B- Larvae from PAAm-AgNPs (NC2) conditions showed spiculogenic cells disturbed by chemical stress, with a few abnormal agglomerations surrounded by normal cells. C- Normal blastocoelar cells from controls had a fusiform shape and long filopodia. D- Under f-SWCNTs+Ag<sup>+</sup> (NC2) conditions, blastocoelar cells from ventro-lateral region got highly vacuolized, with filopodia

still present. E- Same larvae from PAAm-AgNPs (NC2) (as shown in 7B) with intoxicated blastocoelar cells, on the anterior side near animal pole. F- f-SWCNTs+PAAm-AgNPs (NC2) caused injury in spiculogenic cells of late prisms, but blastocoelar cells kept their characteristic shape and organization. Abbreviations- Ac: abnormal clusters, Blc: blastocoelar cells, Cp: coelomic pouches, Fp: filopodia, Git: gastrointestinal tract, Stm: stomodeum.

During gastrulation, SMCs leave continuously the archenteron and travel inside the blastocoel to make contact with the blastoderm wall with thin filopodia. Blastocoelar cells are known to be a distinct SMCs derivative that becomes more organized as far as development goes on. These cells were easily detected with confocal microscopy and allowed us to find out whether or not silver ions and/or nanosilver forms had major effects over another group of non-spiculogenic cells. From larvae in uncontaminated conditions, blastocoelar cells normally got a fusiform aspect (Figure 13 C). This characteristic cellular shape made them more recognizable especially because they tend to display a web-like organization. During this pulsed-treatment, atrophied larvae from higher NC2 concentrations of silver forms had at times two different conditions, either lacking blastocoelar cells or appearing deformed as though they were vacuolized or swelled, both being typical signs of a chemical insult (Figure 13 D). Larvae from PAAm-AgNPs (NC2) also displayed these rounded blastocoelar cells (Figure 13 E), whereas f-SWCNTs+PAAm-AgNPs did not seem to interfere with their general organization and shape (Figure 13 F). At the same NC2 concentrations, we noted that only among f-SWCNTs+PAAm-AgNPs-treated larvae, spiculogenic cells were abnormally congregated, but blastocoelar cells seemed not to be affected.

Later on, a tripartite gut began to be shaped in uncontaminated larvae; but Ag<sup>+</sup> and f-SWCNTs+Ag<sup>+</sup> disturbed gut regionalization in both sublethal concentrations. Abnormal larvae did not produce fecal pellets right after acute exposure. Under lower NC3 concentrations however, pellets production did occur but weakly.

### 1.6.8 Fifth and sixth treatments (T5 and T6)

As development proceeds in both treatments, blastocoelar cells get even more organized inside blastocoel, skeleton bars grow towards animal pole taking the same direction of filopodial extensions, and pigment cells get well distributed both in blastocoel and ectoderm. As mentioned earlier,  $\text{Ag}^+$  and f-SWCNTs+ $\text{Ag}^+$  caused strong larvae atrophy from 48h up to 96h of T5 exposure. However, while larvae exposed to f-SWCNTs+ $\text{Ag}^+$  did not have well organized spiculogenic cells, cellular syncytium appeared under  $\text{Ag}^+$  conditions. Skeleton deposition was poorly detected in both cases. For nanosilver forms, larvae showed well-delimited spiculogenic cells surrounding bigger spicules. Photos showing differences of skeletogenic cells organization and mineralization among uncontaminated larvae and those exposed to PAAm-AgNPs and f-SWCNTs+ $\text{Ag}^+$  are presented in Supplementary material, Appendix 1. Later at T6, only organisms contaminated with PAAm-AgNPs and f-SWCNTs+PAAm-AgNPs had mineralized spicules with well organized spiculogenic cells.

Uncontaminated larvae already had esophagus and stomach separated by the cardiac sphincter and an expanded stomach delimited by a thin tissue layer. Contaminated larvae displayed different stomach shapes well representative of contaminants toxicity compared to controls (Supplementary material, Appendix 1). Following exposure of NC2 concentrations of f-SWCNTs+ $\text{Ag}^+$  at T6, larvae were more shapeless compared to their contaminated siblings and gastrointestinal tract remained as a deformed hollow tube. By far, larvae contaminated with PAAm-AgNPs were almost similar to the controls, with a cardiac sphincter between esophagus and stomach indicating a low toxicity on this development stage. Contamination with f-SWCNTs+PAAm-AgNPs seemed to delay stomach molding whereas under  $\text{Ag}^+$  stress, larvae had very small stomachs compared to controls, no sphincter was detected. At the end of T5, f-SWCNTs+ $\text{Ag}^+$  showed the same abnormal effects over gastrointestinal tract development. As expected, abnormal larvae contaminated with f-SWCNTs+ $\text{Ag}^+$  from T5 and T6 were unable to feed after 96h. A few

cells of phytoplankton were seem inside malformed stomachs of  $\text{Ag}^+$ -exposed larvae at T5, and pellets were always unpacked.

### 1.6.9 Disturbed congregation of spiculogenic cells by silver forms

Under normal conditions, calcite deposition occurs inside a syncytial array of connected cell bodies. Although spiculogenic cells keep their filopodia connected, cell bodies never get massively fused during mineralization. It seemed as though spiculogenic cells had lost their integrity giving rise to amorphous agglomerations when contaminated with silver and nanosilver forms. Using SyberGreen dye allowed us to localize several nuclei inside these clusters (Figure 14 A-C). Sometimes fluorescent signal inside the agglomerations was weak and diffused, which might indicate nuclei collapse. Generally cellular stress condition appeared as a function of contaminant and concentrations in any stage of development (Figure 14 D-I). Observations were made during two different experiences and revealed the same pattern.

$\text{Ag}^+$  and f-SWCNTs+ $\text{Ag}^+$  induced these agglomerations at all concentrations and treatments, but differences in timing occurred. At 48h of T1, only  $\text{Ag}^+$  (NC2)-treated gastrulas had visible swelled cells. At T1 (96h) and T2 (48h), f-SWCNTs+ $\text{Ag}^+$  (NC2 and NC3) led to an intense aggregation of spiculogenic cells not seen in  $\text{Ag}^+$  conditions (Figure 14 D). During T6, malformed clusters arose at 48h after  $\text{Ag}^+$  exposure (Figure 14 G-I), but were not detected at 96h even though larvae struggled to biomimicry. On the other hand, f-SWCNTs+ $\text{Ag}^+$  larvae at T6 showed the same clusters from 48h to 96h. Organisms mostly responded to PAAm-AgNPs stress by not rapidly forming abnormal clusters at 48h as in  $\text{Ag}^+$  treatment. Instead, they mostly came out in NC2 concentrations from T1 to T4 at 96h (Figure 14 E). Little if any deformed agglomerations appeared during f-SWCNTs+PAAm-AgNPs contamination. In this case, they weakly emerged at 96h of T1 at the most sensitive stage; but also at mid-to-late gastrula stage of T4 (Figure 14 F) when all contaminants caused cellular deformities in both 48h and 96h. As larvae became more resilient to silver and nanosilver forms over successive stages, cells tend not to fuse massively and isolated skeletogenic cells got slowly associated to the central cell group. It

frequently happened with nanosilver exposure, and in later stages of prisma to early 2 arms-echinoplateus development contaminated with silver forms (Figure 14 G, H, I). Severity of intoxication caused by  $\text{Ag}^+$ , PAAm-AgNPs and f-SWCNTs+ $\text{Ag}^+$  during T3 are compared in Supplementary data, Appendix 1.

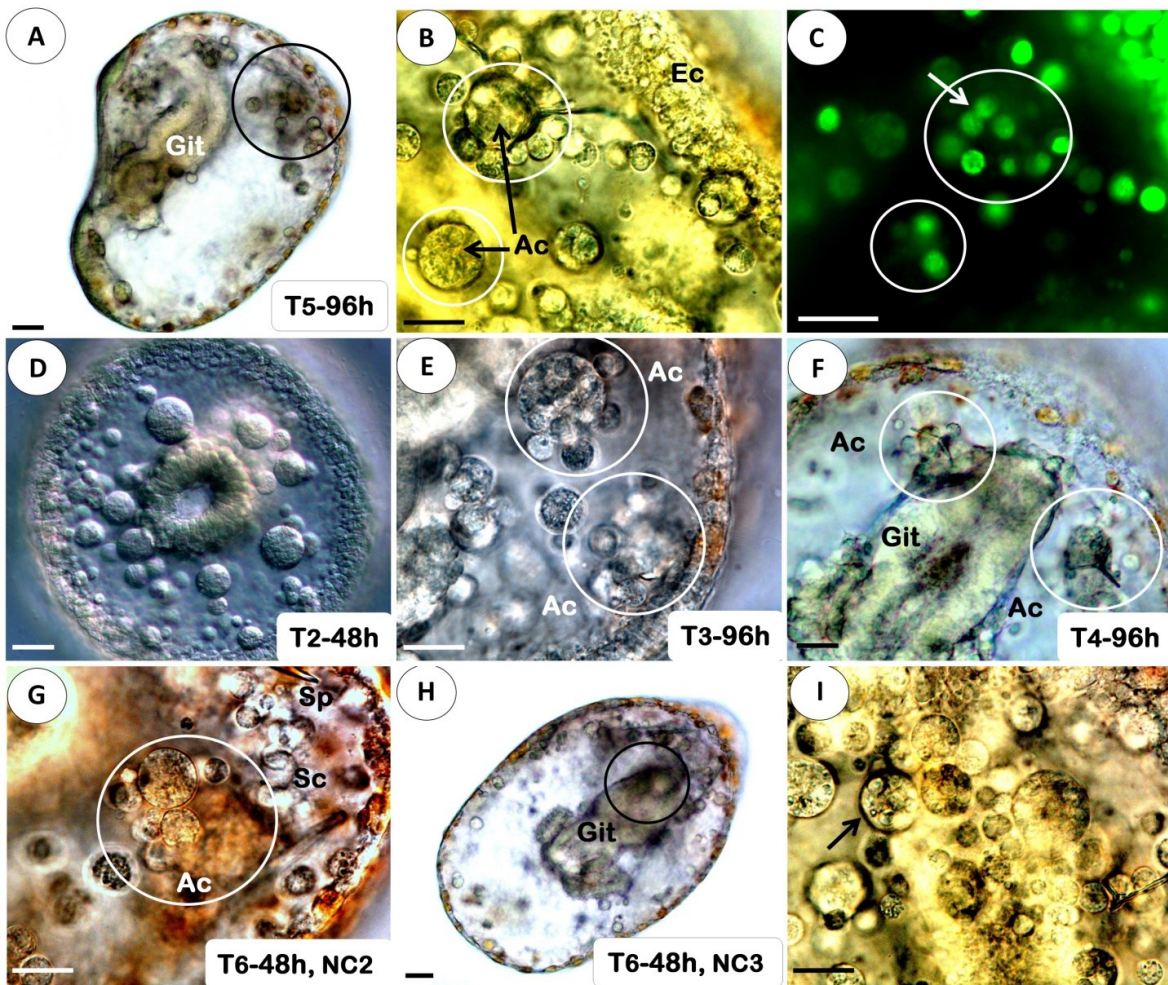


Figure 14: Spiculogenic syncytium cells under silver and nanosilver forms exposures at different times. A- Larvae contaminated with NC2 concentration of  $\text{Ag}^+$  at 96h of T5: delimited area inside black circle indicates abnormal cellular agglomerations shown in detail in (B) and (C). B - Inside white circles, agglomerations of skeletogenic cells. C- Nuclei dyed with SyberGreen revealed associations of chemically stressed cells. D- f-SWCNTs+ $\text{Ag}^+$  (NC3) late gastrulas had numerous anomalous aggregations at 48h of T2. E- Clusters from prisms contaminated with PAAm-AgNPs (NC2) at 96h of T3 had similar structure of those shown in figure A. F- f-SWCNTs+PAAm-AgNPs

induced amorphic agglomerations at 96h of T4. G- Skeletogenic cells were massively associated after contamination with Ag<sup>+</sup> (NC2) at 48h of T6. H, I- Under NC3 concentrations of Ag<sup>+</sup> at 48h of T6, larvae had multiple and free deformed agglomerations near gastrointestinal tract (Git) (black circle). Little granules of calcite were held inside some of them (black arrow) (photo I). Abbreviations- Ac: abnormal clusters, Ec – ectoderm, Sc: spiculogenic or skeletogenic cells, Sp- spicule. (A, H: 20X, scale bar 200µm; B, E, G, I: 63X, scale bar 15µm; C: 63X, scale bar 10µm (laser microscopy); D, F: 40X, scale bar 25µm).

#### **1.6.10 The fate of f-SWCNTs**

At t0, f-SWCNTs readily dispersed in seawater. After 12h, tiny barely visible f-SWCNTs bulks appeared floating in the water or laying at the bottom. Settled nanotubes did not associate immediately with embryos and larvae though. Dispersed bulks were gently caught by ciliary bands, which sometimes disturbed larvae and embryos swimming. On the contrary, phytoplankton cells were completely trapped by these small bulks when larvae were fed after 96h of exposure time. Besides, uptake of f-SWCNTs by early larvae occurred but depuration was also fast. In summary, f-SWCNTs single exposure did not cause any abnormality in early development stages.

#### **1.6.11 Recovery period**

During the first week of recovery period, vegetalized blastulae in Ag<sup>+</sup> exposure of T1 had mesenchyme cells extruded from blastocoel at vegetal plate, and sometimes a tail-like structure with these cells was formed (see Supplementary data, Appendix 1). It looked different from exogastrulation, because a thin rudiment of invaginating archenteron was observed at the inner surface of vegetal plate. All vegetalized blastulae died along the recovery process; and final assessment revealed other categories of embryos and larvae (shown in Supplementary data, Appendix 1). Their main features were as following: (1) arrested gastrula: spherical body with mesenchyme cells randomly distributed over vegetal pole; archenteron failed to get extended inward, but did not exogastrulate; (2) echinoplateus-type 1: triangular body with two bud-arms and one vertex at the posterior region, no-feeding larvae, gastrointestinal tract absent; (3) echinoplateus-type 2: feeding

larvae with gastrointestinal tract completed, bell-shaped body without arms or with very small ones; larvae lack of skeleton or had displaced spicules; (4) small echinopluteus: body shape similar to normal echinopluteus, but very small; vestigial spicules or long and displaced calcite bars appeared, feeding larvae with gastrointestinal tract similar to the controls; and finally (5) normal echinopluteus (2 or 4 arms): larvae with no morphological deformities.

After final 3 x 96h recovery, frequencies of normal and abnormal organisms were related to treatments in NC2 and NC3 concentrations (Figure 15 A and B). Arrested gastrulas were mainly found at T1 from  $\text{Ag}^+$ , f-SWCNTs+ $\text{Ag}^+$  and f-SWCNTs+PAAm-AgNPs recovery conditions of NC2 (Figure 15 A). Echinopluteus type-1 emerged in recovery cultures from T2 to T5 (NC2) of  $\text{Ag}^+$  and f-SWCNTs+ $\text{Ag}^+$ , but also at T1 and T2 of nanosilver forms. Echinoplutei type-2 were taken from T3 to T5 (NC2) of nanosilver forms, and also from T6 of f-SWCNTs+PAAm-AgNPs,  $\text{Ag}^+$  and f-SWCNTs+ $\text{Ag}^+$ . Whereas small echinoplutei developed from T2 to T6 of f-SWCNTs+PAAm-AgNPs, both small larvae and normal plutei appeared at T6 of PAAm-AgNPs. Unlike NC2 concentrations, no arrested gastrulas were found at T1 from lower concentrations conditions of any contaminant. Echinopluteus type-2 was often found in all pulsed-treatments of  $\text{Ag}^+$  after final recovery. Likewise, small echinopluteus emerged from T1 to T6 of PAAm-AgNPs and T1 to T5 of f-SWCNTs+ $\text{Ag}^+$ . Normal echinoplutei were highly frequent in all pulsed-treatments of f-SWCNTs+PAAm-AgNPs, and also present in PAAm-AgNPs and f-SWCNTs+ $\text{Ag}^+$  recovering media.

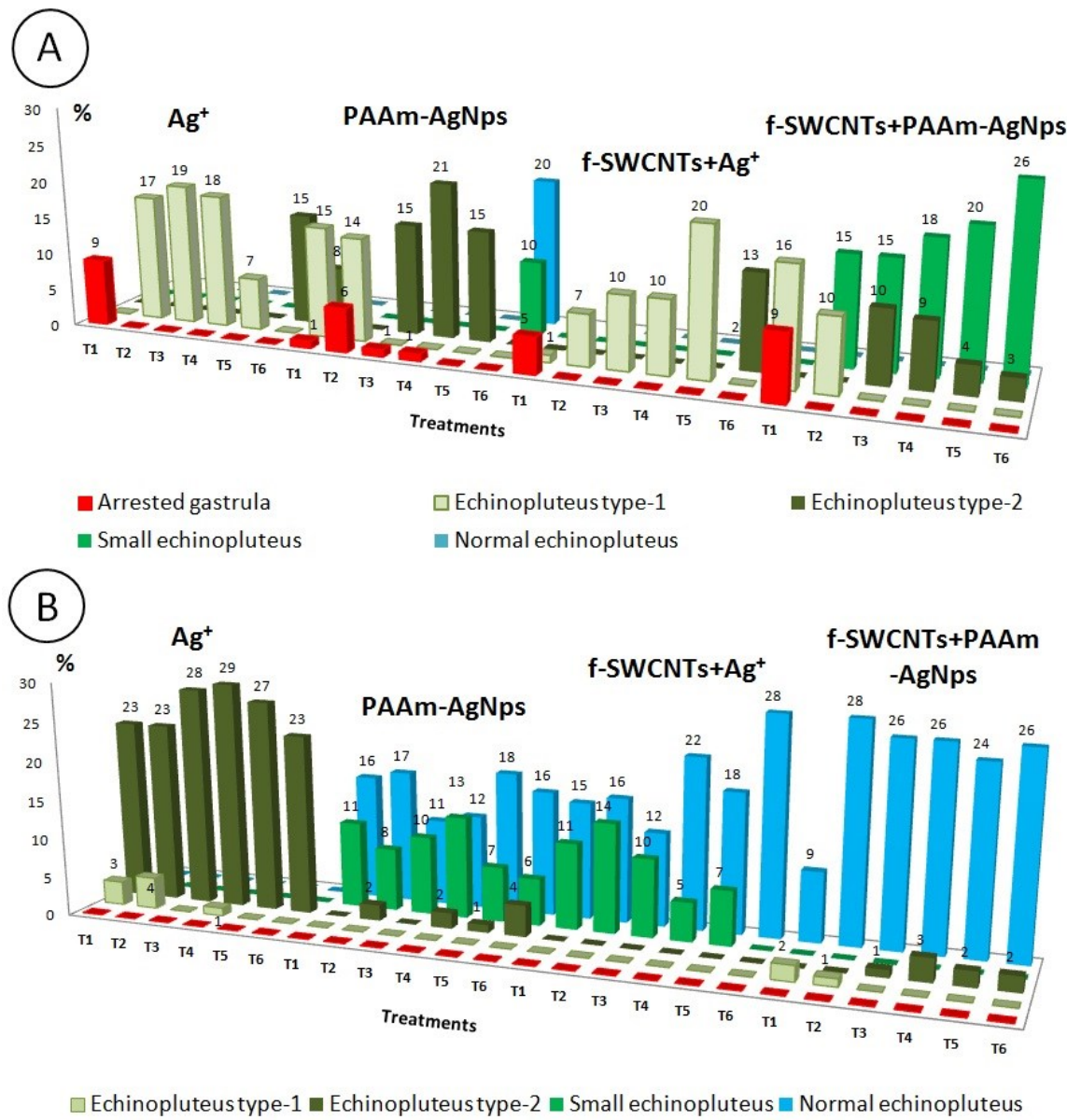


Figure 15: Embryos and larvae groups found after a 3-week recovery period in each treatment (T1 to T6). Organisms were categorized in five groups: arrested gastrula (red), echinoplateus-type 1 (light green), echinoplateus-type 2 (dark green), small echinoplateus (lime green), normal echinoplateus (blue). A- Organisms exposed to NC2 concentrations of Ag<sup>+</sup>, PAAm-AgNPs, f-SWCNTs+Ag<sup>+</sup> and f-SWCNTs+PAAm-AgNPs before recovery. B- Organisms exposed to NC3 concentrations of Ag<sup>+</sup>, PAAm-AgNPs, f-SWCNTs+Ag<sup>+</sup> and f-SWCNTs+PAAm-AgNPs before recovery.

### 1.6.12 Analysis of mortality among contaminated stages

To evaluate if significant differences in mortality appeared among T1 to T6 treatments, a multivariate analysis with PERMANOVA was performed. As shown in Figure 16 we can distinguish a gray cloud at the bottom of the plot and different overlapped clouds aside.

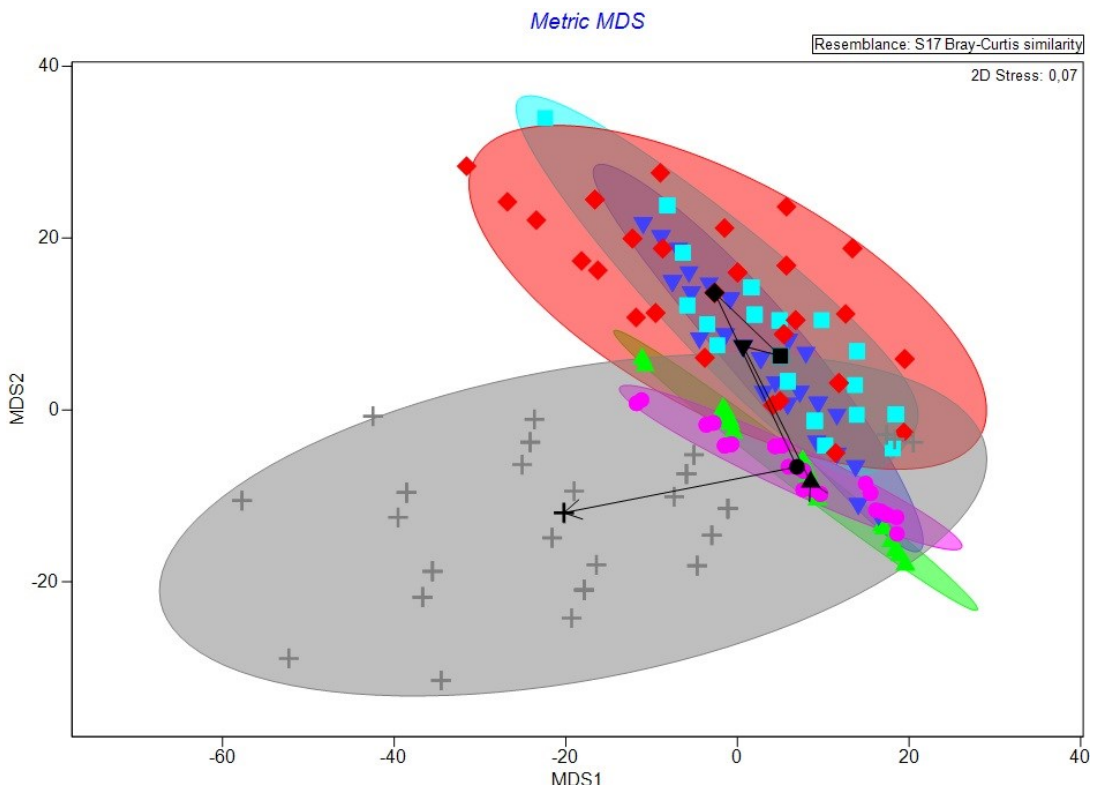


Figure 16: Analysis of mortality among contaminated stages after 3-week recovery period by MDS plot with Bray-Curtis similarity (PERMANOVA) ( $p > 0.01$ ; 2D stress: 0.07). Each cloud represent one time for each treatment from T1 to T6. Green: T1, dark blue: T2, light blue: T3, red: T4, pink: T5, gray: T6. Centroids of each group are represented by black symbols ( $\blacktriangle$ ,  $\blacktriangledown$ ,  $\blacksquare$ ,  $\blacklozenge$ ,  $\bullet$ ,  $+$ ).

Gray cloud represents contaminated mid-to-late prisma stage of T6. By far, we could consider this stage as the most resilient for all contaminants due to low mortality and great variance inside the group. Away from gray cloud centroid we have T5 centroid close to T1. Both green and pink clouds represent respectively, T1 (early mesenchyma blastula

stage) and T5 (late gastrula to very early prisma stage). Contaminants seem to have similar effects on samples of both treatments (T1 and T5), considering their dispersion. Additionally, T4 (mid-to-late gastrula stage), T3 (midgastrula) and T2 (invaginating blastula) formed another set of centroids really close to each other. Surprisingly, T4 had the most dispersed cloud among them. Little differences comparing mortality among pulsed treatments could be detected but were not statistically significant ( $p > 0.01$ ).

#### 1.6.13 Analysis of mortality as a function of contaminants

Statistical analysis of overall mortality for all contaminants and both NC2 and NC3 concentrations was made. A data cloud with four groups was created and each one of them was centered on black points (centroids) (Figure 17).

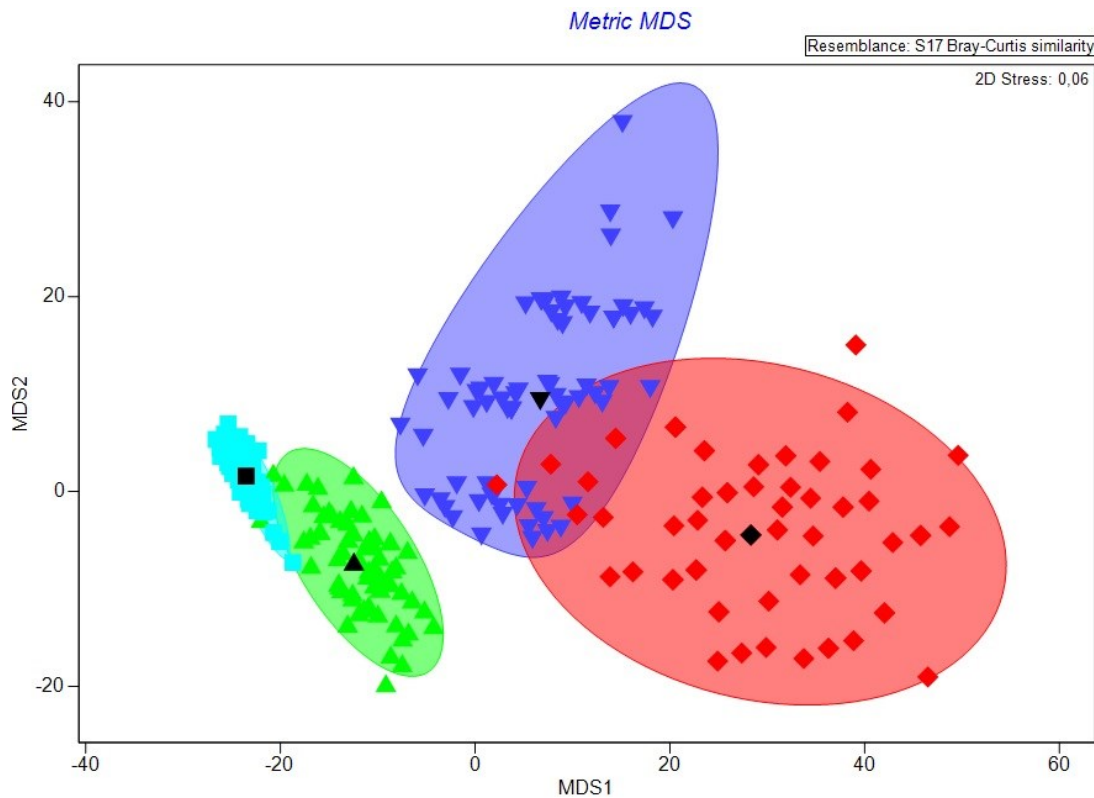


Figure 17: Analysis of total mortality after 3-week recovery period by MDS plot with Bray-Curtis similarity (PERMANOVA) ( $p < 0.001$ ; 2D stress: 0.06) among embryos and larvae previously exposed to  $\text{Ag}^+$  (green), f-SWCNTs+ $\text{Ag}^+$  (light blue), PAAm-AgNPs (dark blue) and f-

SWCNTs+PAAm-AgNPs (red). Centroids of each group are represented by black symbols (**■**, **▲**, **▼**, **◆**).

After PERMDISP analysis we confirmed that our data were homogeneous and comparable ( $p > 0.05$ ). This MDS (non-metric multidimensional scaling) plot indicates a statistically significant interaction of effects of our contaminants tested with two nominal concentrations ( $p < 0.001$ ). Red and dark blue clouds are separated from green and light blue clouds by a shift representing an effect: the light blue and green clouds form a group associated to  $\text{Ag}^+$  forms whereas dark blue and red clouds are related to PAAm-AgNPs forms. Inside these groups, it can be possible to distinguish different directions of each cloud. Variance among samples was reduced in the case of f-SWCNTs+ $\text{Ag}^+$  exposure, with this contaminant mixture being equally lethal from T1 to T6 over time. Close to light blue cloud, green cloud represents  $\text{Ag}^+$  samples less dispersed than red and dark blue clouds. Especially under higher NC2 concentrations,  $\text{Ag}^+$ -exposed embryos and larvae undergoing recovery were less affected than those treated with f-SWCNTs+ $\text{Ag}^+$ , but more than those exposed to nanosilver forms. f-SWCNTs+PAAm-AgNPs caused less mortality than single-exposures of PAAm-AgNPs in each treatment, which is showed by different directions taken by red and dark blue clouds in the multivariate space.

## 1.7 DISCUSSION

### 1.7.1 Embryogenic impairments during chemical stress

The results suggest that  $\text{Ag}^+$  (combined or not with f-SWCNTs) was a disruptive factor causing a scrambled PMCs pattern during T2 and T3; and failed invagination process at T1. In fact, many regulatory pathways could be altered during a toxic insult. Growth factor signaling also regulates multiple developmental processes including early axis specification, germ layer formation and organogenesis in sea urchin embryo. Most growth factor receptors are transmembrane glycoproteins that function in transmitting extracellular signals into the cell (Adomako-Ankomah and Ettensohn, 2014). Among them, FGFs (fibroblast growth factors) are known to regulate cell migration, chemotaxis, cell adhesion and differentiation. The inhibition of signaling factors as FGFA and FGFR1 delays

archenteron invagination and prevents regionalization of the gut in *Paracentrotus* sp. (Röttinger et al., 2008). It is also known that PMCs remain as a disorganized cell population without cellular extensions near the vegetal pole when inhibitors disrupt FGFA signaling. As a consequence, embryos lack of ventro-lateral clusters, ring-like structure and skeleton deposition (Röttinger et al., 2008), which was the situation observed for f-SWCNTs+Ag<sup>+</sup> and Ag<sup>+</sup>-exposed embryos when the % dissolved Ag<sup>+</sup> was the highest at 96h.

Gastrulation requires multiple cellular interactions to coordinate morphogenic process with signaling pathways and a complex gene regulatory network (Angerer and Angerer, 2003). Soon after multiple clivages, sea urchin eggs become polarized along the animal/vegetal axis with different gene regulatory potentials. Thus, early blastomeres begin to accumulate a transcription factor called β-catenin in their nuclei. β-catenin regulates the coordination of cell-cell adhesion and transduction of intercellular signals that specifies cellular fate during embryo development (Miller and McClay, 1997). Several early experiments demonstrated that signaling functions that control cellular fate can be severely changed by metals (as Li<sup>+</sup>, Mn<sup>2+</sup> and Zn<sup>+</sup>) and polycyclic aromatic hydrocarbons in sea urchin embryos (Logan et al., 1999; Pillai et al., 2003; Kobayachi and Okamura, 2005).

Invagination depends on multiple factors as mechanical forces generated by cells division, but also on extracellular matrix elements to keep cellular contact and their interactions along the whole process (Kominami and Takata, 2004). Besides, it is important to note that patterning of nuclear β-catenin at vegetal pole cells is a dynamic process deeply related to PMCs ingestion and invagination process (Logan et al. 1999). It changes continuously from hatched blastulae to pre-invagination (T1) and could be easily perturbed by metal toxicity as noted above. Due to the high toxicity of silver, it is reasonable to consider this metal as a disturber in such a case. Our findings showed arrested blastulae with vegetal plate thickened and mesenchyme cells being extruded from blastocoel when treated with NC2 concentrations of Ag<sup>+</sup>. It seemed that cell contact and fate were severely altered after treatment. Differently from exogastrulation, invagination was early blocked

and outward migration of mesenchyme cells continued to progress in uncontaminated water. Normally, SMCs delaminate from archenteron while primary and secondary invagination processes are going on. Although cells were not specifically marked in our experiments, we suggest that extruded cells were mostly SMCs. Because disrupted LvNotch signaling pathway has been linked to elimination of SMCs specification and cellular extrusion during gastrulation in echinoderms (Sherwood and McClay, 1999), it is reasonable to think this metabolic pathway could be involved in extruded mesenchyme cells found in our experiments.

Detrimental effects of  $\text{Ag}^+$  on pigment cells differentiation were stage-specific. When the first treatment (T1) finished,  $\text{Ag}^+$  and f-SWCNTs+ $\text{Ag}^+$  treated embryos did not have a well-established pigment cells population at the animal pole. It suggests that pigment cells precursors in blastulae stage could have  $\text{Ag}^+$  disrupting Delta signaling before invagination which compromised their differentiation. The *delta* gene expression is down regulated in skeletogenic precursors ingressing into blastocoel, but it gets raised again in non-skeletogenic cells thus inducing first pigment and blastocoelar cells, and later coelomic pouches and muscles (Sweet et al., 2002). Cells in pigment lineage of sea urchin *Hemicentrotus pulcherrimus* are able to switch their fate into blastocoelar lineage under  $\text{Ni}^+$  exposure (Tokuoka et al., 2002) and the same could be expected to happen with  $\text{Ag}^+$ . Another hypothesis is related to the archenteron failure to be stretched. As a consequence, pigment cells precursors were unable to make cell contacts with inner ectoderm of animal pole and get differentiation started. Considering T2, as invaginating blastulae had probably already experienced Delta signaling when they were contaminated, archenteron elevation would become crucial to pigment cell differentiation at animal pole. As such, f-SWCNTs+ $\text{Ag}^+$ -treated embryos had a differentiated pigment cell population, but restricted to the animal region. The same might happen with arrested gastrulae from  $\text{Ag}^+$  conditions whose some orange cells were scarcely distributed near animal pole. Under normal conditions, echinochrome containing-cells became red after ingressing into aboral ectoderm. Hence, signaling or specific cues inside aboral ectoderm might be crucial for a regular differentiation of chromatogenic cells.

Pigment cells scattering over ectoderm was affected by silver and nanosilver forms in a concentration-dependent manner. Particularly in T3, NC2 concentrations showed strong effects over pigment cells migration. This time, cellular differentiation was not altered probably because precursors had already ingressed into animal region. Whereas silver forms rapidly interfered with pigment cells motility, those exposed to nanosilver forms were able to move away but with some delay compared to the controls. The proportion of dissolved silver in PAAm-AgNPs in exposure media was between 30 to 40% lower than in media receiving  $\text{Ag}^+$ . When treated with  $\text{Li}^+\text{Cl}^-$ , pigment cells of vegetal pole remain stuck in blastocoel probably because of extracellular matrix synthesis gets delayed in sea urchin embryos of *H. pulcherrimus* (Kominami et al., 2001). As a rule, cell movement involves signaling, cytoskeleton components and extracellular matrix. Migratory substrates as glycosaminoglycans have been also suggested to guide pigment cells in their pathway to dermis in anuran eggs (Tucker, 1986). Nonetheless, information on factors that drive pigment cells scattering over ectoderm is still unavailable for sea urchins embryos.

### 1.7.2 $\text{Ag}^+$ toxicity mechanism

Ionic silver ( $\text{Ag}^+$ ) effects were highly harmful to all embryonic stages compared to PAAm-AgNPs.  $\text{Ag}^+$  quickly induced to morphological abnormalities in test-organisms for all treatments. We need first to consider the chemistry of  $\text{Ag}^+$  in seawater. Normally  $\text{Ag}^+\text{NO}_3^-$  readily dissolves releasing free  $\text{Ag}^+$  ions, and strong chloro complexes ( $\text{AgCl}_2^-$ ,  $\text{AgCl}_3^{-2}$ ,  $\text{AgCl}_4^{-3}$ ) are immediately formed, enhancing  $\text{Ag}^+$  solubility and dispersion. Secondly, high surface/volume ratio of embryos is also an important factor for  $\text{Ag}^+$  uptake, probably allowing rapid diffusion and bioaccumulation. In general, cellular uptake of xenobiotics from water happens by passive diffusion, facilitated diffusion, active transport or endocytosis (Boelsterli, 2003). However, cationic metals such as  $\text{Ag}^+$  and its chloro complexes are rather uptaken by facilitate transport that involves membrane macromolecular carriers (Campbell and Couillard, 2004). Driven by electrostatic forces,  $\text{Ag}^+$  ions are adsorbed by macromolecules from extracellular matrix where their interactions lead to disruption in the ion-efflux cellular system and increase membrane

permeability (Lapresta-Fernández et al., 2012). As a result, electrochemical gradient of transmembrane proton decreases leading to plasma-membrane potential disruption and cell injury. Of increasing worth as a biomarker during our observations in confocal microscopy, spiculogenic cells readily indicate from T1 to T6 which contaminants had the strongest toxicological effects on cellular metabolism. By far, silver and nanosilver forms exposures had different effects over spiculogenic cells considering their fusion and metabolism. Injured spiculogenic cells of any treatment showed signs of intoxication by silver (ionic or nano). These cells lacked filopodial extensions and get anomalously aggregated appearing as though they had gone through an osmotic swelling. Blastocoelar cells looked the same way, but still keeping tiny filopodia. According to Moore (1985) changes in membrane fluidity lead to altered rates of fusion of internal cellular vesicles being a clear sign of chemical cellular injury. Using 63X magnification in confocal microscopy (immersion) we were able to identify many bright vesicles inside abnormal blastocoelar and spiculogenic cells in the blastocoelar space.

The onset of fusion competence of PMCs is autonomously programmed soon in their micrometer lineage (Hodor and Ettensohn, 1998). As a result, PMCs partially fuse their membranes in order to create a cytoplasmatic cable that facilitates regulation and spacial patterning of skeletal system (Hodor and Ettensohn, 1998). Hence, we suggest that silver strongly interfered with plasmalemma structure and altered fusogenic properties of spiculogenic cells, but not necessarily the basic signaling that lead them to be associated. It is known that xenobiotic-induced cellular stress in sublethal conditions usually reflects perturbations of function and structure at molecular level (Moore, 1985). In fact, deformed clusters mostly found after chemical exposure of  $\text{Ag}^+$  and f-SWCNTs+ $\text{Ag}^+$  firmly exemplified these disturbances. Silver element is a membrane-disrupter that breaks down cellular homeostasis.

According to Vidavsky et al. (2014) recent findings, embryo ectoderm is the first barrier seawater ions have to diffuse to reach out blastocoel and PMCs. Calcium is thus taken up first by epidermic layer and gets imported into blastocoel as a dispersed form,

later it appears inside PMCs as granules that will be incorporated into spicule-forming process. Interestingly, we localized these granules inside pigment cells at ectoderm layer. Also observed in our experiments, abnormal clusters sometimes held some granules of skeleton material inside cellular agglomerations which may indicate  $\text{Ca}^{+2}$  short term accumulation before mineral deposition. Analysis of dissolved silver suggest that  $\text{Ag}^+$  was rapidly taken up by embryos in seawater at T0h as only 18% dissolved silver was in the medium and 17% was adsorbed onto the wells. Hence, it can be hypothesized that dissolved  $\text{Ag}^+$  might somehow have competed as an agonist in transmembrane  $\text{Ca}^{+2}$ -pumps channels from epithelial sheet to spiculogenic cells.

### 1.7.3 PAAm-AgNPs toxicity mechanism

Coming back to PMCs fusion, whilst  $\text{Ag}^+$  and f-SWCNTs+ $\text{Ag}^+$  deformed clusters were mostly formed as a undefined syncytial mass, those caused by PAAm-AgNPs often had limited cells rounded up with a shared membrane presumably because of a lower concentration of dissolved silver in PAAm-AgNPs exposures. This condition characterized nanosilver anomalous clusters and only appeared in  $\text{Ag}^+$  exposure during prisma stage of T5 and T6. In addition, f-SWCNTs+PAAm-AgNPs exposure generally did not result in such deformities. Widely cell fusion indicated the severity of chemical injury. It also showed how strongly silver interfered with both structure and metabolism leading to disrupted cell contact and irregular  $\text{Ca}^{+2}$  mobilization compared to nanosilver. However, to what degree does nanosilver might have driven to cytotoxic effects in such cases?

Several authors have been discussing about the major mechanism that could lead to silver nanoparticles (AgNPs) toxicity. Park et al. (2010) proposed a Trojan-horse type mechanism assuming that inside the cells AgNPs go through ionization releasing silver ions and inducing cytotoxicity. On the other hand, intracellular oxidative stress related mRNA species differentially regulated by AgNPs and  $\text{AgNO}_3$ -treated cells (Kim et al., 2010; Kim and Ryu, 2012). In comparison, Leclerc and Wilkinson (2014) argued that both  $\text{Ag}^+\text{NO}_3^-$  or nanosilver exposures generated intracellular nanoparticulate deposits of silver following *in situ* reduction or precipitation of silver in algae cells. Both  $\text{Ag}^+$  and AgNPs might be

differently involved in cytotoxicity, and this could be strongly related to which type of cells and/or organisms are contaminated. In our work, most of the developmental traits targeted by PAAm-AgNPs were only delayed when compared to the controls or silver forms supporting the hypothesis of a slow release of free silver from incorporated AgNPs. Even though spiculogenic cells underwent to physiological stress (in terms of mineral deposition) mostly in sensitive stages from T1 to T3, their activities got virtually less disturbed from T4 to T6 in PAAm-AgNPs conditions. Chemical data suggests a progressive dissolution of PAAm-AgNPs with a lower amount of  $\text{Ag}^+$  being liberated compared to  $\text{Ag}^+$  exposures. In these conditions, total dissolved  $\text{Ag}^+$  was always inferior to the values found in free silver forms exposures, which may elucidate differences concerning swimming behavior displayed by embryos and larvae intoxicated with  $\text{Ag}^+$  and PAAm-AgNPs.

Nevertheless, in order to properly address the previous question we need to assume that toxicity of nanosilver is doubtfully related to its transformation in environmental media and biological compartments. It includes their surface oxidation, release of silver ions and finally their interaction with biological molecules (McShan et al., 2014). On this purpose, chemical behavior of PAAm-AgNPs in aquatic systems (freshwater, saltwater and briny water) has been characterized in our laboratory. In fact, PAAm-AgNPs behavior in seawater is marked by a relatively slow and constant dissolution, as well as formation of small aggregates (Pelletier, unpublished results). Because of the method of synthesis, it is considered that the PAAm coating is very stable and cannot be displaced from the surface of AgNPs as such a displacement can be postulated for citrate coating AgNPs (Li et al., 2012). These nanoparticles have a complex and thick high molecular weight polyallylamine coating with chains containing amine functions with a negative polar character that may attract surrounding cationic ions from water. After preparation and a long cleanup procedure, proportion of free  $\text{Ag}^+$  caught by polyallylamine chains remained relatively high (2.5 %). Considering again ectoderm as a barrier to external ions and maybe for PAAm-AgNPs in this case, we suggest that silver ions retained by polyamine chains have been one of the sources of toxicity under nanosilver stress.

#### 1.7.4 Influence of f-SWCNTs on mechanisms of toxicity of Ag<sup>+</sup> and PAAm-AgNPs

Previous researchers have explored toxicity of carbon nanotubes (CNTs) using freshwater and marine models. Although previous work provided valuable data concerning the hazards posed by raw SWCNTs, their toxicity has been mostly related to metallic impurities originated from CNTs production by chemical vapor deposition (Hull et al., 2009). In studies reviewed, f-SWCNTs did not cause significant effects on marine invertebrates, and a new key step towards their interactions with other contaminants may shed light on their real impact in the marine environment (Templeton et al., 2006, Ferguson et al., 2008; Galloway et al., 2010). It should be noted that nominal concentrations of f-SWCNTs was 100 times higher than silver concentrations in all our toxicity tests when expressed in weight/volume (Table 1). When concentrations are expressed in molar units (using in first approximation m.w.12 for SWCNTs and 108 for silver), the molar ratio between carbon and silver was about 900 for all concentrations used. But the functionalization level of f-SWCNTs was estimated to 7.5% (Berjeb et al., 2013) which means that about 60 sites of functionalized carbon could be available for each Ag<sup>+</sup> in solution.

The mechanisms by which metal ions interact with carbon nanotubes are complex and are mainly attributed to electrostatic attraction (Rao et al, 2007; Frolov et al., 2010). Protons of carboxylic groups of f-CNTs exchange with metal ions in aqueous solution, thus liberating H<sup>+</sup> and reducing pH (Rao et al., 2007). Frolov et al. (2010) stated that because ions and CNTs are surrounded by water molecules, they both have a layer called hydration shell where interactions of ions-CNTs are expected to take place. Contrarily to small ions, big ions have a low surface charge density allowing them to make some direct contacts with CNTs when they randomly lose water molecules (Frolov et al., 2010). It is quite possible that carboxylic groups of f-SWCNTs would intensify these interactions with Ag<sup>+</sup>, herein considered as a large ion. Our overall analysis of *in vivo* morphological features during Ag<sup>+</sup> and f-SWCNTs+Ag<sup>+</sup> treatments brought many questions about which mechanism would be possibly involved with f-SWCNTs+Ag<sup>+</sup> toxicity. Most sensitive stage

contaminated at T1 with Ag<sup>+</sup> showed overwhelming effects over major events of gastrulation compared to f-SWCNTs+Ag<sup>+</sup>. Over time, however, both contaminants seemed to have similar effects on embryogenesis. Abnormal congregations of spiculogenic cells provided another proof to support this point.

Later on, when early echinoplateus arose in the cultures, f-SWCNTs+Ag<sup>+</sup> became essentially the most toxic of T6 treatment. The chemical data further confirmed high levels of Ag<sup>+</sup> in such conditions. Assuming that gut regionalization in three functional compartments relies upon a complex and sensitive molecular network operating along early pluteus larvae development (Annunziata et al., 2014), we suggest that Ag<sup>+</sup> free ions were carried by f-SWCNTs into gut lumen interfering with differentiation process. Formation of larval gut depends on continuous movements of endodermal cells requiring permanent regulation of adhesive properties of archenteron cells. Cell ability to modify adhesiveness properties is a key factor for remolding the hollow tube into a new gastrointestinal tract (Miller and McClay, 1997). Hence, stomodeum opening would have provided a new route to contaminated seawater when patterning of sea urchin endoderm was still on the process. Contrarily to hindgut that keeps up with cell specification throughout late gastrula and prism stages; foregut and midgut undergo morphological changes readily from late gastrula on, when regions are molecularly defined (Annunziata et al., 2014). Starvation during late stages of prisma and early 2 arms-echinoplateus stage might also have contributed to the severity of intoxication driven by f-SWCNTs+Ag<sup>+</sup>. Some mechanisms that explain f-SWCNTs internalization postulated by Yaron et al. (2011) should be also considered. According to these authors, f-SWCNTs are first absorbed onto cell membrane, where they get trapped. As a result, tension between inner and outer membrane layers increases leading cells to trigger endocytosis in order to regulate this tension. Hence, bundles of f-SWCNTs are taken inside the cells and finally enter cytoplasm when endosomes shrink. Much as this process may be reduced at low temperatures as 4°C (Yaron et al., 2011), this mechanism has to be considered and would allow f-SWCNTs+Ag<sup>+</sup> trafficking directly into the cells of embryos and prisms.

Noteworthy, Rance et al., (2010) demonstrated that interactions between functionalized carbon nanotubes (f-CNTs) and nanoparticles are supposed to be primarily governed by short-range van der Waals forces as well. Nonetheless, our hypothesis to explain general low toxicity of f-SWCNT+PAAm-AgNPs is based on the ability of carboxylated acid groups of f-SWCNTs to rather take Ag<sup>+</sup> free ions liberated from polyallylamine chains; and Ag<sup>+</sup> ions dissolved from nanoparticles core over time. Chemical data showed higher dissolved Ag<sup>+</sup> levels in f-SWCNT+PAAm-AgNPs exposure medium when compared to PAAm-AgNPs, thus supporting our view. Besides that, chlorine (Cl<sup>-</sup>) affinity for silver in seawater might be another factor that complexifies all these dynamic interactions.

### **1.7.5 Recovery period after acute exposures**

The severity of intoxication caused by each contaminant led to late consequences in the larvae development after exposures. In general, abnormal larvae in NC2 and NC3 concentrations had either deformed skeleton or no skeleton even after recovery time, indicating permanent disruption of Mg<sup>+2</sup>/Ca<sup>+2</sup> metabolism and/or mineralization patterning guided by spiculogenic cells. Normal larvae particularly appeared at T6 of PAAm-AgNPs (NC2) recovery media and confirmed our previous findings about gastrointestinal tract molding during T6 treatment. Small echinoplutei mainly found in f-SWCNTs+PAAm-AgNPs (NC2), PAAm-AgNPs (NC3) and f-SWCNTs+Ag<sup>+</sup> (NC3) recovery conditions may exemplify another metabolic response to toxicants. In this case, low levels of dissolved silver combined with starvation at final times of exposure period might have affected normal development. Hence, organisms would likely have had an increase in metabolic maintenance requirements. Because recovery experiments were performed at low temperature (5°C), some arrested gastrula and echinopluteus with dysfunctional gastrointestinal tract were able to live throughout recovery time without feeding.

Sensitivity to contaminants changed over time during early development stages, as seen at T4 with PAAm-AgNPs. Moreover, mid-to-late gastrula (T4) had high variability in mortality ratio and spiculogenic syncytium equally disrupted by silver and nanoforms in

both 48h and 96h. Thus, mid-to-late gastrula might be seen as the first embryological stage (before prisma formation) able to withstand against silver or nanosilver stress combined or not with f-SWCNTs. However, f-SWCNTs+Ag<sup>+</sup> mixtures were so toxic that mortality during recovery was equally high for all treatments (T1-T6). Herein, mortality driven by f-SWCNTs mixtures may be interpreted as a far-reaching consequence of their dynamic interactions with silver.

## 1.8 SUMMARY AND CONCLUSION

To our knowledge this study is first to report on acute and late effects of dynamic interactions driven by f-SWCNTs associated to Ag<sup>+</sup> and polymer-coated silver nanoparticles. Following our detailed observations of effects on six successive development stages of an echinoderm, we proposed the main mechanisms of toxicity that were most probably involved in these cases and their impacts on each early development stage of *S. droebachiensis* living in cold waters. PAAm-AgNPs were less toxic than Ag<sup>+</sup> and their toxicity seemed to be mainly related to silver ions trapped by stabilizing layer and slow core dissolution in seawater. Late effects of prior exposure to f-SWCNTs+Ag<sup>+</sup> in all stages induced the highest mortality during the recovery period. f-SWCNTs seemed to make the small amount of dissolved silver in f-SWCNTs+PAAm-AgNPs conditions more available to the organisms over time. Also, our results give new insights about how each step of embryogenesis and morphogenesis of early larva could be used as targeted endpoints in a real world scenario where contaminants are released in pulses at different intervals over a long period of time. Our results show that the interactions between engineered nanomaterials and dissolved metals such as silver in seawater are real and induce complex effects on all development stages of a model marine invertebrate. The effects were not reversible in most cases and a large number of exposed larvae did not survive to the recovery conditions.

## CHAPITRE 2

### EFFETS PHYSIOLOGIQUES ET REONSES CELLULAIRES DES LARVES METAMORPHIQUES ET JUVENILES D'OURSIN APRES L'EXPOSITION A L'ARGENT IONIQUE ET AUX NANOPARTICULES D'ARGENT

#### 2.1 RÉSUMÉ EN FRANÇAIS DU DEUXIÈME ARTICLE

L'utilisation généralisée de nanoparticules d'argent (AgNPs) amène vraisemblablement à leur rejet dans les eaux usées et à la libération inévitable dans les zones côtières densément peuplées. Il est reconnu que les AgNPs peuvent provoquer des effets néfastes sur la faune marine, mais la façon dont ils affectent les stades de développement reste une question ouverte. Afin de comprendre en détails comment AgNPs enrobés de polymère (PAAm-AgNPs) (0,19 à 4,64 mM comme Ag) peuvent affecter les stades critiques du développement des invertébrés marins, les larves métamorphiques et juvéniles d'oursin ont été utilisées comme modèles biologiques. L'approche multidimensionnelle basée sur une matrice de similarité Bray-Curtis (MDS) avec PERMANOVA a représenté les organismes dans un espace multivarié à des différentes conditions physiologiques en fonction du temps, des formes chimiques d'argent, des concentrations nominales, et de la présence ou l'absence de nourriture. Les effets sublétaux comme la léthargie, la formation d'œdèmes et l'immobilité ont principalement caractérisé les effets des PAAm-AgNPs chez les juvéniles et les postlarves, alors que la nécrose et la mort ont surgi lors des expositions aux Ag<sup>+</sup>. Les larves métamorphiques chroniquement exposés à l'argent ont eu leurs processus morphogéniques interrompus par les PAAm-AgNPs et sont mortes en grand nombre dans la période de récupération. Au contraire, les ions Ag<sup>+</sup> ont causé une mortalité progressive lors de l'exposition, mais une récupération relativement rapide dans l'eau de mer non contaminée s'est produite. A l'aide des marqueurs fluorescents, nous avons montré que les AgNPs pouvaient être transférées entre

les stades consécutifs (des larves planctoniques aux postlarves). De plus, l'importance de la nourriture pour optimiser l'assimilation des PAAm-AgNPs a été remarquée. Nous avons observé par microscopie électronique à transmission que les juvéniles à jeun avaient des agrégats de nanoAg majoritairement limités à leurs sinus cœlomiques, alors que les larves métamorphiques avaient déjà les nanoAg répandues dans différents tissus et la blastocoèle. Notre principale hypothèse pour expliquer la nanotoxicité des PAAm-AgNPs repose sur la lente dissolution du noyau de nanoAg au fil du temps, mais dans cette étude les effets de la nanoparticule elle-même ont également été évoqués. Les mécanismes principaux liés aux réponses tissulaires et cellulaires à la nano-intoxication tels que la réaction inflammatoire et de désintoxication à l'aide des cellules sentinelles (cellules péritonéales et cœlomocytes) sont discutées. Ce document est le premier qui discute en détail les états physiologiques des organismes contaminés par les AgNPs, ainsi que les voies principales d'assimilation et la réponse cellulaire contre le nanoAg dans les stades de développement d'une espèce d'invertébré marin.

Ce deuxième article, intitulé «*Physiological effects and cellular responses of metamorphic larvae and juveniles of sea urchin exposed to ionic and nanoparticulate silver*», fut corédigé par moi-même ainsi que par le professeur Émilien Pelletier. Il fut accepté pour publication dans sa version finale en 2016 par les éditeurs de la revue *Aquatic Toxicology*. En tant que premier auteur, ma contribution à ce travail fut l'essentiel de la recherche sur l'état de l'art, le développement de la méthode, l'exécution des tests de performance et la rédaction de l'article. Le professeur Ciro Ribeiro, deuxième auteur, m'a reçu dans son laboratoire pour une formation en Microscopie électronique à transmission et a participé aux séances d'analyse préliminaire des organismes contaminés. Le professeur Émilien Pelletier, troisième auteur, a fourni l'idée originale. Il a aidé à la recherche sur l'état de l'art, au développement de la méthode ainsi qu'à la révision de l'article.

## **2.2 PHYSIOLOGICAL EFFECTS AND CELLULAR RESPONSES OF METAMORPHIC LARVAE AND JUVENILES OF SEA URCHIN EXPOSED TO IONIC AND NANOPARTICULATE SILVER**

### **2.3 ABSTRACT**

The widespread use of silver nanoparticles (AgNPs) would likely result in their discharge into wastewater and inevitable release in densely populated coastal areas. It is known that AgNPs can cause harmful effects to marine fauna, but how they affect development stages is still an open question. In order to understand in details how polymer-coated AgNPs (PAAm-AgNPs) (from 0.19 to 4.64 mM as Ag) can affect critical stages of marine invertebrate development, metamorphic larvae and juveniles of sea urchins were used as biological models. Multidimensional scaling (MDS) approach based on Bray-Curtis similarity matrix with PERMANOVA showed organisms in a multivariate space undergoing through different physiological conditions as a function of time, chemical forms of silver, nominal concentrations, and presence or absence of food. Sublethal effects such as lethargy, oedema and immobility mainly characterized PAAm-AgNPs effects with juveniles and postlarvae, whereas necrosis and death arose in  $\text{Ag}^+$  conditions in short-term tests. Chronically exposed metamorphic larvae had their morphogenic processes interrupted by PAAm-AgNPs and a high mortality rate was observed in recovery period. On the contrary,  $\text{Ag}^+$  ions caused progressive mortality during exposure, but a quick recovery in uncontaminated seawater was observed. By means of fluorescent markers we showed that nanosilver could be transferred between consecutive stages (swimming larvae and postlarvae) and highlighted how important is food to enhance PAAm-AgNPs uptake. Using TEM we observed that unfed juveniles had nanosilver aggregates mostly restricted to their coelomic sinuses, while metamorphic larvae already had nano-contamination overspread in different tissues and blastocoel. Our main hypothesis for nanotoxicity of PAAM-AgNPs relies on the slow dissolution of nano-core over time, but in this study the effects of particulate silver form itself are also evoked. Main mechanisms governing tissular and cellular responses to nano-intoxication such as inflammatory response and detoxification

based on the role of sentinel cells (peritoneal cells and coelomocytes) for general homeostasis are discussed. This paper is first to detail physiological states, main uptake routes and cellular response against polymer-coated AgNPs in developmental stages of marine invertebrate species.

#### 2.4 INTRODUCTION

The use of silver nanoparticles (AgNPs) in consumer products is widespread in most countries around the world. Considering well-known biocide and thermo-electrical properties of AgNPs, manufacturers have been searching for new applications in areas such as health and fitness, electronics and computers, food industry, goods for children and many others. As a result, AgNPs are largely released into the environment through untreated wastewaters which is leading to their continuous input to coastal marine ecosystems (Fabrega et al., 2011; Kaegi et al., 2015). Because AgNPs release dissolved silver ( $\text{Ag}^+$ ), particularly in seawater, nearshore organisms may face some particular toxicological risks. Therefore, unraveling AgNPs harmful effects in marine ecosystems with realistic scenario approaches is highly suitable (Wang et al., 2014).

The life cycles of most benthic marine invertebrates involve both pelagic and benthic environments with dispersive free-living stages that may be feeding or non-feeding larvae. Thus, owing their different habitats and successive morphological changes, developmental stages become an interesting tool to investigate mechanisms underlying sublethal responses against nano-contamination. It is well established that developmental stages are much more sensitive to environmental disturbances than adults, with sensitivity variating between stages as well (Byrne, 2011; Weis, 2014; García-Alonso et al., 2014). These differences may be explained by multiple aspects related to development such as increasing capacity of detoxification, improved cellular response against chemical insult through time, and growing body providing new barriers or targets that can reduce general steady state with dispersed toxicants.

Nowadays, there is a growing body of evidence showing nano-sized silver as main disruptor in marine invertebrate's development. Under short-term exposures and high concentrations (0.3 - 3.0 mg L), citrate-stabilized AgNPs of different sizes (5-35 nm) were found more toxic than correlated treatments with  $\text{Ag}^+$  ions in embryos and early larvae of sea urchin *Paracentrotus lividus* at 18-19°C (Šiller et al., 2013). Low concentrations (1-100  $\mu\text{g}\cdot\text{L}^{-1}$  range) of 60-nm AgNPs also caused strong deleterious effects on developing embryos of Mediterranean urchins *Arbacia lixula* and *Sphaerechinus regularis* in short-term treatments compared to equivalent  $\text{AgNO}_3$  concentrations at 16-20°C (Burić et al., 2015). García-Alonso et al. (2014) observed that a toxic response of embryos, trophophore, metatrophophore larvae and juveniles of polychaete *Platynereis dumerilii* emerged as a function of silver sources (free  $\text{Ag}^+$ , citrate-capped AgNPs or humic acid-coated AgNPs), silver concentrations, and their life stage at 18°C. Interestingly, the highest lethal toxicity and sublethal responses were associated to higher uptake rates of humic acid-coated AgNPs. Likewise, some tolerance to silver nanomaterials in low concentration ( $< 50 \mu\text{g}\cdot\text{L}^{-1}$ ) appeared with non-feeding larvae of coral *Acropora japonica* exposed to silver nanocolloids (57.2 ± 3.6 nm) (Suwa et al., 2014). In a recent publication, we showed mid-to-late gastrula as the first stage resilient to polymer coated AgNPs (15 ± 5 nm) effects in mid-range concentrations (50 and 100  $\mu\text{g}\cdot\text{L}^{-1}$ ) (Magesky and Pelletier, 2015). We also described the main mechanisms governing PAAm-AgNPs toxicity on different stages of embryogenesis of green sea urchin *Strongylocentrotus droebachiensis* in cold waters (5°C). Our hypothesis to explain general low toxicity of PAAm-AgNPs among final stages of embryogenesis was based on the slow release of free  $\text{Ag}^+$  from AgNPs core compared to  $\text{AgNO}_3$  exposures.

The perimetamorphic period in sea urchin development starts with the acquisition of larval competence and goes to endotrophic postlarva (prejuvenile stage) (Gosselin and Jangoux, 1998). This period has been progressively seen as particularly sensitive to nanosilver toxicity (Suwa et al., 2014; Chin and Chan, 2015). However, it is not clear: 1) Which source of silver (ionic or nanoparticulate) would be more disruptive in this case? 2) How nano-forms are directly or not involved? 3) How they would be interfering with

metamorphosis completion? Suwa et al. (2014) demonstrated that larval survival of coral *Acropora japonica* was not affected, but metamorphic planulae failed to give rise to polyps when treated with  $50 \text{ } \mu\text{g}\cdot\text{L}^{-1}$  of silver nanocolloids at  $27^\circ\text{C}$ . That study reported high dissolution of nanocolloids as a source of toxicity emphasizing the importance of the nature of nanomaterial involved in biotests. Recently, Chan and Chiu (2015) reported that chronic exposures to large oleic acid and polyvinylpyrrolidone-coated AgNPs ( $73.54 \pm 1.34 \text{ nm}$ ) in different concentrations led to significant retardation in growth and development as well as low settlement rates of feeding larvae of polychaete *Hydroides elegans* at  $25^\circ\text{C}$ . Contaminants generate additional stress to organisms undergoing critical stages of early life, particularly metamorphosis and settlement to benthic environment (Weis, 2014). Metamorphosis is a very critical biological process for many invertebrates and so far it is unknown how defensive mechanisms against chemical contamination would operate in metamorphic stages of marine invertebrates.

Considering high density gradient in stratified estuaries and coastal waters and very slow sedimentation rate of AgNPs (Quik et al., 2014), it is expected that nanosilver can be dragged into the mixing layer of saline halocline, eventually aggregating and slowly dissolving for weeks before sedimentation. Thus, free-swimming development stages of invertebrates can be exposed to nanoparticles dispersed in seawater and feed on phytoplankton amended with silver as well. It is already known that zooplankton responds to haloclines in many ways, which include residence in or nearby the halocline and migration through it. Searching for rich feeding ground in temperate waters, echinopluteus larvae can strongly aggregate in presence of phytoplankton patches and eventually cross halocline if under starvation (Metaxas and Young, 1998; Sameoto et al., 2008). After settling, sea urchin juveniles may likely be exposed to auto- and hetero-aggregated AgNPs recently deposited to the bottom boundary layer. In fact, sea floor and benthic organisms are expected to be the ultimate targets for AgNPs in the marine environment (Buffet et al., 2014).

Taking in account the above considerations, we report here a detailed analysis of the effects of polymer coated-AgNPs and sublethal responses to nano-stress using this time, metamorphic larvae and juveniles of sea urchins as biological models. We first aimed to understand dissolved silver and polymer-coated AgNPs toxicity effects during critical perimetamorphic period and in early juveniles. We performed a multivariate analysis (PERMANOVA) with physiological states of exposed organisms in a complex numerical algorithm to construct a graphical representation of the samples pattern in a non-metric MDS ordination. Secondly, we analyzed the main routes for nanosilver uptake in cells and tissues. We also report for the first time cellular and acellular internalization of nanoparticulate silver in both development stages describing: (1) how organisms reacted to nano-contamination in terms of timing for first anomalies to raise; and (2) cell response by immune and detoxification systems correlated to chronic exposures.

## 2.5 MATERIAL AND METHODS

### 2.5.1 Preparation and characterization of silver solutions and PAAm-AgNPs suspensions

Details about synthesis, characterization of poly(allylamine)-coated silver nanoparticles (PAAm-AgNPs) and analysis of dissolved silver have been previously reported (Magesky and Pelletier, 2015) and are briefly summarized hereafter. The size and dispersion of synthesized AgNPs were assessed by transmission electron microscopy (TEM Delong Instruments LVEM 5). The average diameter of organic-coated silver nanoparticles used in our study was  $15 \pm 7$  nm ( $n = 60$ ) with some aggregates reaching about 230 nm in length in nanopure water (Supplementary material, Appendix 2). Stock solution of  $\text{AgNO}_3$  (75 mg in 100 mL) and suspension of PAAm-AgNPs (4.768 mg PAAm-AgNPs in 100mL) were prepared in nanopure water for dilution to nominal exposure concentrations. All solutions and suspensions were stored in the dark at 5°C to minimize photodegradation. For the first series of toxicity tests, larvae and juveniles were exposed to a control and four nominal concentrations chosen according to pre-screening results and named hereafter as: NC1= 500  $\mu\text{g}\cdot\text{L}$  (4.64 mM), NC2= 100  $\mu\text{g}\cdot\text{L}$  (0.93 mM), NC3= 50  $\mu\text{g}\cdot\text{L}$  (0.464 mM) and

NC4= 20  $\mu\text{g}\cdot\text{L}$  (0.19 mM). Quantification of dissolved silver in exposure media at t 0, t 6h, t 24h and t 96h was done with inductively coupled plasma mass spectroscopy (ICP-MS) as well as dissolved silver concentration in nanoAg-FITC dye solution used in experiments using confocal microscopy. First, the supernatants were ultracentrifuged at 7,400 rpm for 10 min at 4°C with centrifugal filters Ultracel-10K (Amicon Ultra-4) to remove suspended particulate matter. Clean samples were immediately stored at 5°C in the dark before analysis. Samples were then diluted in  $\text{HNO}_3$  (1:2 mL) to reduce ionic strength; digested with 0.5 mL of hydrogen peroxide and heated in water bath (60°C) a few hours before the analysis. The detection limit was 0.015  $\mu\text{g}\cdot\text{L}$ .

## 2.5.2 Fluorescent dyes

### a) Preparation of PAAm-AgNPs marked with fluorescein (nanoAg-FITC)

A solution of 10 mM of fluorescein (FITC) was prepared with nanopure water. The solution was first sonicated for 30 min to improve dissolution, and then filtered at 0.22  $\mu\text{m}$  to get rid of undissolved FITC. Then, 1.0 mL of PAAm-AgNPs stock solution was mixed with 1.0 mL of FITC and stirred for 90 min. A few drops of NaOH 0.1N were used to adjust pH to 9.0, then the solution was centrifuged once again at 25,000 rpm for 30 min to sediment nanoAg-FITC complex and leave excess FITC in solution. Supernatant was decanted and pellet resuspended in 3 mL of nanopure water. This cleanup procedure was repeated several times until no sign of fluorescence in the supernatant was observed using a fluorimeter. Final concentration of FITC nanomarker stock solution was 68.79  $\mu\text{g}\cdot\text{L}$ .

According to method developed by Tallury et al. (2009), we assumed that negative PAAm stabilizing layer surrounding AgNPs (due to amine free electron doublets) strongly interacted with neutral fluorescein (at pH 9) to form a stable organo-metal complex that allowed to track internalization of nanoparticles by organisms used in this work. FITC stock solution without nanoparticles was used as a control with 1.0 mL of nanopure water instead of PAAm-AgNPs solution.

b) Quantum dots

Qdots 525 streptavidin conjugate (1 $\mu$ M) (Q10143MP, Molecular probes) were used as a probe to compare with nanoAg-FITC fate inside organisms and had 15-20 nm in diameter. Qdots were made from a nanometer-scale crystal of a semiconductor material (CdSe) coated with a ZnS semiconductor shell. The core-shell material is additionally coated with an organic polymer layer (second shell) allowing them to interact with biological molecules and fully retain their optical properties. The second shell is also coupled to streptavidin. Qdots were immersed with 0.05% sodium azide.

c) SYBR Green

Commonly used as DNA binding dye, SYBR Green I (Molecular probes) was used to help us to understand cellular organization in necrotic and oedemic areas during contamination. It allowed to properly categorize anomalies found in short-term exposures. This marker preferentially binds to double-stranded DNA and in a lower extent to single-stranded DNA and RNA. Samples were dyed with 1.0  $\mu$ L of SYBR Green I in 300  $\mu$ L of seawater and washed with clean seawater before observations.

### 2.5.3 Sea urchin collection, spawning and larvae handling

Collection of young adults sea urchin *Strongylocentrotus droebachiensis*, laboratory conditions, spawning techniques as well as embryos handling have been previously described (Magesky and Pelletier, 2015). Immediately after collection, urchins were acclimatized in large flow-through tanks at 5°C ( $\pm$  2°C) with physical and chemical parameters very similar to the natural environment and the specimens in captivity regularly fed *Laminaria* sp. in *ad libitum* conditions. To obtain healthy cultures of larvae, fertilized eggs from three females were first placed into 3,500 mL of filtered seawater. This suspension was again diluted 70 times in filtered seawater, ending up with a suspension of about 25 larvae per mL. Cultures were kept under gentle agitation in cold chamber at 8°C. To keep them in good conditions, filtered seawater (0.7  $\mu$ m) was changed every three days which resulted in low mortality, optimal conditions and fast development. Early prisma and

larvae were fed with a mixture of 15 mL of *Dunaliella tertiolecta* ( $4.3 \times 10^6$  cells/mL) and 5 mL of *Isochrysis galbana* ( $3.0 \times 10^5$  cells/mL) injected into the cultures. Final concentrations of each species were  $1.84 \times 10^4$  cells/mL and  $4.28 \times 10^2$  cells/mL, respectively. After 5-6 weeks, L8-echinopluteus went through a metamorphosis period. Postlarvae and juveniles were kept in small aquaria at 8°C with unfiltered seawater (4,000 mL) renewed each 5 days. Exotrophic juveniles fed on biofilm from glass walls, but we also added 10 mL of *Chaetocerus muelleri* ( $1.52 \times 10^7$  cells/mL) + *D. tertiolecta* or *I. galbana* to ensure a complementary diet when seawater was changed. This time, final concentration of phytoplankton totalized  $4.9 \times 10^4$  cells/mL. Health conditions of animals were sporadically assessed by measuring oxidative stress with CellRox green Reagent (Molecular probes) in confocal microscopy. Healthy cohorts of juveniles were successfully cultured for over one year.

#### **2.5.4 Experimental Design**

##### a) Toxicity tests

For toxicity tests with echinoderm larvae undergoing metamorphosis, 12-well tissue culture plates with flat bottom (Falcon 353043, polystyrene made) were used, each one filled with 5.5 mL of sea water filtered through 0.45  $\mu\text{m}$  membrane and 30 larvae transferred into it. Only one sublethal nominal concentration (100  $\mu\text{g}\cdot\text{L}^{-1}$ , NC2) was used. Late 8-arm echinoplutei (L8<sub>2</sub>) with about 2 mm in diameter were chosen as test organisms considering short period needed to go through metamorphosis at 8°C. They were exposed to 100  $\mu\text{g}\cdot\text{L}^{-1}$  of Ag<sup>+</sup> and PAAm-AgNPs upon feeding on 200  $\mu\text{L}$  of *D. tertiolecta* of final concentration of  $3.12 \times 10^4$  cells/mL. Larvae were exposed for 3 successive periods of 96h (288h), with conditions renewed each 96h. Recovery period began after final exposure with the transfer of larvae in clean water and food supplied again for 3 periods of 96h. L8<sub>2</sub>/postlarvae-juveniles ratio was assessed in exposure and recovery periods every 96h. All these tests were independently repeated three times.

Endotrophic forms (postlarva) and exotrophic juveniles were also tested separately. Postlarvae 3-4 days old had an average 0.28 mm in diameter while 2-month old juveniles were about 1.05 cm large. We conducted acute exposures (96h) in 48-well cell culture plates (Corning Costar 3548) filled with filtered 1.5 mL of seawater at 8°C. Each test consisted of four nominal concentrations and a control, with six replicate wells for each concentration and the control. A 10 µL aliquot of either Ag<sup>+</sup> or PAAm-AgNPs test solution was added to each well with 5 juveniles already transferred into it. All experiments were done under a 12h light/12h dark cycle, with plates always protected against direct light exposure.

As pre-juveniles (postlarvae) are not able to feed by themselves, only exposures without food were performed with this stage. Opening mouth was not formed (or functional) before about 10 days. However, exotrophic juveniles were exposed to both conditions with and without food. To avoid overlapping effects of contaminants and food limitation during the tests, the lack of food in uncontaminated conditions as well as feeding rate were determined during prescreening tests as a function of size and time (within 96h). Four silver nominal concentrations were used in both cases (with or without food). With animals already transferred before exposure, an aliquot of 25 µL of *C. muellerii* ( $7.8 \times 10^6$  cells/mL) was added to each well, ending up with final concentrations of  $1.3 \times 10^5$  cells/mL of phytoplankton for juvenile feeding conditions tests.

Physiological conditions of postlarvae and juveniles were classified as follows: unaffected, lethargic (with retracted podia, slow movements or hypoactivity), with oedema (epidermic turgid areas), immobility, necrotic (spines falling off and/or wounded epidermis), dead (total lack of response to stimulus) as a function of elapsed time. Observations were made at 3h, 6h, 12h, 24h, 48h and 96h with a stereo-microscope. Toxicity tests were performed according to the Standard guide for conducting static acute toxicity tests with echinoids embryos E1563-98 (ASTM, 2004).

b) Exposure of organisms to fluorescent dyes in confocal microscopy

Tests were performed in 12-well tissue culture plates using 30 larvae and 5 postlarvae or juveniles per well. Each well was first filled up with 5.5 mL of filtered sea water. Experiments were separately performed with 4 different developmental stages: early L8<sub>1</sub> (1), early L8<sub>2</sub> larvae (2), postlarvae (3) and exotrophic juveniles (4). Time for exposure was 96h, with *in vivo* observations at 6, 24 and 96h by confocal microscopy. At t = 0h, 1.0 µL of fluorescent dye (FITC, nanoAg-FITC or Qdots 525 streptavidin conjugate) was transferred into the wells. For fluorescent markers, early L8<sub>1</sub> and exotrophic juveniles were exposed with and without phytoplankton whereas competent larvae, L8<sub>2</sub>, with phytoplankton and post-larvae without it.

c) Exposure of organisms to PAAm-AgNPs for TEM observation

One-month old juveniles (mean diameter 0.51 mm) were chosen as biological model to track PAAm-AgNPs inside tissues by TEM. Animals (n = 5 per well) were exposed to 100 µg·L of PAAm-AgNPs without phytoplankton, under 24h photoperiod, during 288 h (3 x 96h) in 48-well cell culture plates (Corning Costar 3548) filled with 1.5 mL of filtered seawater at 8°C. Seawater was renewed each 96h as well as the contaminant. Two-month old juveniles were also exposed to 50 µg·L of PAAm-AgNPs without food.

Additionally, early 8-arms echinoplutei larvae (L8<sub>1</sub>) contaminated with 100 µg·L of PAAm-AgNPs and 200 µl of *D. tertiolecta* for 288 h (3 x 96h) were analyzed by TEM. In this case we used 12-well tissue culture plates (Falcon 353043) filled with filtered sea water; and 30 larvae feeding on  $3.12 \times 10^4$  phytoplanktonic cells/mL per well. Right after the final assessment, remaining competent larvae L8<sub>2</sub> were taken up and fixed in 2.5% glutaraldehyde in 0.1M cacodylate buffer, pH 7.4 mixed with sea water (1 mL: 0.5 mL) and kept at 5°C for 3 months before observation by TEM. Juveniles were fixed following the same conditions.

### 2.5.5 Observations in confocal microscopy

For each sampling time (6h, 24h, 96h), we randomly took 10 larvae or 3 juveniles for *in vivo* observations using Inverted microscope Axio Cam Observer Z1 and Laser scanning microscope in confocal microscopy (LSM700 Carl Zeiss) under 10X, 40X, 63X magnifications. Specimens were anesthetized with 2.5 µL of 100% ethanol injected into 300 µL of seawater on the glass bottom dishes. A small volume of ethanol did not interfere with florescence observation. Differences between control and nanoAg-FITC exposed samples were determined by measuring the distribution of pixel intensities in freehand profile inside a Euclidean space. We first studied these intensities creating profiles by means of curved or straight lines drawn on the image surface. The high quality steep profiles were acquired with confocal XY measurements profiles (raw data) for comparison. Owing to set significant differences with statistic data among conditions tested, we used histogram function (histo view) measuring regions of interest and obtaining mean intensity, standard deviation ( $\sigma$ ), and number of pixels and size of area ( $\mu\text{m}^2$ ) of reflected light images.

### 2.5.6 Sample preparation for Transmission electronic microscopy (TEM)

Long time preservation (considered here as primary fixation) led to complete decalcification prior to the next steps of sample preparation for TEM. Larvae were first centrifuged and were treated as a pellet. Then, we proceeded to cleanup steps with 3 washes (10 minutes duration each) in cacodylate buffer with sucrose at pH 7.4. Then, we followed secondary fixation, second wash, dehydration, infiltration, embedding, and polymerization steps according to Mukhopadhyay (2003) protocol. Because our samples had high lipid levels, they were placed in oven at 60 °C for 3 days (instead of 24h) to get the best consistency before going to the microtome. We proceeded first with the semi-tin cross-section (0.5-1µm) step and then to ultra-thin sections (50-70 nm) which were assembled onto HCl pre-cleaned metal grids. These grids were immersed in uranyl acetate for contrast enhancement of cellular structures and nanosilver, and then dried. Non-contrasted images exhibiting marked contrast of nanoparticles inside cells or over tissues were considered as

the controls for PAAm-AgNPs contamination, and contrasted images were used to identify specific tissues and cells.

### 2.5.7 Statistical analysis

Due to a complex sampling structure and experimental design with more than one factor, including interactions; we conducted data analysis using a non-parametric rank-based approach provided by PERMANOVA+ (Clark et al., 2014). This method shows robustness and flexibility based on resemblance measures (by distances in dissimilarity and similarity), but also making no explicit assumptions related to distribution of original samples. Thus, we rather worked on rank of dissimilarities of samples using permutations analysis of variance (PERMANOVA) in a multivariate space to obtain *P*-values with Primer 6.1.1.12 and Permanova+ 1.0.2 software.

After factors were chosen, we square root transformed the data before resemblance analysis based on Bray Curtis similarity matrices. Then, groups and their relationships were visualized by MDS (non-metric multidimensional scaling) analysis. MDS plots can be considered as approximations to the true sample relationships obtained in the resemblance matrix; and whose dimensionality is reflected by stress numbers. For instance, stress <0.05 provides an excellent representation with no prospect of misinterpretations (Clark et al., 2014).

To test the homogeneity of multivariate dispersions, we performed PERMDISP and finally to determine the significant effects, the Permanova two-way crossed pairwise tests with permutation of residuals under a reduced model (for two or more factors) and unrestricted permutation of raw data (for one factor) were used. In order to compare values of units of intensity from areas of interest of exposed organisms to fluorescent dyes in different conditions, we used Student's *t*-test with unpaired analysis.

## 2.6 RESULTS

### 2.6.1 Distribution of dissolved, particulate and adsorbed silver in exposure wells

Considering the chemical form of silver as a determining factor of its toxicity for development stages of sea urchin (Magesky and Pelletier, 2015), chemical analysis of dissolved free silver in seawater and residual silver adsorbed to inner wall of the exposure wells was performed for the typical exposure case of 100 µg·L (NC2) for dissolved and nanoparticulate silver. This analysis was made with larvae feeding on phytoplankton to assess the possible adsorption role of plankton cells on silver distribution (Table 1).

Table 3: Distribution of silver chemical forms in exposure wells as a function of time for larvae exposed to nominal concentration of 100 µg L (NC2) of silver nitrate or PAAm-AgNPs in presence of phytoplankton. Particulate silver (%) is obtained by substraction of free and wall adsorbed silver from 100%.

Toxicant	Exposure Time (h)	Dissolved free silver (%)	Adsorbed silver on inner wall of wells (%)	Particulate silver in larvae and plankton (%)
$\text{AgNO}_3$	0	50.0	22.5	27.5
	24	57.5	9.8	32.7
	96	30.3	10.9	58.8
PAAm-AgNPs	0	36.2	20.1	43.7
	24	35.1	12.2	52.7
	96	3.1	8.5	88.4

In the first 24h, the proportion of dissolved silver (labelled as free  $\text{Ag}^+$  and being soluble chloro-complexes and/or soluble organic-complexes of silver) in presence of phytoplankton was higher (50 to 57.5%) compared to exposure media with nanosilver (36.2 to 35.1%). Dissolved silver in media has decreased after 96h to about 30% in  $\text{AgNO}_3$  treatment and 3.1% in PAAm-AgNPs one, most probably due to adsorption and hetero-aggregation to larvae and phytoplankton cells in wells. Adsorption of dissolved and

nanoparticulate silver to inner wall of wells decreased with time in first instance, but remained about the same between 24h and 96h.

When exposing juveniles to 100 µg·L (NC2), a relatively different chemical pattern was observed (Table 2) compared to larvae media. The adsorption of silver on inner wall of wells was generally very low (<1%) with a slow increase with time in wells without phytoplankton. The difference with larvae exposure (Table 1) might be explained by the size of wells being much smaller with juveniles and the grazing activity of juveniles on the wall of the wells.

Table 4: Distribution of silver chemical forms in exposure wells as a function of time for juveniles exposed to nominal concentration of 100 µg·L (NC2) of silver nitrate or PAAm-AgNPs with or without phytoplankton. Particulate silver (%) is obtained by substraction of free and wall adsorbed silver from 100%.

Feeding condition	Toxicant	Exposure time (h)	Dissolved free silver (%)	Adsorbed silver on inner wall wells (%)	Particulate silver on larvae and/or phytoplankton (%)
Without phytoplankton	$\text{AgNO}_3$	0	35.2	< 1	>64.8
		6	52.2	< 1	>47.8
		24	22.1	6.7	71.2
		96	15.7	19.5	64.8
	PAAm-AgNPs	0	32.8	<1	>67.2
		6	28.4	<1	>71.6
		24	21.2	1.8	77.0
		96	38.3	9.2	52.5
With phytoplankton	$\text{AgNO}_3$	0	38.7	< 1	>61.3
		6	56.6	< 1	>43.4
		24	21.2	< 1	>78.8
		96	15.9	< 1	>84.1
	PAAm-AgNPs	0	20.7	< 1	>79.3
		6	22.6	< 1	>77.4
		24	20.3	< 1	>79.6
		96	38.5	< 1	>61.5

Otherwise, the distribution of «free silver» was quite similar with or without phytoplankton for both  $\text{AgNO}_3$  and PAAm-AgNPs with a lower proportion when using PAAm-AgNPs with phytoplankton. The highest values of free  $\text{Ag}^+$  were observed at  $t = 6\text{h}$  for  $\text{AgNO}_3$  exposure, and the lowest ones were also with  $\text{AgNO}_3$ , but after  $96\text{h}$  which is consistent with the expected adsorption of free Ag on larvae and phytoplankton cells. The mean values of free silver with time for  $\text{AgNO}_3$  and PAAm-AgNPs with and without plankton were 31.3%, 31.2%, 33.1% and 25.5%, respectively. These means values are not significantly different from each other ( $p > 0.05$ ), which is an indication that all juveniles have been exposed to similar concentrations of dissolved silver during the course of the toxicity tests.

### **2.6.2 Toxicity tests**

#### a) Toxicity effects of PAAm-AgNPs and $\text{Ag}^+$ during perimetamorphic period

Results of permutational analysis showed organisms going through metamorphosis from competent larvae (early L<sub>82</sub>) to postlarvae and juveniles during contamination and recovery periods (Figure 18). We considered contaminants and periods (exposure and recovery) as factors interfering with completion of metamorphosis. Each label represents 30 animals (per well) in elapsed time of controls and contaminated wells, 18 replicates per condition. Inter-point distances among these labels reflect the same rank order as the dissimilarities between our samples in dissimilarity matrix created for MDS construction. Thus, the multivariate space indicates two crossed axes representing exposure and recovery periods through which larvae completed metamorphosis. Similarities and dissimilarities seen in MDS correspond to proportions between competent larvae L<sub>82</sub> and postlarvae-juveniles that keep changing along perimetamorphic period as a function of time and water conditions (with or without contaminants).

Both plots in Figure 18 indicate two main clouds separated by a central shift showing each one was mostly composed of postlarvae/juveniles or larvae throughout exposure period and recovery. Completion of metamorphosis in PAAm-AgNPs-controls

progressively occurred during exposures reaching 56.4% (96h<sub>1</sub>) to 79.8% (96h<sub>3</sub>) of postlarvae/juveniles emerging into the wells. By the end of PAAm-AgNPs exposure time (96h<sub>3</sub>), only 2.0% of controls remained as competent larvae. As a result, labels representing postlarvae and juveniles in each time (T1, T2 and T3) were rather placed ahead on the juvenile-exposure axis in a space shared with juvenile recovery axis (Figure 18 A).

A few points from controls away from the main cloud indicated replicates with still high proportion of larvae over postlarvae/juveniles. At first week of recovery time (96h<sub>1</sub>), only 48.3% of PAAm-AgNPs-treated organisms were found as postlarvae or juveniles, however, they continued to emerge at 96h<sub>2</sub> (74.4%) and 96h<sub>3</sub> (81.2%) in clean water, which placed labels together with controls cloud. Labels located between L8<sub>2</sub> exposure and L8<sub>2</sub> recovery axes indicate the similarity of samples whose individuals mostly remained as larvae in both periods. During PAAm-AgNPs treatment, proportion of larvae over postlarvae/juveniles remained relatively high at 96h<sub>1</sub> (91%), and also at the first time of recovery 96h<sub>1</sub> (47.5%). Hence, green triangles stayed aggregated between L8<sub>2</sub> axes reflecting larval inability to undergo metamorphosis. Larvae found into the wells at 96h<sub>2</sub> and 96h<sub>3</sub> in exposure period respectively decreased to 83.1% and 66.1%, so dark triangles (at T2) and azure squares (at T3) dispersed away from shared spaces of L8<sub>2</sub> axes.

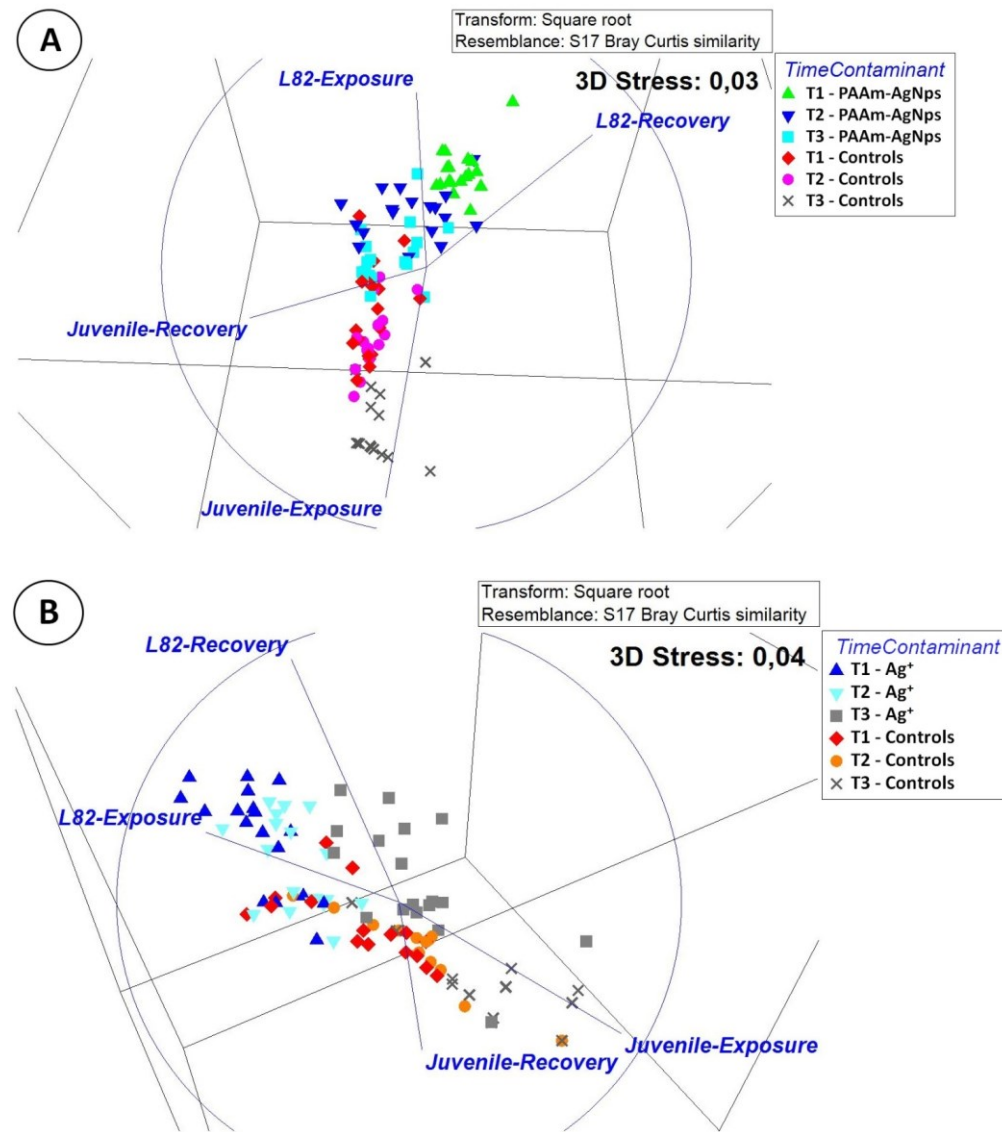


Figure 18: MDS plots with Bray-Curtis similarity analysis (PERMANOVA) of metamorphosis completion of L8<sub>2</sub> echinoplutei larvae chronically exposed to nanosilver and Ag<sup>+</sup> during exposure (3 x 96h), and recovery (3 x 96h) periods ( $p = 0.0001$ ). A- PAAm-AgNPs exposure and recovery (3D stress: 0.03). B- Ionic silver exposure and recovery (3D stress: 0.04). Sampling times for both periods are given as follows: T1= 96h<sub>1</sub>, T2= 96h<sub>2</sub> and T3= 96h<sub>3</sub>. Blue axes represent total time for exposure and recovery. Each label represents a majority of individuals categorized as larvae or postlarvae/juvenile in elapsed time for each contaminant and controls during exposure and recovery

(30 individuals per well, 18 replicates per condition: Ag<sup>+</sup>, nano-Ag<sup>+</sup> and controls, n= 1080 larvae in total).

Differently from PAAm-AgNPs conditions, free Ag<sup>+</sup> slowed down metamorphosis. Again, two main clouds appeared and grouped similar samples (Figure 18 B). The top part of upper cloud composed by dark blue and azure triangles is closer to L8<sub>2</sub>-exposure axis indicating that competent larvae were mainly found at T1 and T2 exposure periods. Yet, their proportion rapidly decreased from 68.5% at 96h<sub>1</sub>, to 59.8% at 96h<sub>2</sub> and finally to 22.4% at T3 (96h<sub>3</sub>). Hence, cloud of gray squares was positioned ahead from dark blue and azure triangles towards juvenile-exposure axis. Meanwhile, larvae from controls decreased even more from 37.5% (96h<sub>1</sub>) to 22% (96h<sub>2</sub>) and later to 9.25% (96h<sub>3</sub>) compared to contaminated siblings. With 85% of postlarvae/juveniles already formed at T3 exposure period, only 3.7% new ones appeared in controls throughout recovery. It led control labels to be restricted to shared space between juvenile-exposure and juveniles-recovery axes.

During all recovery period, only 18.7% more postlarvae/juveniles appeared in free Ag<sup>+</sup> wells compared to final time of exposure (96h<sub>3</sub>) where 75% juveniles had already emerged. This is represented by azure, dark blue gray squares mixed with control labels from exposures on the bottom of exposure axis. So, it turned out that exposure axis explained the majority of our data: metamorphosis occurred during exposure to Ag<sup>+</sup>, but was delayed through time.

Considering time and silver form, differences between free Ag<sup>+</sup> and PAAm-AgNPs treatments were significant ( $p < 0.005$ ) as well as when compared to controls ( $p < 0.0001$ ). Likewise, exposure and recovery periods for both contaminants had meaningful differences ( $p < 0.0001$ ). High mortality was caused by Ag<sup>+</sup> (n = 93; n = 27 in control) compared to PAAm-AgNPs during exposure (n = 27; n = 21 in control) ( $p = 0.0001$ ). Nevertheless, when larvae were brought to clean conditions, mortality in nanosilver media (n = 54; n = 3 in control) became twofold higher than those exposed to AgNO<sub>3</sub> (n= 7; n= 34 in control) ( $p = 0.0001$ ).

b) Physiological states of postlarvae and juveniles exposed to Ag<sup>+</sup> and PAAm-AgNPs

The first sign of intoxication observed in postlarvae and particularly in exotrophic juveniles was lethargy (3-12h). Specimens had retracted podia, slow movements (body and spines), and weaker attachment to the substratum. Within 24h, organisms became sluggish and remained attached to wells developing oedema (Supplementary material, Appendix 2). Oedematous juveniles were often inactive, attached to substratum, with red spherule cells associated with another coelomocyte type getting mobilized towards swollen areas. Turgid areas sometimes appeared in postlarvae, but with no red spherule cells. Whereas postlarvae went through severe necrosis and visible injuries at 48h, exotrophic juveniles barely showed such effects by this time even though sometimes few spines had fallen off (except for lethal NC1 concentrations).

Exotrophic juveniles not turning necrotic at 48h became mostly motionless due to gradual chemical intoxication. So, depending on the degree of intoxication, urchins in immobility state were motionless or stayed firmly adhered to substratum until podia got unattached; then spines laid down. Hence, lethargy and retracted sensorial podia indicated loss of sensory functions at a threshold from where juveniles slightly recovered when immobility state was achieved. Although highly intoxicated, sea urchins kept Aristotle's lantern and pedicellaria active, which provided a useful behavioral marker to contrast immobile from dead individuals (Supplementary Video 1, Aquatic toxicology 174: 208-27).

Necrosis and immobility conditions were grouped as one category for postlarvae because both conditions occurred at the same time (48h). Final category considered for assessment was dead (postlarvae) or necrotic/dead (exotrophic urchins) organisms. In general, exotrophic urchins near to death had strong necrosis, asynchronous movements, and spines massively dropping downward and falling off. Their lack of responses included Aristotle's lantern and pedicellaria features. Contaminated animals were classified as unaffected (no visible physiological or morphological abnormalities), lethargic, oedematous, in immobility (or necrotic/immobility) and necrotic/dead.

c) Toxicity effects of Ag<sup>+</sup> and PAAm-AgNPs in postlarvae and juveniles

Main factors analyzed with postlarvae were contaminants, nominal concentrations and elapsed time. All general interactions of factors related to the chemical stress were statistically significant ( $p = 0.01$ ). Controls are not presented on the MDS because no abnormality was found within 96h. Each label in Figure 19 A represents health conditions of contaminated postlarvae over time. Labels located close to unaffected axis mostly correspond to groups of individuals having no visible effects from 3h to 96h for both contaminants and NC3 and NC4 concentrations. It also includes animals unaffected by PAAm-AgNPs (NC2) at 96h and at the beginning of NC1 exposure. Inside this group, dark blue triangles showed dissimilarities of Ag<sup>+</sup> (NC2) samples at 24h. Other dissimilarities explain dispersing labels close to unaffected axis with a few organisms getting lethargic or oedematous.

Lethal effects emerged with 500 µg·L (NC1) as a function of time. After Ag<sup>+</sup> and PAAm-AgNPs exposures, physiological disturbances rapidly appeared until death with no significant differences between both contaminants ( $p > 0.05$ ) (Figure 19 A). Postlarvae became lethargic in the first 24h in both conditions, but oedema appeared only under Ag<sup>+</sup> (NC1). Necrosis/immobility caused by both Ag forms appeared after 48h. There were significant differences between NC1 and NC2 for nanosilver ( $p < 0.05$ ), but not for Ag<sup>+</sup> ( $p > 0.05$ ).

Noteworthy, only endotrophic forms exposed to Ag<sup>+</sup> (NC2) expressed strong chemical stress compared to AgNPs (NC2) at 96h. Postlarvae exposed to Ag<sup>+</sup> (NC2) were mostly lethargic at 48h, but died only at 96h. By contrast, postlarvae stayed mostly unaffected in AgNPs (NC2) at 96h. Differences in timing for chemical intoxication between Ag<sup>+</sup> and PAAm-AgNPs at 100 µg·L (NC2) were significant at 99.5% level ( $p = 0.005$ ).

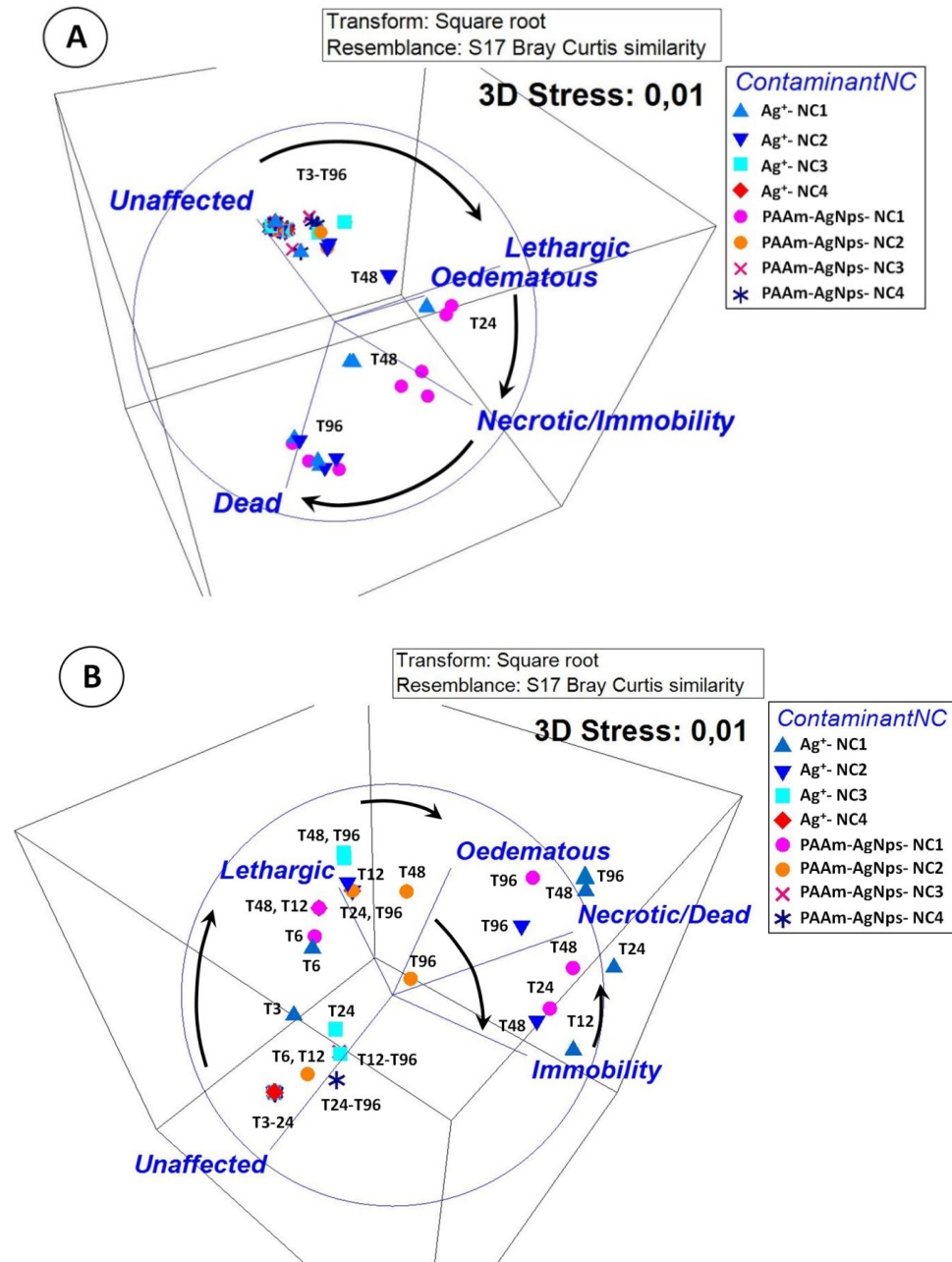


Figure 19: MDS plots with Bray-Curtis similarity analysis (PERMANOVA) of physiological conditions of postlarvae and unfed juveniles (3D stress: 0.01 for each representation) contaminated with Ag<sup>+</sup> and PAAm-AgNPs. A- Postlarvae. B- Unfed juveniles. Black arrows indicate progression of postlarvae and juvenile conditions within 96h. Each label represents a majority of organisms

having one specific physiological condition after exposure to contaminants in 6 replicates (30 individuals per nominal concentration, n= 150 in total including the controls) at different times and nominal concentrations (NC) (see *ContaminantNC* panel). Controls remained unaffected and are not included in the plot for clarity.

The same effects were observed in exotrophic juveniles, but timing for sublethal effects was particularly distinctive (Figure 19 B). Again, contaminants, nominal concentrations and elapsed time were analyzed. Very early, juveniles in starvation exposed to 500  $\mu\text{g}\cdot\text{L}$  (NC1) of  $\text{Ag}^+$  became lethargic from 3h to 6h. Green triangles (T3, T6) between unaffected and lethargic axes illustrated  $\text{Ag}^+$  (NC1) rapid effects compared to other concentrations tested along 96h ( $p < 0.05$ ). At 12h, green triangle position on the top of immobility-axis reflected severe intoxication and inactivity that continued on at 24h, with more than 50% of juveniles already dead or extremely damaged. From 48h to 96h, all specimens were considered dead.

Comparatively, unfed juveniles exposed to PAAm-AgNPs (NC1) slowly displayed similar sublethal responses from 12h to 96h, but no significant differences with  $\text{Ag}^+$  (NC1) were found ( $p > 0.05$ ). 24h was a critical period for intoxication caused by nanosilver when first animals died. At 48h, 63.3% were dead in PAAm-AgNPs media compared to  $\text{Ag}^+$  (100%). And as observed in  $\text{Ag}^+$  (NC1) treatment, 90% of urchins died at 96h; which placed labels near to necrotic/dead axis. Analyzing timing for sublethal responses to  $\text{Ag}^+$  and PAAm-AgNPs, we found significant differences between  $\text{Ag}^+$  (NC1) and (NC2) ( $p = 0.0001$ ); and PAAm-AgNPs (NC1) and (NC2) ( $p < 0.005$ ).

Treatments with 100  $\mu\text{g}\cdot\text{L}$  (NC2) also brought meaningful dissimilarities between both contaminants when timing for anomalies rising were compared ( $p = 0.0001$ ). At 12h, whereas  $\text{Ag}^+$ -treated juveniles got lethargic, no effects were detected in PAAm-AgNPs conditions. Ionic silver caused rapid immobility following 48h, but organisms exposed to PAAm-AgNPs stayed mostly lethargic. 16.3% of mortality caused by  $\text{Ag}^+$  (NC2) at 48h shifted to 63.3% at 96h. Under PAAm-AgNPs (NC2) conditions, only 16.6% of juveniles died at 96h. Under lower concentrations NC3 and NC4, lethargy only occurred in  $\text{Ag}^+$

exposure at 48h and 96h, with no differences between treatments ( $p > 0.05$ ). No lethargy was detected under NC3 and NC4 treatments with PAAm-AgNPs compared to Ag<sup>+</sup>. Oedema appeared at 12h up to 96h with Ag<sup>+</sup> (NC3, NC4) and at 24 up to 96h (NC3, NC4) in PAAm-AgNPs wells.

Under *ad libitum* feeding conditions, juveniles Ag<sup>+</sup>-treated exhibited a cutting-off effect of silver toxicity compared to assays with no food ( $p = 0.0001$ ) (Figure 20 A). Organisms remained unaffected from 3h to 96h for both conditions (w/wo food). Lethargy rapidly appeared with no food conditions at 3h and 6h, while fed animals remained unaffected. Later on (12-24h), starving animals got strongly intoxicated and immobile with Ag<sup>+</sup> (NC1), whereas lethargy had just begun for fed urchins. At 24h, they became sluggish with no attachment to the substratum. From 48h to 96h, starving and feeding juveniles were considered dead. Taken together, these differences were not statistically significant ( $p > 0.05$ ). Meaningful differences appeared between Ag<sup>+</sup> (NC1) and (NC2) treatments with food ( $p < 0.05$ ).

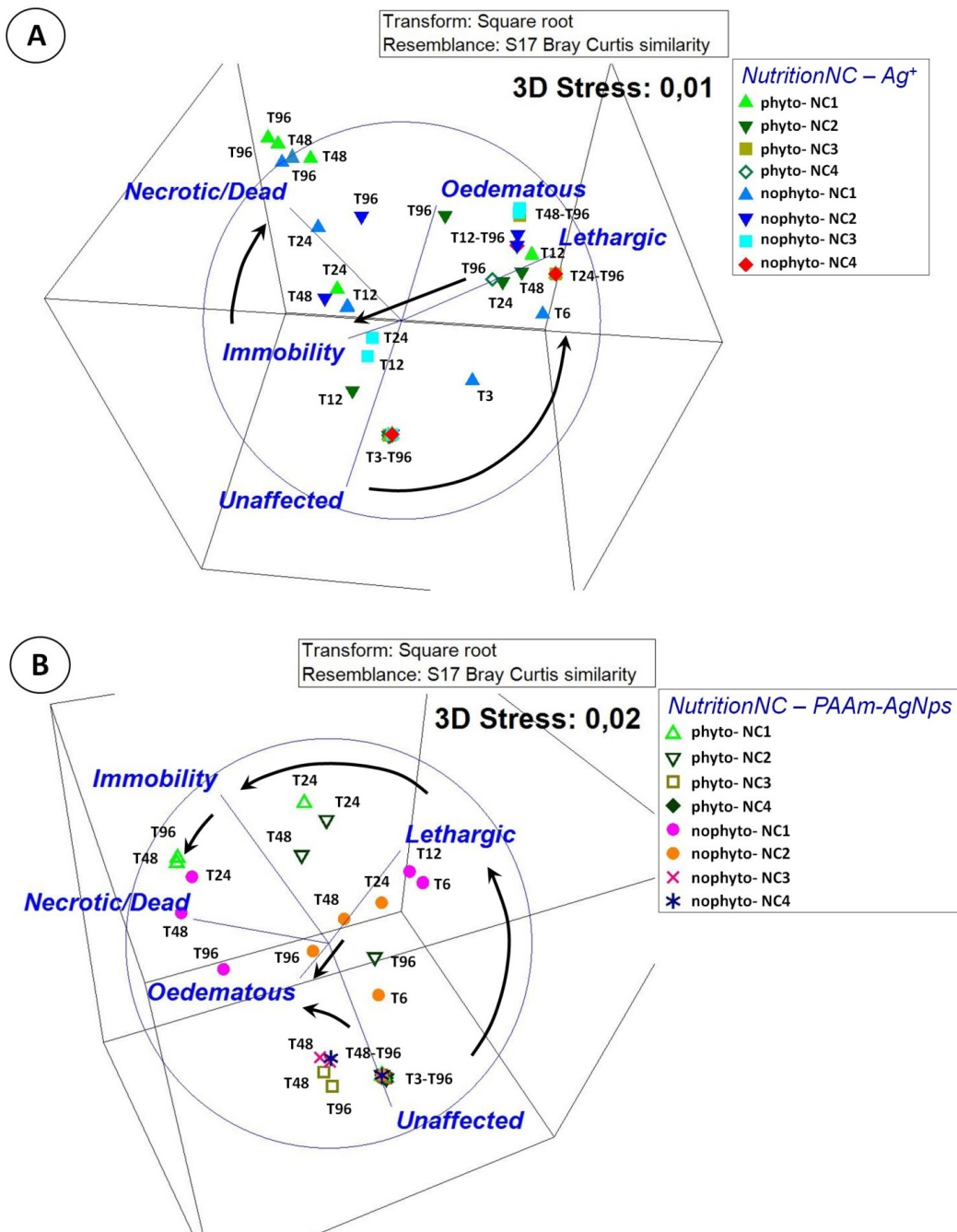


Figure 20: MDS plots with Bray-Curtis similarity analysis (PERMANOVA) of physiological conditions of fed and unfed juveniles contaminated with  $\text{Ag}^+$  and PAAm-AgNPs. A- Ionic silver exposure (3D stress: 0.01). B- Nanosilver exposure (3D stress: 0.02). Black arrows indicate conditions of juveniles within 96h. Arrows and labels as figure 19, for nutritional conditions see NutritionNC panel. Controls not included for clarity.

With Ag<sup>+</sup> (NC2), with and without food treatments, toxic responses differed from 24h up to 96h, ( $p < 0.05$ ). Toxic effects emerged at 24h and fed animals became less active while starving urchins were already lethargic from 12h to 24h. Interestingly, lethargic state was the major condition found in 96.6% fed animals at 48h and 63.3% at 96h (plus 20% oedematous, 3.3% immobile, 13.3% dead). Meanwhile unfed juveniles were already motionless at 48h (76.6%) and reached necrosis/death at 96h (63.3%). Under Ag<sup>+</sup> (NC3) treatment, 80% of fed sea urchins were lethargic (plus 20% oedematous), while 63% had the same physiological condition with NC4 (plus 10% oedematous) at 96h ( $p < 0.05$ ).

Focusing on phytoplankton interference with nanosilver (Figure 20 B), immobility of fed juveniles caused by 500 µg·L (NC1) was significantly delayed until 24h compared to unfed ones ( $p < 0.05$ ). From 48h to 96h, 60% of fed urchins were necrotic or dead while 90% of unfed urchins reached the same condition. Interestingly, PAAm-AgNPs (NC2) exposures with and without food strongly differed ( $p = 0.0001$ ). At 24h, 43% of feeding animals rapidly reached immobility state whereas 93.3% of starving organisms were still lethargic. Because fed juveniles developed oedema and lethargy up to 96h, dark blue triangles moved back to lethargic axis on the plot. Although 43.3% of unfed juveniles continued lethargic at 96h, 16.6% were near death. NC3 treatment caused oedema in 33.3% of fed juveniles compared to 10% of unfed ones at 96h. It clearly differed from NC4 with fed animals showing no sign of intoxication.

In general, phytoplankton cells appeared to delay toxicity effects of Ag<sup>+</sup> and PAAm-AgNPs, a phenomenon already observed in unfed juveniles ( $p = 0.0001$ ). In order to summarize these effects in fed juveniles, another plot is presented in Figure 21. Taking into consideration differences between Ag<sup>+</sup> and PAAm-AgNPs as a function of nominal concentration NC1 ( $p < 0.05$ ), NC2 ( $p < 0.01$ ) and NC3 ( $p = 0.0001$ ), we suggest these results confirmed previous findings with unfed animals. While animals exposed to Ag<sup>+</sup> (NC1) were 100% nearing death, PAAm-AgNPs (NC1) still caused mobility to only 60% of juveniles at 96h. For PAAm-AgNPs (NC2), 53.3% of immobile juveniles became also oedematous compared to 20% of Ag<sup>+</sup> (NC2)-treated juveniles at 96h. Finally, unaffected

specimens were only found in PAAm-AgNPs (NC3) at 66.6%, whereas 80% of juveniles from Ag<sup>+</sup> (NC3) had lethargy. There were no differences between Ag<sup>+</sup> (NC4) and PAAm-AgNPs (NC4) treatments ( $p > 0.05$ ).

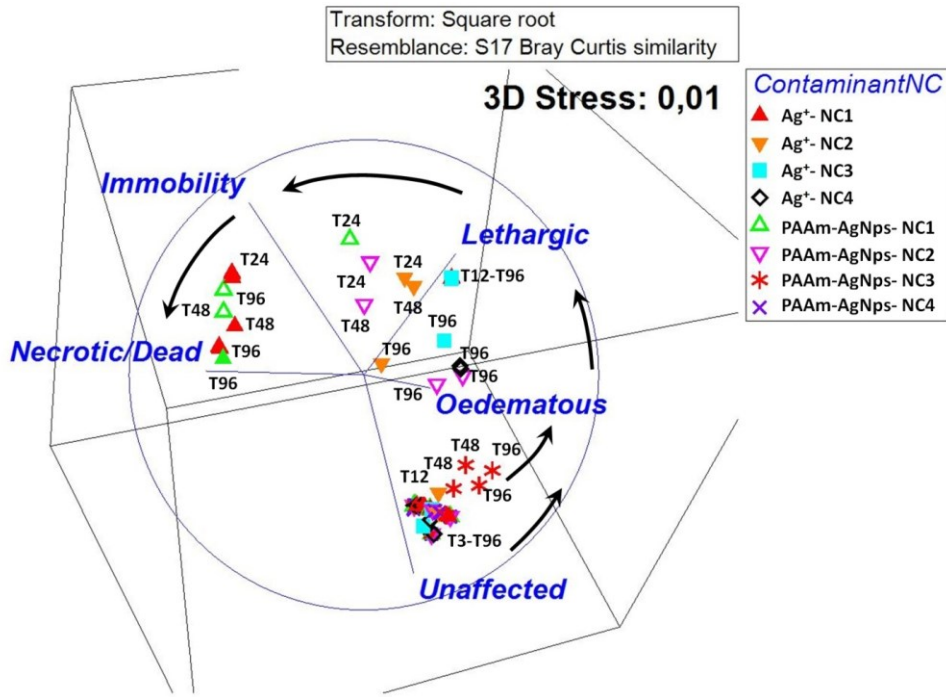


Figure 21: MDS plot with Bray-Curtis similarity analysis (PERMANOVA) of physiological conditions of fed juveniles contaminated with Ag<sup>+</sup> and PAAm-AgNPs (3D stress: 0.01). Arrows and labels as figure 19, for exposure conditions see *ContaminantNC* panel.

Comparing same nominal concentrations for Ag<sup>+</sup> or PAAm-AgNPs, and timing for sublethal responses of exotrophic juveniles and postlarvae; we found no significant differences of Ag<sup>+</sup> or PAAm-AgNPs (NC1)-exotrophic juveniles versus Ag<sup>+</sup> or PAAm-AgNPs (NC1)-endotrophic organisms ( $p > 0.05$ ). However, relevant interactions were detected with NC2 of either Ag<sup>+</sup> or PAAm-AgNPs between both stages ( $p < 0.01$ ) (Supplementary material, Appendix 2). Surprisingly, sublethal responses of postlarval endotrophic stage (to either silver or nanosilver) were often delayed over time compared to exotrophic juveniles.

### 2.6.3 Uptake of nanoAg-FITC and Qdots 525 by larvae (L8<sub>1</sub>, L8<sub>2</sub>), postlarvae and juveniles

Fluorescent markers nanoAg-FITC and Quantum dots 525 (Qdots here after) helped us to track routes and final targets of nanosilver in larvae, postlarvae and juveniles with fed and unfed organisms, either in short or long term assessments. After 6h, Qdots emitted a strong signal from stomach and intestine tissues of L8<sub>1</sub> echinoplutei with little differences between fed (104.78 units of intensity; n = 1; σ = 70.06; 4786 pixels, 29929 μm<sup>2</sup>) and unfed larvae (99.37 units of intensity; n = 1; σ = 64.81; 5886 pixels; 36807 μm<sup>2</sup>). However, fluorescence intensity (total photon influx) indicated that phytoplankton would be mainly responsible for optimizing Qdots transportation to stomach tissues at 24h. This pattern appeared again with nanoAg-FITC (Figure 22).

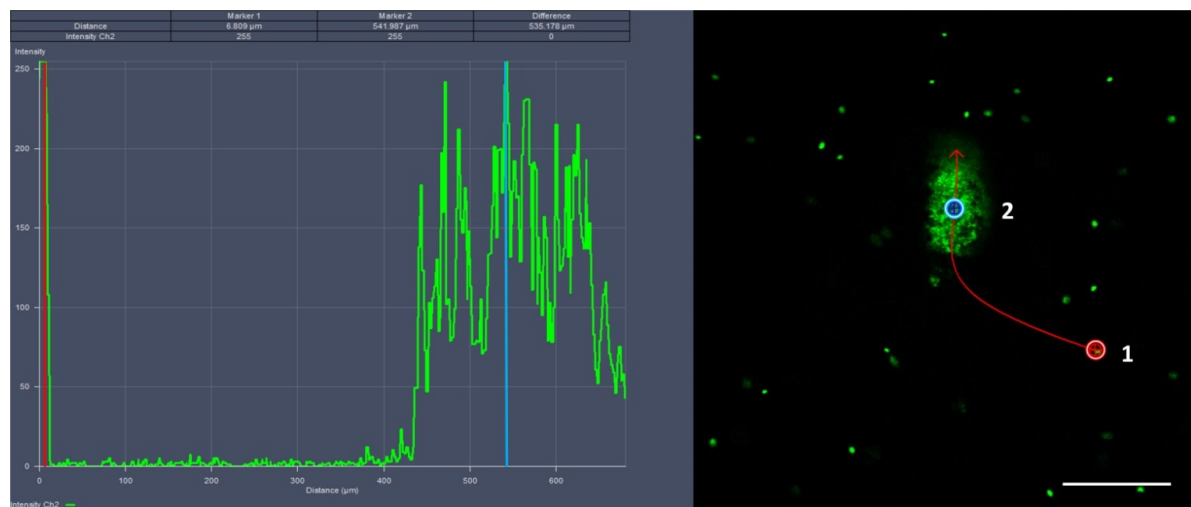


Figure 22: Profile view of levels of fluorescence signal emitted by PAAm-AgNPs-FITC in L8<sub>1</sub> echinopluteus larva feeding on phytoplankton at 24h *in vivo* (10X, scale bar: 200μm). Intensity of the signal is given on y axis, distance (in μm) is on x axis. The distance of marker 1 (phytoplankton cell) from nock of arrow was 72.865 μm while for marker 2 (larval stomach) was 379.210 μm. Difference between both was 306.345 μm.

Following curved red line (points 1 and 2), phytoplanktonic cells (red target) emitted high saturation signal (more than 250 units). In turn, intensity shown by profile

view over stomach areas (blue target) mostly oscillated between 100-250 units. Some areas had low signal due to pigment cells clusters, which appeared as an opaque negative staining on stomach surface. In seawater, less than 50 units were detected between both targets. Early on (6h) we observed that undigested particles egested from hindgut held strong fluorescence with nanoAg-FITC (Supplementary material, Appendix 2) and Qdots. Unfed larvae had gastrointestinal tracts less stained by markers but sometimes holding high peaks of fluorescence. Only Qdots stained larval skeleton bars.

Early 8-arm echinoplutei ( $L8_1$ ) exposed to Qdots, nanoAg-FITC and controls remained as swimming larvae up to 96h. Lipid vesicles were accumulated in stomach until beginning of metamorphosis (Supplementary material, Appendix 2). After 6h of exposure to nanoAg-FITC (with or without food), only gastrointestinal tract appeared highly marked and treated larvae did not differ from controls in fluorescence profile views. Measuring nanoAg-FITC in stomach of unfed larvae, we obtained a mean of 68.46 units ( $n = 3$ , in average: 24670 pixels;  $\sigma = 47.78$ ;  $47148 \mu\text{m}^2$ ) compared to 106.85 for FITC-controls ( $n = 3$ , in average: 13340 pixels;  $\sigma = 70.2$ ;  $30759 \mu\text{m}^2$ ). It was 64% of units in exposed larvae compared to controls. Fed larvae from controls held 123.86 units of intensity ( $n = 3$ , in average:  $\sigma = 62.93$ ; 7671.6 pixels;  $30274 \mu\text{m}^2$ ) while larvae from marked with AgNPs-FITC had 92.98 units ( $n = 3$ , in average:  $\sigma = 58.27$ ; 10648.33 pixels;  $42100 \mu\text{m}^2$ ). It represented 75% of maximum intensity compared to controls. Significant differences between larvae from nanoAg-FITC with and without food treatments were found ( $n = 256$  measurements separately taken in larvae from both conditions;  $p < 0.05$ ;  $t = 2.676$ ;  $\sigma = 510$ ). Differences in fluorescence between nanoAg-FITC-treated fed/unfed larvae and FITC (control) appeared again at 24h and 96h. In order to precisely compare signal intensity from controls and fed larvae with PAAm-AgNPs fluorescent marker, we quantified it circumscribing larval stomachs total areas to obtain pixel intensities values and standard distribution for both conditions (more details are given in Supplementary material, Appendix 2).

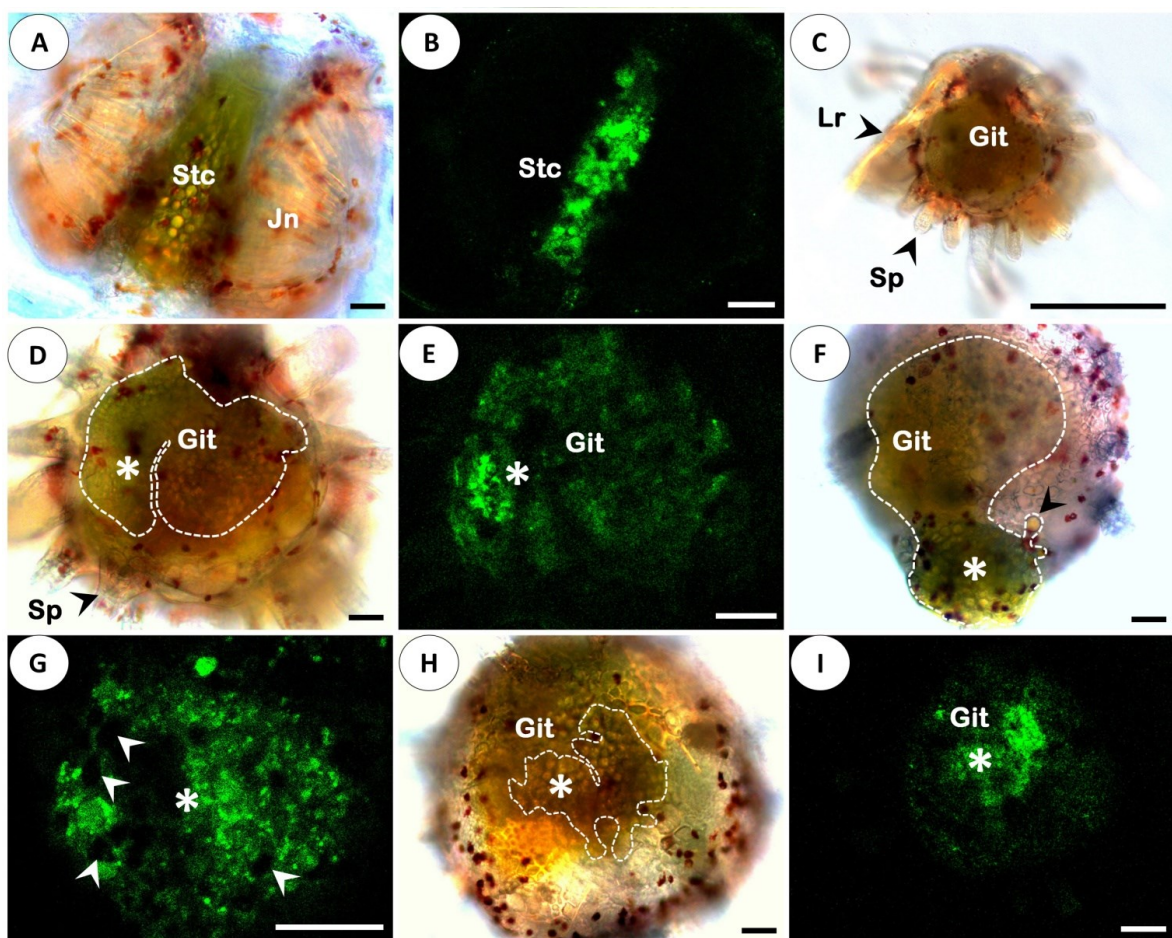


Figure 23: NanoAg-FITC dye transfer between development stages in perimetamorphic period *in vivo*. Panels A and B: bottle-shaped stomach of early L8<sub>2</sub> larva surrounded by rudiment ossicles; lipidic vesicles emitted strong signal of nanoAg-FITC dye at 24h. Panels C, D, and E: late L8<sub>2</sub> (metamorphic larva) with gastrointestinal tract remolded (selected area) and emitting lower fluorescence of nanoAg-FITC compared to competent larvae at 24h. Panels F and G: remolding gastrointestinal tract of postlarva (selected area) and vestigial stomach tissues of larva getting absorbed at 96h (white asterisks). A loosen lipidic vesicle is shown by black arrowhead; high signal was interrupted by pigment cells clusters (white arrows). Panels H and I: advanced postlarval stage with fluorescent vestigial tissues (selected area) already incorporated into new gastrointestinal tract. Asterisks show corresponding regions in both figures. Abbreviations - Git: gastrointestinal tract, Jn: rudiment of juvenile, Lr: larval rods, Sp: spine, Stc: stomach, Stm: stomodeum (opening mouth).

(A, D, F, H: 20X, scale bar: 50  $\mu\text{m}$  in light microscopy; B, I: 20X, scale bar: 50  $\mu\text{m}$ ; C: 10X, scale bar 200  $\mu\text{m}$ ; and E, G: 40X, scale bar: 50  $\mu\text{m}$  in laser microscopy).

As far as development proceeds, early L8<sub>2</sub> (competent larvae) are getting close to the substratum. After 24h, stomach and epidermic cells were equally well marked in nanoAg-FITC and controls (50-200 peaks of units of intensity in profile view). Qdots signal was again distributed over stomach (50-100 units) and skeleton rods (200 units). Larvae from FITC-controls going through perimetamorphic period were thus far more developed than L8<sub>2</sub> siblings contaminated with PAAm-AgNPs fluorescent marker at 96h. Due to ontogenetic processes that quickly took place; our analysis was made in an ongoing process with organisms showing close metamorphic stages (Figure 23 A-I).

As expected, early L8<sub>2</sub> larvae had structures progressively shrinking and rudiment increasingly occupying blastocoel (Supplementary material, Appendix 2). At this time larval gastrointestinal tract became bottle-shaped and tied by growing juvenile plates, but still emitting strong signal of fluorescent nanomarker (Figure 23 A and B). Further, stomach cells and lipid vesicles of late L8<sub>2</sub> (metamorphic larvae) were reorganized to give rise to another gastrointestinal tract (Figure 23 C-E). Cells of early L8<sub>2</sub> bottle-shaped stomach held strong signal of nanoAg-FITC (mean intensity of 115.97 units;  $\sigma = 73.51$ ; 14088 pixels; 9972  $\mu\text{m}^2$ ) compared to late L8<sub>2</sub> (mean intensity of 19.92 units;  $\sigma = 21.79$ ; 23685 pixels; 27972  $\mu\text{m}^2$ ) (Figure 23 C-E). As such a few gut cells of late L8<sub>2</sub> retained high fluorescence among dispersed signal in adjacent areas. Lipid vesicles spread over abactinal surface, indicating energy relocation.

Nonetheless, nanoAg-FITC dye signal remained strong enough in larval tissues throughout this period to observe cellular fate of postlarvae (Figure 23 F to I). Low fluorescence was detected on podia and spines of postlarvae, but restricted areas on supracoronal surface held high intensity values (Figure 23 F and G). Comparing uncontaminated and exposed organisms, we found nanoAg-FITC treated postlarvae with 87.01 units ( $\sigma = 63.05$ ; 8031 pixels; 16056  $\mu\text{m}^2$ ) whilst control had 67.75 units ( $\sigma = 39.50$ ; 4004 pixels; 8958  $\mu\text{m}^2$ ), both with significant differences ( $n= 512$  measurements,  $p < 0.0001$ ,  $t = 9.960$ ;

$\sigma = 499.3$ ). Four days after final observation (2 x 96h), postlarvae from nanoAg-FITC cultures still keeping high signal (mean intensity of 59.13 units;  $\sigma = 44.25$ ; 9139 pixels;  $11621 \mu\text{m}^2$ ) (Figure 23 H and I), whereas controls had 20.42 units ( $\sigma = 27.48$ ; 6543 pixels;  $13081 \mu\text{m}^2$ ) in histogram view (Supplementary material, Appendix 2). Postlarvae from controls had weaker signal coming from few remaining cells, and nanoAg-FITC signal arose from vestigial gastrointestinal tissues of larva still getting reorganized. These results strongly suggest that larvae with tissues contaminated with PAAm-AgNPs at late stages might be successfully transferred to newly settled pre-juveniles.

Epithelial membrane in abactinal surface of postlarvae delimited a swollen space void of skeleton. Later on they developed new internal structures as calcareous plates, radial canal and endocyclic gut (Supplementary material, Appendix 2). From 6h to 96h of a new exposure, postlarvae emitted a strong signal from endocyclic gut in aboral view (50 to 250 units of intensity) mainly under FITC nanomarker treatment. Fluorescent signal was strongly emitted from cells of radial canal in oral view, but only from the first 6h to 24h (Supplementary material, Appendix 2). The signal from controls was often either blurred or weak. At 96h, outer signal increased on cells of podia and epidermis with no differences between controls and nanoAg-FITC. In the following days, exotrophic juveniles fed abundantly on phytoplankton amended with FITC nanomarker, but inner signal was not detected, perhaps due to the well calcified body or degradation of FITC inside gut (Supplementary Video 2, Aquatic toxicology 174: 208-27). Epidermic cells covering plates of test, spines, podia, papulae and pedicellaria got intensely marked in controls, nanoAg-FITC and Qdots 525, with or without food from 6h to 48h. Low toxicity of Qdots allowed fast development of postlarvae and contrarily to nanoAg-FITC, signal was mostly restricted to skeleton at 96h (mean intensity of 70.95;  $\sigma = 56.17$ ; 12305 pixels;  $10223 \mu\text{m}^2$ ). They were also found associated with epidermis of exotrophic juveniles from 6h to 96h. Peristomial membrane and teeth of Aristotle's lantern exhibited fluorescence in fed and unfed animals.

With nanoAg-FITC, fluorescent signal in fed larvae ( $L_8$ ) decreased from 6h to 24h at 49%, but increased again at 96h, which indicates only 32% of fluorescence loss. Controls showed similar tendency with reduction of 33.6% of signal at 96h, still stronger compared to nanoAg-FITC conditions in about 29%. On the other hand, unfed larvae ( $L_8$ ) exposed to FITC nanomarker had lower signal compared to feeding larvae. Higher fluorescence found at 6h in fed larvae from controls was reduced 91% up to 96h compared to those exposed to nanoAg-FITC, with 29% of fluorescence loss. It suggests phytoplankton could optimize uptake of FITC and nanoAg-FITC. It shows indeed how this nanomarker might be persistent in biological tissues even when food is absent, as proved with postlarvae experiment.

#### **2.6.4 Internalization of PAAm-AgNPs by *echinopluteus* larvae and juveniles after chronic exposure**

##### a) Larval digestive system

Nanosilver was internalized by different cell types related to mesoderm derivatives as gastrointestinal tract and coelomic cavities. Proctodaeum of metamorphosing larvae comprises pseudostratified columnar epithelium of one ultrastructural cell type of slender shape, elongated ovoid nuclei and glandular cells. Cells also had long cilia with striated rootlets, vacuoles and anastomosing septate junctions in apical portion, which formed a rough fringed-like surface. Intracellular trafficking of nano-aggregates in enterocytes occurred by means of vacuoles and direct membrane translocation of nanoparticles going inward cytoplasm (Figure 24). Inside panel 1, the larger aggregate loaded into cytoplasm had 130 nm of width and about 400 nm of length. A small aggregate nearby vacuoles, seen in panel 2, had about 130 nm in diameter whereas a larger one showed a size of about 250 nm inside a vacuole (panel 3). Silver aggregates were found in lumen of alimentary canal as well. Non-contrasted tissue revealed the same mechanisms observed in stained tissues (Supplementary material, Appendix 2).

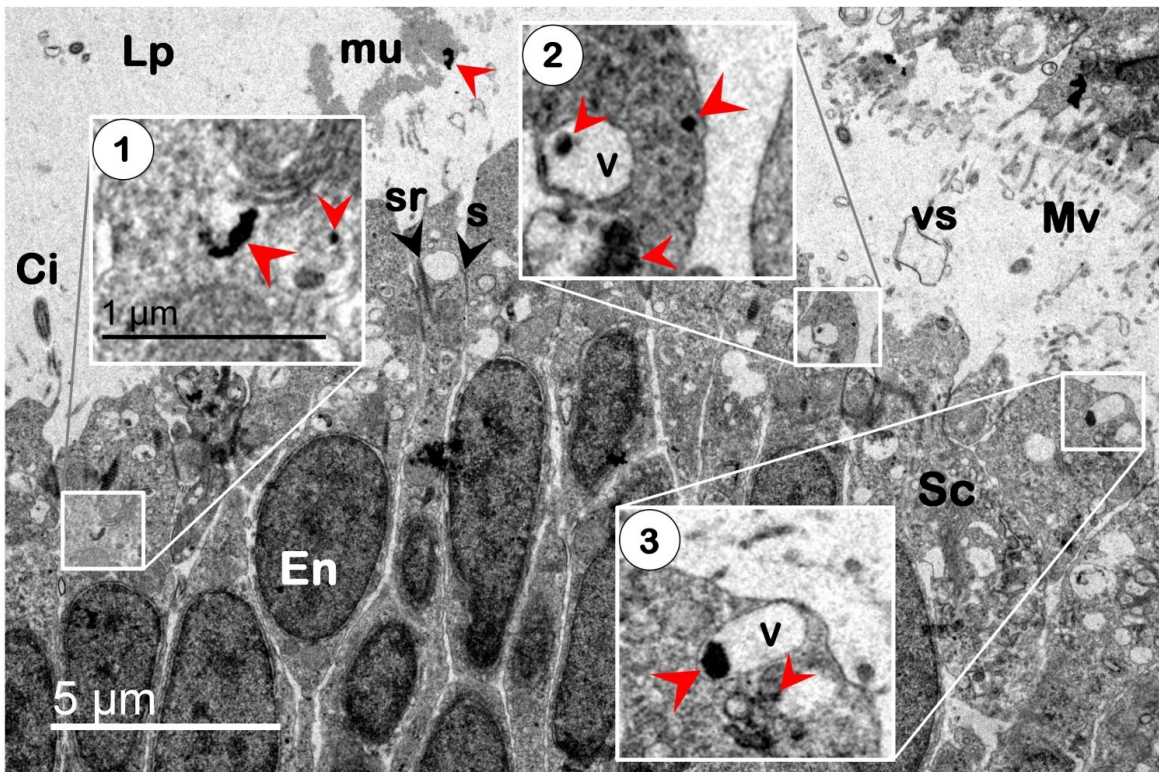


Figure 24: Electron micrographs of hindgut of larva chronically exposed to PAAm-AgNPs ( $100 \mu\text{g L}$ ). Proctodaeum epithelium with different nanosilver trafficking routes (contrasted sample). Insert 1: PAAm-AgNPs aggregates loaded by enterocyte. More aggregates appeared in membrane translocation towards vacuoles/loading vesicles as seen in inserts 2 and 3. Non-contrasted sample is shown in Supplementary material, Appendix 2. Some AgNPs are indicated by red arrowheads and more silver nanoparticles can be observed in tissue and cells. Abbreviations- Ci: cilium, En: enterocyte, Lp: lumen of proctodaeum, mu: mucus, Mv: microvilli, s: septate junctions, Sc: secretory cell, Sr: striated rootlet, V: vacuole, vs: vesicle.

b) Immune cellular response in larval blastocoel

PAAm-AgNPs aggregations between 130 and 400 nm were frequently seen in coelomic space. Phagocytes normally found in larval coelomic fluid seemed to actively internalize nanosilver (Figure 25 A). It confirmed our assumptions about pathways in which nanoparticles were internalized in cells of larvae: occasional internalization in tissues or active phagocytosis in coelomic space. Immune cells at different stages of cellular

activity are seen in Figure 25 A. Phagocytic amoebocyte showed PAAm-AgNPs already incorporated into phagosomes of different sizes. In this case, well developed smooth endoplasmatic reticulum suggests high cellular activity related to the presence of nanoparticles. Petaloid phagocytes with broken vacuoles were also spotted in the area. Spherule cells had some nanosilver attached to cell surface with no typical endosomal nano-vesicles.

c) Parietal layer of coelomic epithelium and circulating phagocytes of blastocoel

Cells from different tissues showed contamination and internalization occurring by means of vacuoles or endocytic vesicles. The epithelium surrounding blastocoel of larvae is composed of trapezoidal cells with large paracellular spaces and subapical septate junctions. Nano-aggregates were found inside coelomic space, cells of surrounding tissue; and trapped by circulating phagocytes (Figure 25 B). Aggregations of nanosilver internalized by means of multiple endocytic vesicles in coelomic epithelial cell had about 150-200 nm in diameter. It should be noted that the pattern of phagocytic response against nano-aggregates described in the previous section was also detected in non-contrasted sample shown in Figure 25 B.

d) Inside epigastric coelom of juveniles

Under short-term exposures (96h), we observed only a few aggregates of nanosilver in coelomic spaces of 2-month old sea urchins (not shown). General morphology of inner cavities is shown in Supplementary material, Appendix 2. PAAm-AgNPs aggregations ( $50 \mu\text{g}\cdot\text{L}$ , NC3) were detected inside coelomocytes from epigastric coelom as well as in mesenteries ( $100 \mu\text{g}\cdot\text{L}$ , NC2) in a lower extent. In a similar way, long-term exposure ( $3 \times 96\text{h}$ ) to  $100 \mu\text{g}\cdot\text{L}$  caused a remarkable internal distribution of aggregates in mesenteries in 1-month old juveniles (Figure 26). Contrarily to metamorphic larvae whose inner contamination mostly gave rise to PAAm-AgNPs aggregates; single nanoparticles (or very small aggregates  $<50 \text{ nm}$ ) seem to be bound to mesenteries of epigastric coelom of juveniles.

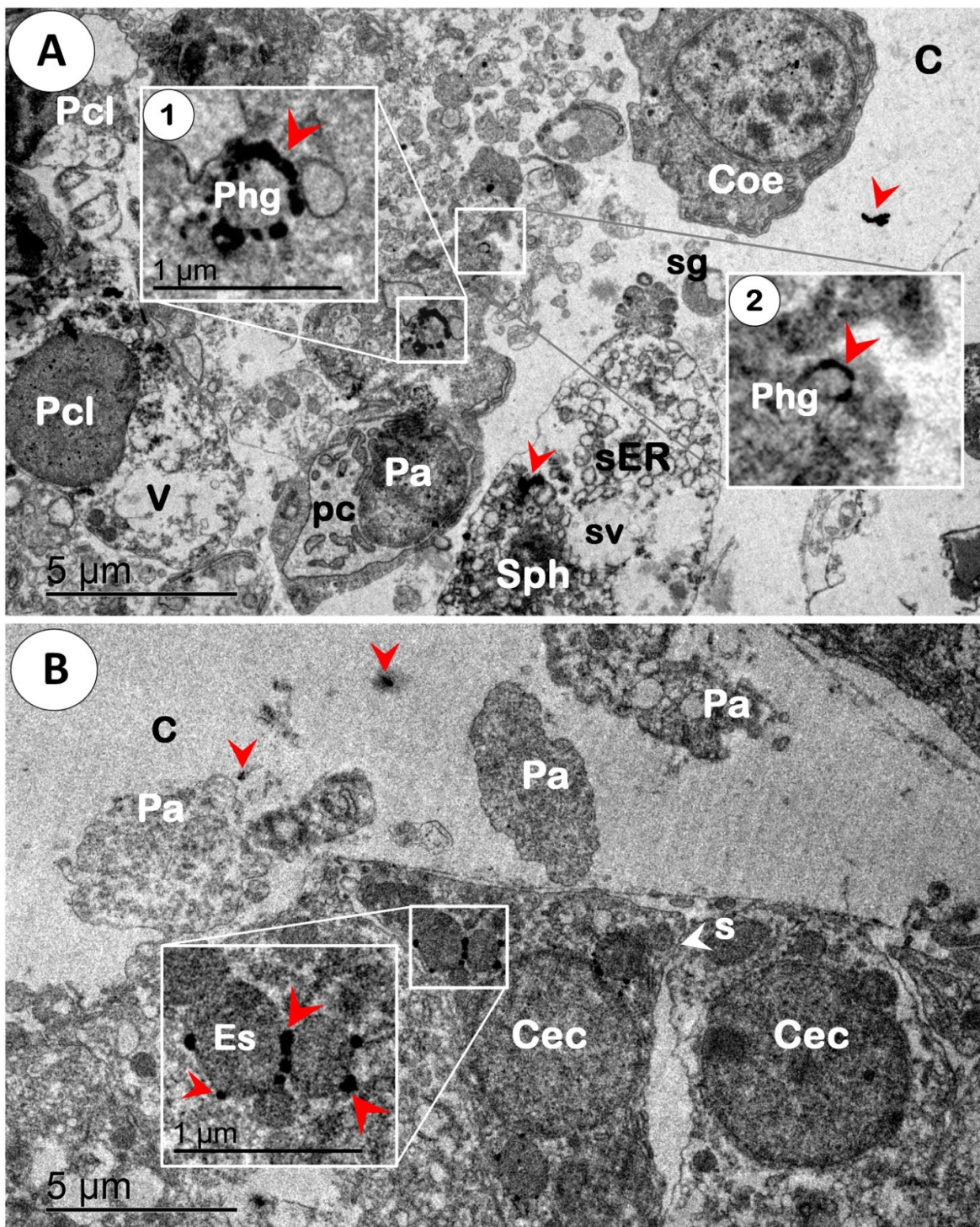


(Figure 25, see legend on next page)

Figure 25: Electron micrographs of coelom of larva chronically exposed to PAAm-AgNPs (100 µg·L). Panel A: immune cells from blastocoel (contrasted sample). Phagosomes of different sizes are indicated by inserts 1 and 2. Spherule cells are seen with aggregates on surface membrane. Panel B: coelomic epithelial cells in somatocoel with endocytic vesicles and free phagocytes in coelom (non-contrasted sample). Some silver aggregates are indicated by red arrowheads and more of them can be seen in the cells and coelom. Abbreviations- C: trunk coelom (somatocoel), Cec: coelomic epithelial cells, Coe: coelomocyte, Es: endocytic vesicle, Phg: phagosome, Pa: phagocyte, Plc: petaloid cell, pn: perinuclear space, Sph: spherule cell, sRE: smooth endoplasmic reticulum, sg: secretion granule, sv: secretory vesicle, V: vacuole.

As observed in Figure 26 left panel (A), a free coelomocyte in hypogastric coelom seemed to internalize PAAm-AgNPs dispersed in coelomic fluid. Meanwhile, epigastric coelom had a main canal running seawater with nanosilver (Figure 26 panels A, B and C). As fuzz balls grabbed in a tissue, nanoparticles were mainly tracked on epigastric coelom walls whatever was width of lumen. Cellular uptake of PAAm-AgNPs eventually happened with circulating coelomocytes in epigastric coelom (Figure 26 panel B). Compared to cell of hypogastric coelom, coelomocyte from epigastric coelom had lower concentration of nanosilver, indicating high attachment of particles on mesenteries and/or moderate cell activity. PAAm-AgNPs with size estimated to about 8 to 17 nm and small aggregates of 25 nm seem to pass through mesenteries towards neighboring cells (as adipocytes and peritoneocytes) (Figure 26 panel C), or haemal vessels. Even so, cells from haemal vessel sometimes showed nanoparticles in vacuoles. Because these sinuses ended up as no through road, PAAm-AgNPs were likely to be restricted to epigastric coelom, eventually crossing this barrier.

e) Peritoneal mesothelial cells in larvae and juveniles

As coelomic canals are extensively interconnected, nanoparticles appeared overspread either in larvae or juvenile's tissues (Figures 27 and 28). PAAm-AgNPs seemed to be randomly caught up by peritoneal cells (peritoneocytes), but also retained in basement membranes as mesothelial membrane that encloses visceral mass in larvae and parietal

mesenteries in juveniles, both separating connecting tissues. Individual or aggregated nanoparticles already internalized by cells appeared to be extruded by vesicles normally produced by peritoneal cells. This could explain why hypogastric coelom of juveniles and larval blastocoel had many free vesicles often associated with nanosilver. Young urchins had some coelomocytes inside intra-peritoneal space exhibiting some internalization of nanosilver. The intra-peritoneal space circumscribes inner walls of test and was bounded by peritoneocytes that eventually packed PAAm-AgNPs inside cytoplasmatic vesicles. Along this trail, nanoparticles had about 30 nm, but were also found forming other small aggregates (40 to 80 nm) and the larger ones (210 to 600 nm) (Figure 26).

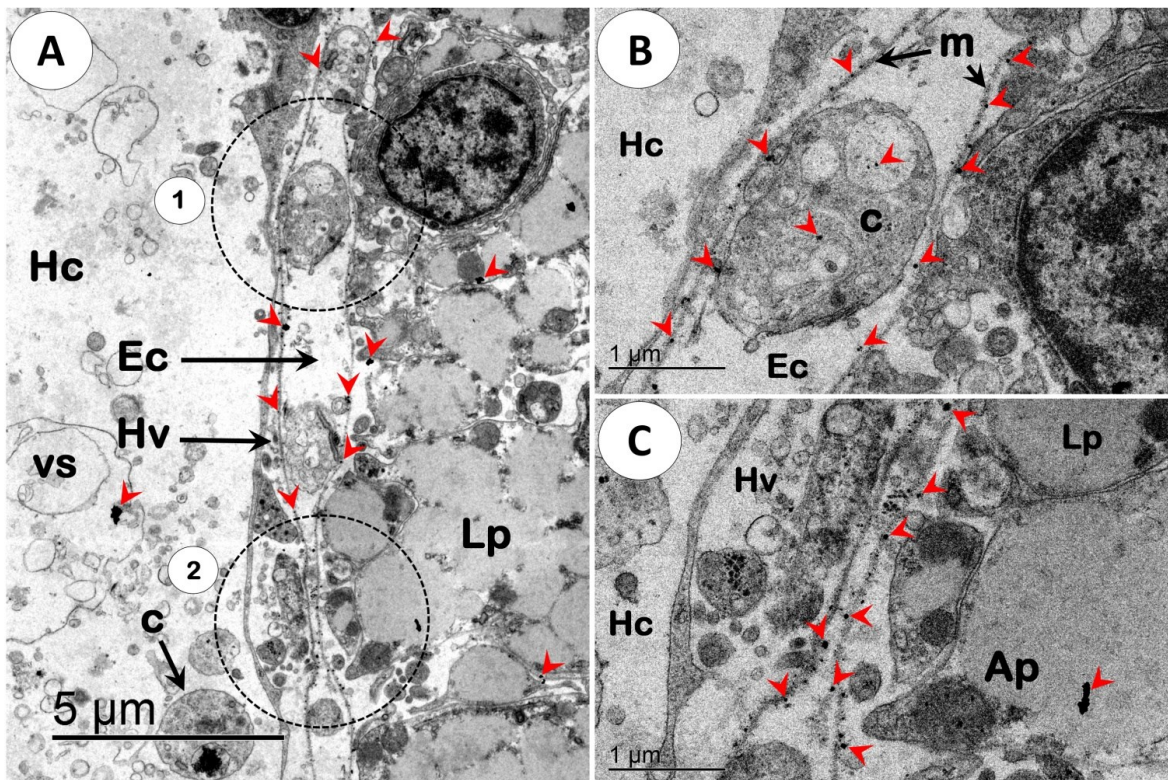


Figure 26: Electron micrographs of perivisceral coelom of juveniles chronically exposed to PAAm-AgNPs ( $100 \mu\text{g}\cdot\text{L}^{-1}$ ) (contrasted samples). Panel A: Epigastric coelom with trail of PAAm-AgNPs in mesenteries. Selected areas in A: (1) Coelomocyte from epigastric coelom engulfing PAAm-AgNPs from mesentery (shown by panel B in detail); (2) Nanosilver pathway in epigastric mesenteries (shown by panel C in detail). Some silver aggregates are indicated by red arrowheads and more of

them can be seen in the tissues and mesenteries. Abbreviations- Ap: adipocyte, c: coelomocyte, Ec: epigastric coelom, Hc: hypogastric coelom, Hv: haemal vessel, LP: lipid droplet, m: mesentery, n: nucleus, Pc: peritoneal cell/peritoneocyte, vs: vesicle.

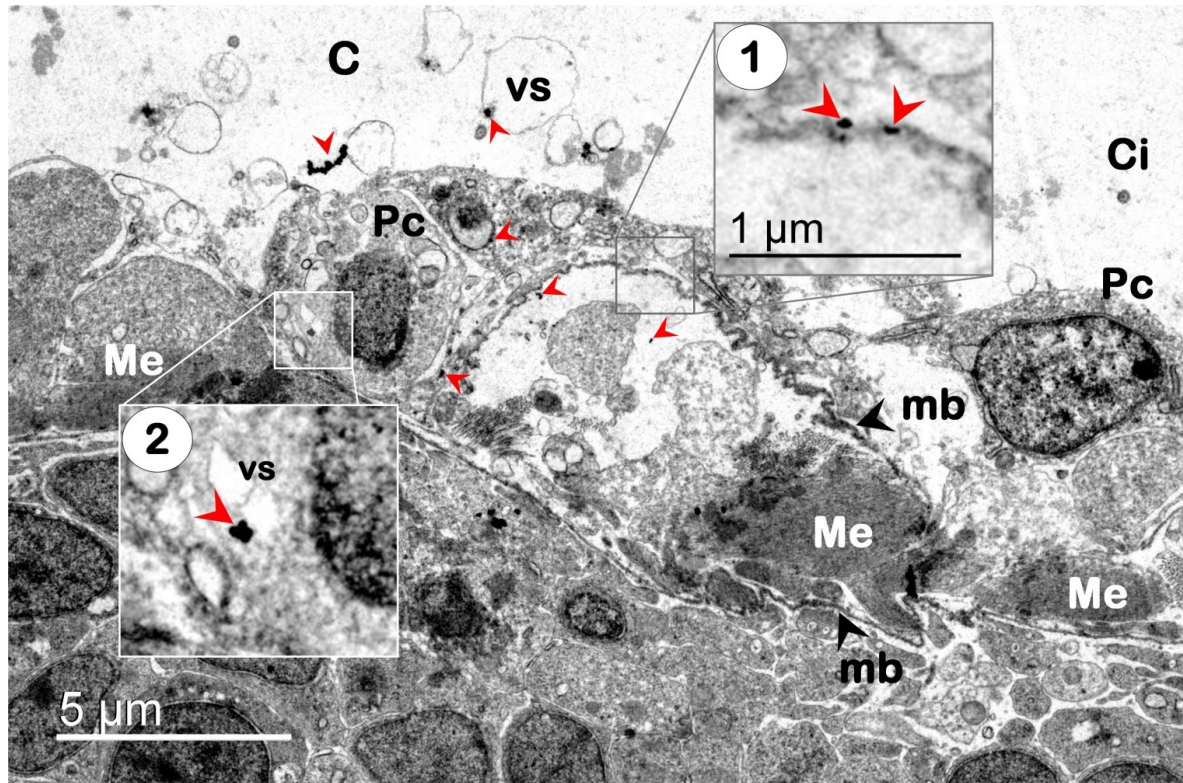


Figure 27: Electron micrograph of mesothelium of larva chronically exposed to PAAm-AgNPs (100  $\mu\text{g}\cdot\text{L}^{-1}$ ). Small aggregations of nanosilver grabbed by mesothelial membrane (insertion 1) were often associated with vesicles produced by larval peritoneocytes (insertion 2) (contrasted sample). Some silver aggregates/particles are indicated by red arrowheads and more of them can be seen in the tissues, coelom and mesenteries. Abbreviations- mb: mesothelial membrane, C: trunk coelom (somatocoel), Ci: cilium, Me: contractile process of myoepithelial cell, Pc: peritoneal cell/peritoneocyte, vs: vesicle.

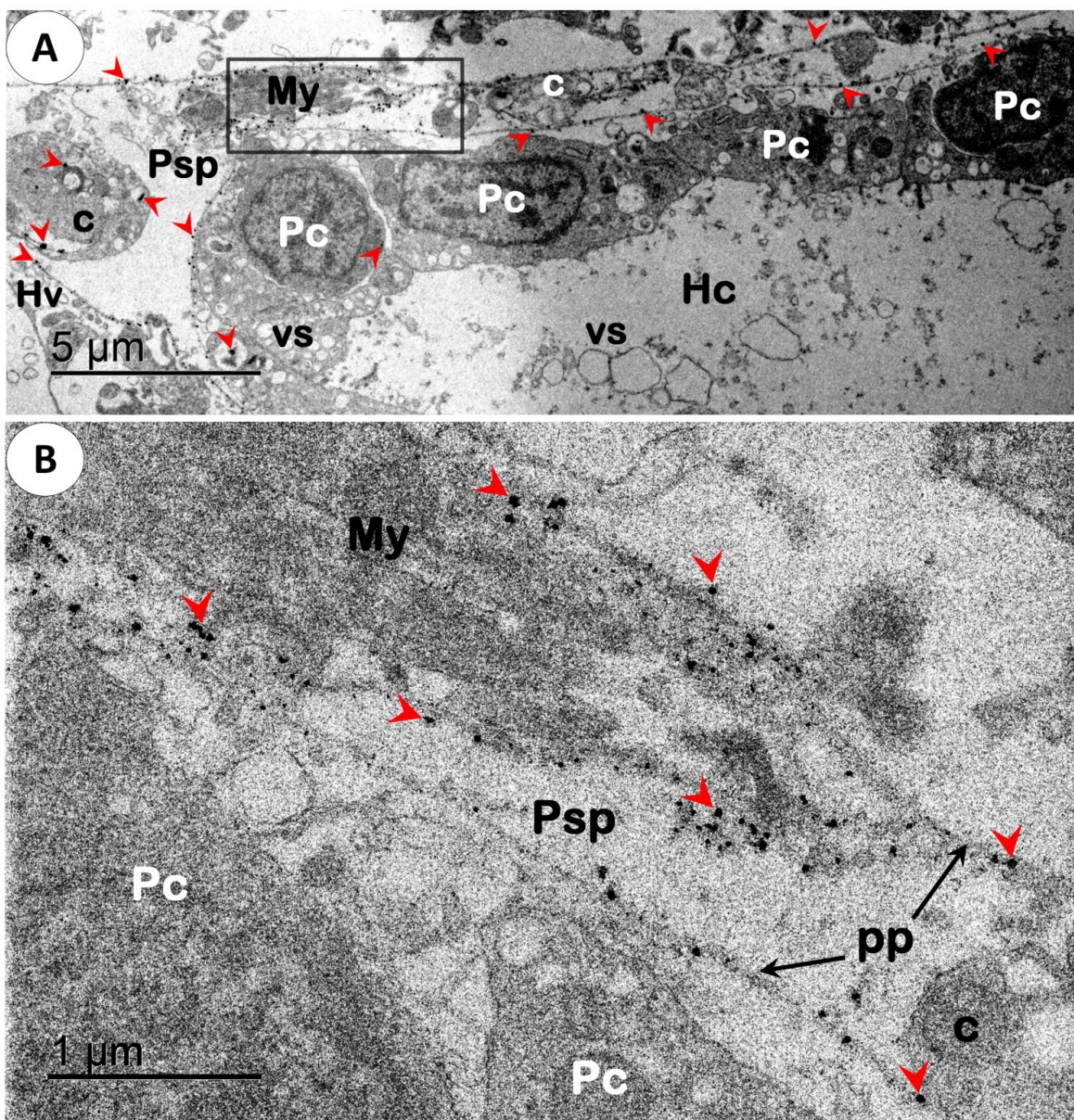


Figure 28: Electron micrograph of mesothelium of juveniles chronically exposed to PAAm-AgNPs (100  $\mu\text{g}\cdot\text{L}^{-1}$ ). Panel A: Parietal peritoneum of juveniles held a trail of PAAm-AgNPs sometimes taken up by coelomocytes; nanosilver was eventually found in vesicles of peritoneocytes (non-contrasted sample). Insertion delimited by black rectangle is shown in detail in Panel B. Panel B: Intra-peritoneal space with small aggregations and individual PAAm-AgNPs trail on parietal peritoneum of juveniles (non-contrasted sample). Some silver aggregates are indicated by red arrowheads and more of them can be seen in peritoneum and cells. Abbreviations- c: coelomocyte,

Hc: hypogastric coelom, Hv: haemal vessel, My: myocytes, Pc: peritoneocyte, Psp: intra-peritoneal space, pp: parietal peritoneum.

## 2.7 DISCUSSION

In this study, complex fate and toxic effects of nanosilver and dissolved silver have been detailed for L8<sub>2</sub>-arm echinoplutei, endotrophic postlarvae and exotrophic juveniles of sea urchin. The presence of food and developmental stages not only revealed how organisms responded to Ag<sup>+</sup> and PAAm-AgNPs in short or extended exposures, but alternative pathways through which contaminants would be taken up and internalized. Organic-coated nano-markers (nanoAg-FITC and Qdots 525) were very useful tools to corroborate PAAm-AgNPs fate observed by TEM. Throughout several exposures, nanoAg-FITC showed significant differences compared to controls and long time resilience to accurately probe different stages of early development in acute and chronic exposures.

### 2.7.1 Juvenile stage

Analyzing MDS plots and ICP-MS data of juveniles we found marked differences between free Ag<sup>+</sup> and PAAm-AgNPs toxicity, mostly in terms of timing for abnormalities to arise. Chemical data confirmed that the proportion of free silver was higher in plates with AgNO<sub>3</sub> compared with those with AgNPs. As a rule, energy reserves have a pivotal role in the rapid provision for increasing energy demands during any kind of stress exposure, including pollutants (Sokolova et al., 2012). Accordingly, high levels of organic compounds in viscera of echinoderms are reserves ready to be used during starvation (Lawrence and Lane, 1982). Under normal conditions, the utilization of stored resources occurs through its allocation into building and maintenance of somatic structure, which is considered a priority in energy budget allocation and cannot be reduced below a certain limit (Van Straalen and Hoffmann, 2000). Deprived of food, specimens contaminated with silver shared available energy not only to sustain basal maintenance, but also to mitigate metabolic losses caused by silver intoxication. Reduction of metabolic activity in acute

exposures in particular are necessary to slow down adverse changes caused by accumulation of metabolic waste in intracellular milieu for a time-limited survival. Low and moderate stresses however induce metabolic and ATP turnover acceleration to continue to fuel key cellular processes along with detoxification and repair (Sokolova et al., 2012).

First effects to emerge following any lethal injury, are pre-lethal injuries (often reversible), followed by a “point-of-no-return” (cell death), and finally postmortem autolytic and degradative changes (necrosis) (Trump et al., 1997; Kroemer et al., 2009). As already known, silver interactions with phospholipids layer can disrupt transmembrane electrochemical gradient which leads cell plasma-membrane potential to collapse (Lapresta-Fernández and Blasco, 2012). It may be part of the explanation for juvenile’s lesions whose necrotic cells appeared swollen with bright vesicles inside cytoplasm in confocal microscopy. In our study, ionic form of silver is likely to be responsible for a large portion of the toxicity of AgNPs in starved juveniles. However, it is not clear which part of toxicity would be attributed to silver nano-form itself and under which circumstances it would be greatly hazardous to their survival. It is well established that coelomic and haemocoelic structures in sea urchin are peculiar and very complex. As observed in TEM images, nanoparticles did spread over connected mesenteries following seawater inflow that normally enter madreporite ampulla and goes through axial coelom. This flow goes through canals equipped with valves and ciliary cells over the body. All echinoderm species possess an axial complex as part of coelomic and haemal system with its vessels; it is broadly described as a structural, functional and topographic interaction between numerous primary and secondary body cavities sometimes ending blindly or interacting with each other (Ziegler et al., 2009; Ezhova et al., 2014). Thus stone canal would be the first main route for PAAm-AgNPs distribution. This is a seawater flow-through passage to ambulacrinal system, but it is connected to axial coelom and partly enwrapped by it. In sea urchin, inner surfaces of epigastric coelom and mesenteries of parietal peritoneum from shell inner walls are lined by a complex network of sinuses sometimes aside with haemal vessels coming from axial organ, the three having circulating cells.

Interestingly, a low aggregation of PAAm-AgNPs was observed with a tight binding to mesenteries inside epigastric coelom and parietal peritoneum. Polyallylamine chains negatively charged likely prevented agglomeration in seawater by steric repulsion (Rivera-Gil et al., 2013). The formation of PAAm-AgNPs stable colloids in perivisceral fluid would maintain its stability and facilitate interactions with mesentery walls. Mesenteries are mainly constituted of elastic and collagen fibers densely organized as a complicated meshwork system where PAAm-AgNPs could have been then entrapped. Having been so well distributed along these sinuses, it can be proposed that single or aggregated PAAm-AgNPs became an inner source of Ag<sup>+</sup> to young urchins. Differently from other nanomaterials, AgNPs are soluble in seawater at a slow rate and dissolution may proceed layer by layer through time (Zhu et al., 2012a). As surface coating allowed stable interactions of PAAm-AgNPs with mesenteries, nanotoxicity became strongly influenced by polymer coating. Therefore, we suggest that polymer-coated AgNPs used in this work have the potential to cause constant chemical release and stress in exposed organisms. Chronic exposure to 100 µg·L of PAAm-AgNPs (0.93 mM) resulted in an apparent coelomocyte response in epigastric/hypogastric coeloms and intra-peritoneal space. Comfort et al. (2014) observed significant cellular consequences under chronic treatments with 50 nm AgNPs in very low concentrations (0.4 µg·L), not generating cytotoxic response, but instead permanent stress, signaling responses and modified gene expression. Similar stress might occur with phagocytic amoebocytes, cells primarily responsible for innate defense in marine invertebrates (Canesi and Procházková, 2014). In a broader view, coelomocytes of echinoderms are highly sensitive to physiological perturbations in internal milieu and a quick cellular response is expected when exposed to metallic nanoparticles (Falugi et al., 2011). Moreover, phagocytes are particularly efficient in identifying and capturing invaders in coelomic fluid - as foreign cells, cell debris and inert particles even at temperature near 0°C as demonstrated by Borges et al. (2002) with Antarctic sea urchin *Sterechinus neumayeri*. On these grounds, we suggest that a continuous cellular response against PAAm-AgNPs in sea urchins, if correlated to intermittent releases, could compromise in some way immune system homeostasis over time.

In general, free Ag<sup>+</sup> and PAAm-AgNPs effects on fed juveniles were remarkably delayed in presence of phytoplankton. Data gathered in the MDS strongly indicate that phytoplankton particularly interfered with PAAm-AgNPs effects. Low levels of free Ag<sup>+</sup> in PAAm-AgNPs + phytoplankton wells was related to moderate toxicity up to 96h. Besides, we need to consider that even though high levels of particulate silver would likely be associated with phytoplankton in PAAm-AgNPs media, nanoAg might only be partially retained by cells in gut. Thence, part of nanosilver combined with undigested waste material gets probably expelled from gastrointestinal tract with pellets. In this context, oedemic condition should be considered as a more complex sublethal response than lethargy since it comprises morphological deformity and migration of a number of cell types. As unfed urchins exposed to 100 and 50 µg·L of nanosilver did not exhibit oedema as fed ones did under same concentrations, it is suggested that phytoplankton cells can interact with free PAAm-AgNPs increasing uptake and leading juveniles to oedematous state. Lowest nominal concentrations of AgNO<sub>3</sub> (NC3 and NC4) with or without food led to similar oedemic conditions, but in a lower extent (15%) indicating that uptake role of phytoplankton is not active with low concentrations of both silver forms. Another point to be addressed is how phytoplankton cells could act as a vehicle for silver uptake. We suggest that *C. muelleri* cells used as a food source can adsorb on surface or even incorporate both dissolved silver and nanosilver. It has been shown that marine diatom cells exposed to AgNPs increased bioaccumulation and tolerance to high Ag<sup>+</sup> levels by producing polysaccharide-rich exopolymeric substances (Miao et al., 2009). TEM studies with marine diatom *Thalassiosira pseudonana* also revealed that outer silica shell did not prevent formation of Ag<sup>+</sup> clusters into intracellular milieu when exposed to AgNPs (García et al., 2014).

Oedematous juveniles were frequently resilient during exposures even under severe necrosis at 96h. Normally, two cell types emerged in turgid areas which pointed to an inflammatory mechanism induced by silver. In fact, red spherule cells have been found surrounding injuries and participating in wound healing in adult sea urchins (Tajima et al., 2007). Swollen areas enclosed by shiny membranes holding red granules and vibratile-like

cells were described in adults *Strongylocentrotus purpuratus* with infected tissues (Gilles and Pearse, 1985). As far as exotrophic juveniles developed, a growing population of red spherule cells occupied the epidermis. Once exposed to a non-infectious stimulus as dissolved silver, cell responses arose in juveniles in a similar mechanism found in adults.

### 2.7.2 Postlarva stage

Pre-juvenile stage is potentially the most vulnerable phase despite showing delayed sublethal responses to silver forms. There are some evidences to support this point. First, red spherule cells were barely found in postlarvae. As far as development proceeds, red spherule pool keeps growing in post-metamorphic life. Then, these cells were not mobilized after exposure to both silver forms in postlarvae as in juveniles. Red spherule cells in echinopluteus are normally distributed to morphogenetically active sites (Ryberg and Lundgren, 1979). This is probably the case for postlarvae as well, once we have found spherulocytes essentially participating in morphogenic process on central place of infracoral region, the forming peribuccal region where mouth will open later on (Supplementary material, Appendix 2).

Since nanoAg-FITC dye remained strongly fluorescent in lipid vesicles along metamorphosis, we wonder how AgNPs would impact a critical period for lipid utilization by postlarvae in this case. High mortality is common during this stage for many reasons, but especially environmental disturbances. During body reorganization, environmental stressors can cause developmental complications, give rise to dysfunctional juveniles and increase mortality (Gosselin and Qian, 1997). As an example, interactions of fullerene ( $C_{60}$ ) altered the size of lipid vesicles among agglomerated droplets increasing degradation in a concentration gradient (Zupanc et al., 2010). In another study, metallic nanoparticles were observed to interact with lipid vesicles and were stabilized by them (Jiménez-Rojo et al., 2015). Therefore, either lipid degradation or AgNPs relocation would certainly be another environmental factor to be interfering with postlarvae development.

Unexpectedly, the time for sublethal effects to rise in postlarvae treated with silver and nanosilver was delayed compared to unfed juveniles. While postlarvae remained unaffected, starved juveniles showed lethargic behavior in PAAm-AgNPs (NC2) exposures at 96h. Likewise, lower concentrations NC3 and NC4 of both silver forms seem not to affect postlarva stage as it does with juveniles. The same mechanisms of toxicity already mentioned doubtless governed these interactions, but the lack of food would imply higher costs for starved juveniles facing chemical injury. For instance, 3-month old juveniles were very active and had a high feeding rate with a functional gut able to digest a wide variety of food whereas short-lived postlarvae stage was less mobile and basically supported by lipidic reserves accumulated during planktonic phase. It is also important to clarify that late L8<sub>2</sub> were as resilient as postlarva in acute exposures (unpublished results), which reinforced our thoughts that postlarvae just do not support chemical stress as juveniles do. Investigating how nanoAg-FITC dye was incorporated by exposed postlarvae, we found high signal intensity coming from gut and radial canals. Without opening mouth, nano-marker may have crossed tiny membrane on supra-coronal surface, or flowed through radial canals and mesenteries where PAAm-AgNPs were found in TEM. At this stage, supra-coronal region already had a hydropore lately becoming madreporite where seawater can flow in.

### 2.7.3 Larval stage (eight-arm echinopluteus stage)

Chemical data revealed a high availability of dissolved silver in AgNO<sub>3</sub> wells, which induced high mortality and delayed metamorphosis of echinopluteus at 8°C. Metamorphosis is considered a hard food-depending process naturally driven by apoptosis and autophagy which already contributes to larval physiological stress (Pechenik et al., 1998; Sato et al., 2006). Echinoderm larvae are able to increase feeding rate beyond maximum sustained ingestion rates found in other suspension-feeders (Strathmann, 1971), and consequently become extremely vulnerable to enhanced intake of phytoplankton amended with contaminants. Other studies indicated that chronic diet borne silver exposure also caused significant effects on growth of echinopluteus of *Lytechinus variegatus* even at

concentrations as low as 0.05 to 0.07  $\mu\text{g}\cdot\text{L}^{-1}$  waterborne  $\text{Ag}^+$  and 0.68  $\mu\text{g}\cdot\text{g}^{-1}$  in dw  $\text{Ag}^+$  amended with algae at 23-25°C (Brix et al., 2012). Luoma et al. (1995) also stated that increasing levels of chloride ions in brackish waters favors  $\text{Ag}^+$  species to become neutral or negatively chloride complexes which are soluble and bioavailable to biota. Contrarily to  $\text{Ag}^+$ , PAAm-AgNPs interrupted morphogenesis at the lowest concentrations of free  $\text{Ag}^+$  in seawater, which strongly suggests effects of silver nano-form itself. Similarly, Gambardella et al. (2014) also observed that echinoplutei of *Paracentrotus lividus* feeding on phytoplankton previously reared with  $\text{SiO}_2$ -NPs and  $\text{CeO}_2$ -NPs oxide nanoparticles had increased mortality and abnormal development at 20°C. It turns out that phytoplankton might be a key factor for nanosilver intoxication for larval stages of marine invertebrates living over a wide range of temperature and salinity.

Results obtained with nanoAg-FITC led to two mechanisms of internalization of nanosilver: (i) direct uptake of the AgNPs dispersed in seawater, and (ii) facilitated uptake by contaminated phytoplankton. In both cases, nanosilver would jeopardize larval survival in coastal waters. In the first mechanism, planktotrophic larvae from oligotrophic waters would have slower development rates to undergo metamorphosis, in addition to the chemical stress. The second one would be representative of coastal areas with eutrophic food levels and closer to contaminant releasing sources. Then, as observed in our assays, it is plausible that nanosilver uptaken by phytoplankton would immediately lead to metamorphosis interruption in echinoplutei. Even worse, it would provoke far-reaching effects with increasing mortality in clean seawater.

As further evidence supporting silver nano-form toxicity, our TEM images showed how nanoparticles can be hazardous to invertebrate marine larvae at different development levels. An ongoing remolding process of coelom and tissues is occurring inside metamorphic larvae. Intestinal epithelium of proctodaeum was composed of cells specialized in food consumption and unspecialized cells lacking microvilli responsible for carrying particles out of the body. Undigested particles stained with nanoAg-FITC formed large lumps before getting expelled by large ciliated cells in distal part of hindgut. Thus,

aggregates of PAAm-AgNPs were found in lumen, beneath of microvilli and taken up by columnar cells as seen in TEM images.

In fact, aggregation of nanosilver could be a result of either digestive process or prior interactions with phytoplankton cells. Bolus of algae material amended with nanoAg-FITC stayed highly fluorescent until egestion, which indicates that AgNPs may be delivered anywhere inside lumen of gastrointestinal tract (in foregut, midgut or hindgut). As a result, trafficking from gut and between tissues would rather happened in larvae compared to perivisceral sinuses in unfed juveniles. Taken together, these results suggest gut as pivotal route for nanosilver uptake in planktrophic larvae in accordance to earlier findings of Chin and Chan (2015).

#### 2.7.4 PAAm-AgNPs cytotoxic effects

The TEM images brought very valuable information about interactions of PAAm-AgNPs with different cells in our model organism. Direct interactions of nanoparticles with cells at the molecular level are expected to induce disturbances in cellular membrane. The cell membrane has an anionic hydrophilic outer surface where cationic particles as AgNPs may attach more readily compared to anionic ones (Karlsson et al., 2013). Physical effects are directly related to particle size and their surface properties while chemical damages are mostly provoked by ionization of nanoparticle core and, as a result, a production of cellular reactive oxygen species (ROS) (Elsaesser and Howard, 2012). Leroueil et al. (2007) mentioned that polymeric nanomaterials from 1.2 to 22 nm can induce nanoscale holes formation in living cell membranes. Depending on the ratio between lipid/protein damage in cell membrane, multiple cellular functions may thus be affected such as transmembrane signaling and molecular transport. This obviously gets more complicated when a whole organism is affected. We do not know if PAAm-AgNPs (about 10 to 20 nm) would provoke such effects, but that being the case, low temperature (8°C) and fluid liquid-gel phases of biological membrane are expected to play a role in such a process (Leroueil et al., 2007).

Loading vesicles associated with nanosilver were observed in larval coelomic epithelial cells and phagocytes. However, it does not mean both cells might have handled it similarly. Phagocytosis is an energy- and receptor-dependent process with uptake requiring invagination of the plasma membrane and subsequent fusion with lysosomes while non-phagocytic pathway might occur in many cell types and is mediated by other operative mechanisms (Stern et al., 2012). In a cellular context, intracellular membrane-enclosed vesicles are naturally involved with trafficking of macromolecules and extracellular fluids regulating specific cell functions (Yameen et al., 2014). By either phagocytic or non-phagocytic pathway, nanoparticles loaded into cell vesicles will most often fuse with lysosomes to be degraded by enzyme-catalyzed hydrolysis, but AgNPs are persistent and known to induce lysosomal perturbation (Ringwood et al., 2010; Stern et al., 2012). So it is suggested that different cell types in larvae responded to nanotoxicity with their own machinery and a unique breakdown of cellular functions (Sohaebuddin et al., 2010). Lysosomal disorders caused by retention of persistent nanoparticles in the lysosome pathway have been proposed as a crucial stage towards cell death. It leads to ineffective intracellular trafficking, disrupted permeability of lysosomes, and altered signaling and gene expression (Stern et al., 2012). Alternatively, the ability of migratory phagocytic cells to accumulate silver as Ag-sulfide in lysosomes and basal lamina in marine invertebrates has been rather considered as another strategy to detoxify inner body from metallic materials (Marigómez et al., 2002). Either way, owing additional costs to physiological maintenance caused by nano-stress in larvae, metamorphosis was shut down and mortality appeared later on in recovery conditions.

Nanosilver aggregates were found in tissues, larval blastocoel, and hypogastric coelom of juveniles, but also inside cells as enterocytes, peritoneocytes and coelomic epithelial cells. Aggregation inside phagocytes might reflect an intense phagocytosis of small particles and/or small aggregates captured in coelomic spaces. Even individual PAAm-AgNPs of about 25 nm (or very small aggregates) that eventually got attached to mesenteries or flowed into coelomic fluid or other tissues might also have travelled through some prior biological processes. Coelomocytes are considered the main mediators of

immune response in Echinoidea, but full understanding of their morpho-functional properties is still under discussion (Pinsino and Matranga, 2015). As noted in larva blastocoel, more than one cell types appeared to be involved in the response against nano-stressors. Cellular cooperation in sea urchins has been reported that cytolytic activity of colorless spherule cells increased in presence of phagocytes (Arizza et al., 2007). Likewise, Furukawa et al. (2009) showed that mesenchyme cells are able to migrate, aggregate, encapsulate and engulf foreign agents in blastocoel of bipinnaria larvae of starfish, but similar mechanism was not found in our experiments with echinopluteus.

#### **2.7.5 Cellular responses and likelihood of detoxification process related to PAAm-AgNPs:**

Enterocytes in proctodaeum are expected to handle undigested material in order to eliminate fecal pellets from gut (Burke, 1981; Temereva, 2010), so their vacuoles might be primarily involved in excretion of waste material. We observed that vesicles and vacuoles were associated with metallic materials mostly detected as nano-aggregates. In a similar way, Marchesano et al. (2013) recently described the translocation of gold nanoparticles through plasmatic membrane in *Hydra* sp. by means of vesicles. Hence, TEM images suggest recruitment of loaded nanoparticles by random excretory vesicles going outward. In fact, metal elimination in many marine invertebrates may be purely incidental and present because their cells are well equipped to grab toxic cations (Ahearn et al., 2004). It is then possible that granular materials (small aggregates and single nanoparticles) would have different fates inside enterocytes: the biggest being loaded while less aggregated material getting randomly extruded. Further studies with proper markers are needed to elucidate how AgNPs of different sizes are handled by excretory cells.

Peritoneal mesothelial cells appeared to be involved in detoxification of PAAm-AgNPs as well. These cells form a monolayer of flattened squamous-like cells actively producing and exporting vesicles into coelomic fluid in both larvae and juveniles. Coelomic fluid circulation is operated by peritoneal cilia from mesothelium layer, so free micro-vesicles contributed to disperse nanosilver into blastocoel and hypogastric coelom. So far,

there is a scarcity of data about the way peritoneocyte functions evolved among coelomate clades, but in a general view they contribute to the normal homeostasis and physiology of visceral cavities. Mesothelial cells are specialized epithelial cells that cover internal organs and body wall in the peritoneal cavity of coelomate animals (Ruppert and Barnes, 1994). They secrete glycosaminoglycans, proteoglycans and phospholipids to ensure protection against infections and provide a slippery layer to avoid mechanical abrasion of inner surfaces with adjacent tissues (during peristalsis, e.g.) (Jangoux, 1982; Yung and Chan, 2007). As observed in our biological models, peritoneocytes of juvenile sea cucumber have been found to produce coelomic fluid components and promote inner circulation (Mashanov and Dolmatov, 2001). Thus, free agglomerates or single PAAm-AgNPs eventually reaching peritoneocytes from adjacent tissues or coelomic sinuses got recruited by cytosolic vesicles and delivered into hypogastric coelom. Considering that peritoneal mesothelial cells synthesize cytokines and other factors responsible for regulating inflammation, cell proliferation and migration (Yung and Chan, 2007), they could also have contributed to the coelomocyte response against PAAm-AgNPs, particularly in larger cavities where circulating cells are normally found. Recently, Zhu et al. (2012b) described exosomes as extracellularly secreted vesicles acting like conveyors for signal induction in nanoparticle-induced immune systemic responses in cells exposed to magnetic iron nanoparticles (m-FeNps). In this way, we consider that several mechanisms being part of natural metabolism in developmental stages would favor accumulation-detoxification processes ultimately responsible for balancing environmental and inner levels of metallic nanoparticles, as AgNPs, and indirectly their water soluble ions.

## 2.8 SUMMARY AND CONCLUSION

Our results revealed marked differences in toxicity mechanisms of organic-coated silver nanoparticles (PAAm-AgNPs) and dissolved silver on larval metamorphosis, postlarvae and juveniles of sea urchin. The sizable effects of AgNPs emerged at the perimetamorphic period in a long-term process including the recovery period. Larval metamorphosis gets interrupted with  $100 \mu\text{g}\cdot\text{L}$  of nanosilver whereas ionic silver slows down the process causing high mortality during exposure. With nano-fluorescent markers we confirmed gastro-intestinal tract as the main route for nano-uptake. Once taken up by larvae, PAAm-AgNPs were mainly found as small and larger aggregates. In fact, AgNPs were detected in different tissues (cellular internalization) as well as dispersed in larval blastocoel (acellular internalization). Even though a slow release of  $\text{Ag}^+$  is expected to happen with PAAm-AgNPs, we suggest that particulate silver itself would be greatly responsible for the toxicity effects during metamorphosis. Thus, high mortality rate of recovering larvae pointed to an inefficiency of detoxification mechanisms to handle nanosilver inner contamination.

Differences in toxicity for free  $\text{Ag}^+$  and PAAm-AgNPs emerged again with postlarvae and juveniles exposed to lethal ( $500 \mu\text{g}\cdot\text{L}$ ) and sublethal concentrations (50 and  $100 \mu\text{g}\cdot\text{L}$ ). On one hand, postlarva can be considered as the most vulnerable stage, owing its low red spherulocyte pool to face chemical injuries and the possibility to carry nano-contaminated tissues transferred by pre-exposed metamorphic larvae. For juveniles, ionic silver was more harmful and starvation seemed to be a critical factor during sublethal treatments. With  $100 \mu\text{g}\cdot\text{L}$ ,  $\text{Ag}^+$  caused immobility and death, while juveniles exposed to PAAm-AgNPs developed only lethargy. In addition, effects of PAAm-AgNPs dispersion in coelomic cavities of juveniles revealed coelomocyte activity and peritoneal cells acting as nano-conveyors.

Finally, the role of sentinel cells (peritoneal and immune cells) in detoxification mechanisms is described for the first time in larvae and juveniles of a marine invertebrate

model. Short and long term exposures revealed that physiological conditions of all exposed organisms evolved through time using Bray-Curtis similarity matrix and Multidimensional scaling (MDS) methods; with Permanova supporting chemical data. Overall, this study put in perspective a broad understanding of maintenance costs of each stage during silver contamination.

## CHAPITRE 3

### SILVER NANOPARTICLES AND DISSOLVED SILVER ACTIVATE CONTRASTING IMMUNE RESPONSES AND STRESS-INDUCED HSP EXPRESSION IN SEA URCHIN

#### 3.1 RÉSUMÉ EN FRANÇAIS DU TROISIÈME ARTICLE

En utilisant des cellules immunitaires d'oursin juvénile *Strongylocentrotus droebachiensis* comme modèle, les mécanismes de protection cellulaire contre l'argent ionique et les nanoparticules d'argent enveloppées par des polyallylamines ( $17 \pm 6$  nm, PAAm-AgNPs,  $100 \mu\text{g/L}$ ) ont été étudiés. Le stress oxydatif (ROS), l'expression des protéines du stress et la production de pigments par les spherulocytes ont été déterminées, ainsi que les voies de nano-translocation et leurs effets multiples sur coelomocytes circulants. Les oursins ont montré une résilience croissante à l'argent au fil du temps. L'argent ionique a été accumulé de manière régulière, alors que les niveaux nanoAg ont chuté entre 48 et 96 h. Une réaction de coagulation est apparue sur les tissus atteints par Ag<sup>+</sup> entre 12 et 48 h à la suite d'une nécrose tissulaire. La production de ROS semble être en grande partie causée par les ions Ag<sup>+</sup>. Après avoir traversé les sinus cœlomiques et de l'intestin, les AgNPs ont été retrouvées dans les coelomocytes. Les images TEM suggèrent que les structures extracellulaires de ces cellules peuvent interagir avec les petites nanoparticules avant le processus d'intériorisation. A l'intérieur des vaisseaux hémaux, les processus apoptotiques chez les coelomocytes semblent être liés à la contamination par les PAAm-AgNPs pendant l'exposition chronique. L'augmentation des niveaux d'argent accumulés par les oursins exposés aux AgNPs ont mis en évidence un mécanisme du type cheval de Troie au cours de 12 premiers jours. Toutefois, pendant les traitements à court terme, les interactions physiques des PAAm-AgNPs avec des structures cellulaires pouvaient être prédominantes et donc responsables de la forte expression des protéines du

stress à 48h. Ce rapport est le premier détaillant plusieurs mécanismes par lesquels les cellules d'oursin peuvent répondre aux AgNPs ainsi que leur translocation dans un organisme marin.

Ce troisième article, intitulé « *Silver nanoparticles and dissolved silver activate contrasting immune responses and stress-induced Hsp expression in sea urchin* », fut corédigé par moi-même ainsi que par le professeur Émilien Pelletier. Il a été soumis pour publication dans sa version finale en mai 2016 au journal *Environmental Toxicology and Chemistry*. En tant que premier auteur, ma contribution à ce travail fut l'essentiel de la recherche sur l'état de l'art, le développement de la méthode, l'exécution des tests de performance et la rédaction de l'article. Le professeur Ciro Ribeiro, deuxième auteur, m'a reçu dans son laboratoire pour une formation en Microscopie électronique à transmission et a participé aux séances d'analyse préliminaire des organismes contaminés. La professeure Lucie Beaulieu, troisième auteure, a participé à ma formation préliminaire aux techniques de Western blott. Le professeur Émilien Pelletier, quatrième auteur, a fourni l'idée originale. Il a aidé à la recherche sur l'état de l'art, au développement de la méthode ainsi qu'à la révision de l'article.

### **3.2 SILVER NANOPARTICLES AND DISSOLVED SILVER ACTIVATE CONTRASTING IMMUNE RESPONSES AND STRESS-INDUCED HSP EXPRESSION IN SEA URCHIN**

#### **3.3 ABSTRACT**

Using immune cells of sea urchin *Strongylocentrotus droebachiensis* in early developpement as a model, the cellular protective mechanisms against ionic and poly(allylamine)-coated silver nanoparticles ( $17 \pm 6$  nm, PAAm-AgNPs) treatments at  $100 \mu\text{g}\cdot\text{L}$  were investigated. Oxidative stress (ROS), heat shock proteins expression and pigment production by spherulocytes were determined and well as AgNP translocation pathways and their multiple effects on circulating coelomocytes. Sea urchins showed an increasing resilience to silver over time as ionic silver is accumulated in a steady way while nanoAg levels dropped between 48 and 96 h. A clotting reaction emerged on tissues injured by  $\text{Ag}^+$  between 12 and 48 h as a result of tissular necrosis. ROS production seemed to be in a large part caused by  $\text{Ag}^+$  ions. After passing through coelomic sinuses and gut, AgNPs were found in coelomocytes. TEM images suggested that extracellular structures of these cells can handle small nanoparticles before internalization. Inside blood vessels, apoptotic-like processes appeared in coelomocytes highly contaminated by PAAm-AgNPs during chronic exposure. Increasing levels of silver accumulated by urchins once exposed to AgNPs pointed to a Trojan-horse mechanism operating over 12-day exposure. However, under short-term treatments, physical interactions of PAAm-AgNPs with cell structures might be in some point predominant and responsible for the highest levels of stress-related proteins detected. This is the first report detailing nano-translocation in a marine organism and multiple mechanisms by which sea urchin cells can deal with toxic AgNPs.

### 3.4 INTRODUCTION

Owing to their remarkable antimicrobial, thermal, electrical and optical properties, silver nanoparticles (AgNPs) have been incorporated into several commercial products and many more new ones are expected in a near future (Mitrano et al., 2015). With the majority of AgNPs likely being released into sewer systems and reaching wastewater treatment plants; questions have been raised about their environmental toxicity. The effects of AgNPs already appear as a pressing problem for aquatic fauna, particularly in areas where industrial and urban sewages could be released into the aquatic environment without an appropriate wastewater treatment (Levard et al., 2012; Thalmann et al., 2015; Kunhikrishnan et al., 2015). Because AgNPs introduced into marine environment tend to aggregate in the water column, precipitate and accumulate on seafloor, benthic organisms are expected to figure among the ultimate receptors for nano-contaminants (Wang et al., 2014a, b). As an example, juveniles of sea urchin have cryptic habits, are particularly sedentary (Scheibling and Hatcher, 2013), and are seen as a primary target to contaminant discharges in coastal waters. As they usually face a hostile environment after settlement, their immune system gets rapidly organized to ensure host survival and can be considered as valuable model to investigate nanotoxicity of silver (Magesky et al., 2016).

Echinoderm's coelomocytes, a heterogeneous population of freely moving cells, occupy perivisceral coelomic cavities, connective tissues, and water-vascular system. They have shown complex responses to metallic nanoparticles such as stannum dioxide ( $\text{SnO}_2$ ), cerium dioxide ( $\text{CeO}_2$ ), iron oxide ( $\text{Fe}_3\text{O}_4$ ) and titanium dioxide ( $\text{TiO}_2$ ) (Falugi et al., 2012; Pinsino and Matranga, 2015). As an example,  $\text{TiO}_2$ NPs (10-65 nm) in low concentrations (1-5  $\mu\text{g}\cdot\text{mL}^{-1}$ ) elicited a typical phagocytic mechanism carried out by phagocytes involving the TLR/p38 MAPK signaling pathway in adults of *Paracentrotus lividus* (Pinsino and Matranga, 2015). Also with *P. lividus*, short exposures to 5-35 nm citrate-stabilized AgNPs ( $\sim 0.3 \text{ mg}\cdot\text{L}^{-1}$ ) induced dose-dependent developmental abnormalities in embryos and larvae, but the cause to effect relationship was not elucidated (Šiller et al., 2013). Burić et al. (2015) also tested the sensitivity of urchin embryo development to AgNPs (50 nm) in the range of 1

to 100 µg·L<sup>-1</sup> using species *Arbacia lixula*, *P. lividus* and *Sphaerechinus granularis* for short-term exposures at 16-20°C. *A. lixula* was the most sensitive one with a high number of aberrant embryos or arrested development at the lowest concentrations tested (1-10 µg·L<sup>-1</sup>/AgNPs). While Šiller et al. (2013) reported AgNPs-derived dissolved silver in seawater to be about 1.0% of total Ag in 50h; Burić et al. (2015) found 3-7% over 48h which is indicative of adverse effects of nanoparticulate silver itself. We recently reported that polymer coated-AgNPs (15 ± 5 nm) slowly dissolved in seawater and were less disruptive than Ag<sup>+</sup> ions on different stages of developing embryos of *S. droebachiensis* (Magesky and Pelletier, 2015). So far, little work has been reported on the way immune system of sea urchin can deal with highly toxic AgNPs dispersed in seawater.

The way coelomocytes of sea urchin face nano-contamination is still unclear, but it appears that phagocytosis of nano-aggregates could be an effective response regardless the type of metallic nanoparticle involved (Falugi et al., 2012; Pinsino and Matranga, 2015; Magesky et al., 2016). Using a marine annelid model, Cong et al. (2014) detected lysosomal and DNA damage in coelomocytes of *Nereis (Hediste) diversicolor* after a chronic exposure to AgNPs (~10nm/2-100 nm) in a wide range of concentrations (5-100 µg Ag·g dw sed.). Notwithstanding, for AgNPs, it is unknown how individual AgNPs or aggregates could affect subcellular compartments of coelomocytes and which protective mechanisms and cell death process would emerge in response to injuries.

Among tools to explore protective mechanisms, heat shock proteins (hsp) have been largely used as an important marker to assess effects of several contaminants in many invertebrate species. For some marine invertebrates, hsp70s have also been involved in wound healing processes and perhaps inflammatory signals (Browe et al., 2007; Jean et al., 2004; Pinsino and Matranga, 2015; Vazzana et al., 2015). Similarly involved in polypeptide folding and protein translocation, hsp60s have shown contrasting responses with different aquatic invertebrates exposed to cationic metals (Singer et al., 2005; Rios-Arana et al., 2005; Pinsino et al., 2010). Yet, mechanism related to hsp60s or even hsp70s expression has not been described for marine invertebrates contaminated by ionic or nanoparticulate silver.

Currently, some efforts have been allowed to find out which portion of AgNP toxicity is related to either nanoparticles themselves or their Ag<sup>+</sup> leaching ions. In a recently proposed Trojan-horse mechanism, ROS species such as H<sub>2</sub>O<sub>2</sub> are suggested to react with AgNPs to form more Ag<sup>+</sup> (Hsiao et al., 2015). It has also been hypothesized that internalization of small AgNPs can result in a signaling cascade that generates ROS and inflammatory markers, leading to mitochondria dysfunction and subsequently induction of apoptosis (Arora et al., 2008; Miethling-Graff et al., 2014; Tomankova et al., 2015). It has already been postulated that nanomaterials can induce cell specific responses as a function of variable toxicity and following cell fate based on the exposed type of cells. Henceforth, not only the chemical behavior of AgNPs will drive their toxic effects in the intracellular milieu, but also the machinery of the targeted cells by themselves. So, finding out what are the main entry routes and how AgNPs translocate in a model organism will contribute to reveal more about the nanotoxicity effects in different groups of cell-types.

In the light of the above-mentioned considerations, we aimed in the present work to understand the toxicity mechanisms of Ag<sup>+</sup> and poly(allylamine)-coated silver nanoparticles (PAAm-AgNPs) on developing cohorts of young sea urchins with the support of chemical data. We analyzed the protective cellular reactions against both toxicants by means of oxygen species (ROS) production, expression of hsp60s and hsp70s and pigment production by spherulocyte cells. Finally, we determined the main entry routes of AgNPs, their translocation pathways and distinctive effects on circulating coelomocytes by means of Transmission electron microscopy (TEM).

### **3.5 MATERIAL AND METHODS**

#### **3.5.1 Test organism conditions**

Young adults ( $6.0 \pm 1.5$  cm in average diameter) of green sea urchin *Strongylocentrotus droebachiensis* were collected at low tide in a rocky intertidal zone along the south shore of the Lower St. Lawrence Estuary, eastern Canada ( $48^{\circ}26'48.47''$ N;  $68^{\circ}34'53.06''$ W). Immediately after collection, the specimens were acclimatized at 5°C ( $\pm$

2°C) in a large flow-through seawater system with 12h light/day. All physical and chemical parameters were very similar to nearby natural coastal environment and urchins in captivity regularly fed *Laminaria* sp. A laboratory protocol to handle echinoderm larvae through metamorphosis and juvenile stage was previously described (Magesky et al., 2016).

### **3.5.2 Preparation of PAAm-AgNPs and characterization**

Poly(allylamine)-coated silver nanoparticles (PAAm-AgNPs) were prepared following the protocol of Al-Sid-Cheikh et al. (2011). PAAm-AgNPs size and dispersion were determined by transmission electron microscopy (TEM Delong Instruments LVEM 5, precision  $\pm$  2 nm). A drop of PAAm-AgNPs stock solution analyzed by TEM showed a multimodal distribution of nanoparticles having 8 nm ( $n=25$ ), 16 nm ( $n=21$ ), and 25 nm ( $n=10$ ) (Supplementary material, Appendix 3).

### **3.5.3 Measurement of dissolved silver in exposure media and sea urchins**

Analysis of dissolved silver in exposure media, total silver in particulate matter, and total bioaccumulated silver in juvenile sea urchins was performed by Induced Coupled Plasma Mass Spectrometry (ICP-MS), after exposure to 100  $\mu\text{g}\cdot\text{L}$   $\text{Ag}^+$  and PAAm-AgNPs at 8°C. Two feeding conditions were tested: under starvation (6 wells) and with added phytoplankton cells (6 wells). Urchins were harvested at 1h, 24h and 96h; washed in clean seawater filtered 0.45  $\mu\text{m}$  and carefully soaked up with paper filter before being dissolved in 2 mL of 100%  $\text{HNO}_3$ . Particulate matter (mainly phytoplankton cells) was separated from exposure media by centrifugation at 7400 rpm for 10 min at 4°C. Pellets were separated from supernatant and weighted on paper filters. Finally, filters with pellets were directly dissolved in  $\text{HNO}_3$  100%. All samples were kept in the dark at 5°C for further analysis.

### **3.5.4 Stock solutions and test concentrations**

Stock solutions of  $\text{AgNO}_3$  (75 mg Ag·100 mL) and PAAm-AgNPs (4.768 mg Ag·100 mL) were prepared in nanopure water for dilution to nominal concentrations. For the main tests, 100  $\mu\text{g}\cdot\text{L}$  of silver (ionic and particulate forms) were used according to pre-

screening results obtained from a range of concentrations (500 µg·L to 20 µg·L). All solutions and suspensions were stored in the dark at 5°C to minimize photodegradation.

### **3.5.5 Experimental set-up for stress proteins, bioaccumulation, oxygen reactive species detection, pigment production and migration of immune cells**

Sea urchins were exposed to 100 µg·L of AgNO<sub>3</sub> and PAAm-AgNPs under starvation for 48h at 8°C in 12-well tissue culture plates with flat bottom (Falcon 353043, polystyrene made), each well filled up with 5.5 mL of filtered seawater and 5 individuals transferred into it. To assess silver toxicity in feeding conditions, diatom *Chaetocerus muellerii* at 15.6 x 10<sup>5</sup> cells as final concentration in 5.5 mL was used as a food source. Each test consisted of 6 replicate wells for controls and exposed ones. All experiments were conducted under 12h light/12h dark cycle, with plates always protected against light exposure. Tests were independently repeated three times.

To understand how immune cells would migrate in different sea urchin cohorts exposed to silver, organisms were separated in different groups as a function of their size (2 categories per month) and age (1 to 3 months). Diameter of shells was measured from the first week after settlement to 8 months to obtain their growth curve (presented in Supplementary material, Appendix 3). Each cohort consisted of 24 replicates, with small and large sea urchins organized, respectively, as age groups (mean diameter): cohort C1-Ag<sup>+</sup>/PAAm-AgNPs (0.46 cm) and C2-Ag<sup>+</sup>/PAAm-AgNPs (0.57 cm) for 1-month old individuals; cohorts C3-Ag<sup>+</sup>/PAAm-AgNPs (0.89 cm) and C4-Ag<sup>+</sup>/PAAm-AgNPs (1.24 cm) for 2-month old; and cohorts C5-Ag<sup>+</sup>/PAAm-AgNPs (1.26 cm) and C6-Ag<sup>+</sup>/PAAm-AgNPs (1.63 cm) for 3-month old urchins. Cohorts were placed in 48-well cell culture cluster flat bottom plates (Corning Costar 3548, polystyrene made) filled with 1.5 mL of filtered sea water at 8°C. Sea urchins were exposed to 100 µg·L of dissolved and particulate silver forms under starvation in 24 replicates for each contaminant (5 urchins per well), 12 replicates for each cohort and the controls. The total exposure period was 12 days (3 x 96h). Observations were made with a stereo-microscope every 96h.

### 3.5.6 Oxygen reactive species assessment

CellROx oxidative stress reagent (Molecular probes® Life technologies), green (485/520 nm) was used to measure reactive oxygen species (ROS) *in vivo*. We first tested animals from rearing batches in order to assess their health conditions before testing. We then assessed ROS under exposure conditions with and without food, including the controls. Urchins were harvested at 96h of exposure to Ag<sup>+</sup> or PAAm-AgNPs/100 µg·L. Taken randomly (n= 5) among 6 replicates (n= 30), juveniles were placed into 300 µL of sea water on the glass bottom dishes with 1µL of stress marker for 30 min then rinsed with clean seawater mixed with phosphate buffered saline before observation. Oxygen reactive species were detected with Z-stack, Ortho and 2.5 D functions in the confocal microscope (LSM700 Carl Zeiss).

### 3.5.7 Pigment extraction and quantification

Three-month old juveniles exposed to 100 µg·L of both contaminants were harvested after 12h, 24h, 48h and 72h exposures. The specimens were then placed into small plastic petri dishes to be air dried at 5°C for 5 days into the dark. For each sampling time, 6 replicates per treatment and controls (5 organisms per well, 30 per condition, 240 per contaminant, for a total of 480) were manipulated. Each specimen had diameter of shell measured before pigment extraction. Dried shells were then placed into glass tubes with 1.5 mL of 6M HCl for 45 min and strongly agitated in vortex each 10 min to optimize tissue dissolution and extraction of free pigments. Absorbance values of extracted pigments were obtained by transferring 300 µL for each sample in wells of a quartz microplate. Absorbance analysis was repeated twice to get an average value for each organism. Maximum absorbance was observed at a wavelength of 450 nm using spectrophotometer Thermo Max microplate reader (Molecular Devices). As pigments could slowly degrade in HCl-aqueous solution, we managed to work with 30 individuals at once taking into account equal period of time for: (1) extraction of all shells, and (2) absorbance measurements in order to keep the same procedure for each group.

### **3.5.8 Immune cell migrations detection:**

Three month-old sea urchins were used as a model for assessment in confocal microscopy after 12, 24, 48 and 72h exposures. Images of sea urchin coelomocytes were taken *in vivo* by Inverted microscope Axio Cam Observer Z1 and Laser scanning microscope under 10X, 40X and 63X magnifications. In order to reveal which cell types (other than red spherulocytes) would be involved in migration towards wounded areas as well as their proportion related to the physiological responses, the nucleic acid stain SYBR Green I marker (Molecular probes® Life technologies) has been used. For regular toxicity assessment in chronic exposures, observations were made with Leica/Wild M3Z stereo microscope.

### **3.5.9 Proteins extraction, SDS-Page and Immunoblotting for Hsp analysis**

Urchins (5 for each condition) were carefully harvested at 12h, 24h and 48h and immediately frozen and stored at -80°C for biochemical measurements. The complete Lysis-M, EDTA-free buffer supplied with protease inhibitors (Roche) was used to extract proteins. To optimize this procedure, animals were transferred to Eppendorf tubes already filled up with lysis buffer and then skeletons were smoothly broken. Samples were placed on ice during 30 min and mixed in vortex each 5 min, warmed to 50°C in water bath for 5 min before cooling on ice for 5 min. This procedure was repeated twice. Finally, samples were sonicated for 2 h on cold water, and centrifuged for 15 min. Proteins were separated by 4-12% Bis-Tris NuPage minigels, 1.0 mm x 12 wells (Introgen) by SDS-PAGE technique. After transferring proteins to nitrocellulose membranes (PVDF membrane, Bio-Rad), they got blocked overnight at 5°C with Casein blocking buffer (Sigma-Aldrich). 60-kDa proteins we probed with monoclonal anti-heat hsp60 antibody produced in mouse (ascites fluid, H3524-Sigma-Aldrich) diluted 1/100. For 70-kDa proteins, monoclonal anti-heat hsp70 antibody produced in mouse (ascites fluid, H5147-Sigma-Aldrich) diluted 1/10000 was used. Goat anti-mouse-HRP conjugated secondary antibodies from Bio-Rad detection were used in second incubation. Finally, protein bands were detected by colorimetric reaction provided by Opti-4CN diluent and substrate anti-mouse solutions (Bio-rad). Bands intensity were

quantified with software Image studio lite version 5.0.21 and expressed as IDVs (integrated density values).

### **3.5.10 Sample preparation for Transmission electronic microscopy (TEM)**

Only one-month-old sea urchins were used for TEM study. General conditions followed those described in section 2.5 for contamination. Samples were fixed in 2.5% glutaraldehyde in 0.1M cacodylate buffer, pH 7.4, mixed with seawater (1 mL: 0.5 mL) immediately after final assessment. Then samples remained preserved and stored at 5°C for 6 months before preparation for TEM observations. This long time preservation was considered here as a primary fixation and led to complete decalcification prior to the next steps of sample preparation. A detailed protocol for sample preparation is given in Magesky et al. (2016).

### **3.5.11 Statistical design**

Owing to our complex experimental design and multiple physiological responses displayed by exposed sea urchins, we opted for a permutational analysis of variance (PERMANOVA) ( $p < 0.05$ ) with Primer 6.1.1.12 and Permanova+ 1.0.2 software. A large number of exposed replicates and individuals per condition allowed analyzing bioaccumulation and absorbance data with PERMANOVA. Unpaired *t*-tests were applied to confirm differences in hsp60 and hsp70 expression at 48h between Ag<sup>+</sup> and PAAm-AgNPs replicates.

## **3.6 RESULTS**

### **3.6.1 Silver distribution in exposure media, sea urchins and phytoplankton**

Chemical analysis of dissolved silver (including all soluble chemical forms in seawater) in exposure media with juveniles at different times is given in Table 1. After 1h-exposure to Ag<sup>+</sup> (100 µg·L) + phytoplankton, about 43% of free silver (chloro-complexes and/or soluble organic-complexes of silver) was available in seawater on contrarily to only 26% in PAAm-AgNPs one (Table 1). After 24h, dissolved silver declined by 19% in Ag<sup>+</sup>

conditions and similarly by about 21% in PAAm-AgNPs, and reached about 3% in both conditions after 96h. Adsorption of silver occurred on inner surface of wells in a similar extent for AgNO<sub>3</sub> and PAAm-AgNPs (about 11% after 1h), but decreased sharply to about 1.5% for the rest of the exposure time, which is attributed to a desorption process from the inner wall as the total free silver was decreasing in seawater. Without phytoplankton, a much larger proportion of dissolved silver was found at all sampling times in AgNO<sub>3</sub> condition when compared to exposure with phytoplankton (Table 1). Silver adsorbed onto inner wall of wells was about the same with and without phytoplankton for all sampling times and both soluble and nanoparticulate Ag species. Seawater of chronic tests with PAAm-AgNPs had 36.5% of free silver at 3h and 17% up to 288h.

Table 5: Chemistry data for dissolved silver as a function of elapsed time for fed and unfed sea urchins exposed to nominal concentration of 100 µg·L of silver nitrate and nanosilver in short term (4 days); and long term treatments (12 days) for PAAm-AgNPs. Dissolved silver in exposure media, adsorbed by inner wall wells and suspended particulate matter as well as accumulated by sea urchins tissues are given as % of total silver added (100% meaning total silver, 100 µg·L).

Feeding condition	Exposure media	Elapsed time (h)	Dissolved free silver in seawater (%)	Adsorbed silver on inner wall of wells (%)	Adsorbed silver in SPM (%) (estimated)	Bioaccumulated silver in sea urchins (%)	Mass balance (%)
With phytoplankton	AgNO <sub>3</sub>	1	43	10.9	25.8	12.7	92.4
		24	24	1.4	19.9	30.0	75.3
		96	3	1.3	20.7	47.9	72.9
	NanoAg	1	26	11.0	21.1	25.1	83.2
		24	5	1.7	14.3	23.2	45.9
		96	3	1.3	12.8	26.4	43.5
Without phytoplankton	AgNO <sub>3</sub>	1	60	12.5	(<1)	31.6	104.1
		24	40	1.8	(23.4)	29.5	76.6
		96	24	1.8	(39.4)	34.8	60.6
	NanoAg	1	34	8.4	(22.8)	34.8	77.2
		24	26	1.3	(30.3)	42.4	69.7
		96	14	1.7	(64.6)	19.7	35.4
		3	36	1.6	(43.1)	19.3	56.9
		288	17	<1.0	(51.8)	31.2	48.2

The amount of silver found in suspended particulate matter (mainly added phytoplankton and feces of sea urchins) was also determined and expressed as a % of total added silver for assays with phytoplankton only (Table 1). The proportion varied between 12.8% at 96h for AgNPs to a maximum of 25.6% at 1h for AgNO<sub>3</sub>. Estimated values in brackets (obtained by subtraction from 100%) are given for both Ag species without added phytoplankton. These values may be overestimated as lost silver in the analytical protocol was unknown and not taken in account in this case.

In assays with phytoplankton, accumulated silver in juveniles increased significantly with time in a similar way for AgNPs and soluble Ag. Without phytoplankton added, the behavior of silver is much less clear and an increase with time is not evidenced. The mass balance of all compartments is not adding to 100% in most cases. The loss of silver seems to increase with time with a maximum of 64.6% for AgNPs at 96h without phytoplankton. It is remarkable that the loss of silver is always higher with AgNPs compared to soluble Ag forms. These losses could be attributed to strong adsorption of AgNPs to well surface, filters and tubing which led to low recovery during silver analysis.

### **3.6.2 Cellular mechanisms against Ag<sup>+</sup> and PAAm-AgNPs**

#### a) Detection of oxidative stress

Silver contamination and nutritional state influenced the production of ROS in cohorts of 3-month old specimens. Juveniles of any cohort from rearing cultures had small aggregates of cells in moderate to low oxidative stress. After short-term exposure (96h), starving juveniles from controls formed ROS as well as those exposed to soluble Ag and PAAm-AgNPs/100 µg·L. Even under a much lower silver concentrations (20 µg·L) individuals produced ROS. Among starving specimens contaminated with both silver forms, only small ones showed highest levels of ROS over spines, podia, pedicellaria and shells. The larger urchins exhibited moderate stress mostly on spines and podia. Oedematous individuals also had high levels of ROS production caused by soluble Ag or PAAm-AgNPs/100 µg·L. Non-exposed feeding urchins had low levels of ROS at 96h similar to

those found among animals from rearing cultures. Optical z-stack series of specimens exhibiting different levels of ROS in Confocal microscopy are given in Supplementary material, Appendix 3.

b) Pigment production and amoebocyte/red spherulocyte cell cooperation under silver exposures

Chemically injured epidermis from shell and spines had swollen cells and a massive migration of spherulocyte and amoebocyte cells towards these areas (Supplementary material, Appendix 3). Using immune cell migrations as an indicator of biological condition, we classified migratory stages in elapsed time as following: induction, mobilization and agglomeration (Supplementary material, Appendix 3). Ionic silver was more toxic than AgNPs for all cohorts (young, medium and old ones) exposed over 12 days. However, younger cohorts (1-month old, C1 and C2) were much more sensitive than medium and older ones ( $p = 0.0001$ ). Immune cells of young urchins experienced all physiological responses from induction to necrosis over 12 days. Observing groups treated with PAAm-AgNPs, cells were only detected in mobilization stage at the final exposure time.

Concentrations ranging from 102.7 to 148.6  $\mu\text{g}\cdot\text{L}^{-1}$  quickly induced immune cells migration in a short period of time. Three-month old urchins went through all cell migration stages until necrosis when exposed to  $\text{Ag}^+$  during 72h. With AgNPs, only induction and mobilization stages appeared. Strong differences related to time for abnormalities to rise in short term exposures with soluble Ag and AgNPs were highly significant ( $p = 0.0001$ ). Red spherulocyte cells are normally dispersed on epidermis and in a lower extent in internal spaces like gut surface, coelom etc. Inside a given cohort, strong differences in spherulocyte pool may occur with consequences on individual responses against stress. Under chemical treatment, there was a clear mobilization of red spherulocytes in a short period of time for soluble Ag ( $100 \mu\text{g}\cdot\text{L}^{-1}$ ) associated with another coelomocyte type, tentatively identified as an amoebocyte-type.

Using primarily spherulocytes as a stress biomarker in this work, stages of their migration based on the number of cells reaching injured areas over time were characterized (Figure 29): (i) induction state when the number of red spherulocyte cells increases around 8.5-fold ( $17 \text{ cells per } 6.0 \times 10^3 \mu\text{m}^2$ ) compared to amoebocytes found *in situ* (Figure 29 A), then (ii) mobilization state with 13.5-fold more cells agglomerating in target areas ( $27 \text{ cells per } 6.0 \times 10^3 \mu\text{m}^2$ ) (Figure 29 B), and finally (iii) agglomeration state (Figure 29 C and D), which might be interpreted as a second stage of amoebocytes mobilization (3D representations of inducted and agglomerated cells in spines are shown in Supplementary material, Appendix 3). During agglomeration state, amoebocytes seemed to greatly exceed red spherulocyte ones (24-fold,  $48 \text{ amoebocytes}/2 \text{ red spherulocyte cells per } 6.0 \times 10^3 \mu\text{m}^2$ ). It could be attributed to lysis of cell granules containing echinochrome in wound areas, justifying why very few red spherulocytes were found in highly pigmented regions. No cells were detected inside these reddish agglomerations (Figure 29 D). Accordingly, more pigmentation also in those areas seemed to be a result of cell multiplication, more granules production per cell and/or degranulation. Post-chemical stress oedema indicated that both cell types continued to repair injured epidermis and skeleton (Supplementary material, Appendix 3).

Figure 29: Cooperation of spherulocytes and amoebocyte-type cells chemically induced by dissolved silver ( $100 \mu\text{g}\cdot\text{L}^{-1}/\text{Ag}^+$ ) in sea urchin from cohort C5 (3 month old) in short term exposure (96h). Each stage of cell migration towards injured areas was primarily characterized by the proportion between red spherulocyte and amoebocyte-type cells through time (white arrowheads indicate spherulocytes; green fluorescent nucleus corresponded in majority to amoebocyte-type cells). A- Induction (12-24h). B- Mobilization (24-48h). C, D: Agglomeration (48-72h): no cells have been dyed by SYBRGreen I marker beneath the surface of tumefied region shown in D (a Z-stack image sequence), which confirmed lysis of spherule cells. Necrosis overwhelmingly began after 72 to 96h depending on urchin age, cohort, contaminant and ionic charges (not shown). See text for more details. (A-D: 20X, scale bar:  $50 \mu\text{m}$  in laser microscopy).

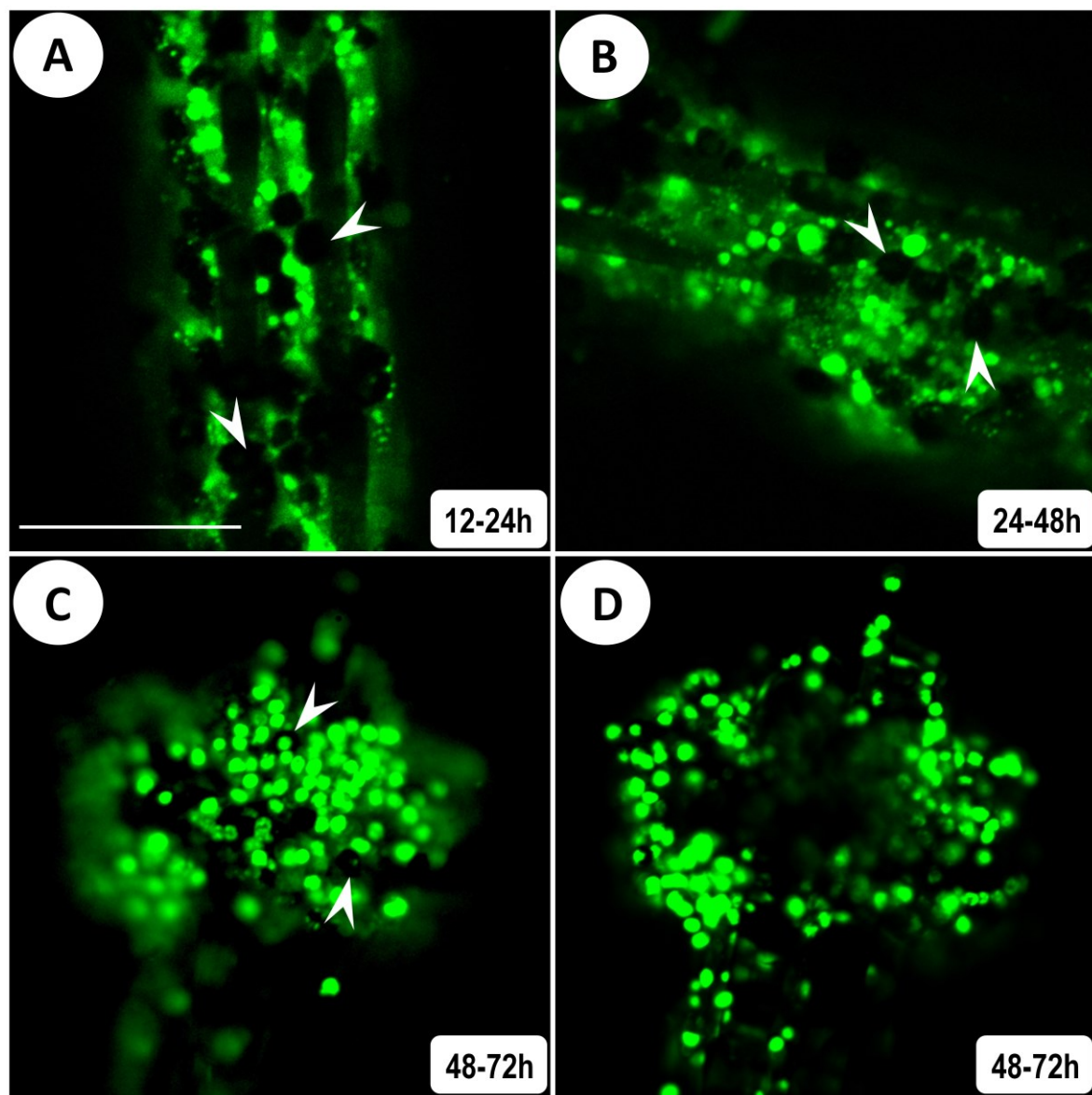


(Figure 29, see legend on previous page)

In developing sea urchins, the number of red spherulocytes was growing as a function of age and size, but a high variability may naturally occur. Differences in urchin size were not significant between controls and exposed organisms ( $p > 0.05$ ). Then after data normalization, the values representing the ratio between absorbance of reddish pigments and volume ( $\text{cm}^3$ ) of shells were obtained for soluble Ag, PAAm-AgNPs treated urchins and controls (Figure 30 A and B). With absorbance values increasing for similar shell volumes for soluble Ag treated urchins, the ratio of pigments absorbance to volume ( $\text{cm}^3$ ) also increased ( $p < 0.001$ ). It dispersed red dots away from the straight line and generated a relatively low  $R^2$  ( $= 0.63$ ). Small differences of pigments to volume ratio between treated and non-treated organisms also appeared at 12h ( $p < 0.05$ ) even though they were less visible by stereo microscopy. Considering nanoAg treatments (Figure 30 B), pigments to volume ratio did not differ between controls and exposed sea urchins, except for 72h exposure when an increasing level of pigments in treated organisms was detected ( $p < 0.05$ ). Highly dispersive points reflected the overall individual variability among sea urchins related to reddish pigment presence even among same size individuals ( $R^2 = 0.15$ ). These points preclude the establishment of a clear relationship between pigment absorbance and AgNP toxicity.

c) Translocation, internalization and elimination of nanoAg by circulating coelomocytes and peritoneocytes

Inside intra-peritoneal space of one month-old juveniles, circulating coelomocytes exhibited phagocytic activity in presence of small aggregates and individual PAAm-AgNPs attached to peritoneum (Figure 31). Nano-internalization by non-phagocytic pathway occurred in neighboring peritoneocytes as a consequence of AgNPs dispersion in haemal vessels from peritoneum. Outside intra-peritoneal coelom, peritoneocytes produced secretory vesicles with which AgNPs may have been randomly associated: (a) by following natural secretory pathway inside the cell after direct translocation or as undigested waste material (mechanisms 1 and 2 in Figure 31); (b) just before vesicle translocation towards perivisceral cavity without cell internalization (mechanism 3 in Figure 31). In this case, nanoAg

eventually crossed peritoneum barrier, to flow through haemal ducts to finally be concentrated on secretory vesicles ready for releasing.

Coelomocytes engulfed PAAm-AgNPs by means of typical phagocytic pathway (mechanism 4 in Figure 31). Phagocytic vesicles fused with a large and dense lysosome forming a phagolysosome holding  $\pm$  276 nm nano-aggregations seen in Figure 32. Primary lysosomes were also detected nearby. A few 15 nm-PAAm-AgNPs and small aggregates (61 nm) remained grabbed on the inner surface of phagolysosome, probably indicating that nanosilver loaded by vesicles could be later packed as a result of cell activity. In comparison, lysosome-endosome hybrid structure in peritoneocyte held nanosilver congregations with 77 to 107 nm in length, an intracellular digestion pathway in addition to the secretory one previously described (Supplementary material, Appendix 3).

Figure 30: Absorbance curve of extracted red pigments (wavelength 450 nm) as a function of sea urchin shell volume ( $\text{cm}^3$ ). Each point corresponded to a sea urchin (controls and treated ones),  $n=480$  organisms individually analyzed in total. A- Absorbance of pigments from  $\text{Ag}^+$  treated sea urchins ( $100 \mu\text{g}\cdot\text{L}$ ) and controls within 72h ( $p < 0.0001$ ): 6 replicates per condition;  $n=30$  individuals, giving 240 in total. B- Absorbance of pigments from PAAm-AgNPs treated sea urchins ( $100 \mu\text{g}\cdot\text{L}$ ) and the controls within 72h ( $p < 0.05$ ): 6 replicates per condition, 30 individuals, 240 in total.

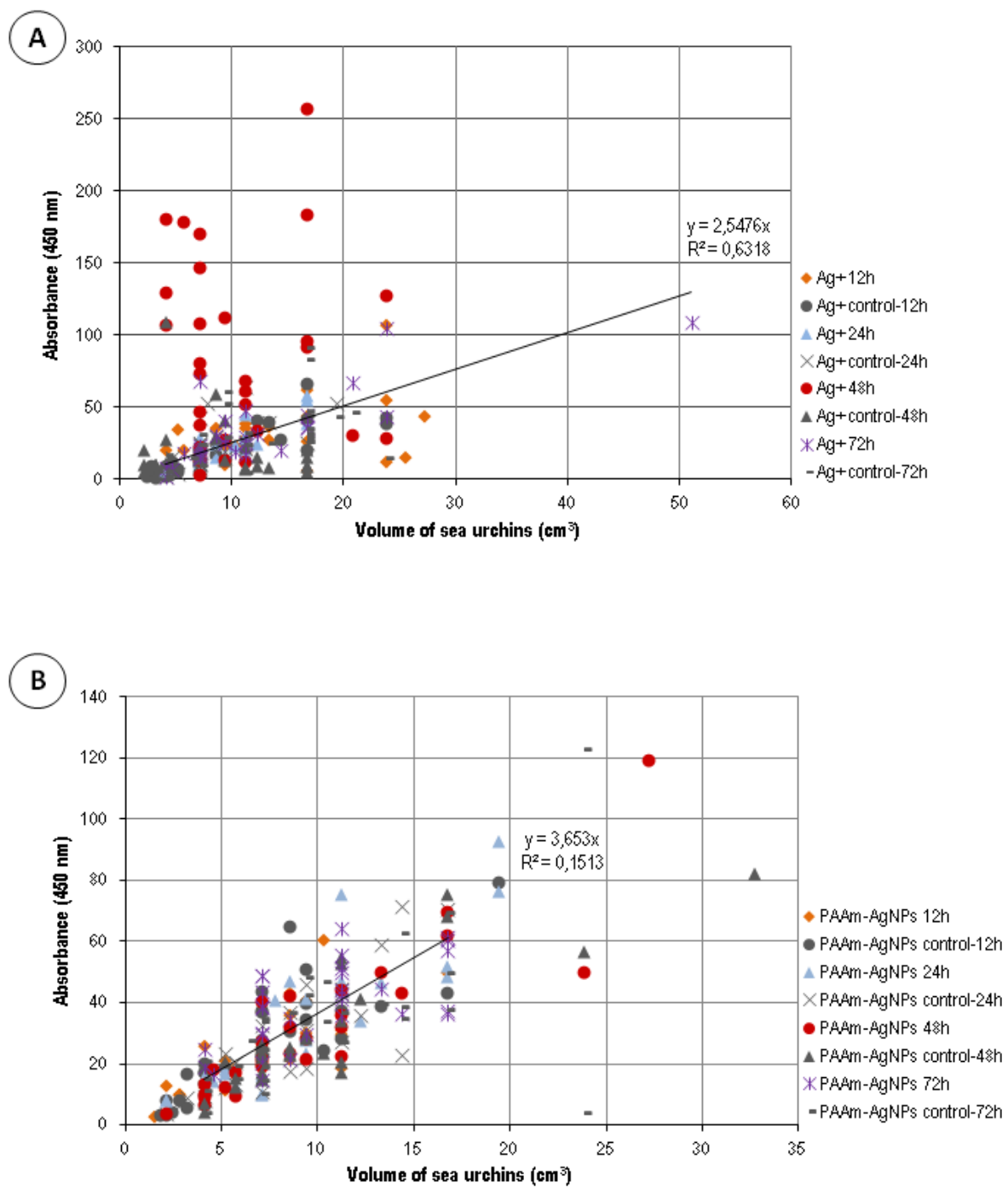


(Figure 30, see legend on previous page)

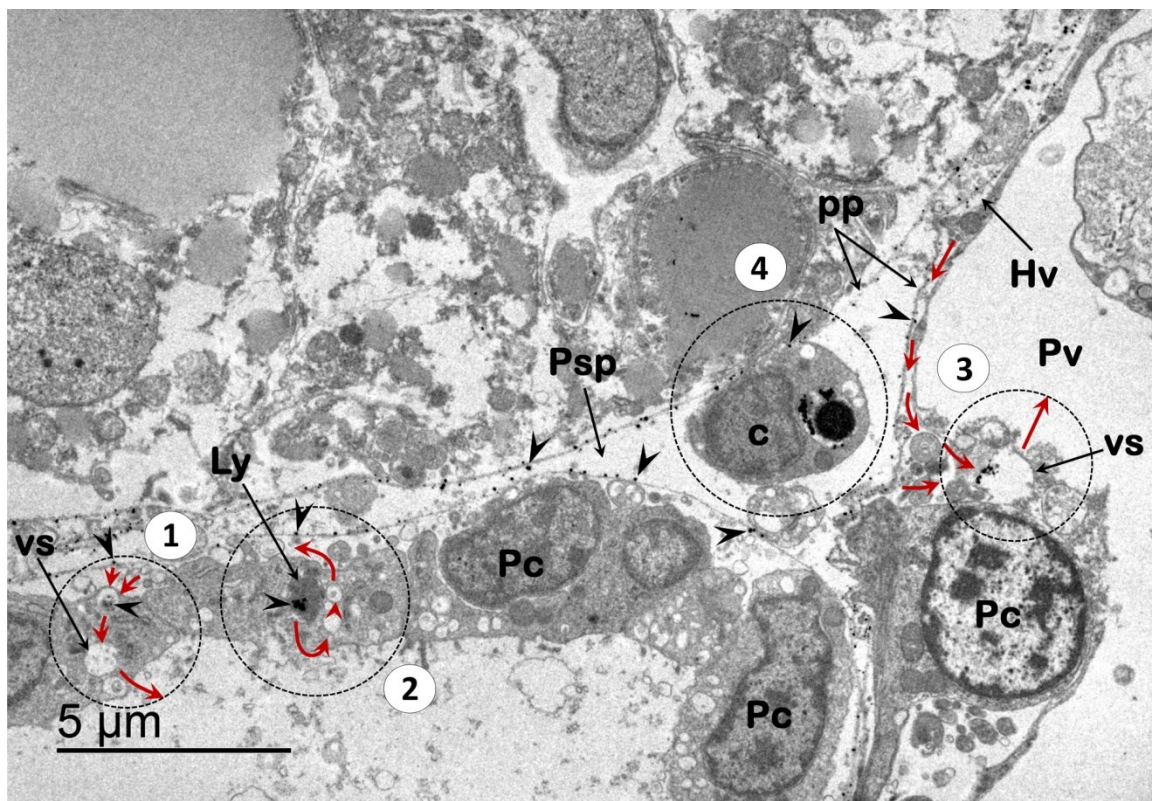


Figure 31: TEM photomicrograph of intra-peritoneal coelom (mesothelium of inner wall of shell) with trail of PAAm-AgNPs on mesenteries (parietal peritoneum) and cellular mechanisms involved with nano-internalization processes (non-contrasted sample). Mechanisms in peritoneocytes (1-3): 1- Translocation of nanoAg from parietal peritoneum to perivisceral coelom by means of vesicles; 2- Elimination of non-digested nanoAg by cytoplasmatic vesicles going to inner space between peritoneocytes and parietal peritoneum (or to perivisceral coelom); 3- Direct translocation of nanoAg from external haemal vessel to excretory vesicles already located on cell surfaces, and then to perivisceral coelom. Mechanism in coelomocyte: 4- Phagocytosis of agglomerates grabbed in mesenteries. Some nanoAg are indicated by black arrowheads, while red arrowheads indicate the direction of the nano-transportation. More AgNPs can be observed in mesenteries, tissues and cells. Abbreviations: Hv: haemal vessel, Ly: lysosome, Pc: peritoneocyte, Pp: parietal peritoneum, Psp: intra-peritoneal space (coelom), Pv: perivisceral coelom, vs: vesicle.

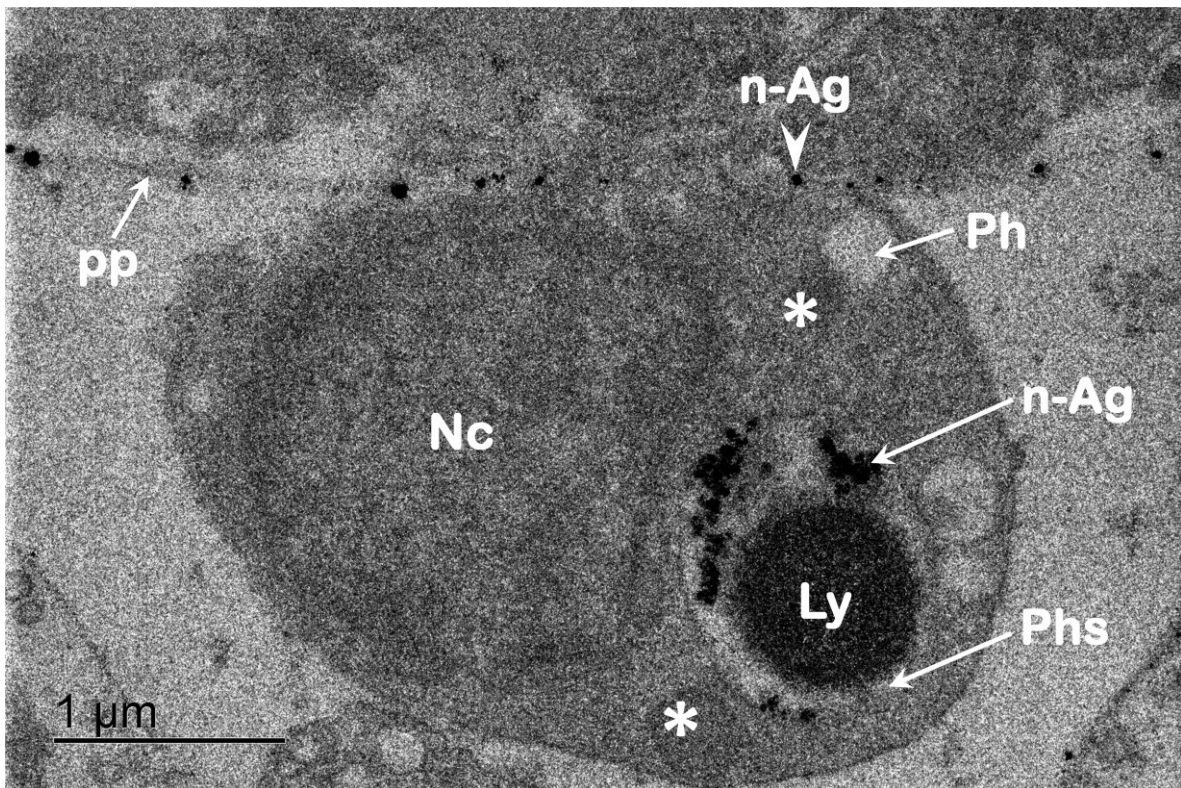


Figure 32: Intra-peritoneal coelomocyte observed in detail (cell mechanism 4 in Figure 31). A typical phagocytic pathway in presence of nanoAg is shown by TEM photomicrograph (non-contrasted sample). Some nanoAg are indicated by white arrowheads on parietal peritoneum. White asterisks indicate early lysosomes close to a phagosome and the larger phagolysosome. More AgNPs can be observed in mesentery. Abbreviations- Ly: lysosome, n-Ag<sup>+</sup>: nanosilver, Nc: cell nucleus, Ph: phagosome, Phs: phagolysosome, Pp: parietal peritoneum.

Another coelomocyte intra-peritoneal space had multiple vesicles being dispersed from cell surface (Figure 33, panel 1). It seemed that AgNPs were concentrated as individual 8 nm-AgNPs on extracellular lamella-shaped surfaces before getting finally trapped by extruding vesicles (Figure 33, panel 2). Inter-NP distances between them was 0.6 nm in average ( $n=13$ ). Measuring the size of AgNPs in stock solution, we found a proportion of 43% of 8 nm-AgNPs. Small (40 to 80 nm) and large aggregates (160 to 176 nm) trapped in large vesicles might thus be the result of nano-concentration on cell surface. Many individual nanoparticles (8 to 15 nm) were found on parietal peritoneum, followed by small

aggregations (from 30 to 61 nm) and seldom by larger ones (about 107 nm). At which point these aggregations could be byproducts of cell releasing is still unclear.

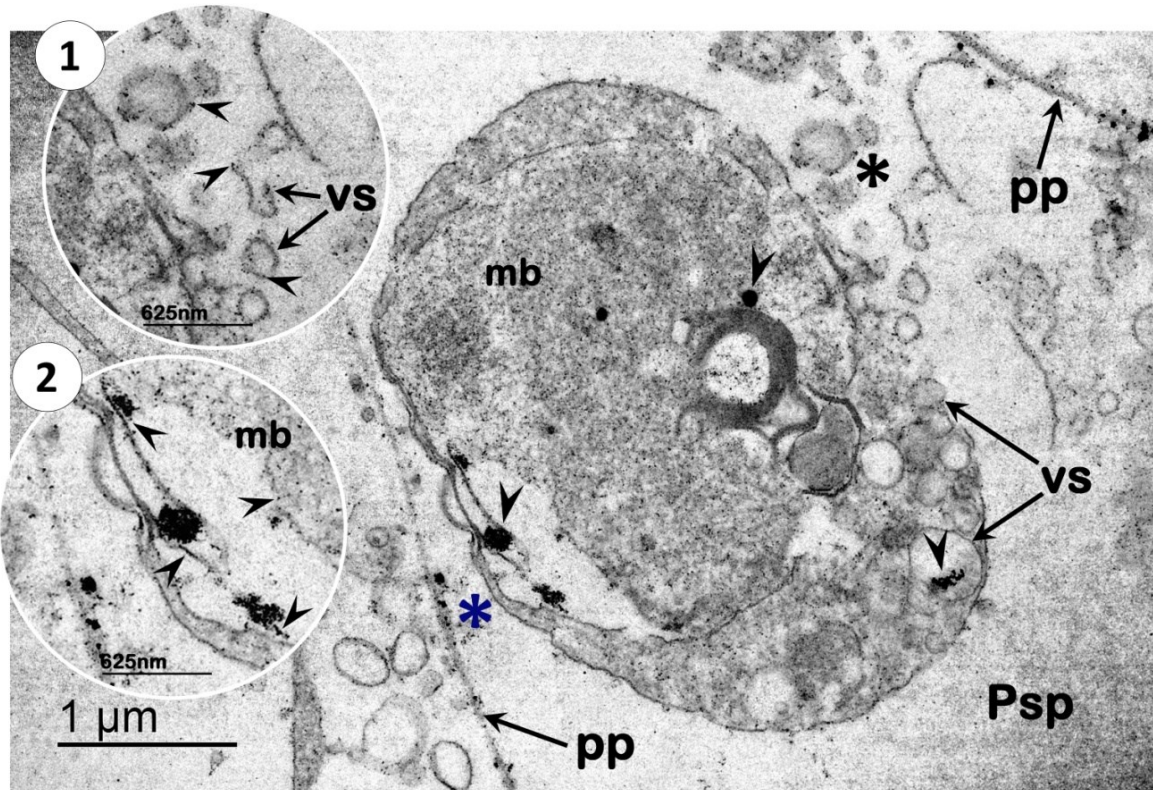


Figure 33: Intra-peritoneal coelomocyte exhibiting extrusion of nano-vesicles formed on cell surface (non-contrasted sample). Multiple 8 nm-PAAm-AgNPs appeared to be released in association with cell vesicles into intra-peritoneal space (panel 1) after nano-concentration in lamellae-like projections on cell surface (panel 2). Black arrowheads indicate nanoAg (individual or agglomerates). Area indicated by black asterisk is shown in detail in panel 1, while blue asterisk referred to panel 2. More AgNPs can be observed in cell, mesentery, vesicles and coelom. Abbreviations- mb: cell membrane, pp: parietal peritoneum, Psp: intra-peritoneal space, vs: vesicle. Coelomocytes from unexposed juveniles are shown in Supplementary material, Appendix 3.

Inside mesenteric haemal vessel (internal haemal duct) running close to esophagus, coelomocytes exhibited cytoplasmatic vesicles with concentrated nano-metallic material (Figure 34).

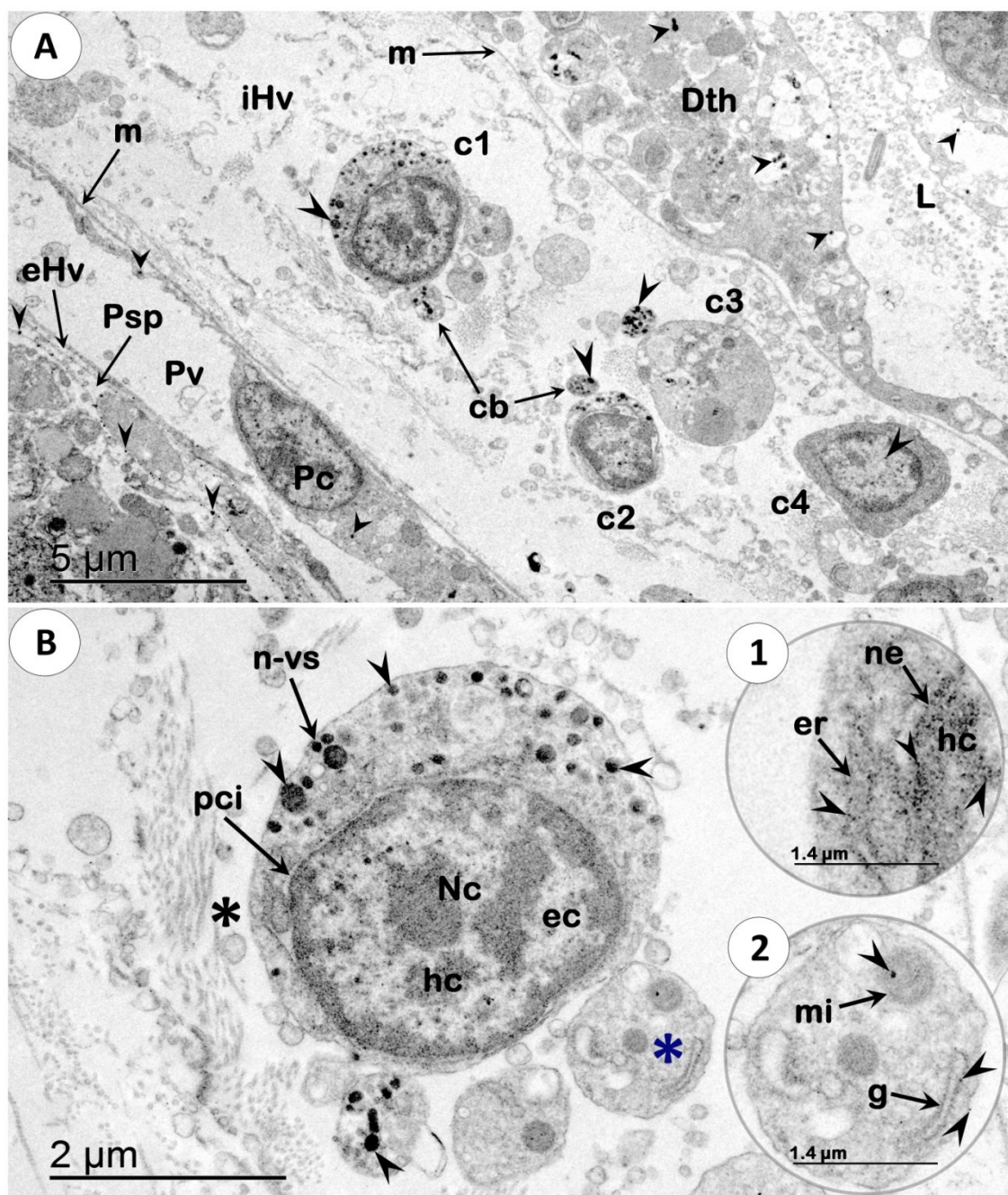


Figure 34: TEM photomicrographs of coelomic sinuses and haemal ducts. The region is localized between gut and inner wall of shell (non-contrasted sample). A- Internal haemal vessel with four circulating coelomocytes close to digestive epithelium, three of them (c1, c2 and c3) holding many nano-dense vesicles, one of them (c4) with PAAm-AgNPs spread inside nucleus. More cell debris can be seen everywhere. B- Coelomocyte c1 in detail. Back asterisk indicate area close to cell

structures seen in panel 1, while the blue one shows a cell breb (panel 2). Black arrowheads indicate nanoAg dispersed inside cells, tissues, coelomic and haemocoelic structures. Abbreviations- c: coelomocyte, cb: cell breb, Dth: digestive epithelium, ec: euchromatin, eHv: external haemal vessel, er: endoplasmatic reticulum, g: Golgi apparatus, hc: heterochromatin, iHv: internal haemal vessel, L: lumen, m: mesentery, m: mitochondria, ne: nuclear envelope, n-vs: nano-dense vesicle, Pc: peritoneocyte, pci: perinuclear cisternae, Psp: intra-peritoneal space, Pv: perivisceral coelom. Non-contrasted tissues (digestive epithelium and internal haemal vessel) of unexposed urchin are shown in Supplementary material, Appendix 3.

While in intra-peritoneal space (Figure 34 A), larger particles and aggregates were grabbed by mesenteries (acellular internalization) as less nanoAg are seen on walls of the internal haemal vessel. Nonetheless, cells from digestive epithelium particularly retained nanoparticles or aggregates (12 to 64 nm) inside vacuoles. TEM image also suggests that coelomocytes from internal vessel were the main target for small PAAm-AgNPs (cellular internalization) (Figure 34 A). They normally held multiple nano-dense vesicles in part eliminated by squeezed cellular fragments (Figure 34 A and B). Compared to coelomocytes from controls (Supplementary material, Appendix 3), cell blebs and nano-dense vesicles were never detected. Nanoparticle-dense vesicles measured between 0.10 and 0.19  $\mu\text{m}$  and concentrated different amounts of nanoAg (Figure 34 B). Smaller nanosilver particles (8 nm) were strongly dispersed over heterochromatin, nuclear envelope and endoplasmic reticulum, but less present over cell membrane and in cytoplasm. Nanosilver from 17 to 42 nm associated with chromatin were depicted as well. In cytoplasm, endoplasmic reticulum and mitochondria became some of the intracellular targets for PAAm-AgNPs as observed in cell brebs (Figure 34 B, panels 1 and 2). Non-contaminated internal haemal vessel and digestive tissues are shown in Supplementary material, Appendix 3.

d) Stress proteins hsp70 and hsp60

With 3-month old urchins exposed to soluble Ag and PAAm-AgNPs/100  $\mu\text{g}\cdot\text{L}^{-1}$  cellular anti-chemical stress responses with Hsps specifically related to each contaminant emerged. We found no appreciable variation above controls in hsp70 levels of large urchins

(cohort C6) exposed to particulate silver at 12h, which means no hsp70s expression related to nanoAg effects (Figure 35 A). At 24h the intensity of hsp70s expression in sea urchins reached similar levels of IDVs with nanoAg treatment (25.8) and controls (26.7). And still, no valuable difference between them was found. Throughout 48h protein expression went to the highest levels when nanoAg clearly up-regulated hsp70s in a twofold increase, 29.7% higher than control levels. At 12h Ag<sup>+</sup>-treated urchins had 12.7 IDVs in band intensity, 3.3% more compared to controls (Figure 35 B). A little increase in protein expression was also detected with contaminated urchins at 24h and in a lower extent in controls. As depicted in PAAm-AgNPs treatments, hsp70s levels drastically raised at 48h and band intensity reached 36.3 IDVs in dissolved Ag wells. On the contrary, densitometric analysis showed hsp70s down-regulated to 7.7 IDVs in untreated organisms.

Early on, both exposed urchins and controls had levels of hsp70s, 25.3 and 23.4 IDVs; respectively. Interestingly, soon at 24h PAAm-AgNPs up-regulated hsp70s expression in small urchins (cohort 5) in a twofold increase, which was 46.2 IDVs in band intensity compared to loading controls (26.1) (Figure 35 C). Protein expression remained relatively high at 48h, whose lane was clearly more intense than control. Likewise, in dissolved Ag wells, protein expression progressively raised from 12 to 48h. Upon Ag<sup>+</sup> contamination, sea urchins harvested at 12h showed 23.3 IDVs of band intensity, which increased to 45.3 (24h) and then 52.5 IDVs (48h), the highest peak found during treatment (Figure 35 D). Up to 48h, hsp70s seemed also to be up-regulated in a lower extent in non-treated urchins of Ag<sup>+</sup> and PAAm-AgNPs exposures. Significant differences of hsp70 expression in large urchins particularly emerged at 48h for dissolved Ag and nanoAg media ( $p = 0.0128$ ) (Figure 35 E). Four replicates for each contaminant supported these findings taking into account increasing amount of proteins analyzed (Figure 35 E). Moreover, with 15.6 and 26.0  $\mu\text{g}\cdot\mu\text{L}$  of proteins, more bands between 70 and 50 kDa were detected in Ag<sup>+</sup> exposures, but not for PAAm-AgNPs.

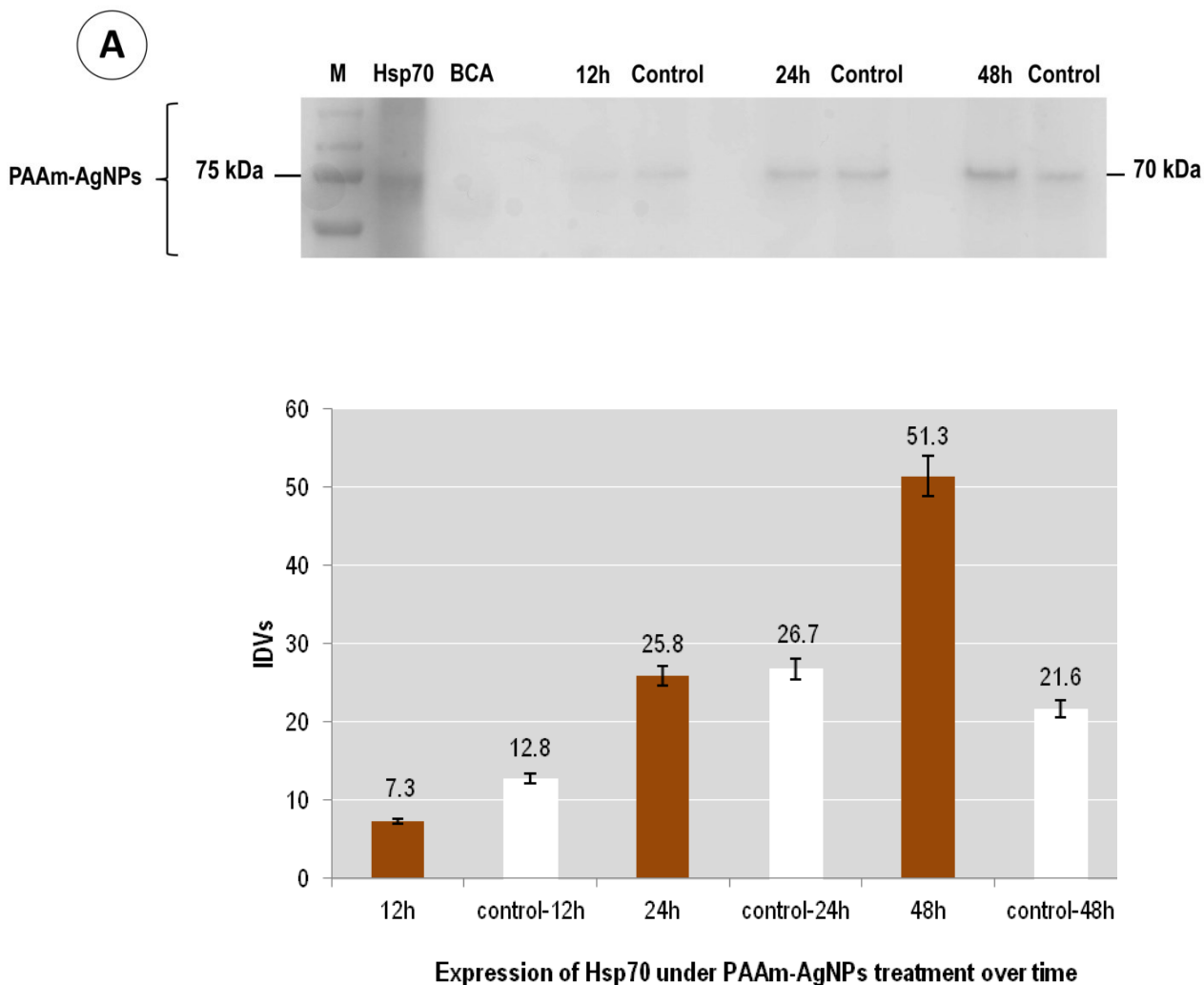
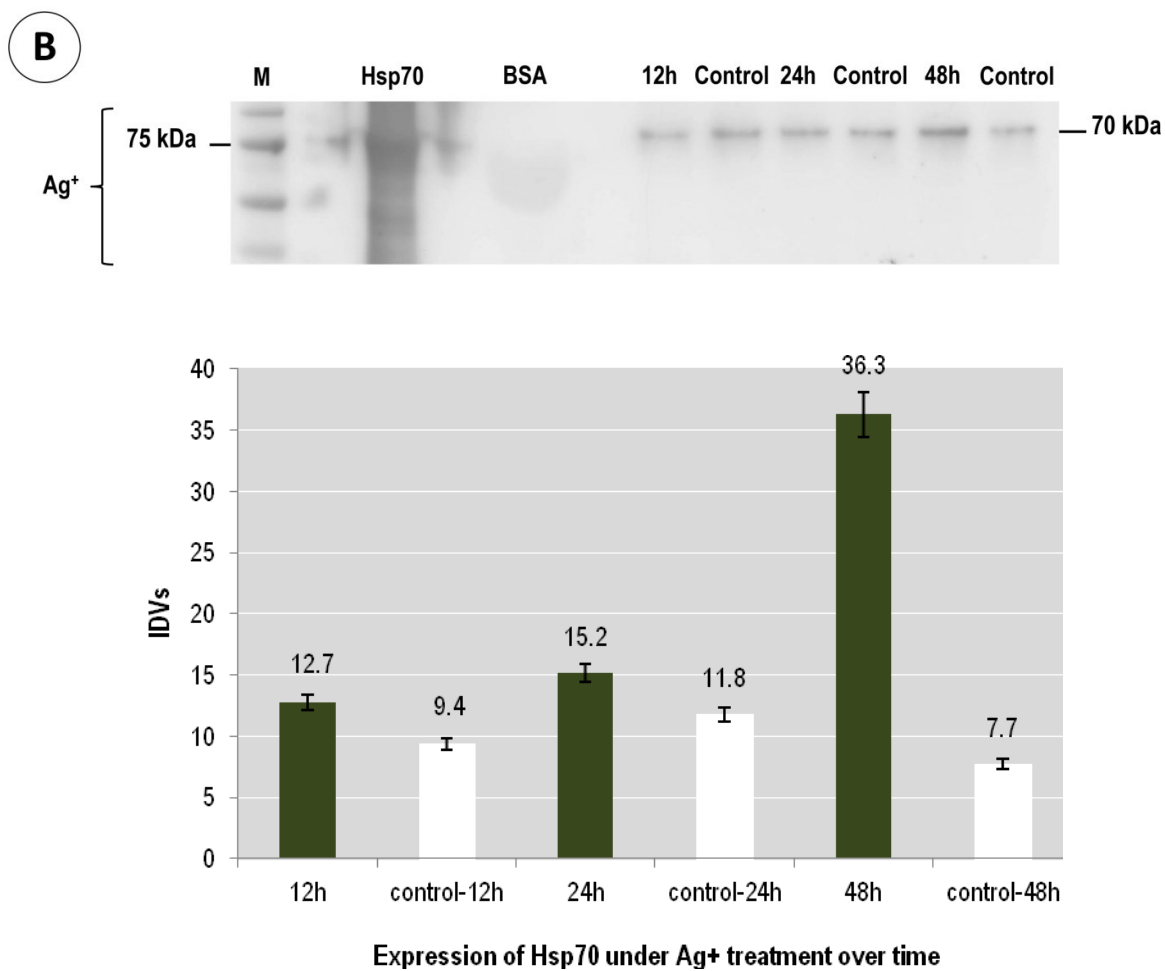
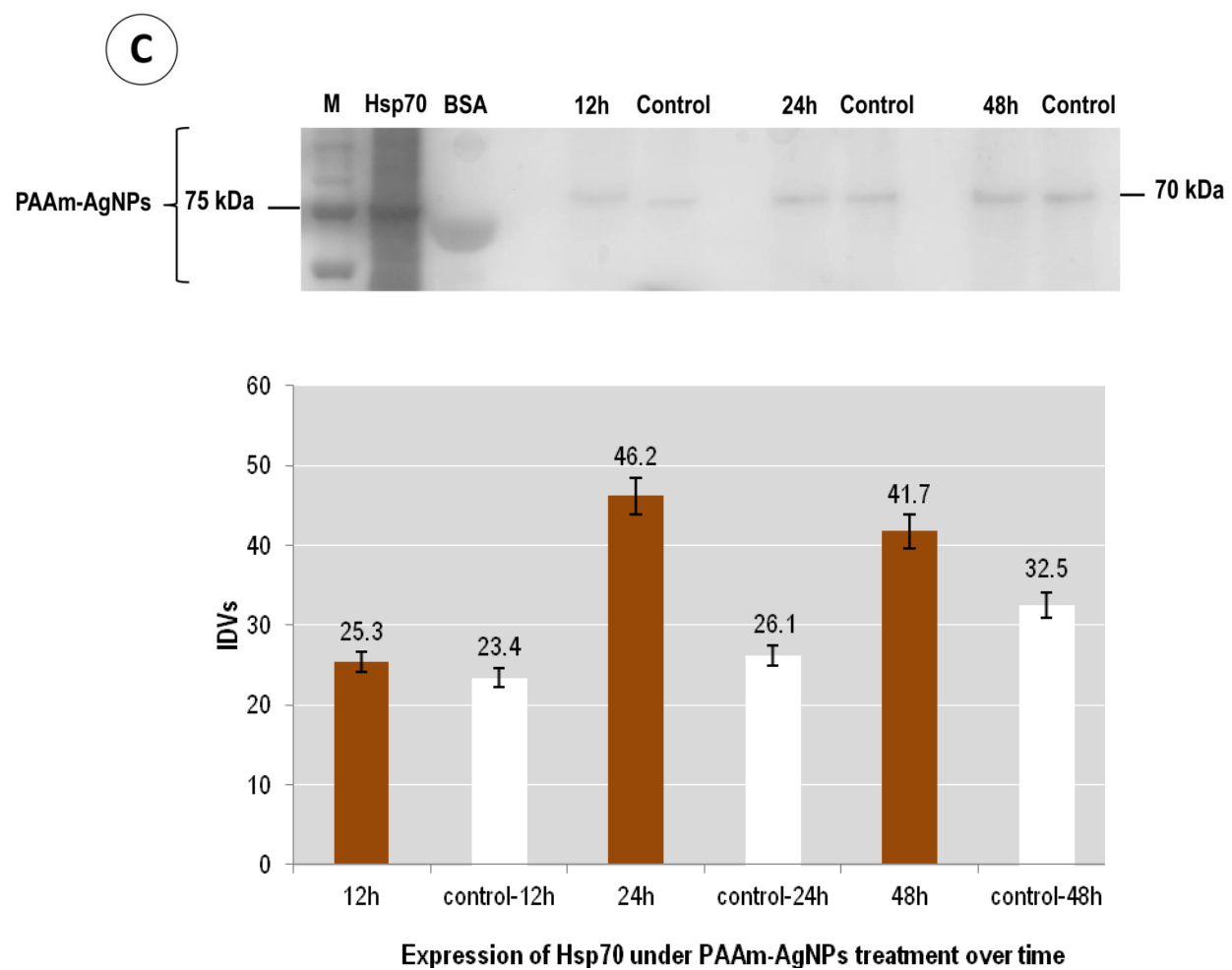
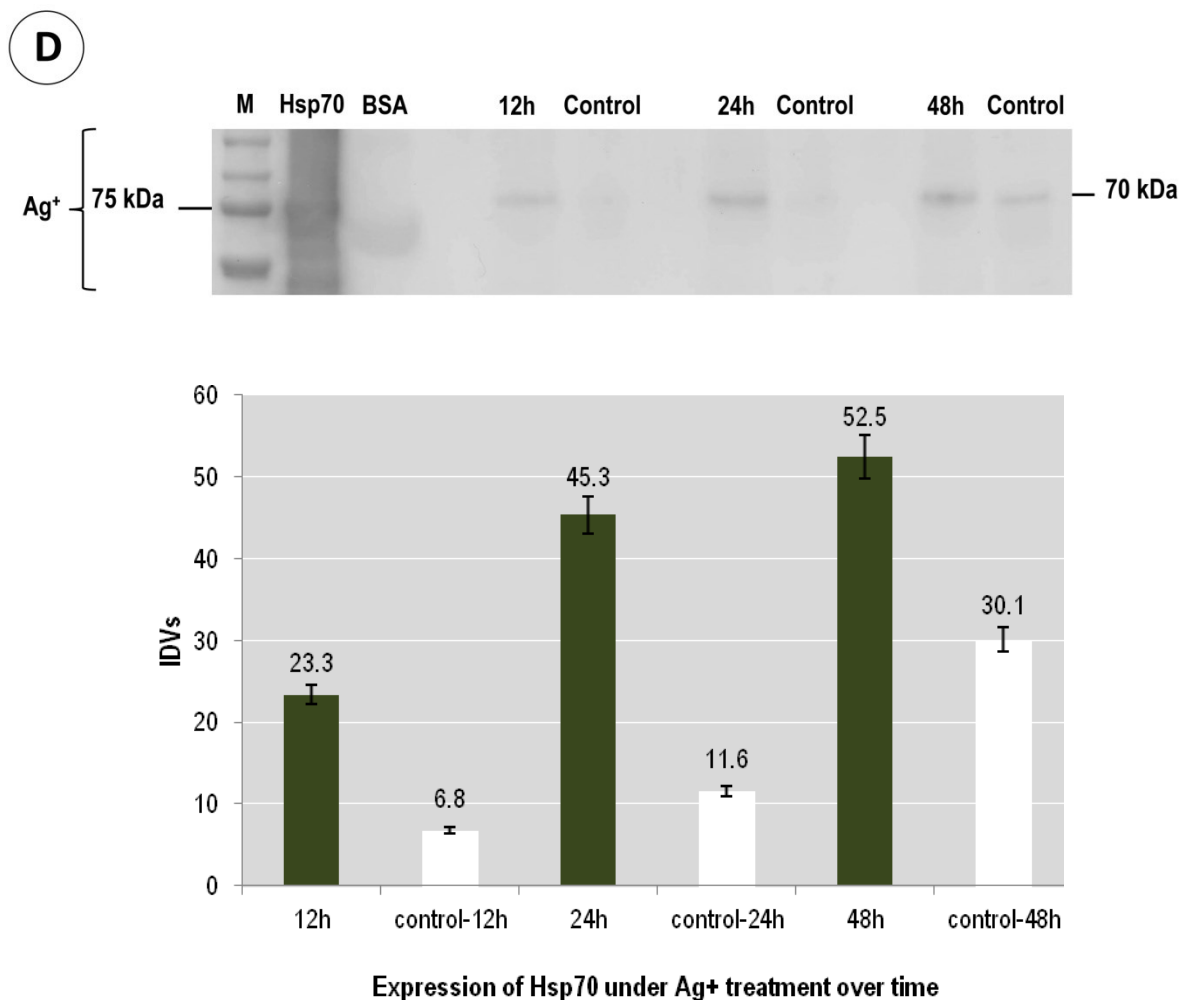


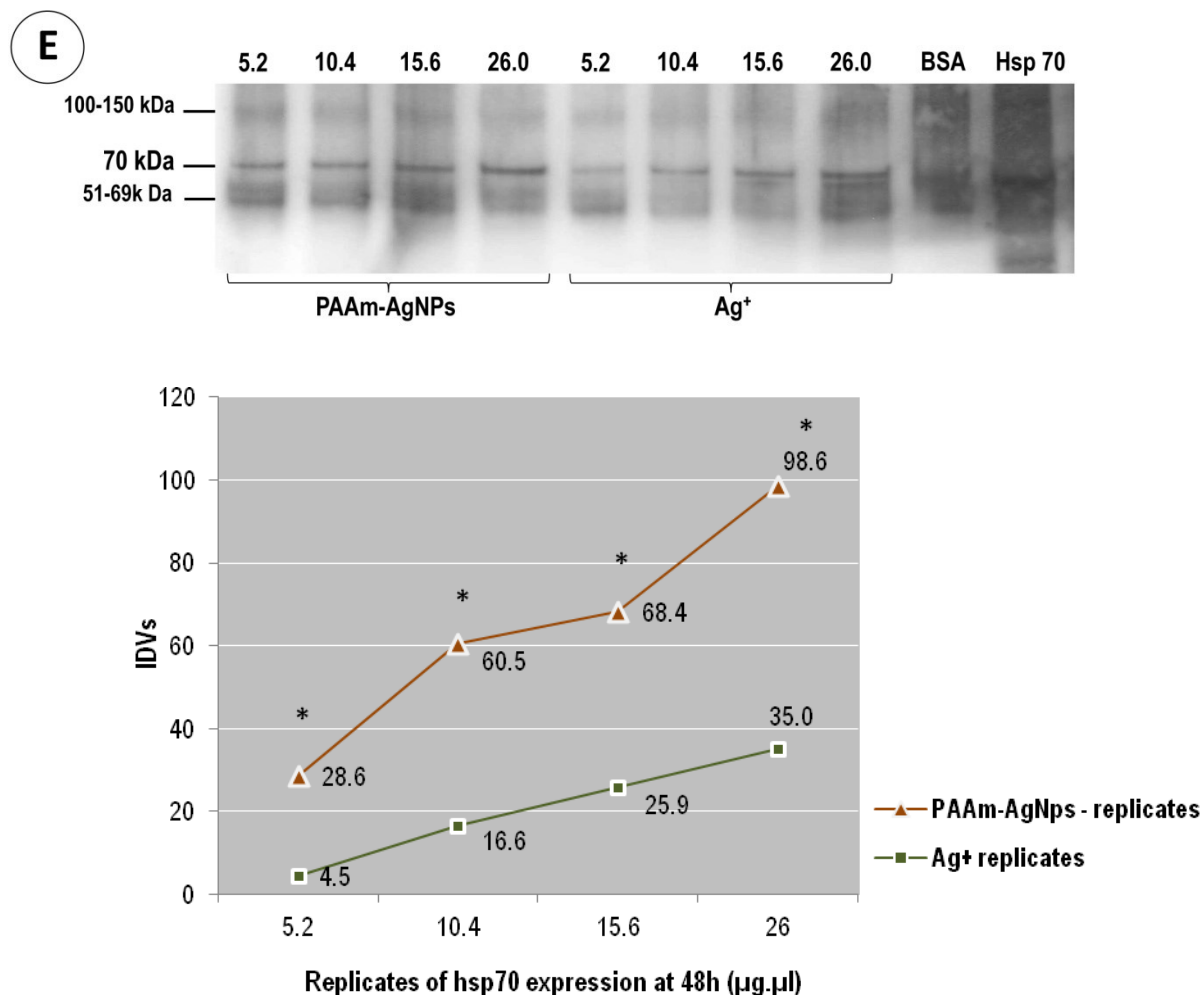
Figure 35: Quantification of hsp70 stress proteins in 3-month old sea urchins exposed to Ag<sup>+</sup> and PAAm-AgNPs/100 µg·L within 48h. Dark orange bars indicate PAAm-AgNPs treatments and dark green bars the Ag<sup>+</sup> ones. White bars indicate the controls for both contaminants. A-B: Hsp70 expression in large juveniles (cohort C6) when exposed to PAAm-AgNPs (A) and Ag<sup>+</sup> (B). C-D: Hsp70 expression in small juveniles (cohort C5) when exposed to PAAm-AgNPs (C) and Ag<sup>+</sup> (D). E: Replicates of hsp70 expression for Ag<sup>+</sup> and PAAm-AgNPs treatments at 48h with different amounts of proteins loaded into the wells (µg·µl) (\*p < 0.05). Data was obtained by densitometric scanning (IDVs: integrated light density values). For large sea urchins, histograms represent the means of the two independent experiments ± SE after normalization. For small urchins, only one immunoblotting

experiment was performed for each contaminant. Abbreviations: M: molecular-weight size marker, BSA: bovine serum albumin (negative control).









The highest level of hsp60 expression in large urchins from nanoAg media arose at 48h, with 9.4 IDVs in protein expression compared to controls (6.8) (Figure 36 A). From 12 to 24h, both contaminated and uncontaminated urchins had an up-regulation of hsp60s without appreciable variations. With dissolved Ag media, exposed sea urchins had 16.5 IDVs in protein hsp60, 3.2% more than controls at 12h (Figure 36 B). Then, this expression decreased to 10.4 (24h) and 7.2 IDVs at 48h under dissolved silver treatment. Immunoblotting results also suggest a down-regulation trend up to 24h in non-treated sea urchins, with hsp60 levels getting stable until 48h in similar levels to those at 24h (8.0% in average). Differences for Ag<sup>+</sup> and PAAm-AgNPs at 48h were significant and grounded with replicate analysis ( $p = 0.0242$ ) (Supplementary material, Appendix 3).

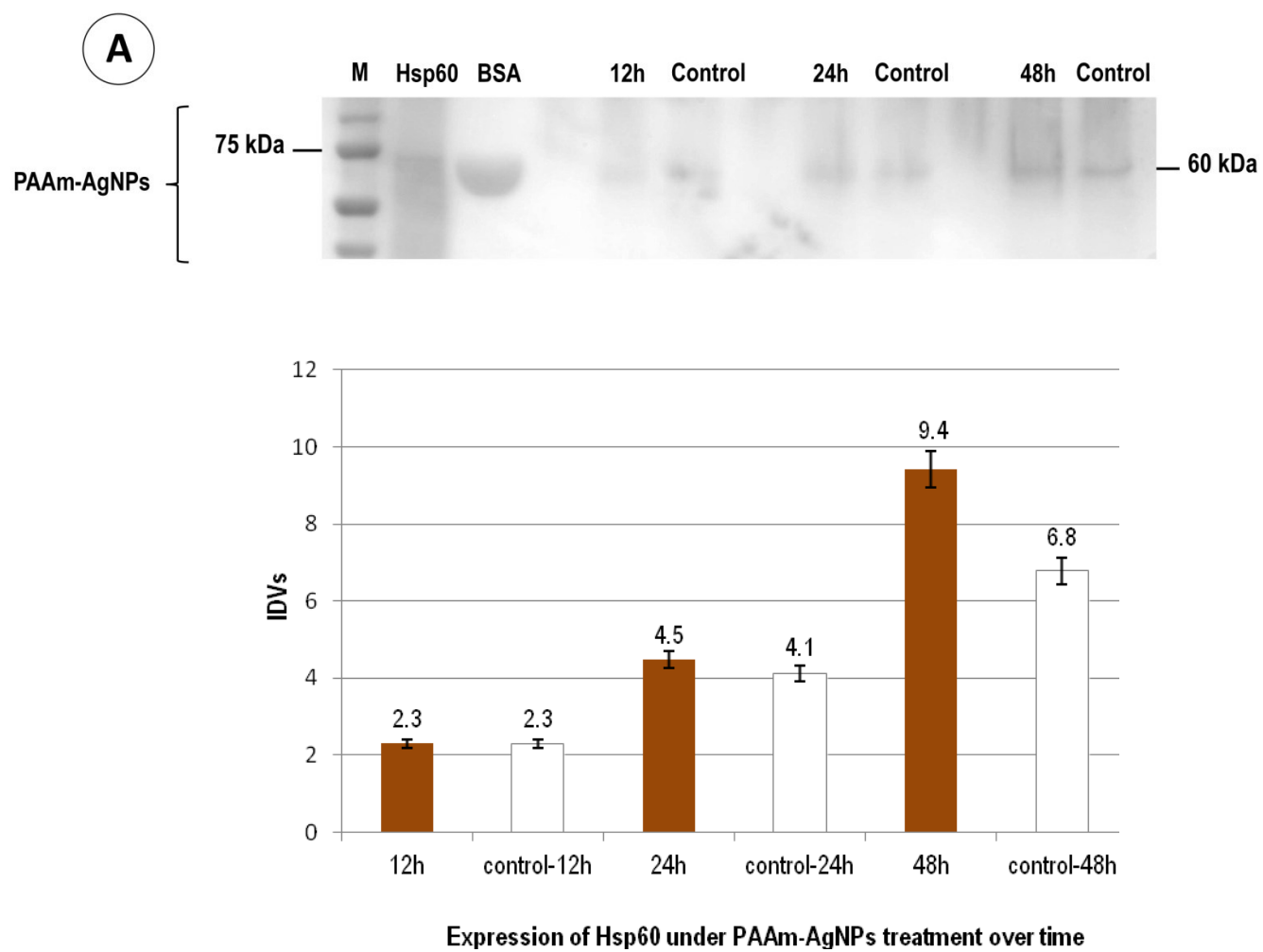
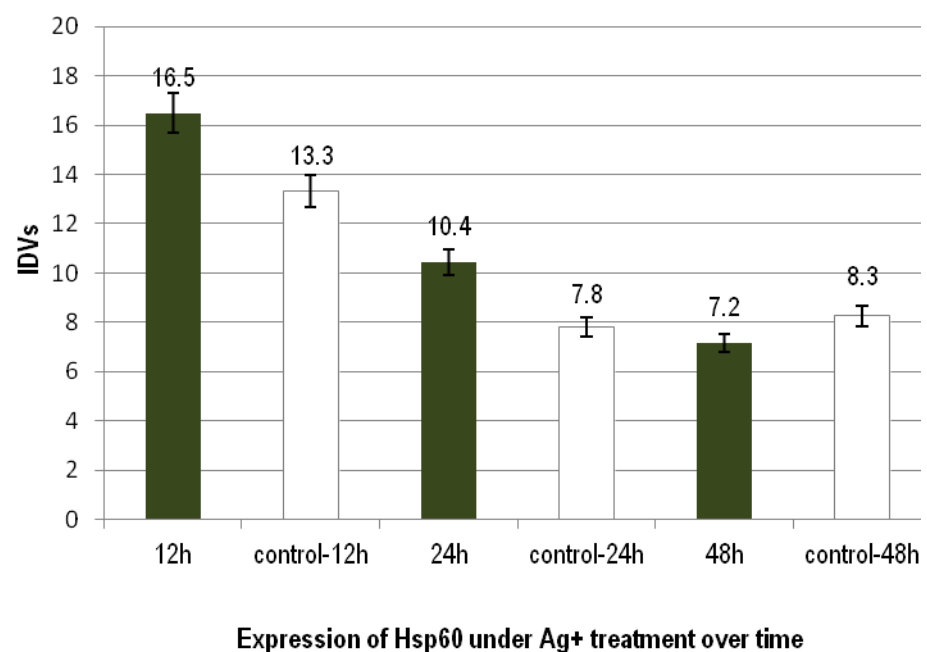
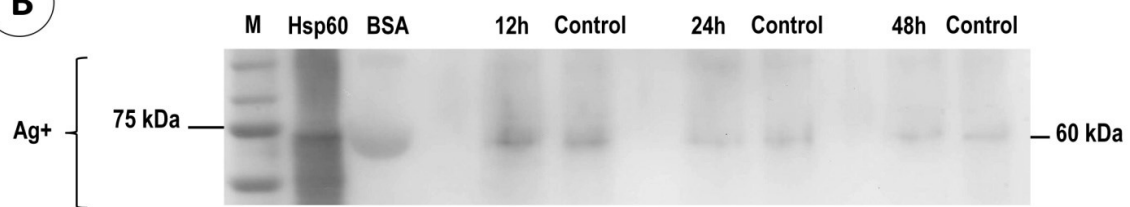


Figure 36: Quantification of hsp60 stress proteins in 3-month old sea urchins exposed to Ag<sup>+</sup> and PAAm-AgNPs/100 µg·L within 48h. Dark orange bars indicate PAAm-AgNPs treatments and dark green bars the Ag<sup>+</sup> ones. White bars indicate the controls for both contaminants. A- Hsp60 expression in large urchins (cohort C6) exposed to PAAm-AgNPs. B- Hsp60 expression in large urchins (cohort C6) exposed to Ag<sup>+</sup>. Data was obtained by densitometric scanning (IDVs: integrated light density values). For dissolved silver, histograms represent the means of the two independent experiments ± SE after normalization. For PAAm-AgNPs, only one immunoblotting experiment was performed. Abbreviations: M: molecular-weight size marker, BSA: bovine serum albumin (negative control).

**B**

### 3.7 DISCUSSION

This report is first to explore multiple mechanisms of stress response *in vivo* sea urchin cells against nanoparticulate and dissolved silver using the juvenile stage as a biological model. The way sea urchin cell types responded to nanoparticulate and ionic silver allowed us to differentiate their toxicity in details and determine how immune system is operating to restore systemic homeostasis through time. Innate immune response was modulated to repair chemically injured tissues within a short period of time and to effectively capture particulate silver dispersed in coelomic cavities after chronic exposures. Nano-translocation through internal haemal vessels confirmed the complexity of internalization, retention and elimination processes.

#### 3.7.1 Effects of Ag concentrations in sea urchins

Concentrations of dissolved silver in sea urchins tissues reflected the mechanisms of silver accumulation depending on the chemical form and presence of phytoplankton in exposure media. Interference of food with contaminant uptake was clearly a strong effect that reduced metal concentration in tissues and its toxicity. As soon as injected into seawater, phytoplankton cells dispersed and were poorly ingested by urchins over exposure time. It also appeared that the first hour was crucial for rapid capture of free silver by suspended particulate matter. To reach stability in water, cationic silver rapidly associates with negatively charged ligand-bound forms. So in natural waters, metal-ligand complexes are formed with anionic ligands such as fluoride ( $F^-$ ), chloride ( $Cl^-$ ), and sulphate ( $SO_4^{2-}$ ), but also with dissolved or particulate organic matter. With nanoAg exposure media, interactions of phytoplankton are supposed to be more complex and involve dynamic adsorption processes of free  $Ag^+$  and AgNPs on cell surfaces, extracellular exudates or within the intracellular space (Moreno-Garrido et al., 2015; Magesky et al., 2016). It is known that silver is strongly adsorbed by the wall of marine diatom cells when exposed to AgNPs but gets more accumulated in cell compartments if exposed to dissolved Ag (Bielmyer-Fraser et al., 2014). This chemical fate can be part of an explanation for the

contrasting amounts of silver found in diatom cells exposed to soluble Ag forms and PAAm-AgNPs.

Without food, soluble Ag was steadily bioconcentrated whereas nanoAg showed a more transient process within 96h. Body wall and gut are the main organs involved in metal accumulation in echinoderms depending on the source of the contaminant; either by water or food (Coteur et al., 2003). With sea urchin *P. lividus*, Danis et al. (2005) also shown that organic contaminants from seawater are easily bioaccumulated, and body wall and spines were the main targets. In our experiments, a 24h period seems to have been a steady-state time for silver to decrease or rise; and a crucial period for immune reaction as well. It can be hypothesized that integument of juveniles clearly arose as a favoured site for rapid ionic silver uptake. Digestive epithelium must also be considered as an additional route for diffusion of soluble silver in juveniles as well as tiny tissues of pedicellaria, podia and papulae (Bianchini et al., 2007). In fact, Aristotle's lantern was always very active, functioning as a pump even for starved urchins, providing a facilitated seawater throughway that enhanced circulation in gut and likely ionic silver uptake. Following Scott (1955), water always circulates through the urchin mouth, pharynx, oesophagus, siphon and intestine specially when a sea urchin is not feeding, which may serve as a respiratory function.

Lethal cell injury caused by dissolved silver in our experiments definitely points to a swelling process (oncosis), followed by a final necrotic phase (Balvan et al., 2015). Silver ions are well known to compromise cell membrane integrity. Basically the disruption of cell ion-flux system occurs either due to membrane-protein interactions with  $\text{Ag}^+$ -ions by protein thiol groups or else results from electrostatic attractions with  $\text{Ag}^0$  (Lapresta-Fernández et al., 2012). Thereby, the outer membrane and transmembrane proton gradient get destabilized; and plasma-membrane potential and energy-dependent reactions collapse causing ATP intracellular levels to be depleted (Bianchini et al., 2005). In turn, a de-

energization of the  $\text{Na}^+/\text{K}^+$ -ATPase provoke an increase in intracellular  $[\text{Na}^+]$  and  $[\text{Cl}^-]$ ; which is obviously accompanied by water influx and cellular swelling.

### 3.7.2 Immune cell cooperation after dissolved silver and nanosilver contamination

The tumor-like formation in spines and cell agglomerations on shells can be classified as granulomas essentially induced by  $\text{Ag}^+$  effects on cells. These proliferative lesions were proportional to damages caused by silver and corresponded to a typical wound repair mechanism with clotting formation. A cooperative interaction between spherulocytes and amoebocyte cells in echinoderms under stress has already been demonstrated. Arizza et al. (2007) stated that uncolored spherulocytes are cell effectors and cause cytotoxic activity by releasing soluble factors as lysins in the presence of amoebocytes in *P. lividus* at 10°C. Recently, Dheilly et al. (2011) reported that 185/333 proteins released by uncolored spherulocytes facing pathogens were later found incorporated with microbial debris in coelomocytes of *Heliocidaris erythrogramma*. It has been also proved that 24h  $\text{Zn}^+$ -treatments at 20°C concomitantly give rise to amoebocytes transformation from a petaloid to a filopodial-like form and an increase in number of red spherule cells also in *P. lividus* (Pagliara and Stabili, 2012). Our data confirm this spherule cell-amoebocyte cooperation being remarkably organized and protective against silver toxicity in post-settlement life of sea urchins living. Nevertheless, by which molecular mechanisms red spherulocytes and amoebocyte would be synergistically interacting with one another in juveniles remain unanswered. Tentatively, it could be a massive inflammation triggered by intracellular contents released by dying cells early on at 12h after contamination with dissolved Ag or following multiple exposures of young cohorts to PAAm-AgNPs.

Each step of cellular migrations was examined and even though they represent a short and progressive response to a chemical insult, we observed that continuous process until spherulocyte lysis might not necessarily occur. As not all spines supported agglomeration process, capacity to withstand without degranulation should be related to the

degree of tissue damage and/or at which extent other mechanisms would additionally interfere to avoid spherulocyte lysis. This study demonstrated that a series of cellular events took place in a fine-tuned cooperation of at least two cell-types to isolate and repair injured area to virtually form an amorphous material, probably a mix of cell debris and byproducts of cell secretion as previously observed by Canicatti and Farina-Lipari (1990) with clotting reaction in *Holothuria polii*. Early damages to epidermic cells and/or amoebocytes are thought to initiate stimuli for spherulocytes migration in a moderate response in a lag period of about 12h. At this time, early production of pigments might occur. Then an initial clotting reaction took place with amoebocyte cells and final spherulocyte degranulation. A large acellular matrix is probably formed only in the worst cases inside large cell plugs. Likewise, Coffaro and Hinegardner (1977) mentioned that spherule cells rapidly break down and despherulate at injury sites in sea urchin *Lytechinus pictus*, perhaps producing a collagen material to form the fibrous matrix of the integument. Second induction of amoebocytes which swamped necrotic areas with a new pool of migrating cells and/or *in situ* proliferation must similarly be a continued response in such cases. The same cell plugs randomly appeared in supra-coronal surface of shells and shown effectiveness in repairing epidermic and skeleton tissues. Against Ag<sup>+</sup> and even more clearly for AgNPs, this cellular protective cooperation rapidly improved in a short period of time (12 days) among the cohorts.

The weaker nanoAg cell-modulated response was a clear effect of low concentration of free silver after 24h and over 12-day exposure in addition to a developing defense system increasingly less sensitive to silver. Contrarily to the stronger values of absorbance for 48h-soluble Ag urchins related to pigment production and release; significant differences at 72h-PAAm-AgNPs could be also attributed to a slow release of pigments throughout exposure time. In nanoAg exposures we often observed some slight pigmentation only on shell surface with more spherulocytes being irregularly distributed, but it still difficult to properly characterize it in confocal microscopy. So, it could be argued that during PAAm-AgNPs short term treatments, combined forms of silver would slowly be

responsible for inducing inflammation processes and, in turn, spherulocytes slow reaction. Even though we did not find PAAm-AgNPs uptaken by epidermic cells after long term exposures in TEM-photomicrographs, slow inflammation reaction in integument could be attributed to nanosilver effects. These findings are also in accordance to typical chemical profile of PAAm-AgNPs in seawater characterized by a slow and constant release of «free Ag<sup>+</sup>» through time. This mechanism might occur either due to gradual release of Ag<sup>+</sup> entrapped by amine functional groups of poly-allylamine coating and under the action of competing cations; or a true dissolution of the AgNPs core by oxidation processes in seawater over time. Before exposures, we observed that stabilizing layer (PAAm) of AgNPs held 2.5% of dissolved silver even after exhaustive cleaning-up procedures. Amines have one electron doublet available and can capture cations such as Ag<sup>+</sup> and exchange them within the surrounding solution. The hypothesis of slow release of captured Ag<sup>+</sup> is nevertheless suggested here as the sustainable and dominant mechanism leading to toxicity over time, owing the weak dissolution of PAAm-AgNPs in highly oxygenated seawater (Magesky and Pelletier, 2015).

### 3.7.3 Silver effects and anti-stress hsp60 and hsp70 expressions

Assuming that cellular protective mechanisms in soluble Ag-treated urchins were essentially related to fast cell impairment and tissue repair, hsp70 expression might be directly related to these processes. Both immune cell migrations and hsp70-chaperones expression operated at the same time. In fact, more ~70 kDa bands detected in larger soluble Ag-treated individuals at 48h might also reflect tissue repairing mechanisms already started with clotting reaction in addition to general proteomic stress. A larger surface area/volume ratio allowing faster chemical uptake per unit weight in small cohorts would likely have contributed to raise hsp70s expression sooner than in C6 cohorts. In our experiments a new confined environment with no food or a careful manipulation for transferring urchins to exposure media might likely have induced hsp70s expression. At least for untreated C5 cohort, chaperones expression continued to increase up to 48h

supporting the premise that a drastic lack of food can additionally change metabolic homeostasis during contamination. Feed deprivation has been considered as a stressor for aquatic animals; it is also been related to ~70-kDa chaperones expression specially after organisms get suddenly in need for food source and after long time periods in starvation (Hand et al., 2012; Antonopoulou et al., 2013). There is a constant need for chaperone assistance during *de novo* protein folding and refolding of inactive polypeptide chains, mostly because stability of cellular proteins is low and aggregation competes with productive folding in normal conditions (Richter et al., 2010).

In addition, ~90 kDa peptides detected in immunoblotting illustrated the complexity of pathways in which hsp70 protein family is involved. Cytosolic hsp70 types can interact with nascent polypeptides as soon as they emerge from ribosomes, work together with another chaperones and cochaperones (cofactors) as hsp40/J-domain-containing protein activators and nucleotide exchange factors (NEF) inside intricate machinery (Richter and al., 2010; Mayer, 2013). In fact, to accomplish multiple cellular tasks, the hsp70s can have their molecular conformation twisted. Basically the hsp70 molecule has a high dynamic structure with an N-terminal nucleotide-binding domain with ATPase activity (NBD) and a C-terminal substrate-binding domain (SBD); and two affinity states: the low affinity ATP-bound state and the opposite high affinity ADP-bound state when hsp70 binds substrates (Young, 2010; Mayer, 2013). As such, 70-kDa chaperones can eventually be linked to other molecules of high/low molecular weight, which can explain the additional bands detected in our immunoblotting. Owing to the fact that we used a monoclonal anti-heat shock protein 70 (mouse IgG1 isotype) to probe the stress-inducible form (hsp72) and constitutive cognates (hsc73) of hsp70s, a broader detection of bands in these conditions should be expected as well. Increasing levels of hsp70 from 12 to 24h coincided with first stages of Ag<sup>+</sup> injury (induction-mobilization stages). It has been proposed that hsp70 units released from sea urchin immune cells promote inflammatory responses with both constitutive and inducible forms of hsp70 involved in clotting reaction and down-regulation on

inflammation, but more studies are necessary to further the current understanding on these processes (Browne et al, 2007, Pinsino and Matranga, 2015).

Decreasing levels of 60-kDa chaperonins in soluble Ag media compared to nanoAg may lie in drastic mitochondrial membrane disturbance or degradation of hsp60 units, their cofactors and/or co-working chaperones. Even with high up-regulation of hsp70s in cytoplasm, expression of 60-kDa chaperonins appears to get progressively shut down. As hsp70s were strongly expressed and probably protective to cytoplasmic proteins at some level, we can first hypothesize that a progressive disruption of mitochondrial membranes by soluble Ag would likely have interfered with co-chaperones trafficking through cytoplasm and mitochondrial matrix, which prevented final assembling of the hsp60. Therefore, because soluble Ag ions stress impaired cell machinery, the chaperonines reaction to proteins denaturation would have been depleted over time. Actually, hsp60 hydrophobic substrates-binding sites are responsible for keeping an unfolded conformation of proteins to facilitate their channeling by transmembrane transport for import and export across mitochondria inner membrane. For instance, it is known that hsp60 co-works with co-factor hsp10 to catalyze folding of a subset of mitochondrial hsp70 (mt-hsp70) client proteins. Before, mt-hsp70 is supposed to independently interact with hsp10 to promote assembling of hsp60 precursors and form the mature hsp60 in mitochondria (Böttinger et al., 2015). To accomplish this task, however, mt-hsp70 needs to be imported to mitochondria by functional transmembrane proteins (Blamowska et al, 2012).

On the other hand, it has also been suggested that hsp60s are present in the cytoplasm in a different molecular conformation, but are quickly imported to mitochondria by cytoplasmic hsp70s under severe conditions (Itoh et al. 2002). So after stress period cells are able to compensate chaperonins levels between opposite compartments, a mechanism that may explain the high levels of Hsp60 and Hsp70 at 48h both in AgNPs wells. Between 24 and 96h, silver accumulated in juveniles exposed to soluble Ag remained high compared to nanoAg conditions and in some way interfered with hsp60

expression, whereas reducing levels in those treated with PAAm-AgNPs allowed hsp60 up-regulation. Considering that monoclonal anti-hsp60 antibody (mouse IgG1 isotype) used in our work was reactive to both constitutive and inducible hsp60s, protein expression detected in controls could correspond to both hsp60 types. It has been demonstrated that the expression of 60-kDa chaperonines might be inhibited in a dose-depending manner for some invertebrates in the field or laboratory essays (Werner and Nagel, 1997; Clayton et al., 2000; Arts et al., 2004; Rios-Arana et al., 2005). Down-regulation or no expression of hsp60s have been particularly found in aquatic invertebrates exposed to increasing concentrations of metals such as Cd<sup>+</sup> (0.5-50 µg·L) in amphipod *Hyalella azteca* (Werner and Nagel, 1997), or higher concentrations as 100 µg·L of Cu<sup>2+</sup> in zebra mussel *Dreissena polymorpha* and 50 µg·L of As<sup>3+</sup> in rotifer *Platynus patulus* (Clayton et al., 2000; Rios-Arana et al., 2005).

### 3.7.4 Silver nanoparticles route mechanisms in sea urchin

The toxicity effects of polymer coated-AgNPs observed in this study were much more complex and less acute than soluble silver ones. In order to broadly understand these effects we need first to address nano-translocation inside juvenile physiological structure. The facilitated water inflow through madreporite and mouth conducted directly or indirectly nanosilver into coelomic sinuses, perivisceral cavity, digestive epithelium and blood circulatory system (haemal system). Biological activity generated in response to nano-uptake by cells was a clear indication of PAAm-AgNPs toxicity effects. We previously discussed about the rule of stone canal as a main route for nanosilver uptake and inner dispersion in one month-old sea urchins (Magesky et al., 2016). Seawater taken up through the madreporite is thought to be propelled down the axial coelom and stone canal, then the ring canal. Because this vascular system is made up of blind-ended chambers, a portion of water flows likely across them and could reach perivisceral coelom (Ferguson, 1984). Nonetheless, it is clear that AgNP-loaded seawater flow in coelomic sinuses goes across intra-peritoneal space and epigastric coelom which may come from a connection point between secondary

coelomic cavities and hydraulic system and/or axial coelom in the juvenile body, originated from larval axohydrocoel. Dispersed PAAm-AgNPs in coelomic sinuses would likely act as a source of dissolved Ag through time, increasing silver accumulation in sea urchins over 12 days.

Coelomocytes from internal haemal vessel were targeted by PAAm-AgNPs that likely crossed digestive epithelium. This fact indicates a second way where nanoAg can easily penetrate in the deeper juvenile organic system, even though blood circulatory network (haemal system) is a closed system in sea urchins (Ezhova et al. 2014). The large layer of adipocyte cells surrounding the digestive epithelium in intestine must function as another barrier for free translocation of AgNPs towards the epigastric coelom and the external haemal vessels. Internal haemal vessel arises from oral haemal ring, runs along the esophagus, stomach, and intestine and finally disappears (De Ridder and Jangoux, 1982). It has been suggested this duct may serve as a reservoir for nutritional support of digestive tissues rather than haemal material transport to other parts of the body (Scott, 1955; Ferguson, 1984). Therefore, even though this system was shown to be involved in nutrient translocation, new insights about the real potential of long way nano-transportation through other tissues need more clarification by TEM analysis.

### **3.7.5 Mechanisms of cellular internalization and elimination of AgNPs**

Two cell types responded to PAAm-AgNPs transported by seawater inside coelomic sinuses: neighboring peritoneal cells and coelomocytes. Secretory functions of peritoneal cell-types are used as nano-conveyors once nanosilver reached haemal vessels bordering epigastric coelom and intra-peritoneal sinus, but their cell machinery can alternatively attack nanosilver as observed in TEM images. Different functions of peritoneal cells have been described in echinoderms, and they might be related to multiple mechanisms in which these cells can handle AgNPs. Thus, they may either clean up coelomic sinuses and external haemal ducts, or prevent nanosilver from invading perivisceral coelom from internal haemal vessel. Likewise, mechanisms pointing to cytotoxic processes in coelomocytes showed how

these cells dealt with flowing AgNPs: (a) regular nanosilver internalization with larger agglomerates getting congregated inside cytoplasm, (b) extrusion of empty vesicles carrying small particles on cell surface, and (c) shrunken cell bodies signaling beginning of cell death. We do not know if these mechanisms separately emerged over time or might be part of a building-up process; either way they were only spotted in circulating coelomocytes.

Results confirmed physical stress on cell membrane of coelomocytes caused by very small PAAm-AgNPs, sometimes organized as a pearl chain on extracellular surface. The loading process depends on nanoparticle size, membrane tension and nanoparticles concentration on cell membrane (Yue and Zhang, 2012). This process clearly follows a threshold particle size that prevents endocytosis of small single nanoparticles below the optimum size (25-50 nm) (Roiter et al., 2008; Jiang et al., 2008; Zhang et al., 2009). As small nanoparticles did not cause enough membrane deformation to trigger internalization, their clustering facilitates the wrapping process, so they are uptaken as a whole. From the beginning, a cooperative effect with separated small particles needs to happen to provoke membrane bending, a negative pressure and final internalization of nano-clusters (Yue and Zhang, 2012). This mechanism may govern PAAm-AgNPs uptake of small clusters in coelomocytes other than active phagocytosis of larger nanoparticles or aggregates as observed in TEM photomicrographs. Yet, very small PAAm-AgNPs (about 8 nm) were observed laying on an extracellular net where the inter-nanoparticle distances were about 0.6 nm, may be preventing AgNPs from being aggregated and loaded. According to Treuel et al. (2013), small nanoparticles (10 nm) are supposed to coat plasma membrane before incorporation. So, it can be a hint that aggregation of small AgNPs or their association with larger ones (16-25 nm) may be crucial for 8 nm AgNPs internalization.

Once small PAAm-AgNPs invaded the intracellular milieu of coelomocytes, they targeted many cell compartments, particularly nucleus and secretory vesicles exported by Golgi apparatus. Comparatively, larger AgNPs were mainly present within endo-lysosomal structures. In agreement with Sakhtianchi et al. (2013), Golgi nano-vesicles in our study were identified as a conventional secretion system through which nanoparticles will likely

leave the cell. Working with larger SnO<sub>2</sub>, Fe<sub>3</sub>O<sub>4</sub> and CeO<sub>2</sub> nanoparticles (20-105 nm) orally injected in adult sea urchins, Falugi et al. (2012) detected harmful modifications of the trans-Golgi and endoplasmic reticulum compartments in coelomocytes from coelomic fluid. These processes can take place in the proximal portion of gastro-intestinal tract before intestinal epithelium as shown by our data. It is known that metallothioneins are up-regulated when cells are exposed to AgNPs and the presence of these proteins in Golgi apparatus may in some way explain why this organelle appears to be an important target for metallic nanoparticles (De Matteis et al., 2015). Conversely, when nanoparticles are taken up by slow turn-over structures as endo-lysosomal structures, a larger number of proteins and receptors are necessary to get rid of them (Sakhtianchi et al., 2013).

### **3.7.6 Intracellular effects of AgNPs in coelomocytes**

As shown in our results, intracellular displacement of small AgNPs resulted in excretion, but also in translocation into other compartments like nucleus. As it is unknown if PAAm-AgNPs would behave in a typical Trojan-horse type mechanism in such environment, their final fate is difficult to address. The water dispersed structure of PAAm-AgNPs corresponds to a little metallic core surrounded by high molecular weight long and intertwined [CH<sub>2</sub>CH(CH<sub>2</sub>NH<sub>2</sub>)]<sub>n</sub> polymeric chains. Hence, it is not known to which point PAAm-AgNPs surface could be easily attacked by oxidant agents over time. Therefore, considering long term exposures for instance, trapped Ag<sup>+</sup> ions could still be liberated from polymeric chains together or not with those from core dissolution. If PAAm-AgNPs do dissolve though, Ag<sup>+</sup> can lead to apoptotic chromatin changes (Banfalvi, 2014). Actually, genotoxic effects should be expected with AgNPs in any case. Coelomocytes from internal haemal duct were severely damaged by nanoAg and appeared to undergo an apoptotic-like cell death process (Balvan et al., 2015). It is very unusual for echinoderm immune cells to fall apart losing cellular components on a regular basis as seen by TEM. The cell bodies identified as apoptotic ones held crucial organelles for cell metabolism and a high amount of nanosilver, pointing to a severe toxic effect of 8 nm-PAAm-AgNPs. So far, no

mechanism has been described for marine invertebrates interacting with nanoparticles. With mammalian cells, AgNPs (5-10 nm) are known to be more cytotoxic than larger ones and to induce more ROS production, DNA damage and apoptosis (Kim and Ryu, 2013).

Considering that important cytotoxic mechanisms described here were greatly related to the smallest nanoparticles, they might be greatly involved in protein damaging in the intracellular milieu. Important features in hsp60 and hsp70 expression in sea urchins exposed to AgNPs can be attributed to an additional nanoAg effect. So we suggest that both dissolved Ag and especially nanoAg physical-chemical effects would damage cellular structures like proteins and other macromolecules. Otherwise, hsp70s expression pattern in small sea urchins showed a 24h up-regulation very similar for both toxicants, clearly indicating silver ions effects in both media. It has been reported that cytoprotective effects of hsp60 expression rise as a response to mitochondria dysfunction in marine invertebrates (Choresh et al., 2004). If we consider that silver bioaccumulation decreased over time, the peak of hsp60 expression at 48h would be rather attributed to nanoAg already dispersed in coelomic sinuses of sea urchins in short exposures (Magesky et al., 2016).

The generation of reactive oxygen species (ROS) is seen as a response to soluble Ag and PAAm-AgNPs, both worsened by starvation condition. ROS production is considered as the main underlying chemical process in nanotoxicity. In fact, the metabolism of ROS is under a fine cellular control and their concentrations normally do not go beyond  $10^{-8}$  M (Halliwell and Gutteridge, 1989). Currently, reactive intracellular H<sub>2</sub>O<sub>2</sub> has been suggested to promote oxidation of internalized AgNPs with final Ag<sup>+</sup> liberation, which is another element to support the Trojan-horse mechanism in our work (Hsiao et al., 2015). Proteins may be particularly sensitive to changes in intracellular pH, redox state and ionic media, leading to misfoldings and then activating the Hsp (Kalmar and Greensmith, 2009). Because food deprivation causes depletion of antioxidant stores and ROS increase (Morales et al., 2012), we may consider that starvation might had an important impact over anti-oxidant defenses during chronic exposures, particularly for small urchins.

### 3.8 SUMMARY AND CONCLUSION

This is the first report detailing multiple cellular mechanisms related to ionic silver and organic coated-AgNPs in juveniles of sea urchin. With 100 µg·L, both chemical forms of silver affected juveniles in a very particular way. Increasing bioaccumulation of silver due to high bioavailability of soluble Ag in seawater rapidly set off a series of cellular responses such as clotting reaction operated by spherulocytes and amoebocyte cells, oxidative stress and 70-kDa chaperones expression. Compared to direct Ag<sup>+</sup> effects on epidermis, we found PAAm-AgNPs interacting with tissues, cells and coelomic sinuses where nano-contaminated seawater flowed through. A phagocytic pathway is proposed for cell internalization of larger nano-aggregates and translocation of small nano-clusters likely escaping the protective extracellular nets to go into cytosol and cell organelles. For individual PAAm-AgNPs, physical interactions of nanoparticles with cell macromolecules and organelles might be, in short term, the main mechanism that induced higher expression Hsp proteins and an apoptotic-like process in sea urchins exposed to nanosilver. The toxicity of silver ions and nanoparticulate silver in sea urchin is differentiated by specific mechanisms through which cells handled each toxicant.

## CONCLUSION GENERALE

L'objectif de ce chapitre est de reprendre les principaux éléments physiologiques et toxicologiques décrits dans les trois chapitres précédents pour élaborer un modèle général des interactions de l'argent dissous et nanoparticulaire avec les différents stades du développement de l'oursin vert, de l'embryon jusqu'au juvénile, et de mettre en évidence les mécanismes de protection cellulaire déployés par l'organisme pour se protéger de l'agression toxique. La toxicité de l'argent est donc évaluée en rapport avec les changements morphologiques subis par les organismes en développement. Les fonctions de base de chaque tissu et leurs dérivés pendant l'exposition aux xénobiotiques sont discutées, ainsi que leurs effets dans différents groupes cellulaires d'importance à chaque stade. Les voies d'assimilation, de distribution interne et d'élimination du nanoAg sont pris en compte au niveau cellulaire et de l'organisme entier. Le devenir de l'argent dans nos modèles est interprété à l'aide des résultats obtenus lors des biotests et de l'étude des organismes en microscopie confocale. En somme, la compréhension des mécanismes cellulaires étudiés nous permet d'établir le mode d'action de chaque forme chimique de l'argent chez ces organismes. Le terme « argent ionique (ou Ag<sup>+</sup> dans le texte) » inclut toutes les formes chimiques hydrosolubles de l'argent.

**1- Les interfaces biologiques en interaction directe avec les contaminants: l'ectoderme, l'endoderme et ses dérivés (l'épiderme et le tissu digestif)**

Dans chaque compartiment marin (microsurface de l'eau, colonne d'eau, sédiment), le rôle de l'interface tissu/cellule-nanoparticule/Ag<sup>+</sup> à chaque stade de développement semble être essentiel pour caractériser les mécanismes de toxicité. Le feuillet externe, l'ectoderme des embryons qui devient l'épiderme chez les autres stades, doit être vu comme une couche essentiellement protectrice contre les nanoparticules chez la majorité des stades embryonnaires, les larves et les juvéniles (Appendice 4, Figure 1 A et B). Cette conclusion est basée sur l'analyse de l'internalisation des AgNPs par microscopie électronique à transmission, essentiellement produite par des tissus internes. Il est probable

que l'interaction des nanoparticules avec les cellules de la couche externe subisse une sorte d'interférence par le mouvement des cilles, ce qui crée un tourbillon autour des gastrules et des larves.

Une quantité infime de nanoAg-FITC a été observée dans les cellules épidermiques des larves indiquant que peu d'internalisation doit passer par ce tissu, un fait confirmé par les analyses TEM (Appendice 4, Figure 1 B). Les marqueurs fluorescents (nanoAg-FITC, Qdots525) se maintiennent faiblement sur l'épiderme des juvéniles jusqu'à 48h, un tissu où les PAAm-AgNPs n'ont pu être détectées (Magesky et al., 2016). En conséquence, ceci nous amène à conclure que l'internalisation à travers l'ectoderme reste négligeable en comparaison avec le proctodaeum (partie finale de l'intestin), un fait confirmé par le marqueur nanoAg-FITC. Un autre événement lors de l'embryogénèse renforce l'argument de l'ectoderme comme barrière protectrice contre les PAAm-AgNPs et peut être même les Ag<sup>+</sup> est la différentiation et la migration des spherulocytes rouges sur l'épiderme (Appendice 4, Figure 1 A). Comme observé par les micrographies TEM, les AgNPs semblent ne pas dépasser les limites de la membrane plasmique des spherulocytes.

En outre, il apparaît que les spherulocytes rouges produisent des espèces oxygénées réactives (ROS) pendant le processus de dégranulation dans l'épiderme des oursins lorsque contaminées avec les AgNPs en mélange avec les nanotubes de carbone fonctionnalisés (f-SWCNTs) (Appendice 4, Figure 2 A et B). Ceci pourrait correspondre à un effet direct de l'argent ou à une activation progressive du processus de dégranulation. En fait, les spherulocytes rouges constituent sans doute un groupe cellulaire d'importance majeure chez les stades de développement des oursins réguliers et irréguliers. Leur distribution sur des régions morphogénétiquement actives, surtout chez les larves et les juvéniles de *Strongylocentrotus droebachiensis*, démontre un rôle particulièrement multifonctionnel à la fin de la gastrulation quand elles sont capables d'importer du Ca<sup>2+</sup> et protéger les larves en formation (prismes). Chez les larves, les cellules pigmentaires s'occupent de la réparation des tissus nécrosés par l'argent dissous et répondent à l'intoxication des ions Ag<sup>+</sup> et des

AgNPs en coopération avec des amoebocytes dans le blastocoel. Dans ce cas, le mécanisme est totalement relié à la mobilisation des cellules pigmentaires du mésoderme. À la fin du développement des postlarvae, les spherulocytes couvrent en grande partie les régions du corps encore en organisation et doivent moins servir à la réparation immédiate au moment de la contamination par l'argent (Appendice 4, Figure 3 A-D).

D'autre part, le mécanisme d'interférence engendré par la ciliature de l'ectoderme des embryons et de l'épiderme des larves semble amplifier l'adsorption des f-SWCNTs (Appendice, Figure 4 A et B), perturber le mouvement des organismes dans la colonne d'eau et optimiser le transfert des ions  $\text{Ag}^+$  vers les cellules épidermiques (Magesky et Pelletier, 2015). Chez les postlarvae, cette couche cellulaire ciliée externe est progressivement remplacée par l'épiderme des juvéniles, donc il est difficile à préciser jusqu'à tel point ce mécanisme pourrait être fonctionnel à ce stade.

Chez les blastules en début de gastrulation, les cellules mésenchymateuses primaires démarrent la construction du squelette, ce qui fait de l'ectoderme un tissu de « libre passage » du  $\text{Ca}^{2+}$  vers le blastocoel. Dans le milieu contaminé par l' $\text{Ag}^+$ , notre hypothèse est que l'argent peut être internalisé par les blastules, ainsi perturber l'importation du  $\text{Ca}^{2+}$  et le métabolisme des cellules mésenchymateuses minéralisatrices, empêchant la minéralisation (Figure 37). Quelques études montrent que le  $\text{Ca}^{2+}$  passe de l'ectoderme vers le blastocoel pour être ensuite importé par les cellules minéralisatrices qui ont des transporteurs de faible affinité chimique avec le  $\text{Ca}^{2+}$  (Pinsino et al., 2011). Les spicules de calcite et magnésium sont le résultat de la formation transitoire du  $\text{CaCO}_3$  amorphe dans les vésicules intracellulaires des cellules mésenchymateuses primaires (PMCs); exportés ensuite vers la cavité où le squelette est produit. Pour alimenter ce processus, le  $\text{HCO}_3^-$  est absorbé à partir de l'eau de mer (40%), en plus de la contribution du  $\text{CO}_3^{2-}$  métabolique (60%) (Sikes et al., 1981).

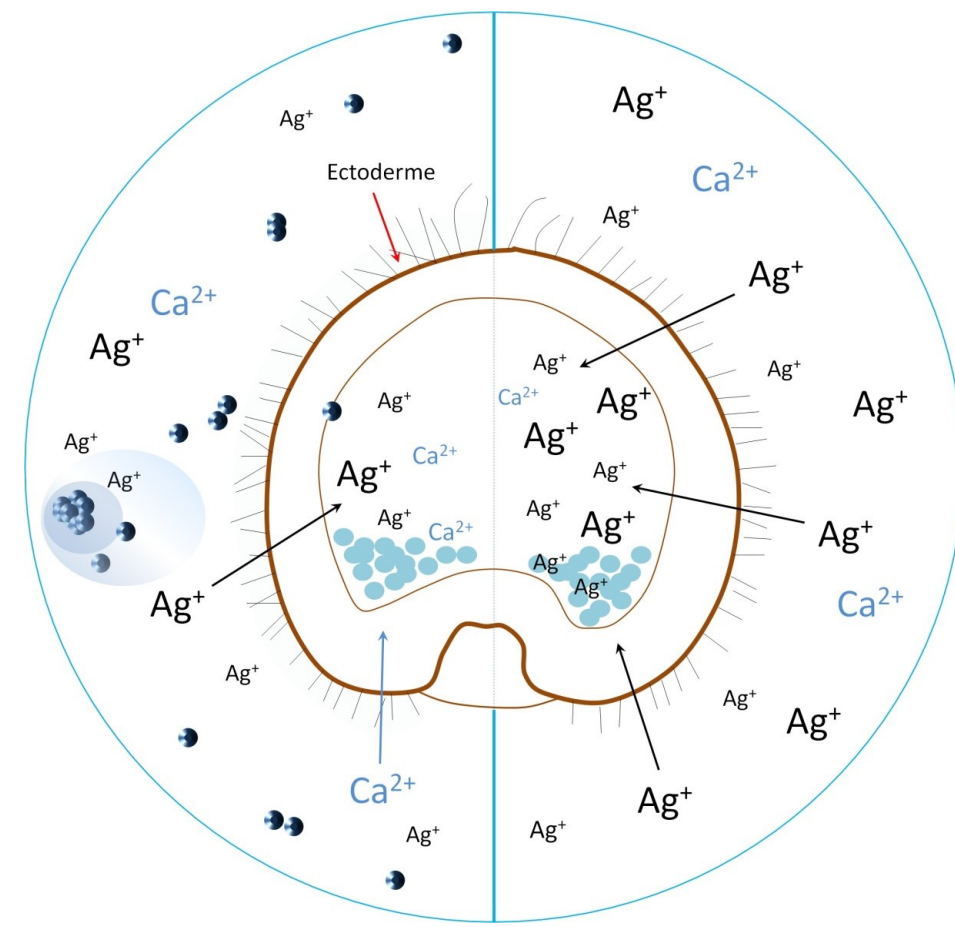


Figure 37: Modèle d'interaction contaminant-ectoderme (couche brune) proposé pour les blastules en début de gastrulation exposées aux AgNPs (petites sphères bleues à gauche du schéma) et aux ions  $\text{Ag}^+$  (à droite du schéma). La grande sphère bleue est la couche d'interaction. L'agent ionique apparaît comme le principal perturbateur du métabolisme des cellules mésenchymateuses minéralisatrices (en bleu), représentantes du mésoderme en formation. Les flèches noires représentent l'assimilation des ions  $\text{Ag}^+$ ; les bleues, l'assimilation des ions  $\text{Ca}^{2+}$ .

Bien que les principes généraux de la calcification soient relativement connus, aucun mécanisme précis sur les transporteurs de  $\text{Ca}^{2+}$  n'a été démontré jusqu'à présent chez ces cellules (Stumpp et al., 2012). Nos résultats suggèrent que l'argent doit endommager la structure et toutes les fonctions de la membrane des PMCs, comme le rassemblement et la formation du syncytium, ainsi que l'importation des ions importants à la formation des

spicules (Figure 38). Puisque les AgNPs libèrent une certaine quantité d' $\text{Ag}^+$  avant la dissolution de la particule *per se*, nous considérons que ce mécanisme peut expliquer similairement les malformations observées lors des expositions au nanoAg, mais à une plus faible intensité.

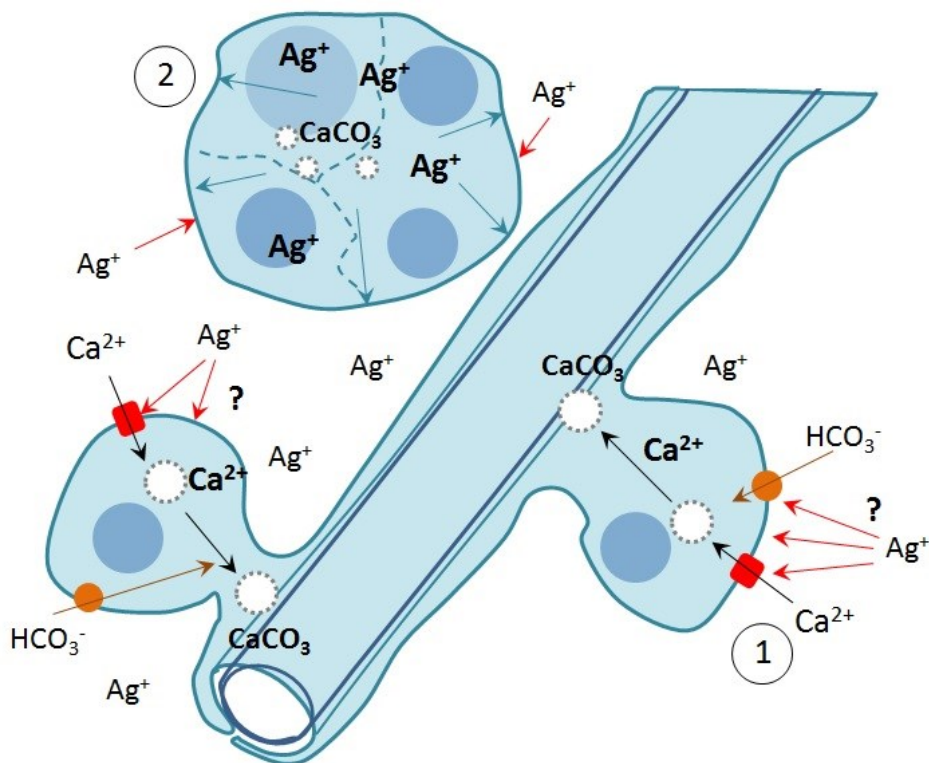


Figure 38: Modèle d'interaction argent-cellules mésenchymateuses primaires (PMCs) chez les stades embryonnaires (adapté de Stumpp et al., 2012). (1) L'effet des ions  $\text{Ag}^+$  doit se faire sur les membranes des PMCs, ce qui perturbe l'importation du  $\text{Ca}^{2+}$  et des  $\text{HCO}_3^-$  et le dépôt du  $\text{CaCO}_3$ . (2) L'oncrosis produit des clusters aberrants dont les cellules semblent subir un processus de mort cellulaire. Les flèches vertes indiquent le gonflement des cellules; les flèches rouges les cibles probables de l'argent (membrane et protéines de transport des ions; les flèches noires montrent le déplacement des vésicules de sécrétion contenant du  $\text{CaCO}_3$  amorphe).

Dans le même ordre d'idées, ayant le stomodeum (bouche) formé, le tractus gastro-intestinal (dérivé de l'endoderme) devient logiquement l'une des voies d'entrée principale aux contaminants ( $\text{Ag}^+$ , PAAm-AgNPs et f-SWCNTs) chez les prismes. À partir du

moment où la régionalisation de l'œsophage, l'estomac et l'intestin de la larve prisme se met en place (et même après l'ouverture de la bouche chez les postlarves juvéniles), l'assimilation de l'argent dissous ou particulé par les cellules de l'épithélium digestif se produit avec ou sans l'apport de nourriture (Figure 39).

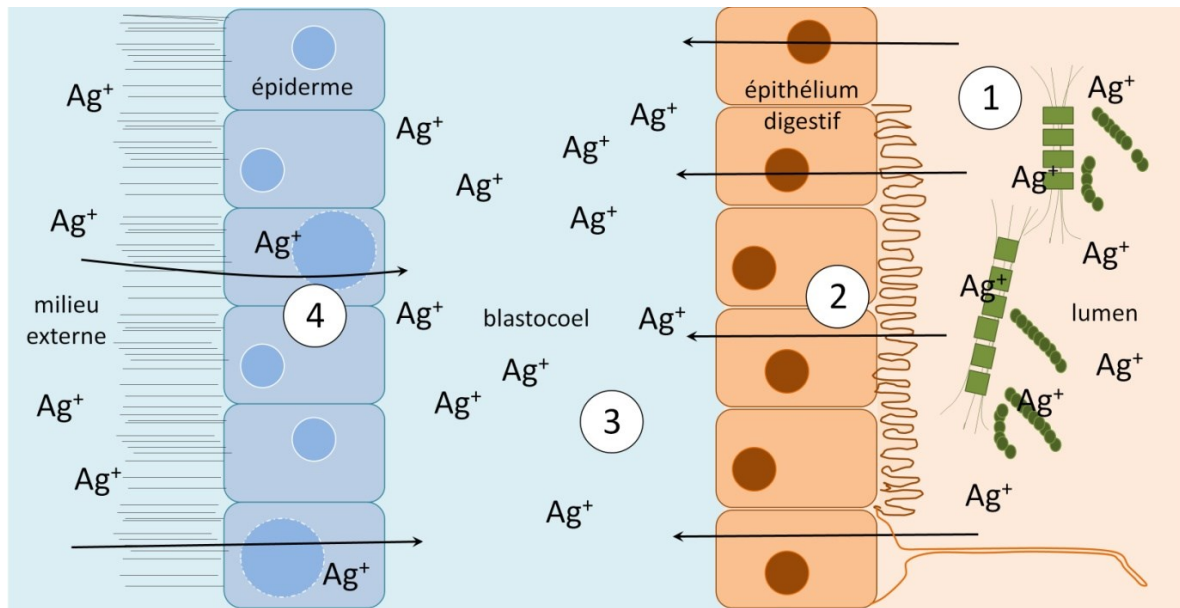


Figure 39: Modèle d'assimilation des ions  $\text{Ag}^+$  chez les larves d'oursin nourries avec du phytoplanктон : (1) le phytoplanктон transporte des  $\text{Ag}^+$  dans le tube digestif; (2) le passage des  $\text{Ag}^+$  par l'épithélium digestif (endoderme) est considéré comme une voie préférantelle; (3) l'argent assimilé par la larve rentre dans le blastocoel; (4) aussi bien que le nanoAg-FITC, l'assimilation des ions  $\text{Ag}^+$  par l'épiderme doit être prise en compte, mais comme un mécanisme secondaire d'entrée des  $\text{Ag}^+$  dans le blastocoel . Les flèches noires représentent l'assimilation des  $\text{Ag}^+$ .

La filtration de l'eau par les échinoplutei et la capacité de pompage de l'eau par la lanterne d'Aristote ouvrent le passage à un flux d'eau de mer contaminée dans les organismes. Les marqueurs nanoAg-FITC et Qdots 525 confirment, au moins chez les larves, que le tube digestif est la voie principale d'assimilation des contaminants. Comparativement, l'internalisation acellulaire (blastocoel) des AgNPs devient alors

possible par ce mécanisme. Chez les larves échinoplatei à 2 bras en formation finale (2 bras-echinoplateus tardive), les malformations du tube digestif correspondent à l'ordre de toxicité suivant : f-SWCNTs- $\text{Ag}^+$  >  $\text{Ag}^+$  > PAAm-AgNPs > f-SWCNTs-PAAm-AgNPs et confirment les relations de toxicité trouvées par PERMANOVA, avec les organismes en récupération. À partir du libre passage dans le tractus digestif, les AgNPs sont assimilées par l'endoderme ce qui permet ensuite leur entrée facilitée vers le blastocoel (Figure 40).

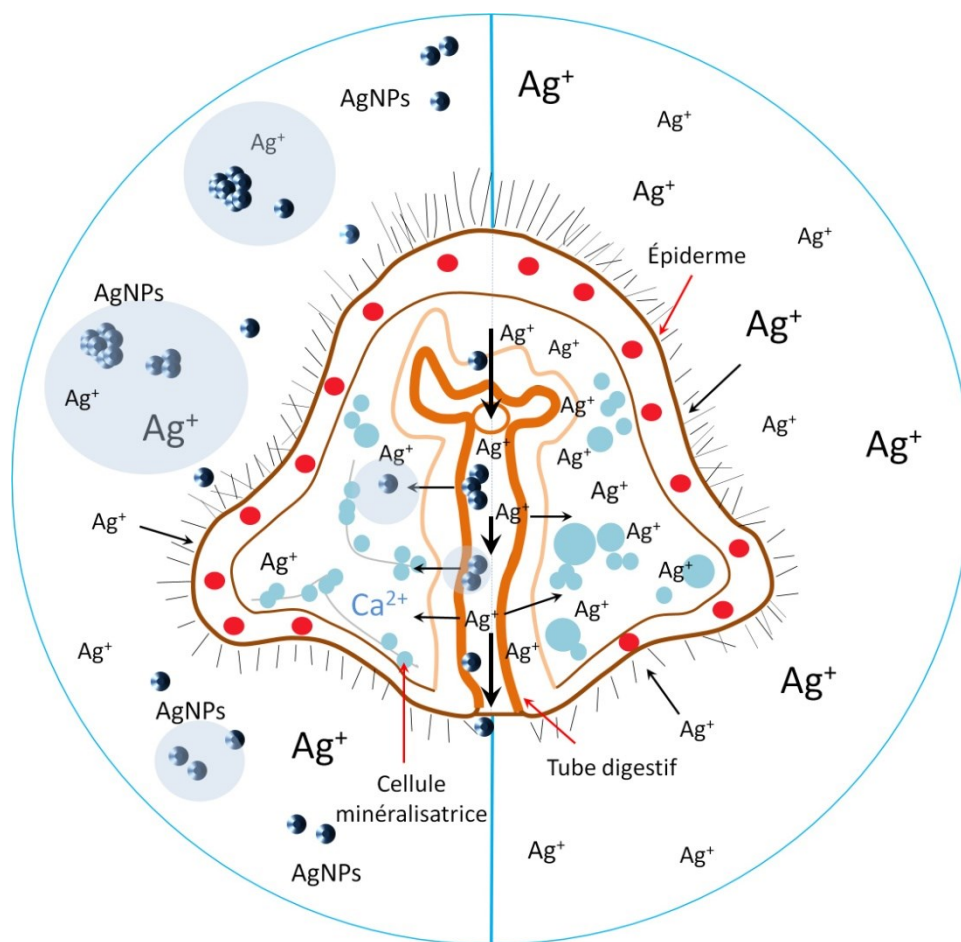


Figure 40: Modèle d'interaction contaminant-épiderme/contaminant-épithélium digestif proposé pour les larves échinoplatei (prismas) récemment formées après l'exposition aux AgNPs (à gauche du schéma) et aux ions  $\text{Ag}^+$  (à droite). La couche brune représente l'épiderme avec les spherulocytes rouges; la couche orange est l'épithélium digestif. Les flèches noires en gras montrent le flux d'eau contaminé dans le tractus, celles plus fines indiquent l'assimilation des AgNPs et des

$\text{Ag}^+$  par les tissus. La sphère bleue est la couche d'interaction. L'agent ionique est encore considéré comme le principal perturbateur du métabolisme des cellules mésenchymateuses minéralisatrices dans la larve (en bleu).

Pour déterminer si le changement du pH et de la force ionique dans le tube digestif provoque l'agrégation des nanoparticules emportées par l'eau (condition sans phytoplankton) ou bien si l'agrégation prend place lors de la digestion du phytoplankton nano-contaminé, il faudrait mener des expériences plus dirigées vers l'analyse de chaque compartiment du tube digestif et non seulement le proctodaeum. En reconnaissant que ces processus chimiques dominent le comportement des AgNPs dans le lumen du tube digestif, l'agrégation locale pourrait se produire avec ou sans la destruction du PAAm avant que le nanoAg traverse l'endoderme vers le blastocoel (Figure 41).

De façon similaire, il est possible d'évoquer des processus chimiques qui pourraient catalyser la libération des ions  $\text{Ag}^+$  et/ou les AgNPs capturés par les groupements acides de la surface des nanotubes ingérés. Il apparaît logique de proposer que le passage des ions  $\text{Ag}^+$  par l'épithélium digestif soit déterminant pour l'intoxication des larves à tous les stades (Figure 42). Que ce soit pour les stades filtreurs dans la colonne d'eau (échinoplatei) ou pour des consommateurs de détritus à la surface du substrat (juvéniles), l'épithélium digestif permettrait la diffusion directe de l'argent (dissous et particulé), et probablement son élimination à partir du blastocoel et de la cavité périviscérale. La réponse phagocytaire des coelomocytes circulant dans la larve surgit quelque soit la forme chimique (nanoparticulé ou libre). L'argent ionique provoque une très forte réponse des coelomocytes et des spherulocytes dans le blastocoel (Magesky et Pelletier, 2014).

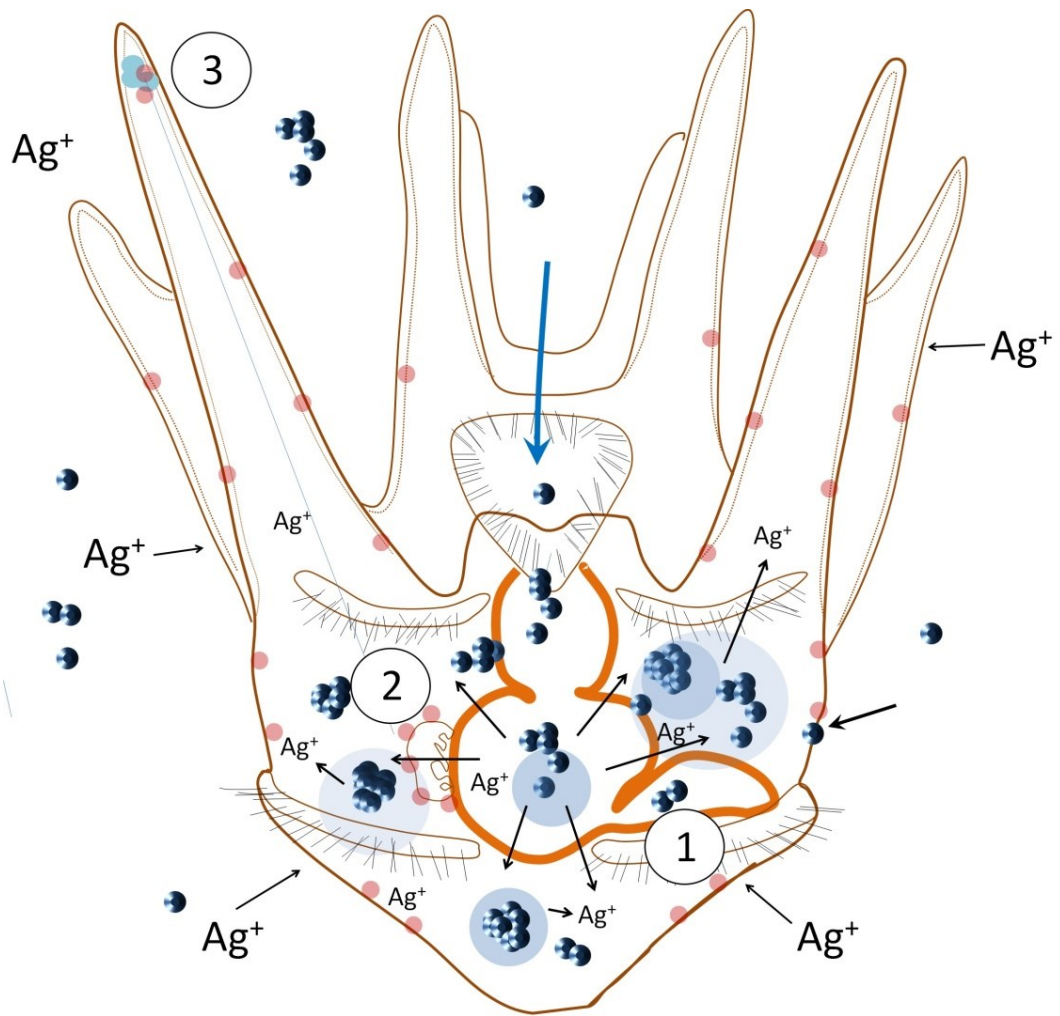


Figure 41: Modèle d'interaction des AgNPs avec l'épiderme, l'épithélium digestif et le mésoderme (cavités coelomiques et tissus associés) chez les échinoplutei. Peu d'assimilation par l'épiderme (en brun) par opposition à l'entrée facilitée des nanoparticules par l'épithélium digestif (en orange). Les flèches indiquent l'assimilation des AgNPs et des  $\text{Ag}^+$ . (1) l'agrégation des nanoparticules pourrait se produire dans le lumen du tube digestif comme conséquence du changement de pH (en manque de nourriture), des processus digestifs du phytoplankton (en présence de nourriture) ou le passage des AgNPs par les cellules de l'endoderme. (2) les agrégats des AgNPs dans le blastocoel sont liés à la contamination du mésothélium, la cytotoxicité des cellules de défense ainsi que la réponse phagocytaire. (3) L'argent dissous dans le blastocoel doit perturber la minéralisation menée par les clusters à l'extrémité des bras.

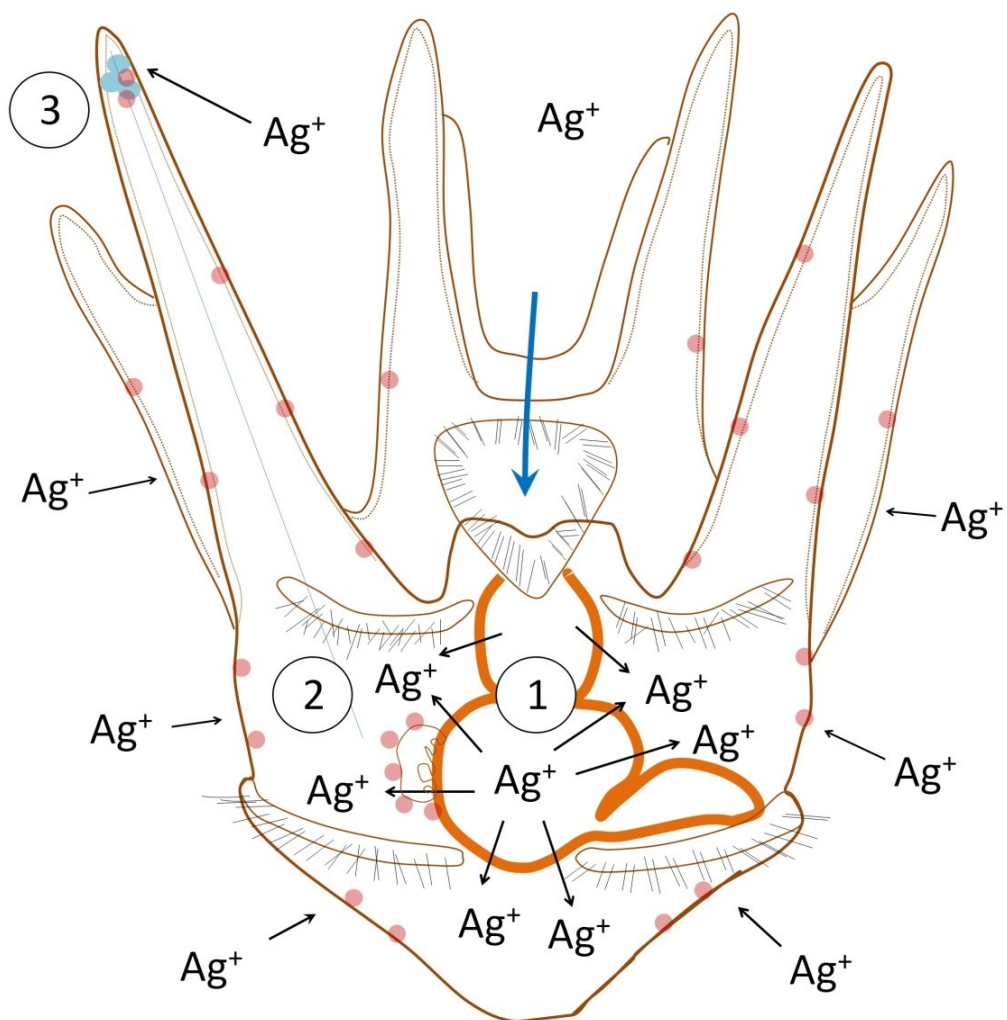


Figure 42: Modèle d'interaction des ions  $\text{Ag}^+$  avec l'épiderme, l'épithélium digestif et le mésoderme (cavités coelomiques et tissus de l'entourage) chez les échinoplutei. Les flèches indiquent l'assimilation des  $\text{Ag}^+$ . Peu d'assimilation par l'épiderme (en brun) par opposition à l'entrée facilitée des  $\text{Ag}^+$  par l'épithélium digestif (en orange). (1) assimilation du contaminant par des processus de transport. (2) la diffusion des ions dans le blastocoel provoque aussi une réponse cytotoxique des coelomocytes et des spherulocytes. (3) L'argent dissous perturbe l'activité des clusters à l'extrémité des bras.

## 2- Les fonctions du mésoderme et ses dérivés coelomiques lors de la nano-contamination : défense, translocation et détoxicification

Pendant la gastrulation, les cellules blastocoeliaires et les précurseurs des cellules rouges migrent de la surface de l'archentéron vers le blastocoel et l'endoderme (pôle animal), respectivement. Les spherulocytes ré-envahissent ensuite le blastocoel une fois leur différentiation commencée au pôle animal de l'embryon. Ainsi, cette individualisation tardive du mésenchyme secondaire représente, avec le mésenchyme primaire, l'établissement définitif du troisième tissu fondamental: le mésoderme. Les spherulocytes rouges et les cellules blastocoeliaires constituent le système de défense cellulaire primaire des embryos. D'ailleurs, les cellules blastocoeliaires sont déjà capables de phagocytter des bactéries aussitôt qu'elles quittent l'archentéron, d'après Silva (2013). En ce qui concerne les AgNPs, il est impossible de préciser si ces cellules auraient une réponse phagocytaire comme celle des échinoplutei (amoebocytes phagocytaires) ou des juvéniles (coelomocytes), parce que les ions  $\text{Ag}^+$  libérés dans l'eau semblent perturber assez rapidement leur métabolisme. En admettant que les AgNPs arrivent à accéder au blastocoel embryonnaire en traversant l'endoderme avant les  $\text{Ag}^+$ , les cellules blastocoeliaires répondraient probablement d'abord à la présence des nano-agrégats, comme constaté avec les images MET des larves.

Au dernier stage larvaire (échinoplutei L8), le coelom de gauche forme le système aquifère, le système perihémal et une partie des mésentères juvéniles, celui de droite forme le sinus axial et aussi une partie des mésentères (Brusca et al., 2016). En supposant que l'hydropore larvaire formé chez les larves puisse contribuer à l'assimilation des ions  $\text{Ag}^+$  ou à l'internalisation des nanoparticules dans les cavités en transformation, cette contribution serait moins importante comparée au tractus gastro-intestinal. Il semble que les nanoparticules individuelles chez les larves et les juvéniles sont internalisées par les coelomocytes circulants du cœlome (blastocoel et cœlome hypogastrique) grâce à leur capacité inhérente d'envahir les cellules. Les processus actifs d'internalisation semblent

être restreints à des petits ou grands nano-agglomérats (Figure 43). D'ailleurs, la nano-agrégation dans les cavités coelomiques (secondaires ou périviscérale) peut constituer une condition importante pour déclencher une réponse phagocytaire plus fonctionnelle à n'importe quel stade de développement chez les oursins.

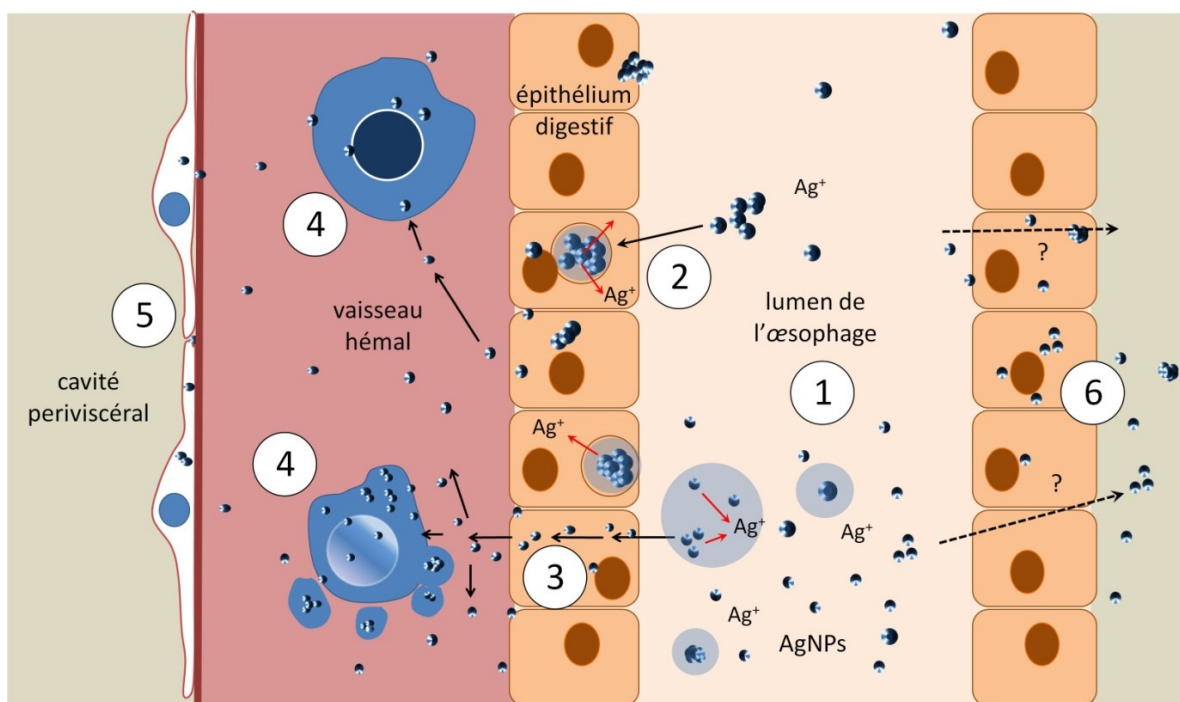


Figure 43: Modèle des mécanismes d'agrégation et d'internalisation des AgNPs après l'assimilation par voie orale chez les juvéniles. Les flèches noires continues représentent des voies confirmées, les pointillées les voies probables ou possibles, alors que les rouges indiquent la dissolution des AgNPs. (1) les AgNPs (8 nm, 16 nm, 25 nm) rentrent dans l'œsophage et se dispersent sur l'épithélium digestif; (2) les nanoparticules de plus grande taille semblent être aggrégées dans les vacuoles des cellules de l'épithélium; (3-4) les 8 nm-AgNPs traversent l'endoderme et atteignent les coelomocytes circulants du vaisseau hémal interne en causant des processus apoptotiques; (5) les AgNPs qui continuent à traverser le mésentère sont capturées par les peritoneocytes; (6) les surfaces du tractus non couvertes par les vaisseaux doivent permettre le passage des AgNPs vers le cœlome.

En général, le fluide de circulation corporel chez les échinodermes - le fluide coelomique - diffère très peu de l'eau de mer. Le pH de ce fluide est normalement inférieur à celui de l'eau de mer par environ 0,5 à 1,5 unité. Ce liquide comporte des aminoacides, des sucres réduits, des lipides, des cellules circulantes, des peptides de fonction structurelle et un large répertoire de protéines associées à la réponse innée et à la détoxicification (Dheilly et al., 2011). Dans le cas des juvéniles, le courant d'eau contaminée passant par les cavités coelomiques secondaires pourrait transporter les nanoparticules non-agrégées. On peut logiquement évoquer l'action des protéines de reconnaissance du non-soi pour expliquer la phagocytose dans l'espace intra-péritonéal. Cependant, il semble que l'action cytotoxique des 8 nm-AgNPs sur la surface membranaire entraîne une réaction d'élimination par les coelomocytes et une nano-agrégation dans la cavité comme résultat final.

De cette façon, ces nano-agrégats mélangés avec des débris cellulaires pourraient contribuer au déclenchement de la réponse phagocytaire par les coelomocytes. Comme les nano-agrégats traversent les vaisseaux de circulation envoisinant les cavités secondaires (épigastrique ou intra-péritonéal), ils sont à nouveau capturés, exportés par les peritoneocytes vers la cavité périviscérale (probablement associés avec des contenus cellulaires), où ils sont encore une fois phagocytés. En somme, les peritoneocytes aident à la nano-détoxicification des cavités coelomiques secondaires des juvéniles alors que chez l'échinoplateus, ces cellules décontaminent surtout le mésothélium qui enveloppe le tract gastrointestinal (Figure 44). La réponse immunologique dans la cavité périviscérale ou le blastocoel en fonction de l'agglomération des nanoparticules constitue en soi une question à résoudre par de nouvelles observations. De toute façon, le comportement des AgNPs dans l'épithélium digestif et le mésothélium vont influencer leur devenir dans le cœlome (Figure 44).

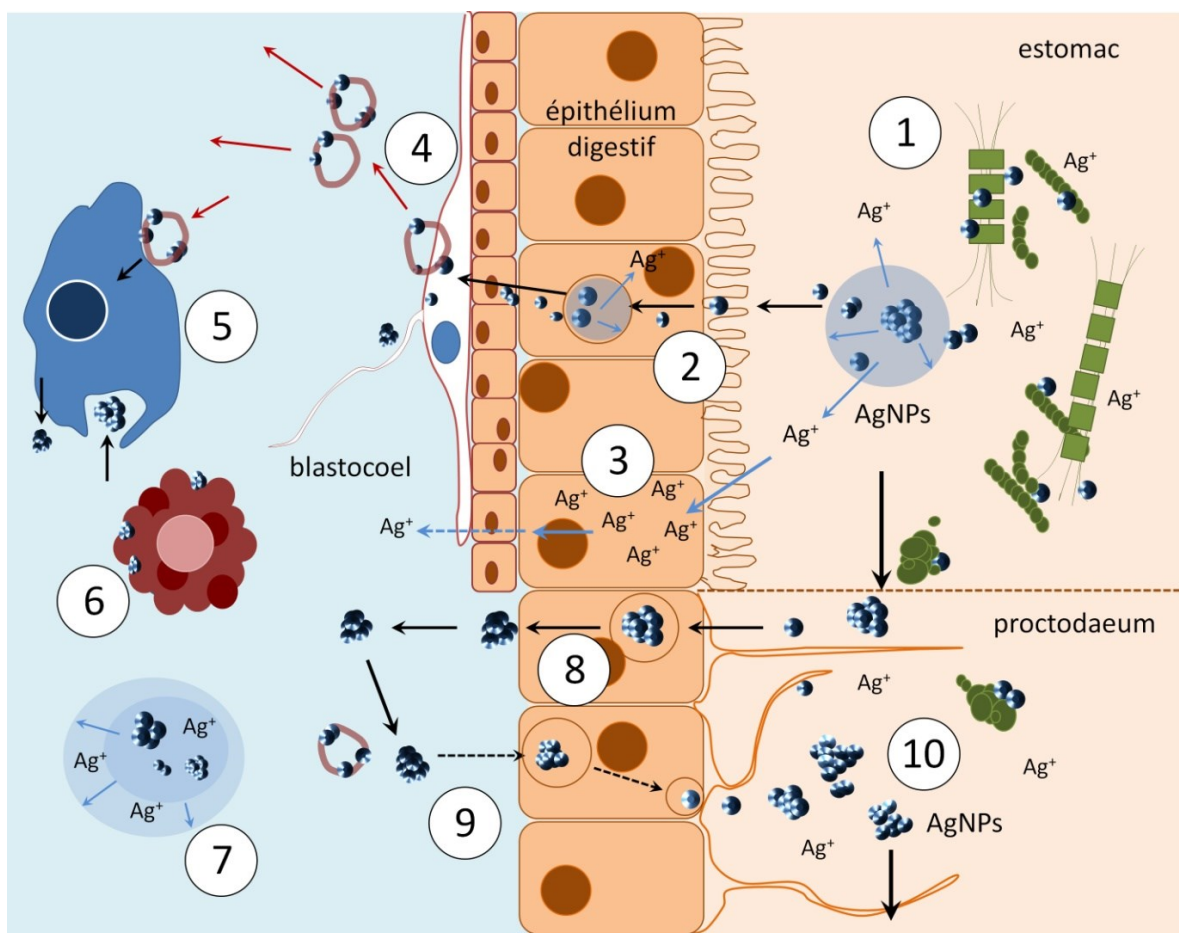


Figure 44: Modèle des mécanismes d'assimilation, agrégation et internalisation des AgNPs chez les échinoplutei en métamorphose. Les flèches noires représentent les voies de translocation des AgNPs, les bleues indiquent la dissolution du nanoAg. (1) Entrée des nanoAg avec le phytoplancton dans l'estomac; (2) passage des AgNPs à travers l'épithélium digestif; (3) capture des ions  $\text{Ag}^+$  par le tissu digestif; la flèche bleue indique la possibilité de passage des ions vers le blastocoel; (4) production des vésicules porteuses des AgNPs par les peritoneocytes du mésothélium; (5) interactions des AgNPs libres dans le blastocoel (avec ou sans les vésicules) avec les phagocytes (capture et possible élimination); (6) possible coopération des spherulocytes avec les phagocytes pour élimination des AgNPs; (7) dissolution du noyau des agrégats dans le cœlome pouvant contribuer à des effets toxiques à long terme; (8) translocation des AgNPs dans le proctodaeum vers le blastocoel; (9-10) élimination possible des nanoparticules par ce tissu.

Toujours d'après cette approche mécanistique, d'autres questions se posent et quelques réponses peuvent être tentées en s'appuyant sur des données de morphophysiologie des échinodermes. Comment les coelomocytes peuvent-ils se débarrasser de l'argent particulaire internalisés après la phagocytose? Utiliseraient-ils des récepteurs spécifiques aussi trouvés chez l'homme? Quels seraient les véritables mécanismes d'expulsion des AgNPs du système organique des larves et des juvéniles? Chez l'échinoplatei, on voit que cette élimination est problématique étant donné que les larves en récupération meurent en grand nombre. Nous pouvons alors considérer le tissu du proctodaeum comme pouvant permettre l'expulsion complète du nanoAg (Figure 44). Chez les oursins juvéniles, les coelomocytes des vaisseaux hémaux qui sont liés à l'intestin sont la cible finale des nanoparticules présentes dans lumen du tube digestif. Bien que le circuit hémal soit fermé, les coelomocytes sont censés suivre le flux circulatoire vers l'organe axial, où ceux qui sont chargés de débris non-digérés sont stockés et dégradés. L'urée est détectée à forte concentration dans la région du sinus axial-organe axial chez les oursins, ce qui suggère une dégradation locale des protéines (Jangoux, 1982). L'élimination des coelomocytes alourdis peut aussi se passer à l'extrémité des branchies et des podia chez les échinidés, une sorte de diapédèse cellulaire (Jangoux, 1982). Paradoxalement, le complexe axial (madréporite, ampulla du madréporite, canal du sable, organe axial, sac dorsal, cœlome axial) est une porte d'entrée aux AgNPs, et un possiblement un endroit de détoxicification.

Quoique ces mécanismes n'aient pas été démontrés lors de la contamination avec l'argent dissous, ils sont considérés comme des mécanismes réguliers de détoxicification chez les étoiles de mer, les oursins et les holothuries. La dissolution lente du nanoAg et les mécanismes de détoxicification peuvent être les raisons principales qui expliquent la toxicité modérée chez les oursins comparée aux effets produits par l'argent dissous.

### 3- Le changement de toxicité au cours du développement en lien avec les transformations morphologiques de chaque stade

Le changement de toxicité de l'argent dissous et de l'argent nanoparticulé, combinés ou non avec les nanotubes de carbone, peut prendre place tout au long d'un processus dynamique de l'embryogénèse et jusqu'à la fin du développement des larves et des juvéniles. En fait, la sensibilité à chaque stade peut être vue initialement comme le résultat final entre les processus d'assimilation, transformation et élimination du contaminant. Dans notre étude, cette sensibilité pourrait aussi être directement reliée au fonctionnement des systèmes anti-stress (comme les *heat shock proteins*), anti-oxydation (population croissante de spherulocytes), de détoxicification (peritoneocytes) et de réparation (spherulocytes-amoebocytes) progressivement plus performants à chaque stade et même entre cohortes d'individus au même stade. Pendant l'embryogénèse, de l'induction et des fluctuations de la production de métallothionéines sont déjà connues comme un mécanisme fondamental de protection des embryons d'oursins (Nemer, 1984); ce qui peut expliquer des différences de toxicité trouvées lors des expositions à l' $\text{Ag}^+$ , aux AgNPs et leurs mélanges avec les f-SWCNTs. Récemment, cette voie de protection contre la contamination métallique a été aussi évoquée chez les oeufs de la limace terrestre *Cantareus aspersus* en développement (Baurand et al., 2015; Pedrini-Martha et al., 2016). L'idée selon laquelle les différences d'expression de métallothionéines pendant le développement est de plus en plus vue comme un mécanisme physiologique crucial pour contrer les effets nuisibles des métaux chez les invertébrés en développement.

Il est d'autre part important de mentionner que les processus d'assimilation, transformation et élimination peuvent aussi être, d'une certaine façon, associés à l'ontogénie des organismes. Autrement dit, évaluer la toxicité de chaque stade d'un organisme en développement signifie reconnaître d'abord la probabilité que les processus métaboliques clés d'un stade soient sévèrement bouleversés. Aussi, comprendre que la morphologie et le comportement de chaque stade peuvent optimiser la capture des

xénobiotiques et leurs effets toxiques ou créer des nouvelles barrières à leur assimilation. L'interruption du développement ou son ralentissement comme conséquence de la contamination résulte du budget final des coûts de maintenance organique, investissement sur la croissance somatique/ontogénie et la détoxicification qui en suit. Toutefois, l'intensité du stress chimique en termes de temps d'exposition et de concentration nominale du contaminant peut compromettre définitivement le développement.

Quelques exemples peuvent illustrer la complexité des processus de transformation des stades de développement de l'oursin vert et comment chaque stade réagit à la toxicité de l'argent. D'abord, l'ingression des cellules mésenchymateuses dans le blastocoel au début de la gastrulation, la migration des cellules spherulocytes rouges ou le rassemblement des cellules minéralisatrices au tour de l'archentéron affectés par les ions Ag<sup>+</sup> constituent un bon exemple. L'embryogénèse est un processus dynamique qui inclut la complexité des mécanismes de signalisation chimique entre plusieurs groupes de cellules, un système qui peut être facilement inversé. Une fois que la population de spherulocytes est établie sur l'ectoderme, l'ouverture du stomodeum à l'entrée des xénobiotiques dans le tube digestif en remaniement devient l'étape cruciale qui contribue significativement à l'intoxication des larves prisme.

Or, le ralentissement de la métamorphose sous l'exposition à l'Ag<sup>+</sup> et son arrêt par les AgNPs en présence de phytoplankton et à la même concentration nominale (100 µg·Ag L) nous a montré un autre aspect de la toxicité des AgNPs. À cette étape, les larves disposent de plus de bandes ciliaires (épaulettes) au tour du corps et un vestibule, ce qui se reflète sur leur capacité de natation en tant que larves compétentes, mais aussi l'optimisation du taux d'ingestion de ressources alimentaires. En conséquence, l'assimilation de l'argent avec la nourriture se fait davantage. Comme leur système organique (tissus et cavités coelomiques) est en train de se remodeler, l'élimination déficiente des agrégats d'AgNPs pourrait être une autre cause qui engendrait une forte mortalité lors de la récupération. Dans ce cas, l'assimilation du contaminant est optimisée

ainsi que sa rétention finale. La métamorphose en soi est un processus extrêmement coûteux où l'autophagie et les processus apoptotiques sont naturellement présents. Pendant l'exposition des larves métamorphiques L8<sub>2</sub> (tardives), les coûts de maintenance, d'activité (filtration) et de développement sont probablement diminués à une certaine limite pour que les processus de détoxification se mettent en place. Dans l'eau propre, les larves qui meurent sans compléter la métamorphose indiquent possiblement la hausse des coûts de maintenance pour contrer l'intoxication causée par les AgNPs (Sokolova et al., 2012).

Durant la formation du rudiment juvénile dans les larves compétentes L8<sub>2</sub> (hâties), de nouvelles couches épidermiques (des dérivatives de l'ectoderme, des tissus de la somatocoel et de l'hydrocôle en formation) s'entreposent de façon à former un sac dont la surface est couverte par des sphaerulocytes rouges. En examinant le stress oxydatif des larves compétentes contaminées par l'argent ionique sans phytoplankton, la production de ROS n'a pas été détectée dans les tissus du rudiment en croissance (Magesky et Pelletier, 2014). Cela peut indiquer une faible concentration d'argent dans le blastocoel et moins de toxicité pour le rudiment. Puisque les larves meurent en grand nombre quand contaminées en présence de phytoplankton, il semble que l'épithélium digestif contribue à une forte assimilation de l'argent ionique pendant la digestion à tel point que les mécanismes anti-stress chimiques n'arrivent pas à compenser les dommages provoqués par les ions Ag<sup>+</sup>.

Finalement, on observe que le squelette des juvéniles est définitivement une barrière contre les AgNPs. Le stéréome peut être décrit comme un labyrinthe de canaux constamment en minéralisation de façon à former une sphère soudée en plaques. Plus l'oursin se développe, plus l'endosquelette devient résistant et grand, ce qui peut constituer une barrière contre l'assimilation directe des AgNPs et leur translocation vers la masse viscérale. Chez l'étoile de mer *Asterias rubens* trouvée dans les sites contaminés, la partition des métaux lourds se fait principalement entre la masse viscérale et la paroi corporelle, dont la concentration de chaque métal obéit à des processus d'affinité chimique (Coteur et al., 2003). Étant donné que le stéréome est aussi composé d'une matrice

organique, il est possible que la dispersion de l'argent ionique se fasse par affinité avec des groupements chimiques de protéines ou de cellules associées à la structure minérale. Cependant, on ne trouve pas de données chimiques dans la littérature pour confirmer cette hypothèse. L'épiderme rapidement ciblée par la dissolution des ions  $\text{Ag}^+$  dans l'eau saumâtre pourrait cependant indiquer le début de la dispersion ionique vers le stéréome.

#### 4- Les différentes voies d'assimilation, translocation et les mécanismes de toxicité cellulaire

La toxicité de l'argent ionique est normalement reliée à son affinité chimique pour les groupements thiols et sa capacité d'endommager la structure des membranes par le disfonctionnement des protéines transmembranaires et donc perturber l'équilibre ionique des cellules (Wang, 2001). En conséquence, la cellule perd sa capacité de réguler le flux ionique et les fluides extracellulaires. De surcroît, il apparaît que les cellules dont la perméabilité cellulaire est plus importante, comme les cellules minéralisatrices et celles de l'épithélium digestif, pourraient être plus facilement perméables à l'argent dissous. Les clusters qui minéralisent le squelette des larves à l'extrémité des bras sont également rapidement perturbés, ce qui provoque une réponse réparatrice des spherulocytes. Or, chez les embryons, les PMC (cellules mésenchymateuses primaires) sont les premières à indiquer la cytotoxicité de l'argent.

En affectant la perméabilité de l'épithélium d'absorption (digestif), l'entrée de l'argent serait facilitée vers le fluide coelomique; ce qui pourrait expliquer pourquoi les cellules du blastocoel deviennent rapidement gonflées. Ceci est une indication claire de la toxicité de l'argent qu'on en a décrit comme un processus oncotique (oncosis), d'après les concepts établis par Balvan et al (2015) lors de leur étude holographique des cellules en processus de mort cellulaire. Quand les larves ingèrent les nanotubes de carbone mélangés avec l'argent dissous ou les AgNPs, plus d'argent ionique pourrait être capturé et lâché dans le tractus digestif. Ceci serait probablement le résultat des réactions chimiques propres

à la digestion ou le remaniement naturel de l'argent suivant son affinité chimique dans un milieu biologique. Puisque les groupements  $-OH$ , et  $-O\bullet$  des f-SWCNTs et les groupements amines  $-NH_2$  des polymères PAAm sont négativement chargés, les liaisons chimiques avec les ions  $Ag^+$  seraient vraisemblablement privilégiées dans le milieu d'exposition (Figure 45).

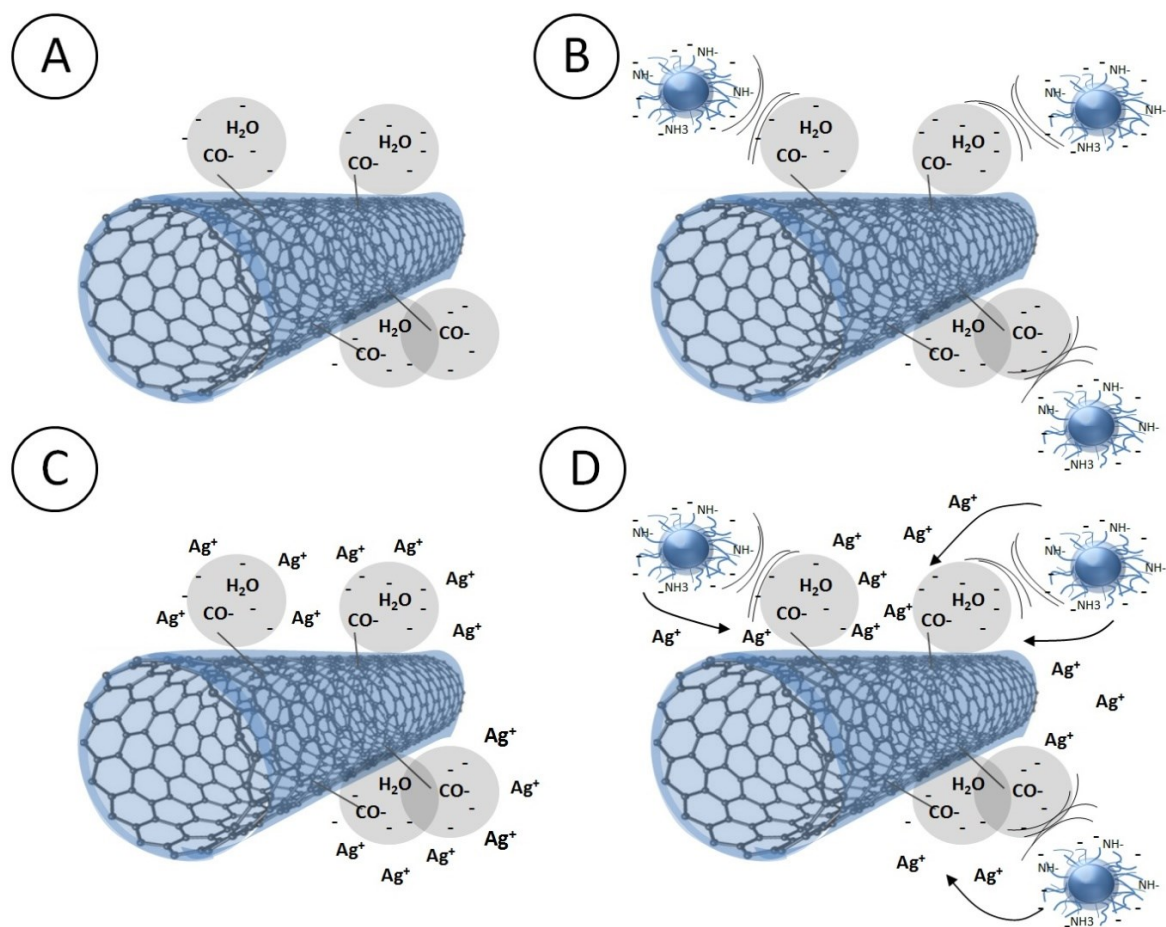
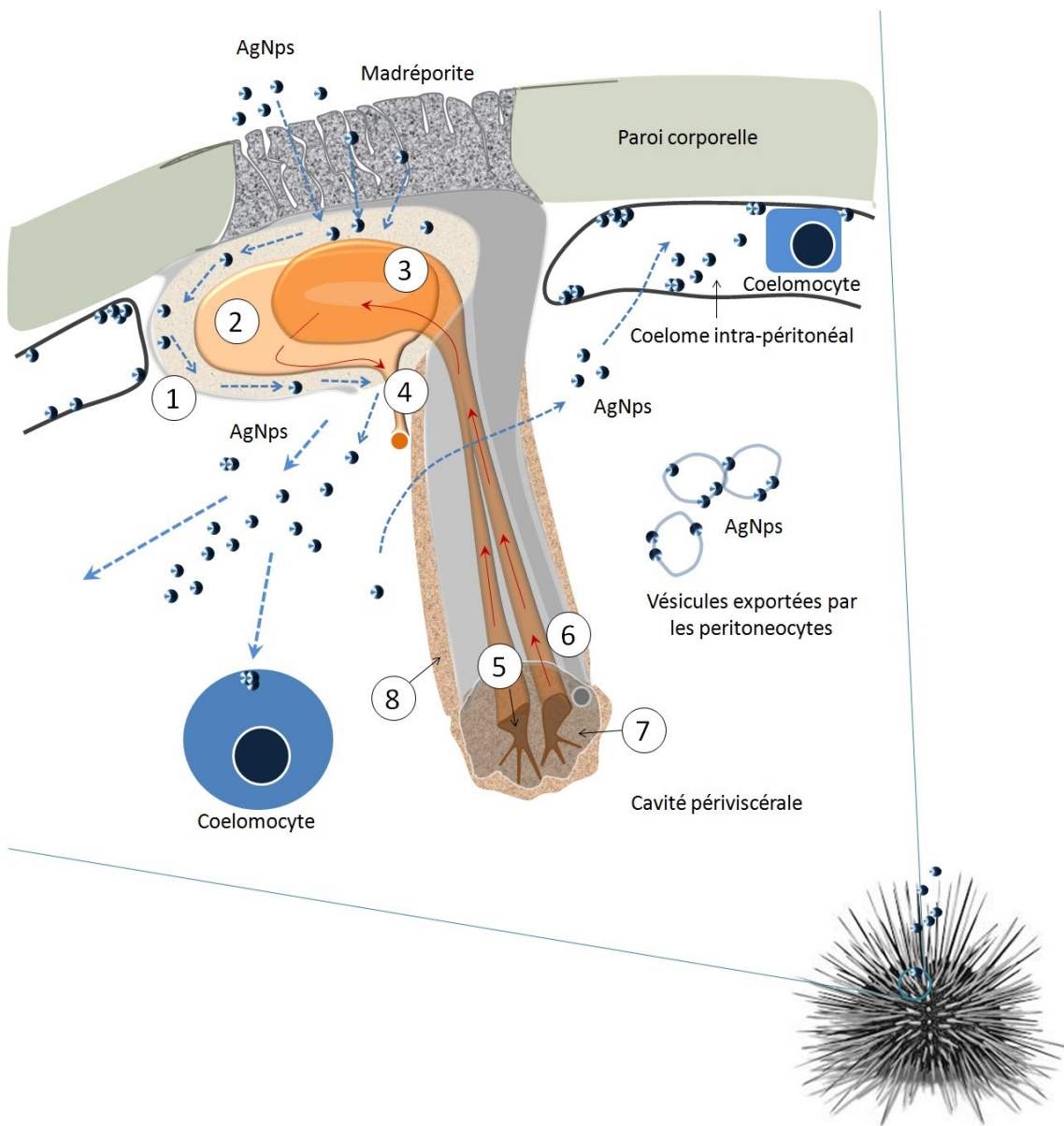


Figure 45: Modèle d'interaction de l'argent dissous et des PAAm-AgNPs avec les f-SWCNTs. (A) Sphère d'hydratation des f-SWCNTs avec des groupements acides libres. (B) Les interactions entre les PAAm-AgNPs et les f-SWCNTs doivent être dominées par des réactions électrostatiques répulsives. (C) La sphère d'hydratation des f-SWCNTs permet des approximations sporadiques et des liaisons directes avec de plus gros ions comme l' $Ag^+$ . (D) Les  $Ag^+$  libérés des polymères ou du

noyau d'argent doivent aussi être privilégiés lors des interactions entre les nanotubes et les PAAm-AgNPs.

Notre hypothèse centrale pour expliquer le flux de nanoparticules chez les juvéniles est basée sur l'entrée de l'eau par le madréporite, les pores aquifères puis les connexions coelomiques (l'axocôle) à proximité de ce complexe, comme décrit par Boolootian et Campbell (1964) (Figure 46). La distribution des AgNPs dans les cavités coelomiques secondaires suit le flux de l'eau contaminé de l'extérieur des oursins. La possibilité de dispersion des AgNPs à partir de la cavité périviscérale vers le cœlome épigastrique est moins plausible vu que le vaisseau hémal de cette région ne semble pas être contaminé. Concernant l'espace intra-péritonéal, les 8 nm-PAAm-AgNPs devraient tout d'abord traverser les mésentères et interagir avec les coelomocytes en circulation avant d'agglomérer et se lier au péritoneum. Si l'agglomération des nanoparticules avec la matière organique se présente comme le principal processus chimique dans l'environnement, l'entrée des AgNPs par le madréporite pourrait être moins importante et la voie orale privilégiée. Également, en considérant l'entrée des nano-agglomérations sans matière organique, une réponse plus effective des coelomocytes de la cavité périviscérale pourrait se produire.

Figure 46: Modèle d'interaction contaminant-tissus dérivés du mésoderme proposé pour les juvéniles d'oursin vert après l'exposition aux nanoAg. Ce mécanisme prend en compte le complexe axial, les cavités coelomiques et le mésothélium (l'illustration schématique de l'organe axial et les vaisseaux hémaux modifiée à partir d'une illustration de Boolootian and Campbell, 1964). Les flèches bleues pointillées indiquent le parcours des nanoparticules et les flèches rouges montrent le flux du liquide hémal et des coelomocytes circulants des vaisseaux. (1) après avoir circulé dans la cavité de l'axocôle, le flux continue vers la cavité périviscérale, (2) compartiment aplati de l'organe axial, (3) compartiment arrondi de l'organe axial, (4) vaisseau hémal de l'intestin du sinus hémal interne, (5) branche de droite du vaisseau hémal dans le lumen de l'organe axial, (6) canal du sable (*stone channel*), (7) lumen de l'organe axial, (8) membrane.



(Figure 46: voir sous-titres dans la page précédente)

Les AgNPs enveloppées par les polyallylamines semblent être stables dans l'eau de mer, le fluide coelomique des cavités coelomiques secondaires et dans le vaisseau hémal interne. L'interaction des 8 nm-PAAm-AgNPs avec la membrane cellulaire et leur internalisation par des coelomocytes prouvent qu'une certaine quantité de AgNPs rentre sous une forme dispersée dans les juvéniles. Les coelomocytes en circulation dans le système hémal, une fonction physiologique normale, aident au transport des nutriments absorbés à partir de l'épithélium digestif du tractus gastrointestinal vers d'autres organes (Allen, 1974). Donc, lorsque l'exposition aux nanoparticules se produit, leur transport interne peut être majoritairement mené par ces cellules. Comme les nano-agglomérations se lient facilement aux mésentères, leur libre transport dans les espaces cœlomiques secondaires pourrait arriver de façon plus lente et aléatoire, ou être tout simplement moins possible. Bien entendu, le déplacement du contenu circulant dans le système hémal est assez lent quoique quelques vaisseaux soient contractiles de façon non-rythmique.

Comparativement aux larves, les voies de translocation des AgNPs chez les oursins juvéniles sont nettement plus compliquées. Dans cette étude, nous avons remarqué que le complexe axial et le tube digestif sont essentiels pour l'internalisation acellulaire et cellulaire chez l'oursin (Figure 47). Quoique les 8 nm-PAAm-AgNPs qui passent par l'œsophage gardent leurs formes individualisées dans les coelomocytes du vaisseau interne, il est moins certain que ce fait se reproduise tout au long de l'intestin où des agglomérations de grande taille sont fréquemment observées dans les adipocytes. Le circuit de l'eau circulant avec des AgNPs dans les cavités coelomiques secondaires démontre que la contamination peut se disperser dans tous les tissus. Il est plausible que les cavités secondaires soient plus interconnectées chez les juvéniles, au moins plus directement avec l'axocœle (cœlome axial).

Les lacunes absorbantes du système hémal forment un riche réseau sur les surfaces de l'intestin à partir duquel des sous-réseaux rayonnent (Figure 48). Néanmoins, ces dispositions sont variables en termes de nombre et de connexions selon les clades supérieurs d'oursins (Spantagoidea, Echinoidea, Cidaroidea, Cassiduloidea, etc). Dû à l'organisation propre du système hémal, le transfert des AgNPs aux coelomocytes serait

possible dans n'importe quelle partie du tractus. Hypothétiquement, plus il y aurait de vaisseaux en connexion, plus l'organisme se montrerait capable de se dépurer des AgNPs. En contre partie, plus de transfert des nanoparticules vers la cavité périviscérale à partir des surfaces libres des vaisseaux augmenterait la contamination du cœlome. La façon dont les processus de détoxicification se présentent en fonction des différences morphologiques chez les groupes d'oursins (réguliers et irréguliers) pourrait avoir des conséquences intéressantes à découvrir expérimentalement.

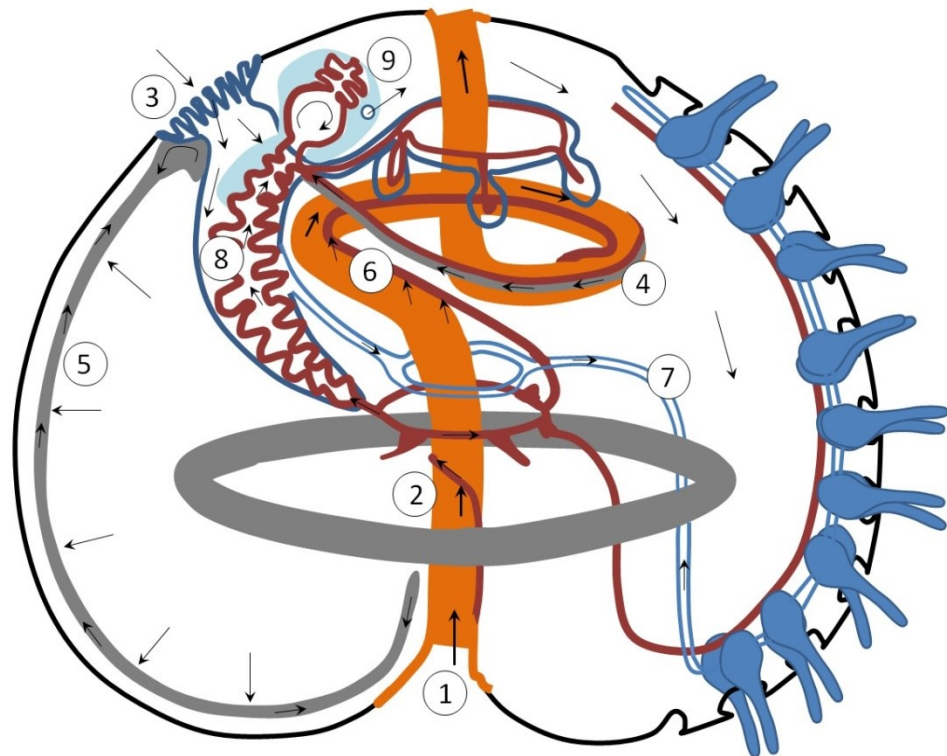


Figure 47: Modèle des voies d'entrée et de nano-translocation chez les oursins en développement. Les flèches noires montrent la direction du flux d'eau contaminée avec les PAAm-AgNPs (l'illustration schématique modifiée d'après Ezhova, 2014). Les structures marquées avec un astérisque ont été observées comme endroits de passage des nanoparticules par les images TEM: (1) voie orale\*; (2) transfert des 8 nm-PAAm-AgNPs aux coelomocytes du vaisseau hémal interne\*;

(3) entrée des AgNPs par le complexe axial; (4) cœlome épigastrique\*; (5) cœlome intra-péritonéal et periviscéral\*; (6) transfert vers les vaisseaux au long de l'intestin; (7) système aquifère; (8) organe axial; (9) incision entre l'axocôle et la cavité periviscérale.

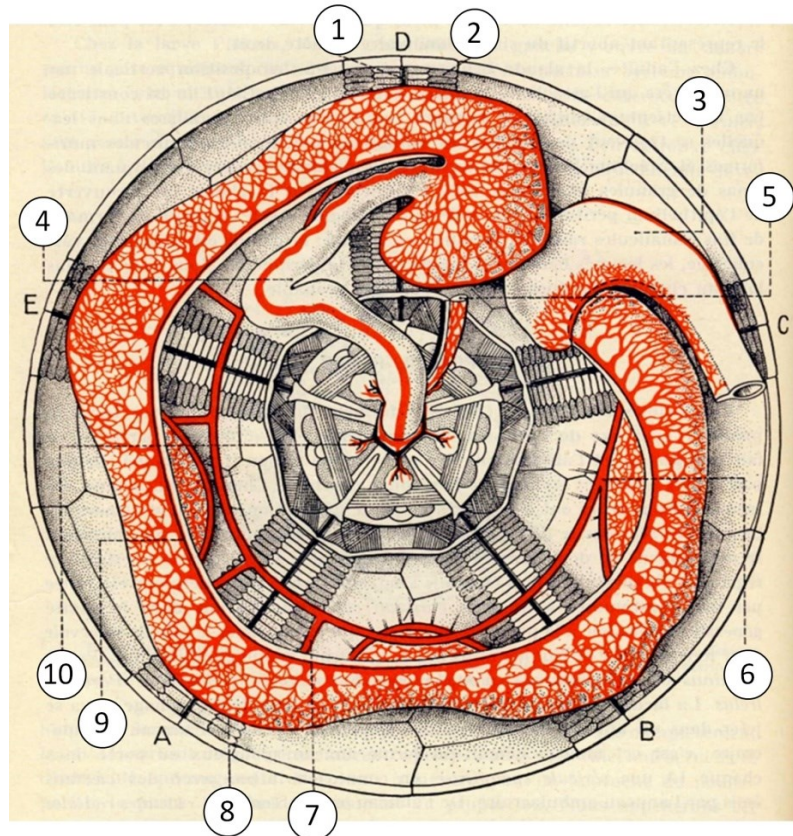


Figure 48: Réseau du système hémal lié au tractus digestif de l'oursin *Echinus esculentus* (Echinidae) en coupe radiale (illustration tirée de Grassé, 1966). L'importance du système hémal (en rouge) pendant la contamination peut indiquer des voies de détoxification complexes chez les oursins. 1- canal ambulacraire radial, 2- vésicules podiales, 3- début de la 2<sup>e</sup> courbature de l'intestin, 4- œsophage, 5- glande brune (organe axial) et tube aquifère, 6- confluent de la lacune collatérale, 7- canal transversal de communication entre la lacune collatérale et la lacune marginale externe, 8- lacune marginale externe, 9- lacune marginale interne, 10- amas spongieux. (A-D : structure ossiculaire des ambulacres).

Aussi bien chez les larves que chez les juvéniles, le transport interne des AgNPs est complexe et jusqu'à présent leur dispersion interne semble être principalement liée à la distribution libre des AgNPs dans la cavité périviscérale, l'activité des peritoneocytes et des coelomocytes en circulation. Le mécanisme cellulaire d'internalisation proposé avec les coelomocytes a des implications directes sur le devenir des PAAm-AgNPs dans les espaces coelomiques et leur remobilisation par les peritoneocytes. L'assimilation cellulaire des petites PAAm-AgNPs sous forme de clusters ou légèrement agrégées avec d'autres nanoparticules de 16 à 25 nm doit en principe déclencher les premiers mécanismes de toxicité et les réponses cellulaires restreintes aux membranes. Les images TEM dans cette étude peuvent servir de support au modèle théorique sur l'endocytose de plusieurs nanoparticules récemment présenté par Yue and Zhang (2012). Leur base théorique repose sur des simulations géométriques pour des fluides complexes et démontre l'effet coopératif de plusieurs variables, comme la taille, les concentrations des nanoparticules sur les membranes et la tension membranaire vis-à-vis l'inertie ou l'internalisation des nanoparticules. Pourtant, le comportement physico-chimique des AgNPs dans le cytosol (la formation de la *corona*, la dissolution, les phénomènes d'agrégation des nanos individuelles, désagrégation des clusters, leurs liaisons avec les organites, etc) reste encore à être étudié en détail. En outre, la dissolution des AgNPs dans les cavités coelomiques et les cellules exigent des nouveaux protocoles expérimentaux en microscopie TEM et des méthodes chimiques pour détecter la spéciation chimique dans les organismes exposés (e.g. Synchrotron X-ray Absorption Spectroscopy and micro-X-ray fluorescence Imaging, Chemosensor RC-1 pour l'analyse des ions  $\text{Ag}^+$  intracellulaires, Lm-edge X-ray absorption near-edge spectroscopy – XANES) (Wang et al., 2014; De Matteis et al., 2015; Hsiao et al., 2015).

L'interface membranaire plus externe stabilise d'abord les nanoparticules sur la couche extracellulaire (Figure 49). Une sorte d'extrusion vésiculaire se produit sur la surface des coelomocytes contaminés (Figure 49 A), ce qui peut correspondre à un mécanisme d'élimination à partir de la membrane cellulaire elle-même. Il est encore

difficile à dire jusqu'à quel point ce mécanisme implique des coûts énergétiques irréversibles pour les coelomocytes. Il se peut aussi qu'un réseau de protéines extracellulaires récemment découvertes chez les cellules du système immunitaire humain puisse attraper les nanoparticules aussi chez les coelomocytes d'oursin (Figure 49 B). Ce résultat converge vers la pensée scientifique actuelle qui propose le système immunitaire des oursins comme étant très similaire à ceux des autres deutérostomiens, y compris les humains. En traversant ce réseau de macromolécules, les interactions nanoparticule-surface biologique passeraient directement à la membrane plasmatische. Puisque l'enveloppe organique des nanoparticules doit probablement aussi capturer et relâcher d'autres molécules du fluide coelomique, il paraît plausible d'évoquer en premier lieu l'importance des effets physiques des nanoparticules sur les composantes membranaires menant à la perturbation des activités membranaires, les processus de transport, et la conformation des protéines.

Une fois intériorisées en forme de petits clusters, les AgNPs peuvent probablement subir des processus d'agrégation-désagrégation avant d'atteindre les compartiments cellulaires (Figure 49 B). Cependant, rien n'a encore été démontré dans la littérature. À ce propos, la microscopie TEM liée à l'analyse des rayons X (EDX) pourraient être un précieux outil pour discerner les tailles des nano-agrégats formés dans les coelomocytes en culture, par exemple. Dans l'espace périnucléaire, le réticulum endoplasmatic et le noyau, les AgNPs maintiennent leur forme en très petites agrégations ou en particules individuelles. Ceci contribue à l'idée selon laquelle ces compartiments sont facilement ciblés par les AgNPs.

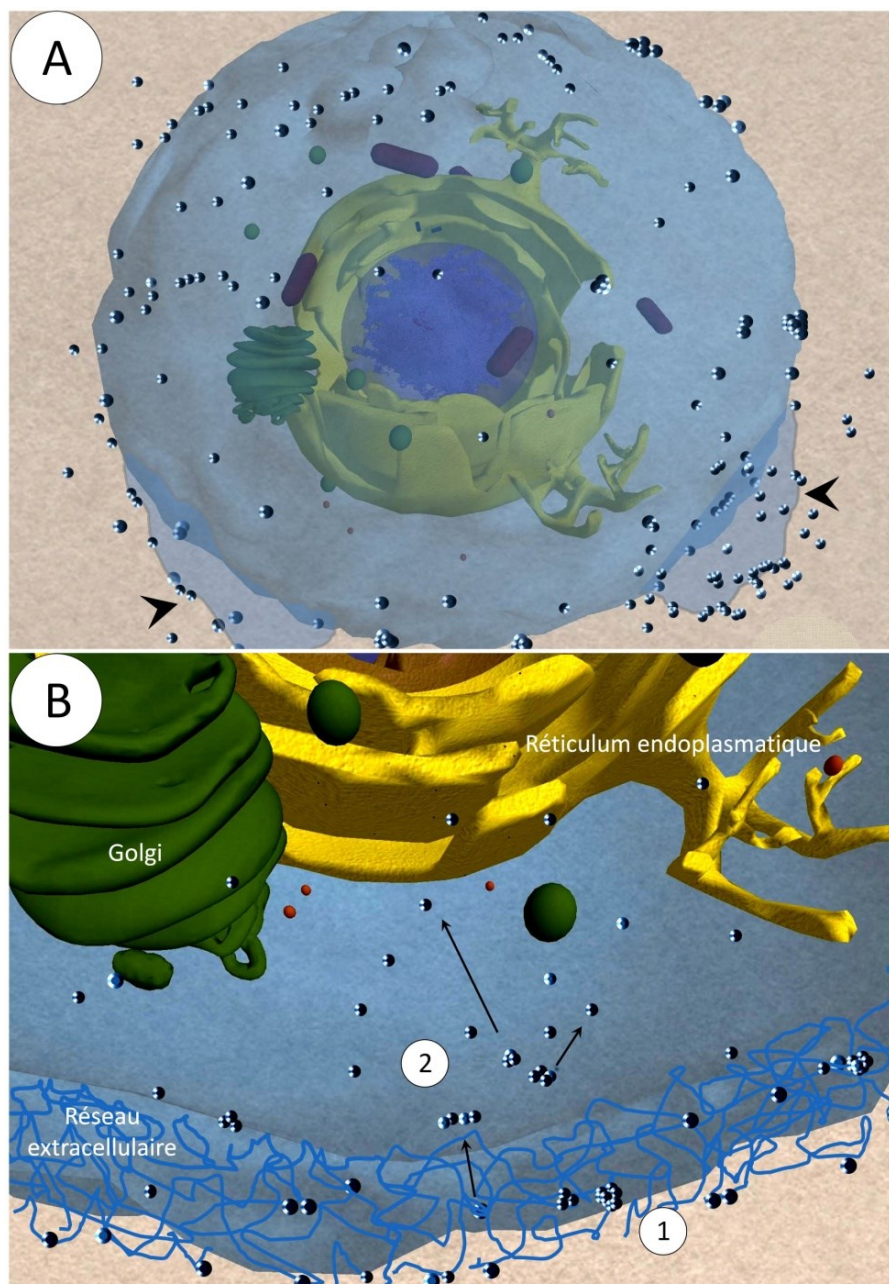


Figure 49: Modèle d'interaction des AgNPs avec la membrane cellulaire des coelomocytes: (A) production des vésicules d'extrusion comme effet cytotoxique; (B) le mécanisme d'internalisation des AgNPs sous forme de clusters qui se dispersent dans le cytosol (2) après leur passage par le réseau extracellulaire (1).

Dans ce cas, leur effet génotoxique serait sans doute renforcé par leur oxydation et la libération des Ag<sup>+</sup> (mécanisme cheval de Troie), considéré comme l'effet toxique à long terme dans nos expériences. Tout cela mène à d'autres questionnements qui n'ont pas encore été abordés dans ce travail: les AgNPs s'oxydent-elles de la même manière dans le cytosol et le noyau? Où l'oxydation des AgNPs dans le noyau se fait-elle d'abord en fonction de la surproduction de ROS au cytosol (« effet de boucle »)? L'importance de ces questions repose sur la possibilité d'investigation des processus apoptotiques des coelomocytes d'échinodermes. Les processus cellulaires qui conduisent à l'apoptose sont moins connus chez les invertébrés marins en général, surtout quand ils sont contaminés par les AgNPs.

L'activation des protéines chaperonnes hsp70 a été cruciale pour ajouter de nouvelles évidences sur les effets toxiques propres à l'argent dissous et l'argent particulé. L'interaction des hsp70s avec les cochaperones hsp90 et hsp40 et même avec les hsp60s dans la matrice mitochondriale sous l'action des nanoparticules demeure néanmoins encore méconnue. Dans le cytosol, l'expression accrue des hsp70s doit contrôler l'agrégation et la dénaturation des protéines provoquées par l'action additive de l'argent dissous et les AgNPs (stress protéomique). En fait, les effets physico-chimiques de l'argent particulé doit influencer l'agrégation des protéines dans le cytosol (Shemetov et al., 2012). La forte expression des hsp60s montre en parallèle la différence entre l'action physico-chimique modérée de l'argent nanoparticulé dans la cellule comparée à l'argent dissous, d'effet ici considéré immédiat (Figure 50).

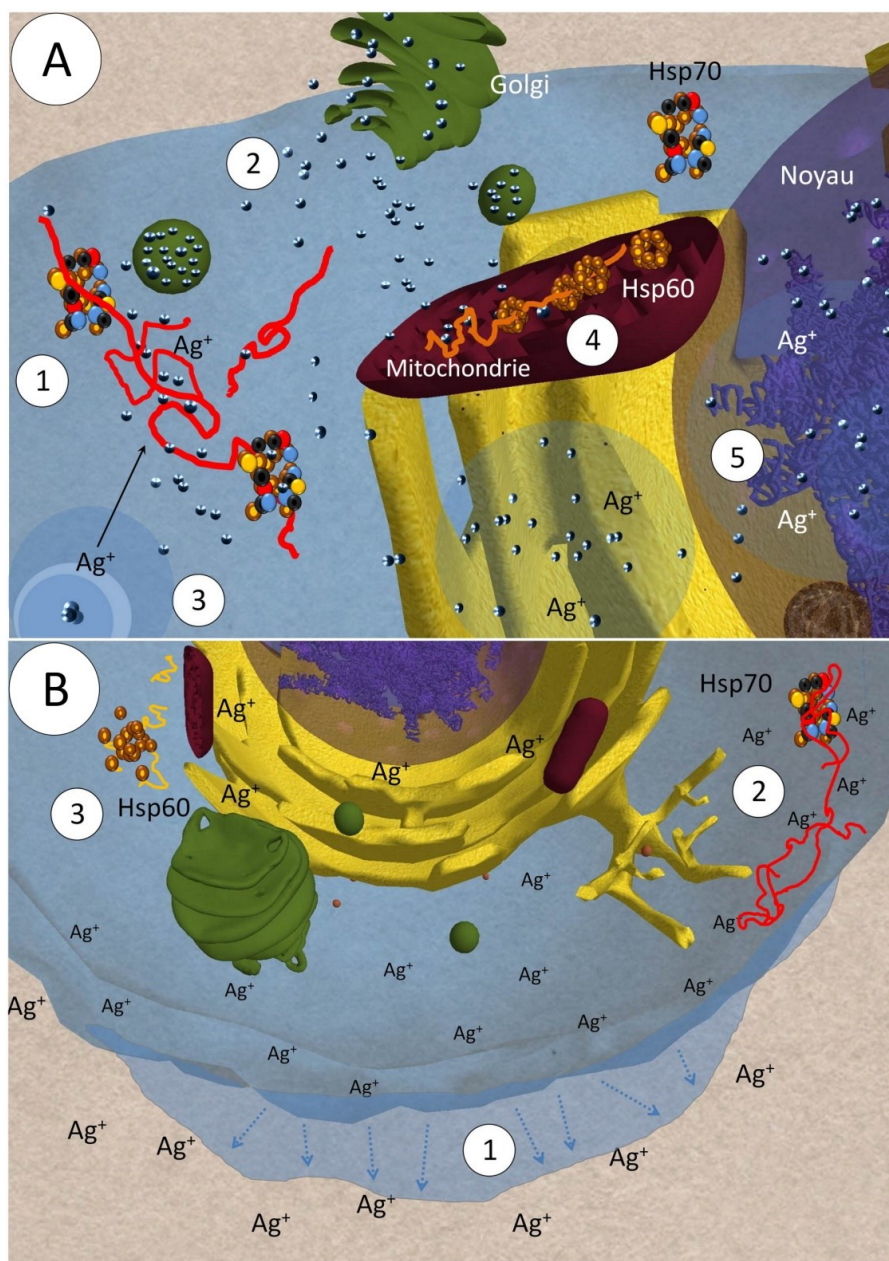


Figure 50: Différences entre les mécanismes de toxicité cellulaires des AgNPs et des ions Ag<sup>+</sup> chez l'oursin vert en stade juvénile. (A) nano argent : 1- l'agrégation/dénaturation des protéines cytoplasmatisques causés par les AgNPs cause une forte expression des hsp70s; 2- l'appareil de Golgi et la voie de sécrétion cellulaire sont ciblés par les 8 nm-PAAm-AgNPs; 3- les effets physiques doivent dominer la toxicité dans un premier moment, suivi par la dissolution de l'argent dans la cellule peut-être par l'action du ROS; 4- l'expression des chaperonines 60 KDa confirme

l'effet toxique des AgNPs sur les protéines des mitochondries; 5- la présence des nanoparticules dans le noyau démontrant leur effet génotoxique, peut être relié avec les processus apoptotiques des coelomocytes. (B) argent ionique : 1- l'oncosis (gonflement) de la cellule se produit comme résultat direct de l'action déstabilisatrice des  $\text{Ag}^+$  sur la physiologie de la membrane cellulaire; 2, 3 - l'expression des hsp70s contre le stress protéomique des  $\text{Ag}^+$  dans le cytoplasme contraste avec l'absence de l'expression des hsp60s.

D'après quelques données trouvées dans la littérature sur les invertébrés aquatiques, les métaux cationiques à forte concentration de l'ordre de 100  $\mu\text{g}\cdot\text{L}^{-1}$  semblent empêcher l'expression des hsp60s. L'effet déstabilisateur des ions  $\text{Ag}^+$  sur les membranes de la mitochondrie (ou l'équilibre ionique cellulaire en général) doit interférer sur l'expression des hsp60s : (1) en empêchant le passage des cochaperons cytoplasmatisques précurseurs des hsp60s vers l'organite ou (2) les endommageant avant leur assemblage dans les mitochondries. Parmi les nanoparticules métalliques d'Ag,  $\text{Fe}_3\text{O}_4$ , Al,  $\text{MoO}_3$  et  $\text{TiO}_2$ ; les AgNPs sont celles qui affectent le plus l'intégrité mitochondriale par la réduction du potentiel de membrane, la diminution de la glutathionne (antioxydant mitochondrial) et la forte production de ROS (Unfried et al., 2007).

## 5- La structure des PAAm-AgNps et la nanotoxicité

Les deux grands groupes de nanoparticules (non-solubles et solubles) sont impliqués dans des mécanismes uniques d'internalisation et de génération du ROS; l'un des effets chimiques perçus comme un déclencheur de la nanotoxicité cellulaire. L'internalisation des nanoparticules est fonction de leurs propriétés physico-chimiques (composition, taille, forme et état d'agglomération), des conditions expérimentales du milieu d'exposition, et aussi des caractéristiques de la cellule-cible, ainsi que leur différentiation. Tous ces facteurs peuvent déterminer si l'assimilation cellulaire sera active et/ou dépendra de récepteurs cellulaires spécifiques. Bien que plusieurs études n'examinent pas les effets de la dissolution des nanoparticules métalliques dans le cytosol à cause de difficultés méthodologiques, notre travail montre que le rôle des ions dissous (comme

l' $\text{Ag}^+$ ) pour expliquer leur toxicité ne doit pas être négligé. Outre la libération ionique dans le milieu intracellulaire, le mécanisme non-oxydant est aussi responsable par des dommages cellulaires. La façon dont les nanoparticules interagissent avec des molécules organiques dans le milieu cellulaire est une condition qui dépend de la taille de la particule, la forme, et des caractéristiques de la surface (charge, groupes fonctionnels, énergie disponible). En conséquence des interactions électrostatiques qui prennent place avec les macromolécules, des effets biologiques adverses comme agrégation protéomique, fibrillation et perte d'activité enzymatique apparaissent (Lynch et Dawson, 2008).

Le stress oxydatif est étroitement associé à la toxicité des ions  $\text{Ag}^+$ , mais il y a des nouvelles données qui pointent vers les nanoparticules comme inductrices de signaux qui causent l'endommagement de l'ADN, l'arrêt du cycle cellulaire et l'apoptose (Eom et Choi, 2010). La série de résultats présentés ici avec les stades de développement de l'oursin vert montrent que parfois la toxicité des PAAm-AgNPs peut être plutôt attribuée à l'argent libre (embryons), l'effet de la particule en soi peut être combiné avec les  $\text{Ag}^+$  (larves métamorphiques) et la dissolution à long terme (juvéniles). Par exemple, les effets des nanoparticules d'or (AuNPs) au niveau cellulaire sont très similaires aux AgNPs comme: les interactions avec la membrane cellulaire, le stress oxydatif, l'endommagement des mitochondries et de l'ADN. Cependant, les AuNPs catalysent la production de l'oxyde nitrique (NO) à partir des groupes thiols (S) ce qui n'est pas un mécanisme connu pour l'argent (Lapresta-Fernández et al., 2012).

Les nanoparticules d'argent PAAm sont formées par un noyau d'argent et d'une enveloppe polymérique de polyallylamine relativement stable à partir d'où les interactions avec le milieu externe devront d'abord prendre place (Figure 51).

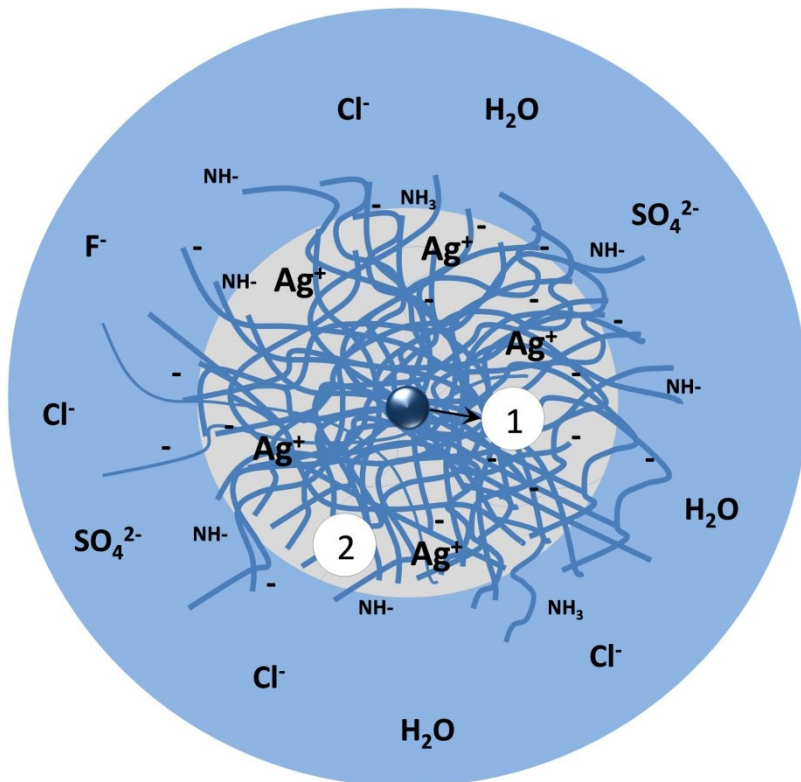


Figure 51: Schéma de la structure des nanoparticules d'argent PAAm. (1) noyau métallique d'argent; (2) enveloppe polymérique contenant les  $\text{Ag}^+$  près à être libérés. La couche bleue indique la sphère d'hydratation et le milieu aqueux d'exposition.

L'enveloppe donne une stabilité colloïdale par les forces d'attraction électrostatiques et la répulsion stérique qui s'exercent entre les particules. Les polymères gardent une certaine quantité d'argent dissous ( $\sim 2.5\%$ ) pouvant être libérée lorsque les nanoparticules arrivent dans un milieu aqueux comme l'eau de mer. On peut donc considérer la présence d'une couche de rétention où une partie des ions sont encore retenus et libérés au fur et à mesure, et une région où des échanges plus dynamiques « capture-recapture » se produirait (Figure 52 A). Ce comportement semble expliquer une partie de la toxicité trouvée lors des expositions aigues chez les organismes étudiés, marquée par une hausse initiale de la concentration de l'argent dissous (24-48h), suivi par une baisse (96h). L'augmentation de l'argent accumulé ou adsorbé par les oursins en une seule exposition

chronique suggère que la dissolution des PAAm-AgNPs s'est fait lentement à 8°C (Figure 52 B).

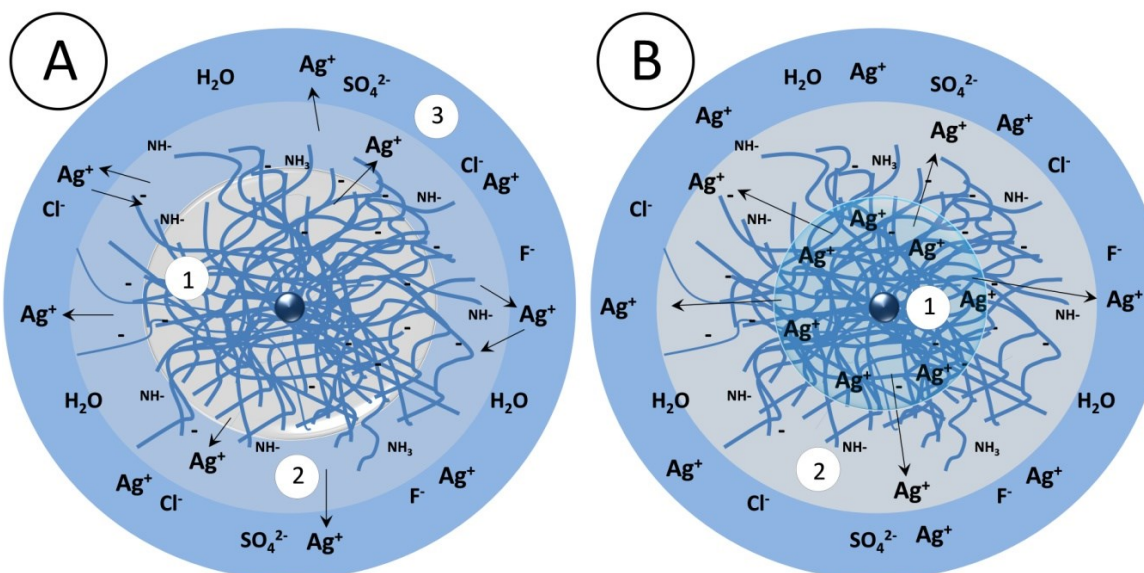


Figure 52: Modèle d'action des PAAm-AgNPs dans un milieu aqueux. (A) 1-région de rétention de l'argent ionique, 2- région d'interaction avec le milieu externe, 3- milieu aqueux. (B) 1- dissolution du noyau métallique, 2- régions de rétention et interaction.

Les molécules de PAAm, négativement chargées, devraient constituer une force répulsive à l'interaction des AgNPs avec la couche phospholipidique des membranes, pourtant ce ne semble pas toujours le cas. Dans le cas des petites PAAm-AgNPs, il se peut que les clusters exercent une force qui surmonte les interactions répulsives ou que la couche négativement chargée soit déjà neutralisée par d'autres molécules organiques du milieu interne des oursins. Dans le cytosol, en considérant que les molécules de PAAm soient intactes, un remaniement de la coquille organique (diminution ou augmentation) avec des nouvelles interactions dans le cytoplasme serait possible. Si la couche organique et le PAAm sont dégradés dans le cytosol, le milieu intracellulaire contribuerait aussi à la complète dissolution de la particule (Treuel et al., 2013). En conséquence, les débris moléculaires qui sont issus de ces interactions ainsi que les ions Ag<sup>+</sup> provoqueraient la toxicité. Le fait que les PAAm-AgNPs individuelles (ou en petits clusters) soient trouvées

dans la région périnucléaire et dans le noyau des coelomocytes suggère qu'elles ont un comportement typique des particules cationiques utilisées pour délivrer des gènes ou des agents thérapeutiques aux cellules (Wang et al., 2015).

Les coelomocytes d'oursin accumulent une quantité relativement importante d'AgNPs dans les vésicules endocytiques. Puisque les cellules semblent être en pleine activité de digestion (avec la mobilisation des lysosomes à différentes tailles), nous pouvons suggérer que la toxicité des agrégats pourrait être moins importante que celle des 8 nm-PAAm-AgNPs. La compréhension des mécanismes de toxicité des nanoparticules en milieu biologique demande une recherche plus approfondie sur la formation des coquilles organiques (*coronas*) et son potentiel de mitiger la toxicité. Cet aspect n'a pas été abordé dans nos études avec les PAAm-AgNPs, mais soulève des réflexions intéressantes. Il est bien établi que les nanoparticules dans le milieu biologique sont recouvertes par des protéines et d'autres biomolécules formant une couche plus ou moins perméable à leur surface. Cette couche est retenue par les nanoparticules même après leur entrée dans les cellules (Gunawan et al., 2014).

Après les interactions des nanoparticules avec les lysosomes, la couche est possiblement détruite et ainsi expose la surface nue des nanoparticules qui déclenche des effets toxiques auprès des lysosomes (Wang et al., 2013). La toxicité cellulaire apparaît donc par la perméabilisation de la membrane des lysosomes, ce qui engendre la libération de leurs hydrolases dans la cellule et l'acidification du cytosol. Tous ces processus sont connus avec les AgNPs et conduisent finalement à la nécrose cellulaire. Alternativement, la libération des nanoparticules et des hydrolases à partir des endosomes rompus peut générer de l'inflammation, la production du ROS, les dysfonctionnements de la mitochondrie et du réticulum endoplasmique et l'apoptose (Wang et al., 2015). Cependant, les grands agrégats des AgNPs dans les coelomocytes comparées à celles de l'extérieur suggèrent, à un certain point, une capacité de stockage pas forcément liée à un processus toxique majeur. Il est difficile de préciser si ces cellules arrivent à éliminer le nanoAg au fil du

temps, avant que les effets nuisibles surgissent. Déterminer si le PAAm ou la formation d'une couche organique seraient des variables importantes lorsque les coelomocytes digèrent les AgNPs agglomérées est également compliqué sans le marquage de ses couches en microscopie. Dans cette étude, l'enveloppe polymérique des nanoparticules d'argent rend le paradigme de la théorie du cheval de Troie encore plus complexe.

La vraie structure des nanoparticules d'argent PAAm doit plutôt ressembler à un petit point d'argent entouré des très longs polymères  $[CH_2CH(CH_2NH_2)]_n$  entremêlés et à un fort poids moléculaire. Ainsi, il est difficile de savoir jusqu'à tel point les PAAm-AgNPs pourraient être dégradées par des agents oxydants en milieu externe ou dans le cytosol (avec le  $H_2O_2$ , pas exemple). Il est connu que dans les lysosomes on trouve environ 40 enzymes hydrolytiques différentes, mais il faudrait aussi considérer quelle serait la vitesse de digestion des PAAm et des coronas à 8°C. Selon Sakhtianchi et al. (2013), différentes cellules peuvent répondre différemment à la même nanoparticule de même corona, ce qui empêche une compréhension claire du devenir intracellulaire des nano-agrégats chez les coelomocytes, pour le moment. La réponse à cette question devrait prendre en compte les coûts métaboliques des cellules de continuer une digestion lente des agrégats ou de procéder à leur élimination par exocytosis, un processus coûteux qui demande plusieurs récepteurs intracellulaires. Quoiqu'il en soit, plus la taille des AgNPs est importante, plus elles seront difficilement éliminées (Sakhtianchi et al., 2013).

Alors, il est possible d'hypothétiser que la libération des  $Ag^+$  retenus par les polymères des AgNPs peut se faire à partir (1) de la région plus externe de la coquille polymérique dans n'importe quel moment vu qu'ils sont plus labiles et échangeables et (2) de la région plus proche du noyau, ce qui demanderait probablement une prédigestion du polymère. L'autre possibilité est que les molécules d' $O_2$  aillent complexer l'argent en attaquant ensuite le noyau d'argent. D'après les modèles actuels, les composés  $Ag_2O$ ,  $AgO^-$ ,  $AgNO_3$ ,  $AgCl$  et  $Ag_2S$  sont formés dans les larves échinoplutei après une courte exposition à des 5-35 nm-AgNPs enveloppées au citrate (Piticharoenphun et al., 2012). Les

oxydes des types  $\text{Ag}_2\text{O}$  sont plus hydrosolubles et doivent donc libérer les  $\text{Ag}^+$  et régénérer l'agent oxydant. Les  $\text{AgCl}$  sont aussi labiles et biodisponibles, mais les  $\text{Ag}_2\text{S}$  sont très peu solubles dans l'eau. Admettant que cette dissolution de l'argent se produise très lentement dans nos modèles, l'effet physique de la particule en soi doit être fondamental pour expliquer une partie de la toxicité.

6- La compréhension des mécanismes en fonction du temps d'exposition et récupération, les observations *in vivo* et par microscopie MET :

Il est important que noter que si pour l'argent dissous les modèles proposés peuvent représenter l'intoxication dans les expositions courtes (96h) et longues (12 jours), les mécanismes qui expliquent la nano-internalisation cellulaire et non-cellulaire se produisent lentement au cours du temps. À 96h d'exposition, le cœlome épigastrique des juvéniles se montre moins contaminé par les AgNPs. D'ailleurs, les expériences avec le nano-FITC à plus de 96h renforcent cette idée ainsi que les données ICP qui montrent une chute des niveaux d'argent nano accumulé. En ce qui concerne les oursins exposés pendant 96h, nous n'avons pas remarqué l'activité des phagocytes en réponse à la présence des nanoparticules en MET. Donc, il faut considérer que les expositions continuées à chaque 96h (pendant 12 jours) doivent optimiser les processus cellulaires de façon à les rendre plus évidents lors des analyses en microscopie. Du fait que les oursins récupèrent bien au fil de trois semaines, on pourrait supposer que les systèmes d'élimination du nanoAg doivent être efficaces, mais les données nous manquent pour tracer une véritable cinétique des événements.

7- Considérations finales

Les grands domaines d'application des nanoparticules et leur usage quotidien en général ne laissent aucun doute quant à l'importance de connaître en profondeur leurs mécanismes de toxicité sur les organismes marins, en particulier pour les nanoparticules

d'argent. Les processus morphogéniques du développement à chaque stade sont cruciaux pour expliquer les différences de toxicité de chaque contaminant étudié. Les feuillets (ectoderme, mésoderme et ectoderme) et leurs dérivés en contact direct avec les xénobiotiques se modifient progressivement au long du développement, ce qui mène à des réponses multiples suite à l'interaction toxique. D'une certaine manière, reliés aux changements ontogéniques, certains groupes cellulaires apparaissent plus importants à certains stades que d'autres (les cellules mésenchymateuses primaires, les coelomocytes, les cellules sphérules rouges, les cellules digestives, les cellules blastocoeliaires, les peritoneocytes, les amoebocytes, etc). Ces cellules constituent des *proxys* d'une grande valeur pour étudier la nanotoxicité et les effets de l'argent ionique.

Dans l'ensemble, nos résultats confirment que les stades de développement de l'oursin vert *S. droebachiensis* sont d'excellents modèles pour les travaux sur la toxicité des xénobiotiques au niveau cellulaire et de l'organisme des écosystèmes tempérés et polaires. Grâce à une vitesse de développement plus modéré en eau froide, comparée à d'autres espèces étudiées en nanotoxicologie, de nouveaux processus de détoxicification, réparation et toxicité (à court et long terme) ont été décrits à un niveau beaucoup plus détaillé que précédemment.

## APPENDICE

### APPENDICE 1: CHAPITRE 1

#### DETAILED DESCRIPTION OF EMBRYOLOGICAL AND LARVAL STAGES:

A- **No toxic treatment:** hatching blastula stage. Blastula formation is followed after the fertilized egg undergoes successively several rounds of cleavage. A single layer of cleaved blastomeres is formed enclosing the blastocoel (Bc). Later, the blastula develops cilia, and hatches from its fertilization membrane (Fm). No treatment was performed for this stage.

B- **First treatment (T1):** early mesenchyme blastula exposed. Before gastrulation, the epithelium at the vegetal pole (Vp) of the blastula flattens and thickens to form the vegetal plate. Later, the primary mesenchyme cells (PMCs) move from the vegetal plate into blastocoel (Bc) and give rise to the larval skeleton later.

C- **Second treatment (T2):** invaginating blastula exposed. Primary invagination starts, vegetal plate begins to bend inwardly and a short and squat archenteron (Aq) is formed. The PMCs are still somewhat diffusely distributed, but tend to form a ring with two ventro-lateral clusters (Vlrc).

D- **Third treatment (T3):** early gastrula stage exposed. A ring-like arrangement of PMCs is formed, surrounding the invaginating archenteron. The PMCs population inside the blastocoel forms a spiculogenic syncytium where the calcite deposition begins. These granules rapidly display a triradiate shape that is elongated to form finally the extending spicules (Sp) from the ventro-lateral clusters (Vlrc).

E- **Fourth treatment (T4):** mid-to-late gastrula stage exposed. The half way extended archenteron forms a short stub-like gut rudiment (end of primary invagination). That form continues to be stretched becoming a slender archenteron closer to the animal pole

(secondary invagination). Secondary mesenchyme cells (SMCs) continuously delaminate from the tip of the archenteron, and they later extend thin branching filopodia (Fp) towards the animal pole (Ap).

**F- Fifth treatment (T5):** late gastrula to very early prism stage exposed. Once gastrulation is finished, some SMCs begin to differentiate into four types of non-skeletogenic mesodermal cells: pigment cells, blastocoelar cells, coelomic pouch cells and circum-esophageal muscles. Chromatogenic mesenchyme that has already entered the animal pole (Ap) becomes pigment cells (Pgc). They shift into two subpopulations: one moving toward vegetal plate in epidermis and the other ingressing into blastocoel (Bc). A third population is also detected in vegetal pole. Later on, mouth opening appears (stomodeum invagination), archenteron gets remolded and the gastrointestinal tract (Git) is regionalized (foregut, midgut, and hindgut).

**G- Sixth and last treatment (T6):** mid-to-late prism stage exposed. Organogenesis takes place quickly. Endoderm becomes even more subdivided by constrictions into a series of 4 main regions: coelomic pouches (Cp), oesophagus (Esp), stomach (Stc) and intestine (Int). Sphincters (Sphc) also appear through the gut. Additionally, spicules are bigger and give support to the growing body. Swimming behavior is related to the apical tuft at the foremost end of the larva and where apical organ (Apo) is supposed to be located.

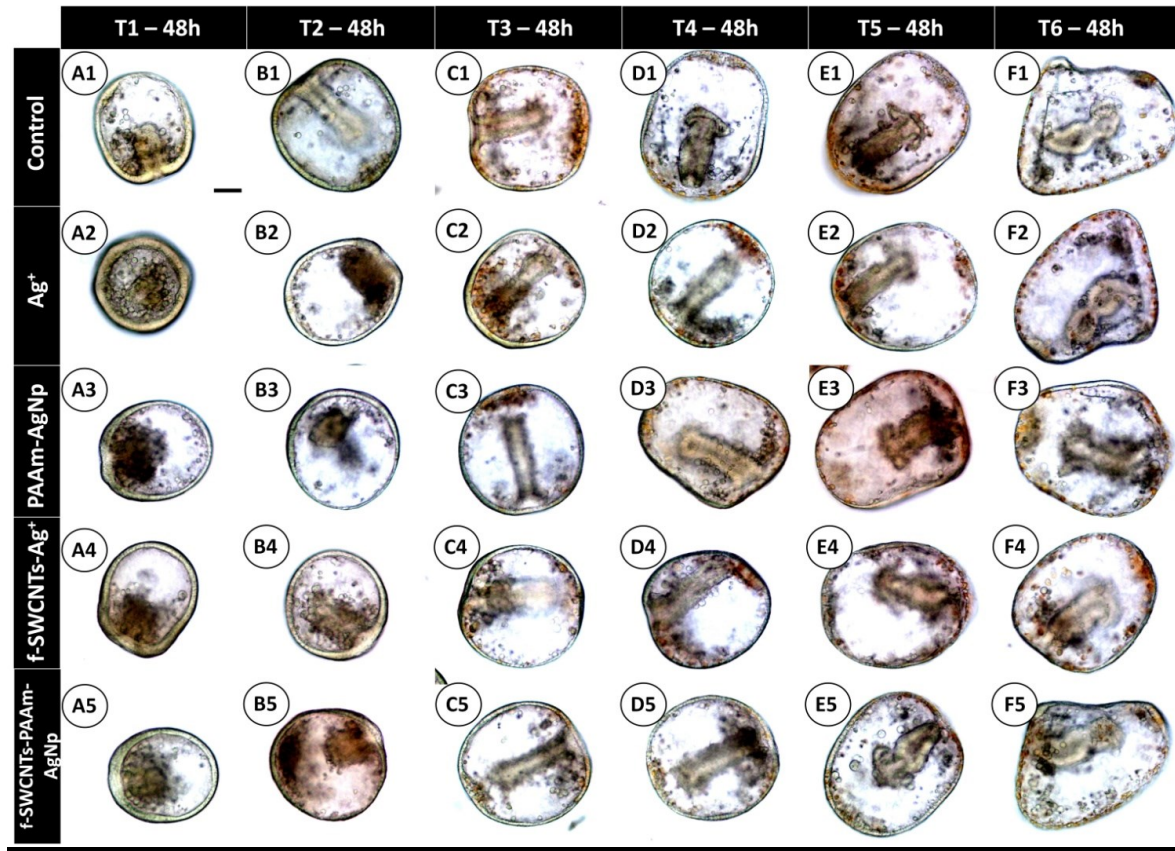


Figure A: General view of development stages of embryos and larvae in controls and under treatment using NC2 concentrations of  $\text{Ag}^+$ , PAAm- $\text{AgNp}$ s, f-SWCNTs+ $\text{Ag}^+$  and f-SWCNTs+PAAm- $\text{AgNp}$ s after 48h (20X, scale bar: 200 $\mu\text{m}$ ). Timing for treatments are on the top line, and contaminants are given on the left axis. Description of controls (A1-F1): A1: midgutula, B1: late gastrula to early prisma, C1: early-to-mid prisma, D1: mid-to-late prisma, E1: late prisma, F1: late prisma to early 2 arms-echinopluteus. Main observations in presence of contaminants at T1-48h (A2: arrested blastula, A3-A5: midgastrula); T2-48h (B2, B3: midgastrula; B4-B5: mid-to-late gastrula); T3-48h (C2-C5: mid-to-late gastrula); T4-48h (D2: late gastrula, D3: midprisma, D4, D5: early-to-mid prisma); T5-48h (E2, E4: atrophied prisma; E3, E5: late prisma) and T6-48h (F2-F5: atrophied late prisma to early 2-arms echinopluteus).

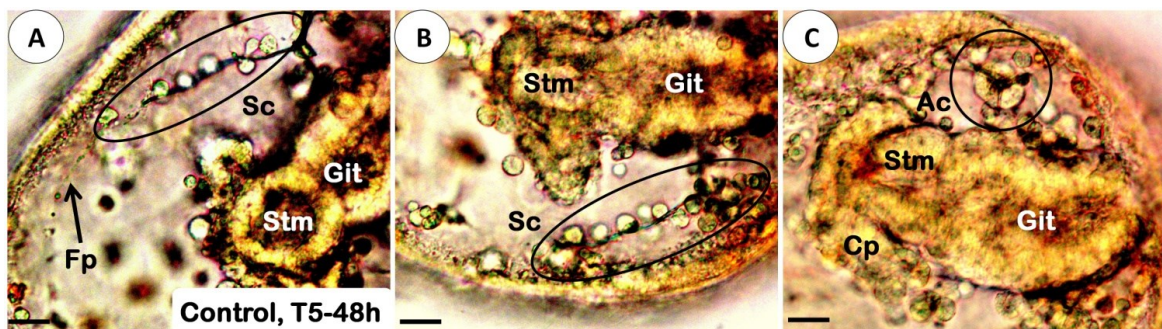


Figure B: Larvae at 48h of T5 (40X, scale bar 25 $\mu$ m). A- Controls showed advanced skeleton mineralization, well developed gastrointestinal tract and extended filopodia near blastocoel walls. B- Larvae contaminated with PAAm-AgNPs (NC2) were similar to the controls with ongoing mineralization, well organized skeletogenic cells and shaped gastrointestinal tract. C- f-SWCNTs+Ag<sup>+</sup> (NC2) larvae had small triradiate spicules held by abnormal clusters and delayed stomodeum invagination. Abbreviations- Ac: abnormal clusters, Cp: coelomic pouches, Fp: filopodia, Git: gastrointestinal tract, Sc: spiculogenic or skeletogenic cells, Stm: stomodeum.

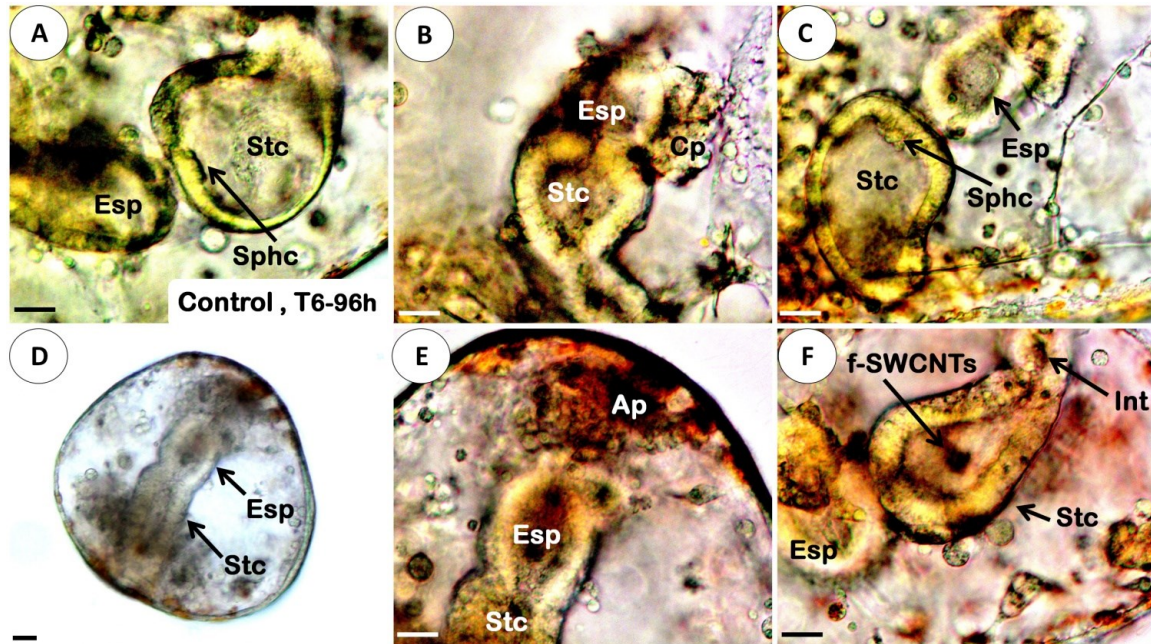


Figure C: Morphology of gastrointestinal tracts at 96h of T6, NC2 concentrations and control. A- Larvae from controls had large esophagus and expanded stomachs delimited by cardiac sphincter. B- Ag<sup>+</sup> larvae had reduced stomachs with thickened walls and no sphincter. C- PAAm-AgNps larvae showed a delayed development of gastrointestinal tract; stomach and esophagus were similar to the controls with cardiac sphincter present, but with stomach walls were thickened. D, E- Larvae contaminated with f-SWCNTs+Ag<sup>+</sup> got atrophied; gastrointestinal tract did not develop and became a hollow tube. F- Under f-SWCNTs+PAAm-AgNps stress, stomach was almost similar to PAAm-AgNps-treated larvae, but with highly thickened walls; bulks of f-SWCNTs are seem in stomach lumen. Abbreviations- Ap: animal pole, Cp : coelomic pouches, Esp : esophagus, Sphc : sphincter, Stc : stomach, Int : intestine. (A, B, C, E, F: 40X, scale bar 25μm; D: 20X, scale bar 200μm).

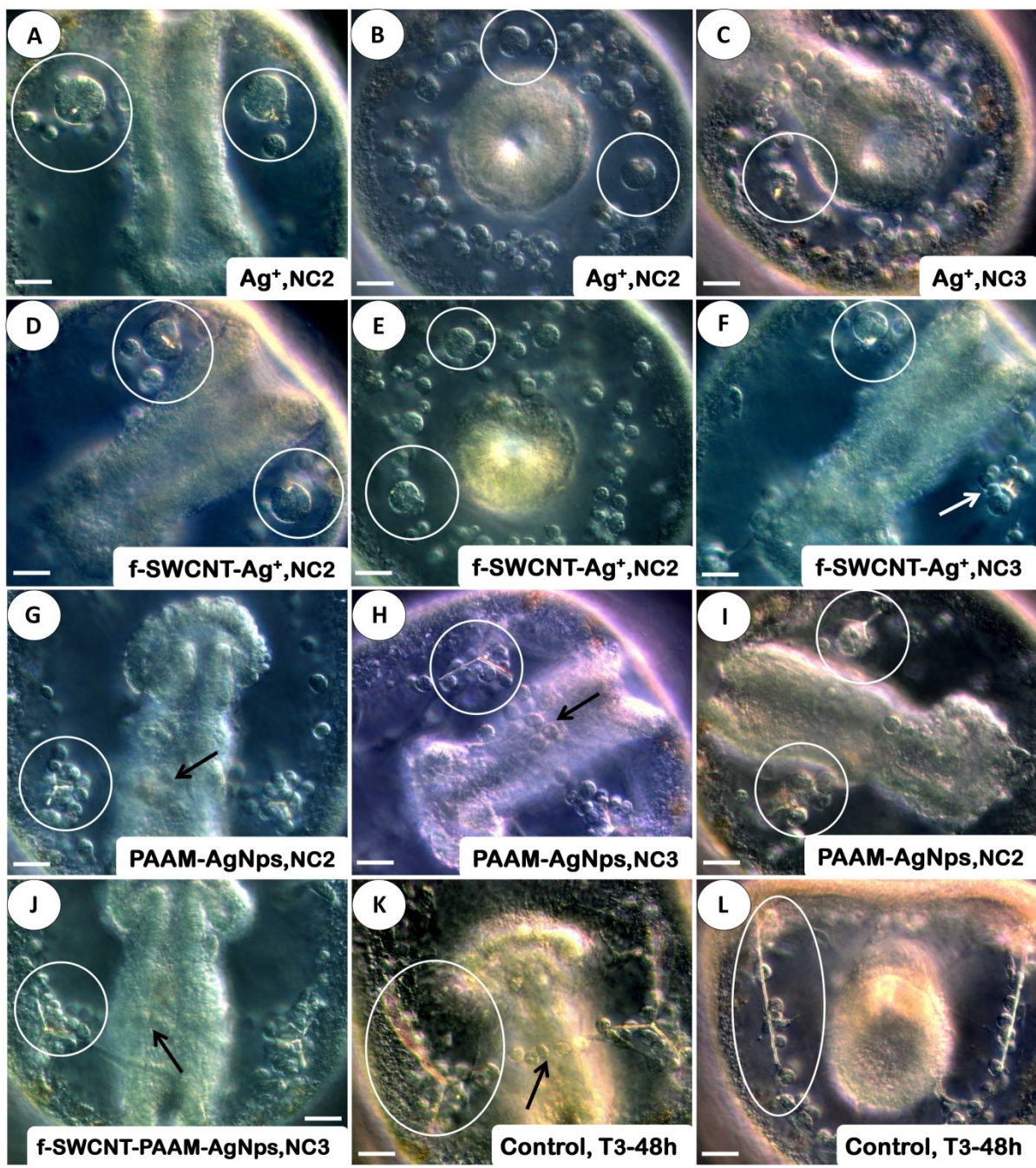


Figure D: Congregations of spiculogenic cells in ventro-lateral clusters (white circles) at 48h of third treatment T3 (A-H, J, K, L) and T4 (I), black arrows indicate syncytium ring formation (40X, scale bar 25μm). A- Lateral view of two amorphous clusters with small triradiate spicules contaminated with NC2 concentrations of Ag<sup>+</sup>, some separated cells were seem nearby. B- In

vegetal view, spiculogenic cells with abnormal clusters in  $\text{Ag}^+$  (NC2) conditions. C- With NC3 concentrations of  $\text{Ag}^+$ , few abnormal clusters were detected; and organization of the ring structure emerged. D- f-SWCNTs+ $\text{Ag}^+$  (NC2) also had the same effect observed in  $\text{Ag}^+$  (NC2) conditions, amorphic clusters also held small spicules near vegetal pole. E- f-SWCNTs+ $\text{Ag}^+$  (NC2)-treated larvae in vegetal view, amorphous clusters are indicated inside white circles. F- NC3 concentrations of f-SWCNTs- $\text{Ag}^+$  caused deformed agglomerations and inhibited mineralization; small associations of normal cells also came out (indicated by white arrow). G- Skeleton deposition less inhibited in PAAm-AgNps (NC2) exposures, spiculogenic cells did not fuse as observed in  $\text{Ag}^+$  or f-SWCNTs+ $\text{Ag}^+$  (NC2) conditions. H- Delay in mineralization was also detected in PAAm-AgNps (NC3) exposure. I- Comparatively, prisms contaminated with PAAm-AgNps (NC2) had no skeleton elongation at 48h of T4, syncytium ring was not visible. J- Pattern of skeleton deposition found in f-SWCNTs+PAAm-AgNps conditions was similar to the controls. K, L: Skeletogenic cells in controls elongated spicules from ventro-lateral positions of clusters inside the syncytium space.

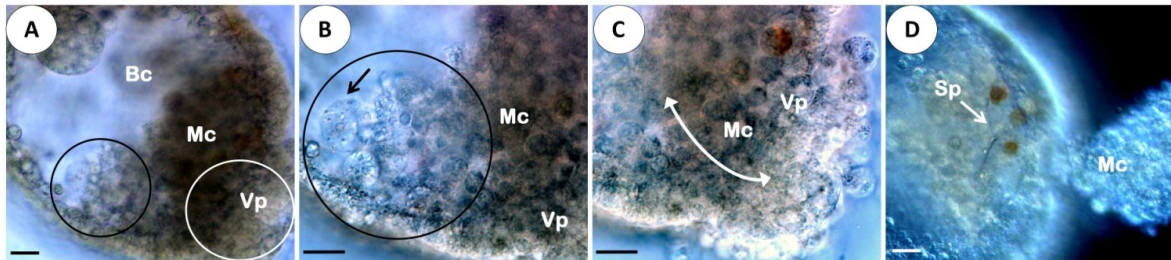


Figure E: A- Abnormal blastulae found during recovery period after  $\text{Ag}^+$  (NC2) exposure: some swelled mesenchyme cells (black circle) occupied the region near vegetal plate in blastocoel, while other cells got extruded (white circle). B- Swelled cells (black arrow inside black circle) showed little bright vesicles in cytoplasm. C- Mesenchyme cells getting squeezed from blastocoel (white circle indicated in detail of figure A). D- Extruded cells were sometimes connected to the vegetal plate as a tail. Abbreviations- Bc: blastocoel, Mc: mesenchyme cells, Sp: spicule, Vp: vegetal pole. (A, D: 40X, scale bar 25 $\mu\text{m}$ ; B, C: 63X, scale bar 15 $\mu\text{m}$ ).

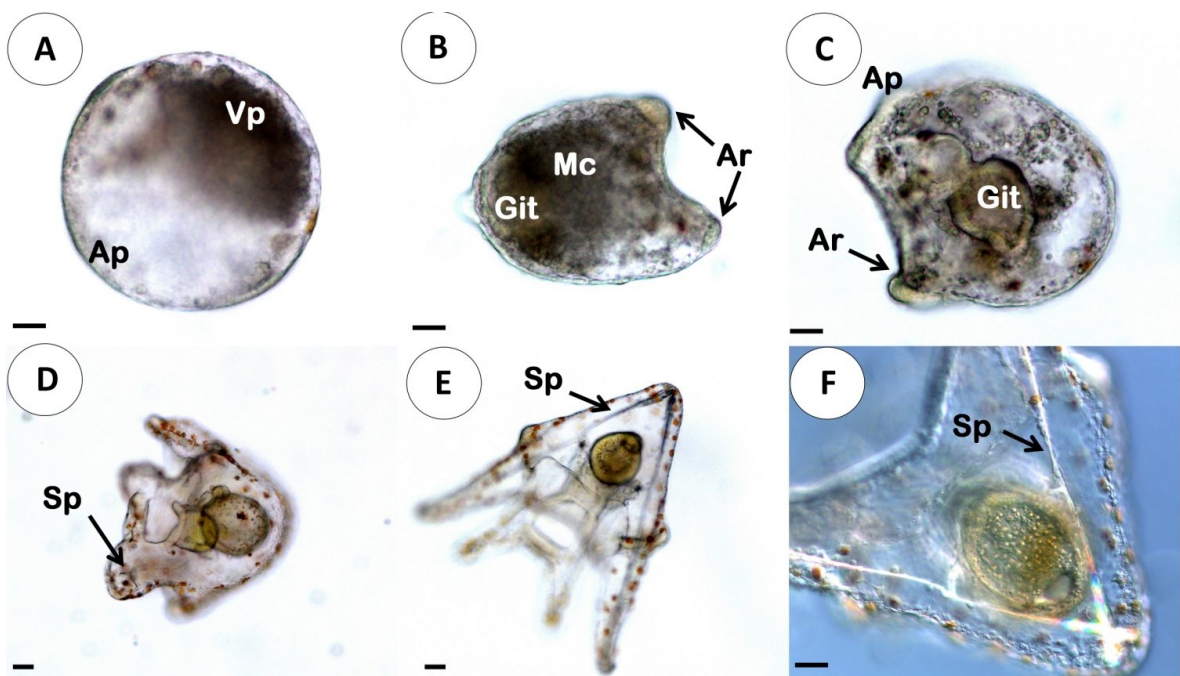


Figure F: Larvae and embryos found after recovery period. A- Arrested gastrula. B- Echinopluteus-type 1. C- Echinopluteus-type 2. D- Small echinopluteus. E- Normal echinopluteus. F- Control. Abbreviations: Ap – animal pole, Vp – vegetal pole, Git: gastrointestinal tract, Mc- mesenchyme cells, Ar- arm, Sp- spicule. (A-C, F: 20X, scale bar 200 $\mu$ m; D, E: 10X, scale bar 100 $\mu$ m).

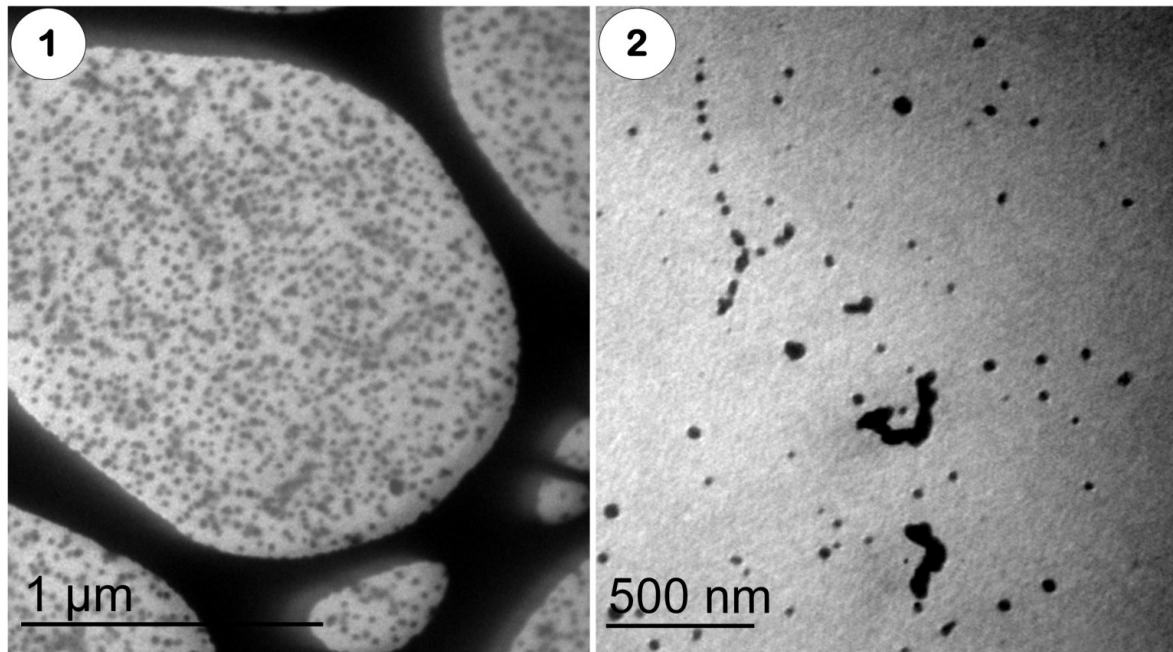
**APPENDICE 2: CHAPITRE 2**

Figure A: TEM images of PAAm-AgNPs from stock solution dispersed with ethanol 100% on lacey carbon grid (panel 1) as well as some aggregates that eventually appeared in seawater (panel 2).

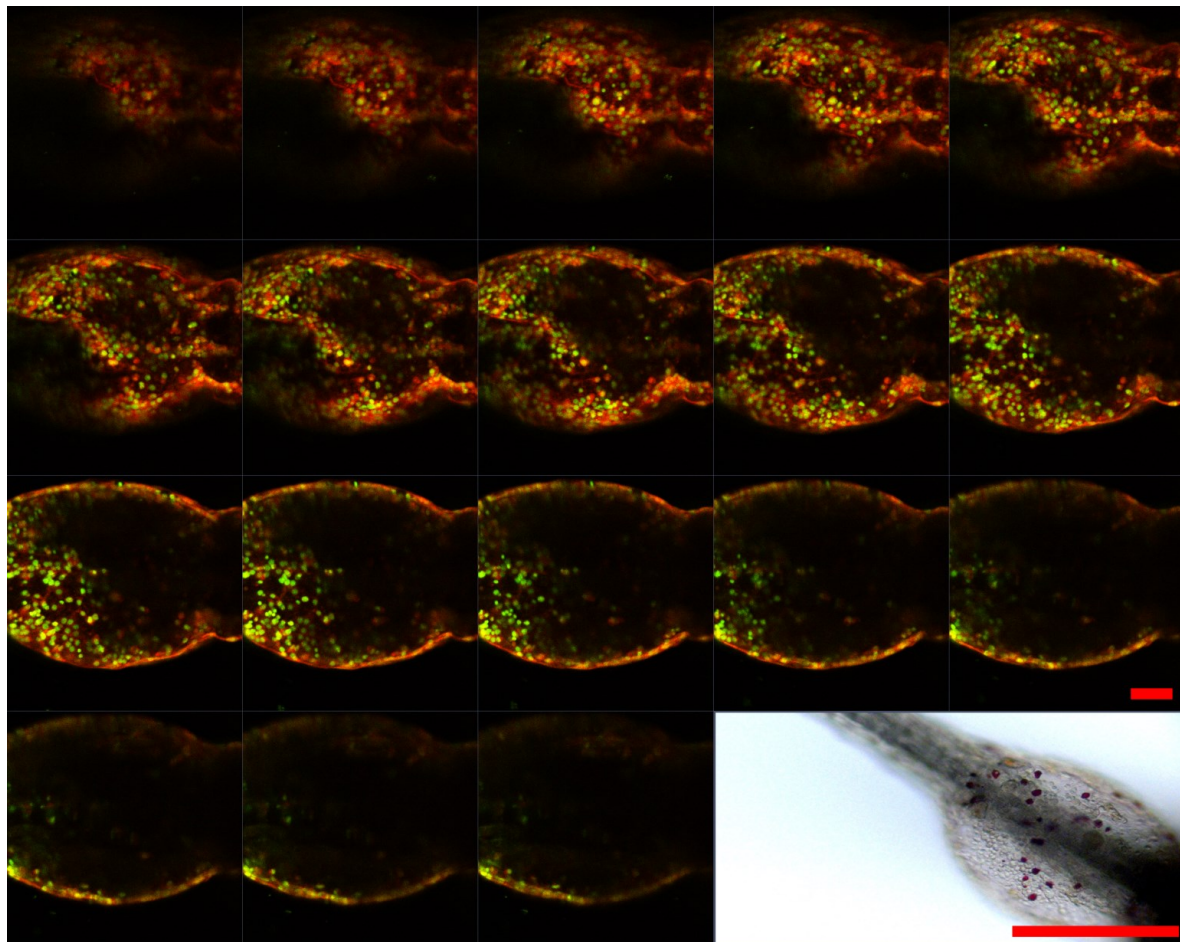


Figure B: Z-stack series of oedema in spine of sea urchin juveniles contaminated with  $\text{Ag}^+$  (NC2) in confocal microscopy *in vivo*. Nucleuses of cells are marked by SYBR Green dye (scale bars: 20  $\mu\text{m}$  in laser microscopy and 200  $\mu\text{m}$  in light microscopy). At least two cell types were mobilized towards oedemic areas (see text for more details).

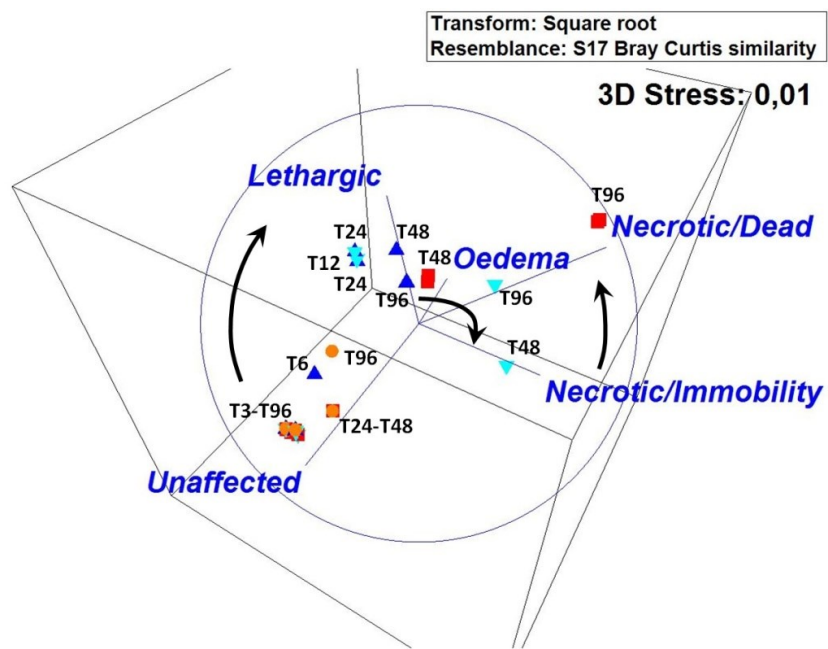


Figure C: MDS plot with Bray-Curtis similarity (PERMANOVA) analysis of physiological conditions of endotrophic forms (postlarvae) and exotrophic juveniles (not fed) contaminated with  $\text{Ag}^+$  (NC2) and PAAm-AgNPs (NC2) (3D stress: 0.01). Black arrows indicate progression of juvenile's conditions within 96h. Corresponding labels are shown as follows: postlarvae-  $\text{Ag}^+$  (NC2) (■), PAAm-AgNPs (NC2) (●); juveniles -  $\text{Ag}^+$  (NC2) (▼), PAAm-AgNPs (NC2) (▲).

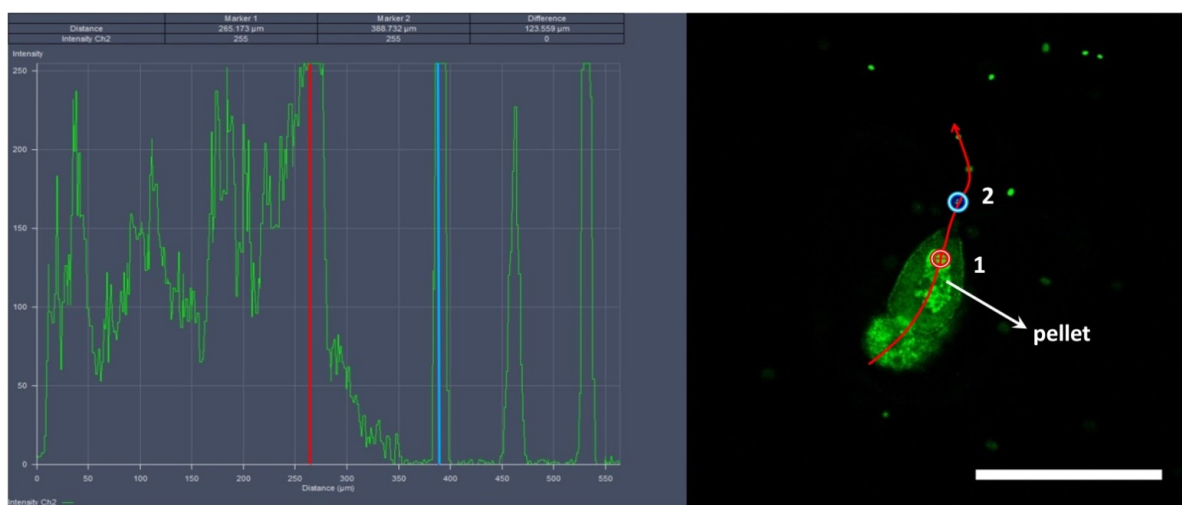


Figure D: Profile view of levels of fluorescence signal emitted by PAAm-AgNps-FITC in L8<sub>1</sub> echinopluteus larva feeding on phytoplankton at 6h *in vivo* (10X, scale bar: 200 $\mu\text{m}$ ); waste material (pellet) is seen inside hindgut. Red market (1) indicates undigested phytoplankton debris, blue market (2) swimming phytoplankton cell. Intensity of signal is given on y axis, distance (in  $\mu\text{m}$ ) is on x axis. From arrow nock to marker 1, distance was 265.173  $\mu\text{m}$  while for marker 2 it was about 388.732  $\mu\text{m}$ . Difference between both markers was 123.559  $\mu\text{m}$ .

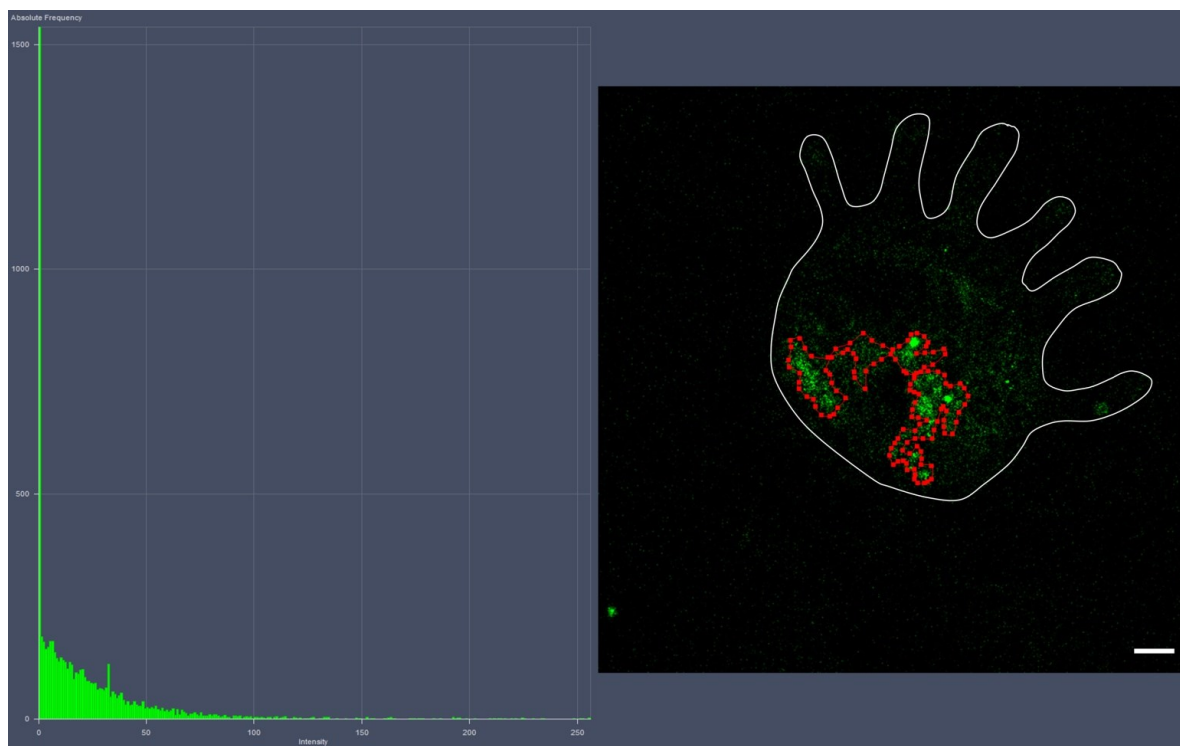


Figure E: Histogram view of levels of fluorescence signal emitted by PAAm-AgNps-FITC in postlarvae *in vivo* (2 x 96h) (20X, scale bar: 50 $\mu$ m). Intensity of signal of area limited by red squares is given on x axis, absolute frequency is on y axis. Area selected in red corresponds to remaining tissues of larval gut still being incorporated to aboral surface of postlarval body

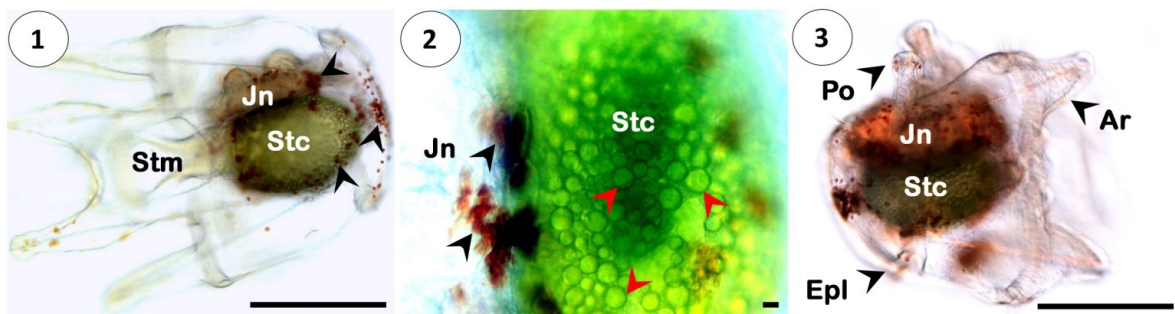


Figure F: (1) Early L8<sub>1</sub> swimming larvae: pigment cells clusters are indicated by black arrowheads. (2) Lipidic vesicles stored in stomach (red arrowheads), and pigment cells clusters in detail (black arrowheads). (3) Early L8<sub>2</sub> (competent larva): rudiment occupied large space of blastocoel. Abbreviations- Ar: arm, Epl: epaulettes, Jn: rudiment of juvenile, Po: podia, Stc: stomach, Stm: stomodeum (opening mouth). (A, C: 10X, scale bar 200  $\mu$ m; B: 40X, scale bar 25  $\mu$ m).

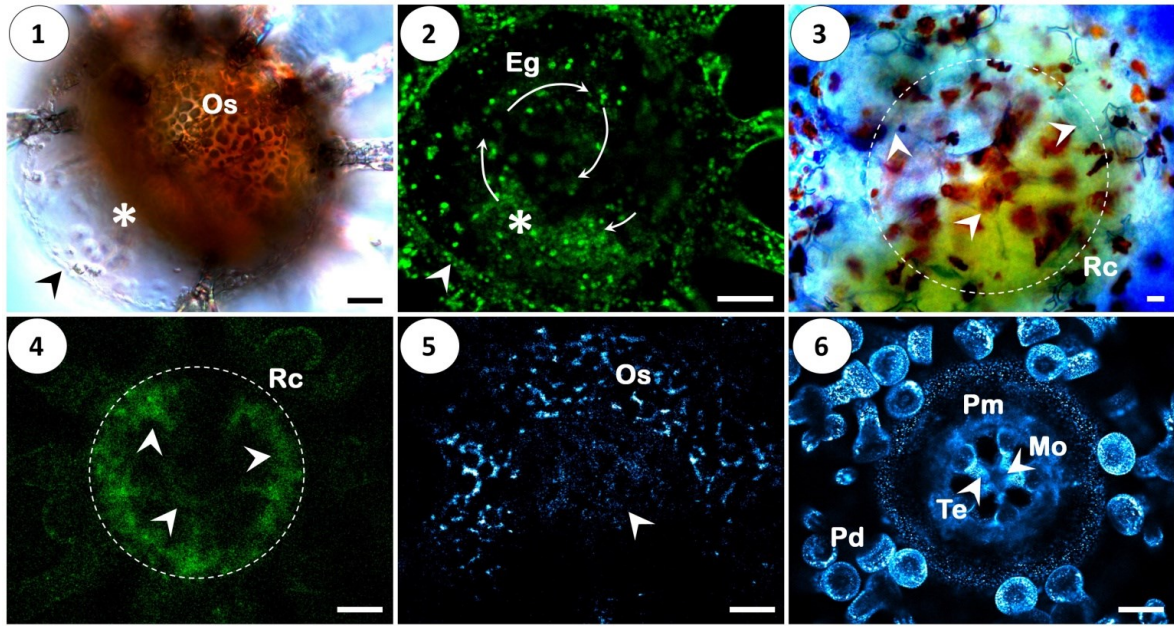


Figure G: Uptake of PAAm-AgNPs-FITC and Qdots 525 by late postlarvae to early juvenile stage and exotrophic juveniles *in vivo*. (1, 2) Late postlarvae to early juvenile stage in aboral view at 96h: PAAm-AgNPs high signal came from cells of endocyclic gut in formation (white asterisk), abactinal surface had no skeleton plates by this time. (3, 4) Oral view of late postlarvae at 24h in light (3) and laser microscopy (4): circum-oral ring canal and radial canals of water vascular system emitted high signal in a Z-stack frame (delimited by dashed lines), white arrowheads indicate corresponding areas in both figures. (5) Skeleton plates were strongly marked by Qdots 525 at 96h, a weak signal came out from inner soft tissues as well (white arrow). (6) Outer surfaces of juveniles emitted strong fluorescence of Qdots 525 in soft tissues as podia, peristomial membrane and hard structures (teeth). Abbreviations: Eg: endocyclic gut, Mo: mouth, Os: ossicles, Pd= podia, Pm: peristomial membrane, Rc: ring canal system, Te: teeth. (1): 20X, scale bar: 50  $\mu$ m and (3): 40X, scale bar 25  $\mu$ m in light microscopy. (2): 20X, scale bar: 50  $\mu$ m and (4-6): 20X, scale bar: 50  $\mu$ m in laser microscopy).

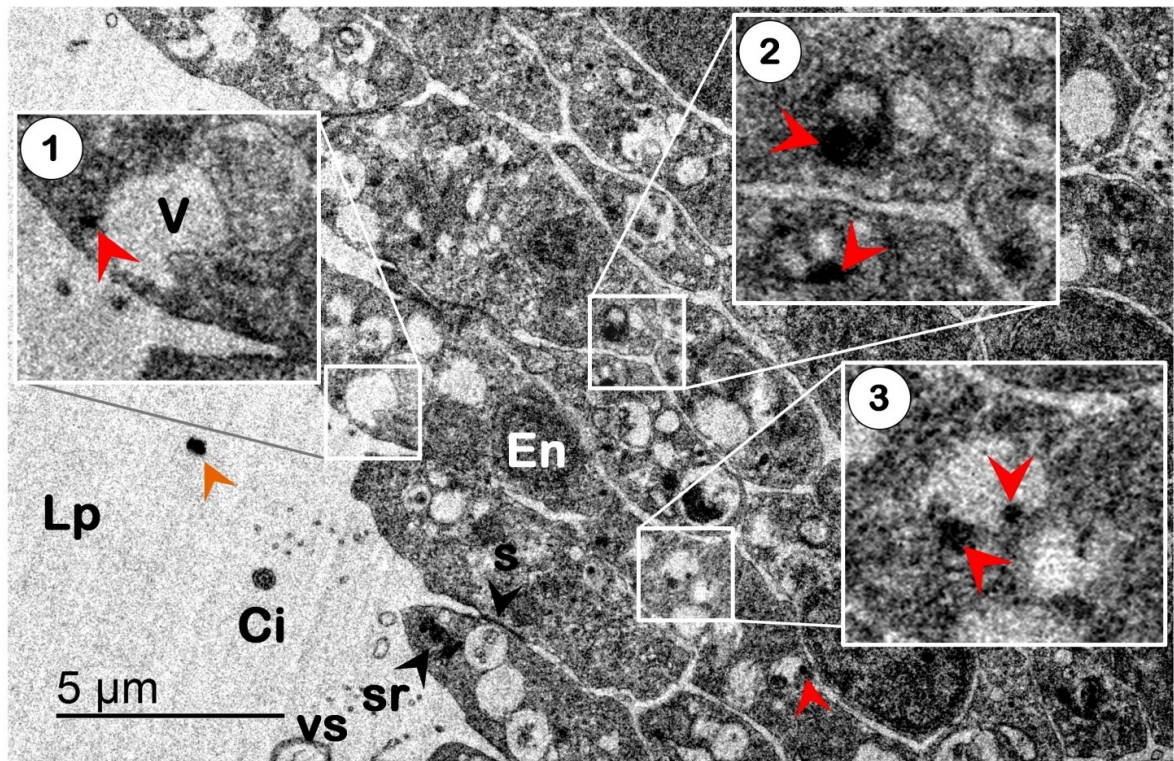


Figure H: Proctodaeum epithelium with small silver aggregates (1, 3) and bigger ones (2, 3) attached to cytoplasmatic vesicles/vacuoles (red arrowheads); orange arrowhead indicates nanosilver dispersed in lumen (non contrasted sample). Abbreviations- Ci: cilium, En: enterocyte, Lp: lumen of proctodaeum, s: septate junctions, Sr: striated rootlet, V: vacuole, vs: vesicle.

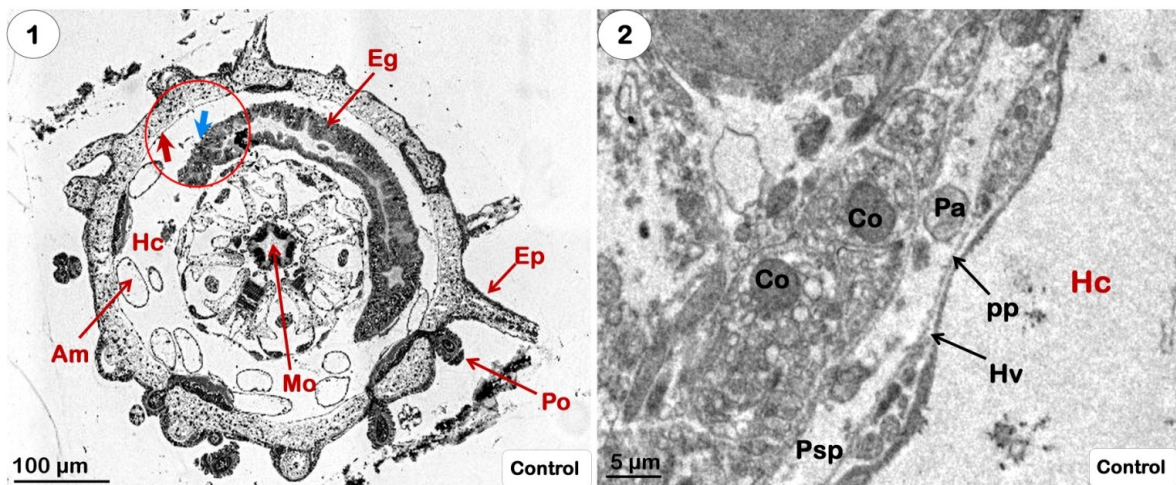


Figure I: Internal morphology of sea urchin juvenile 1-month old. (1) Scanned general view of uncontaminated juvenile in transverse plan. Selected area in red corresponds to peritoneal coelom (thick red arrow), and epigastric coelom (thick blue arrow). (2) Parietal mesothelium of uncontaminated animal (non-contrasted sample). Abbreviations: Am: ampulla, Co: constitutive cells, Eg: endocyclic gut, Ep: epidermis, Hc: hypogastric coelom, pp: parietal peritoneum, Mo: mouth, Pa: phagocytes, Po: podia.

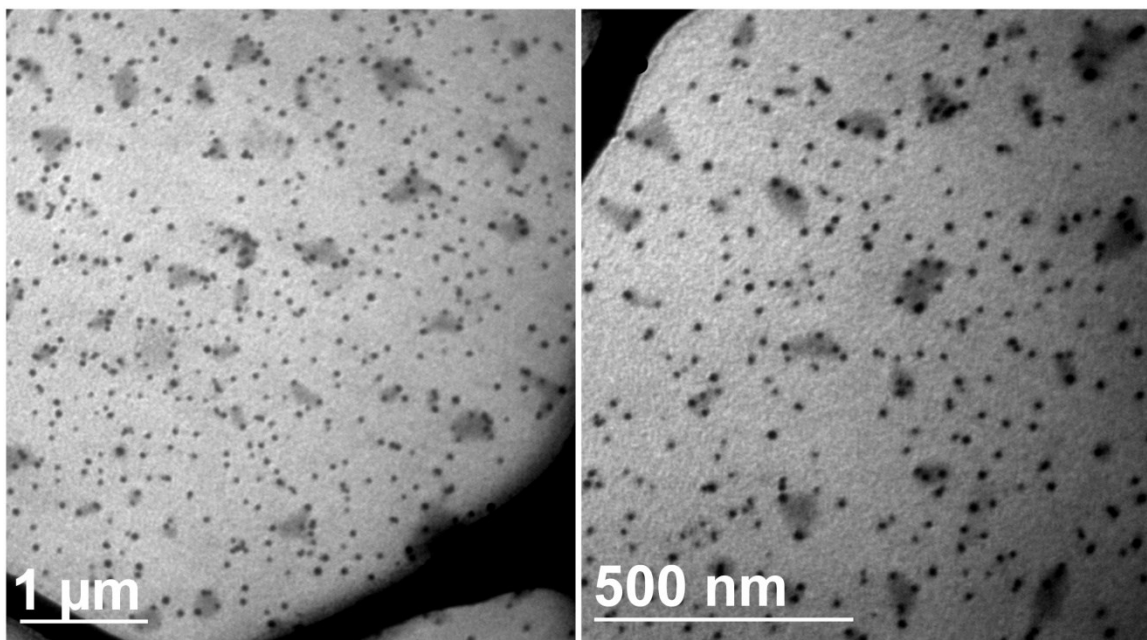
**APPENDICE 3: CHAPITRE 3**

Figure A: TEM images of organic-coated silver nanoparticles dispersed in ethyl alcohol 100%. Organic polymer (PAAm) is identified as dense areas around some AgNPs.

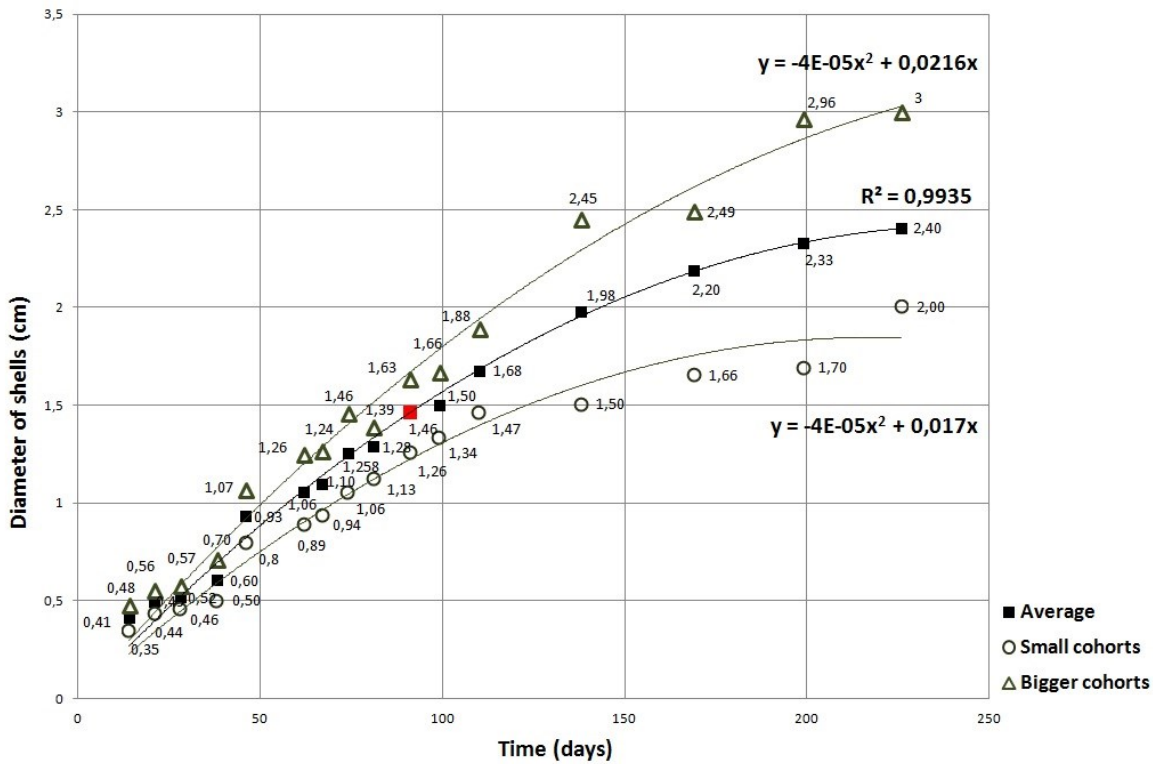


Figure B: Juvenile growth from 7<sup>th</sup> day after settlement to 8 months in laboratory conditions at 8°C. Smaller cohorts are shown by green circles and larger ones by green triangles. Average in size for each time is given by black squares. Red square represents 3-month old urchins. Each point had 40 measurements in average. At 3<sup>th</sup> month, cohort 1 ranged from 1 cm to 1.44 cm (average 1.26 cm), and cohort 2 from 1.48 to 2 cm (average 1.63 cm). At 11<sup>th</sup> day, individuals with more than 0.52 cm showed well developed gut. At 1<sup>st</sup> month, red spherulocytes population increased on shells compared to settlers. As far as time goes, a growing population of red spherulocytes tends to occupy surface of shells especially in larger urchins. Yet, even among large ones red spherulocyte pool may strongly differ.

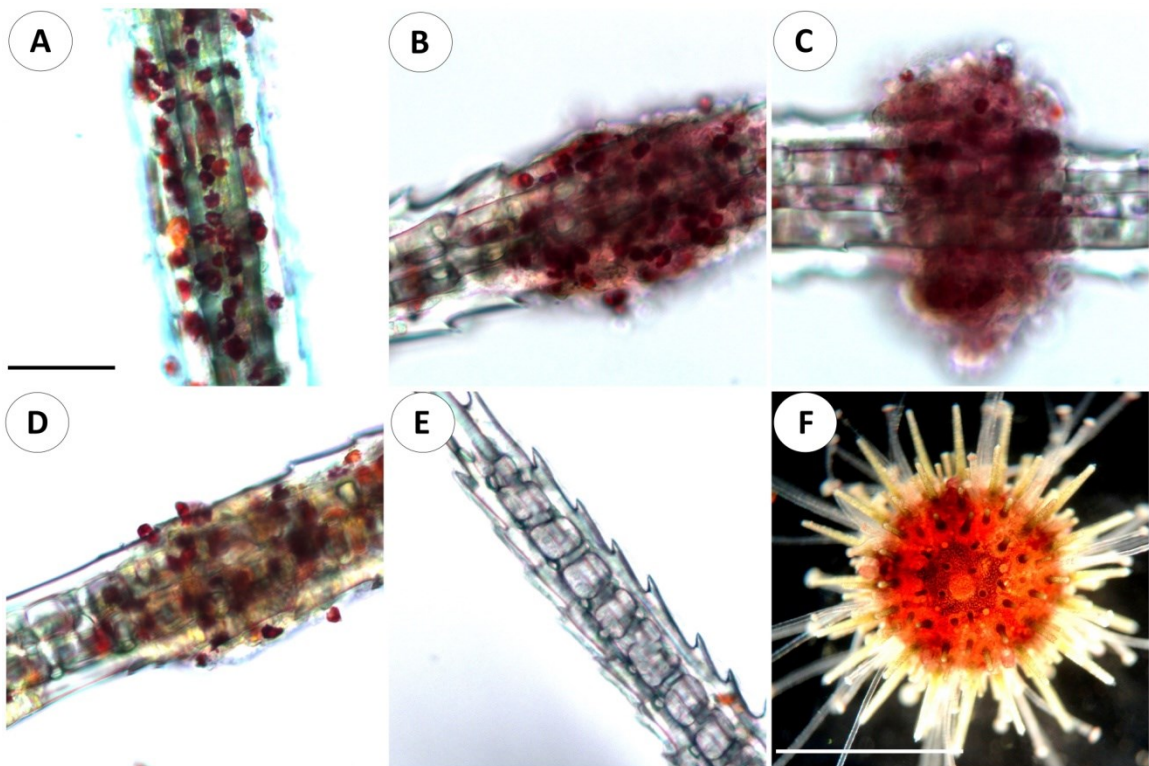


Figure C: Migrations of sea urchin immune cells towards chemically injured areas during silver exposure ( $100 \mu\text{g L}^{-1}$ ) - A: Induction state. B: Mobilization state. C: Agglomeration state. D: Necrotic state. Uncontaminated urchins – E: Apical part of normal spine with one red spherule cell on the bottom. F: 3-month old juvenile from rearing cultures. (A-E: 10X, scale bar: 50  $\mu\text{m}$  in light microscopy; F: 25X, scale bar: 2.5 cm in stereomicroscope).

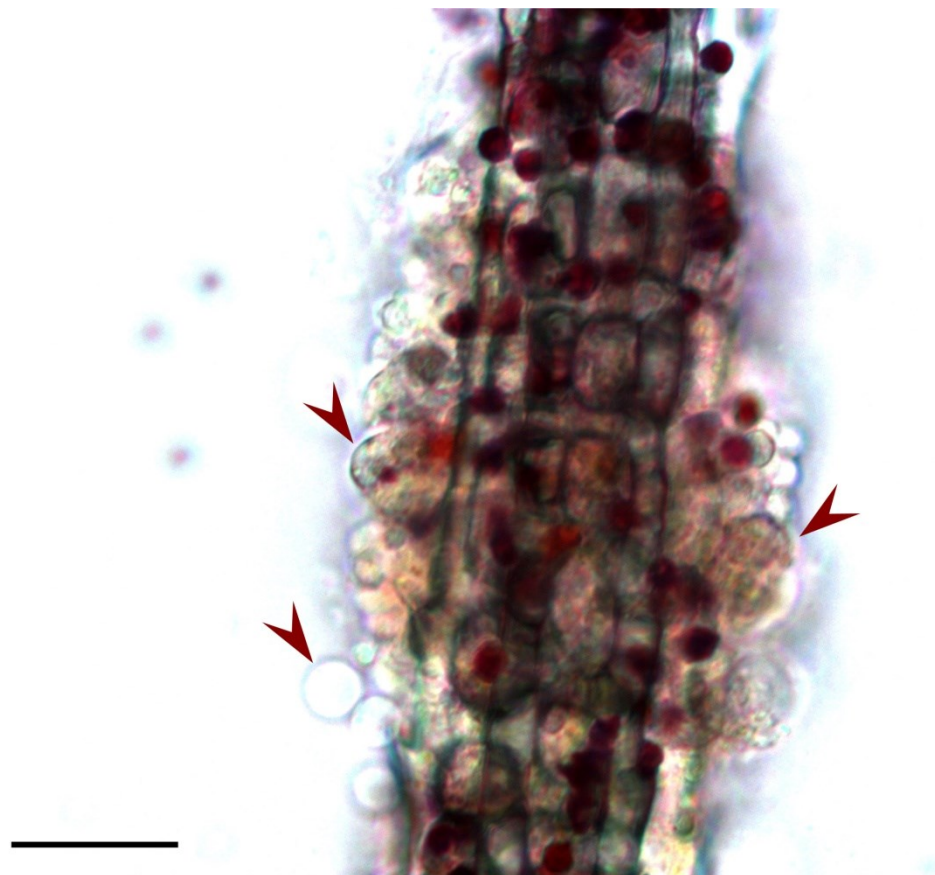


Figure D: Spines of 3 month-old sea urchins under  $\text{Ag}^+$  chronic exposure ( $100 \mu\text{g L}$ ): Some swollen cells chemically affected by silver are indicated by dark red arrowheads (288h). (A: 10X, scale bar:  $50 \mu\text{m}$  in light microscopy).

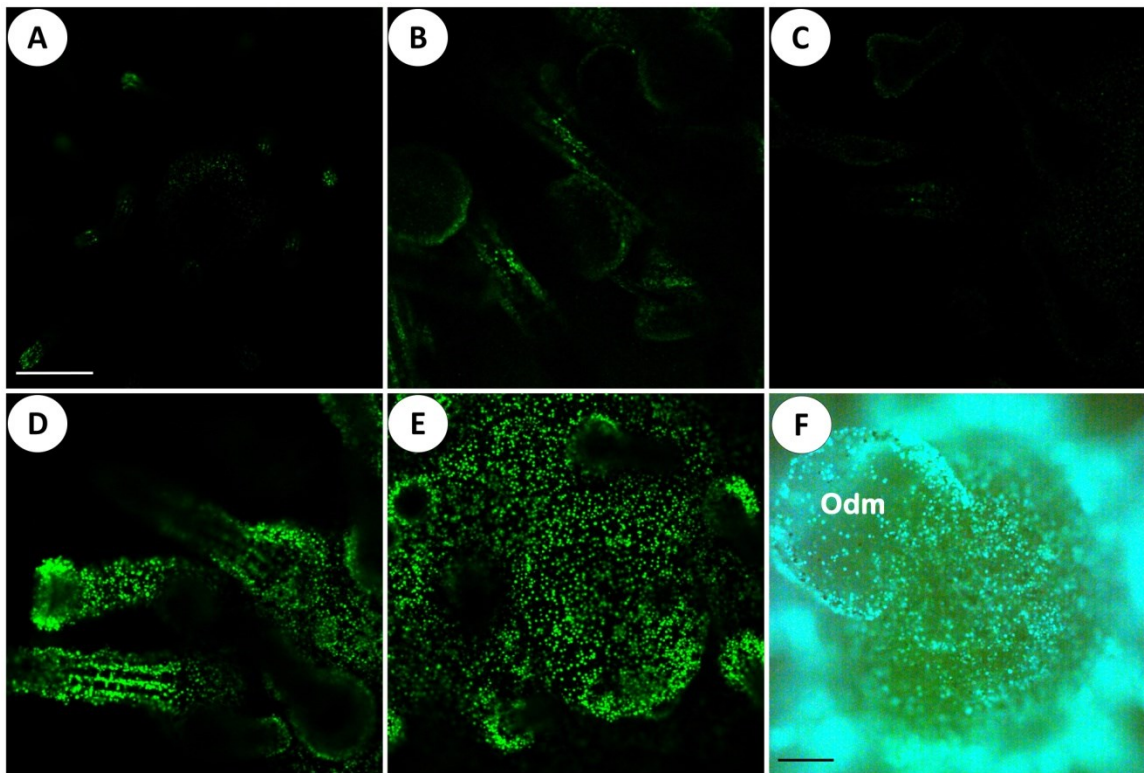


Figure E: Detection of reactive oxygen species (ROS) in juveniles of sea urchins aged of 3 months with confocal microscopy. A- Small specimen from rearing cultures (cohort 5). B- Large specimen from rearing cultures (cohort 6). C- Fed urchin from test-controls at 96h (cohort 6). D- Unfed urchin from test-controls showing oxidative stress on spines and podia. E- Same organism observed in (D), with abactinal region showing strong oxidative stress. F- Small specimen (in oedemic state) previously exposed to PAAm-AgNPs (100 µg/L) and exhibiting ROS production at 96h. Abbreviation: Odm- oedema. (A-E: 10X, scale bar: 50 µm in laser microscopy; F: 10X, scale bar: 50 µm in confocal epifluorescence).

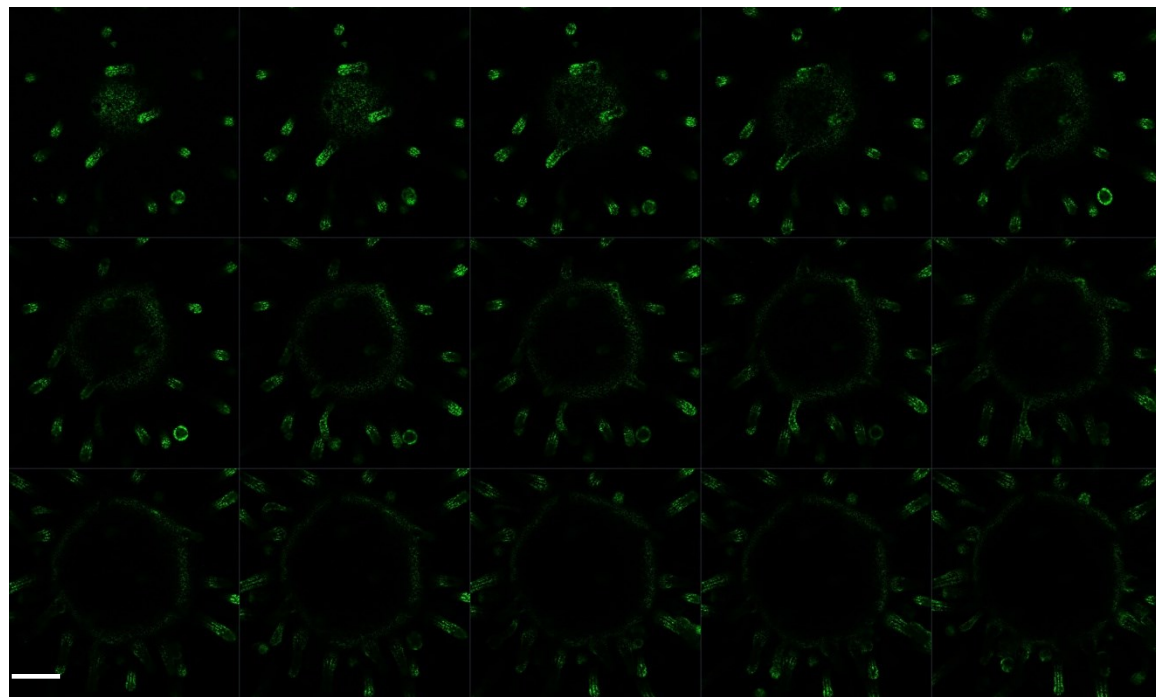


Figure F: Z-stack optical sequences in laser microscopy of an unfed sea urchin (cohort 6) exposed to PAAm-AgNPs (100 µg/L) showing moderate ROS production on the shell. (10X, scale bar: 50 µm).

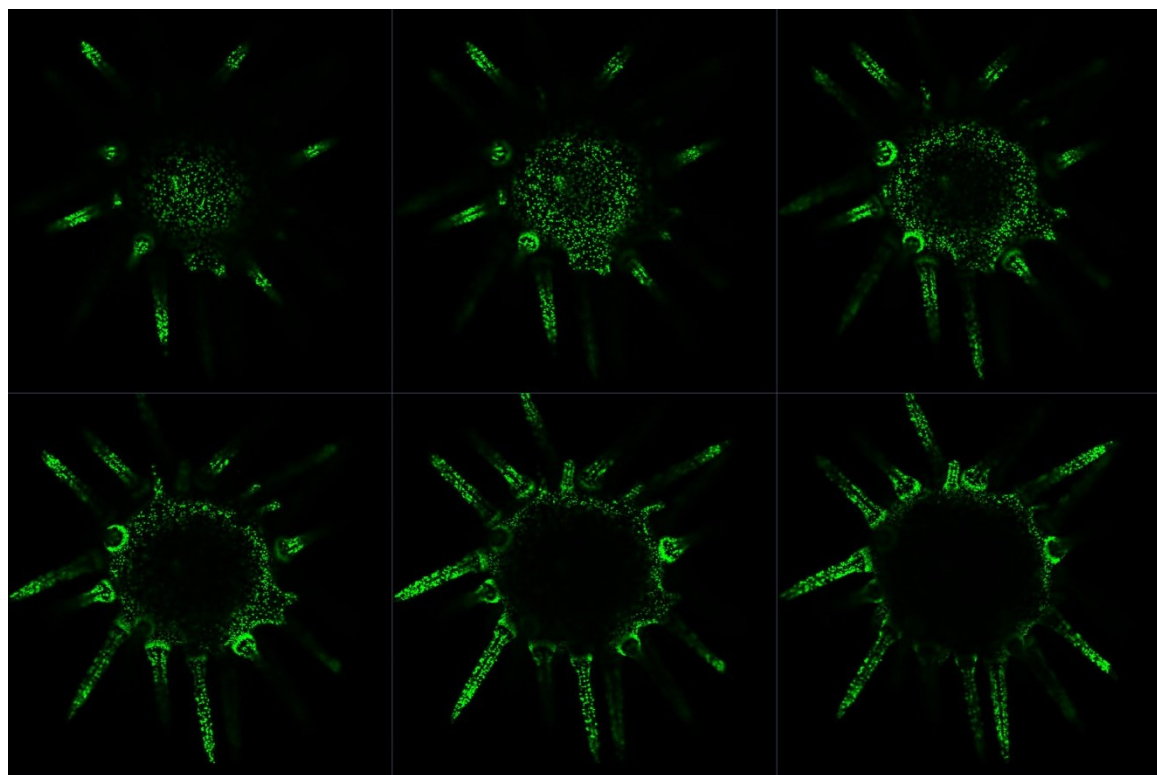


Figure G: Z-stack optical sequences in laser microscopy of unfed sea urchin (cohort 5) exposed to PAAm-AgNPs ( $20 \mu\text{g L}^{-1}$ ) showing strong ROS production on the shell. (10X, scale bar:  $50 \mu\text{m}$ ).

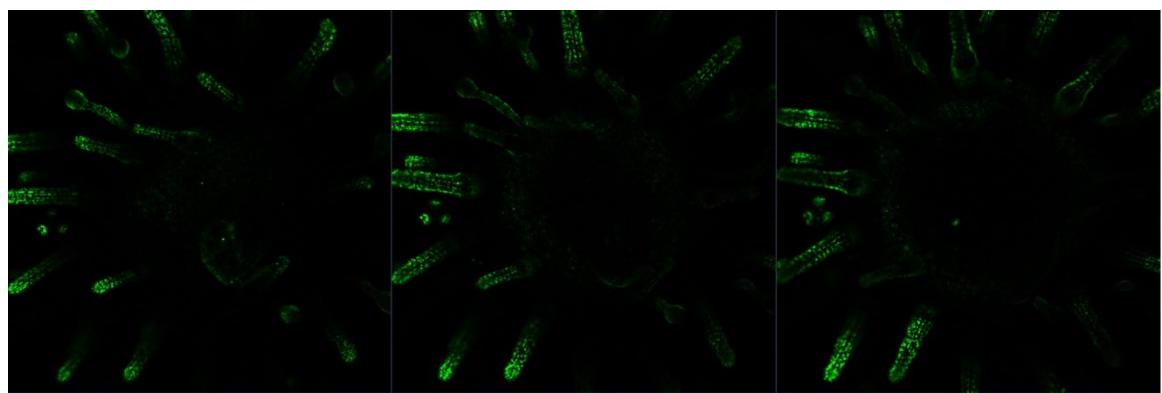


Figure H: Z-stack optical sequences in laser microscopy of an unfed sea urchin (cohort 6) exposed to  $\text{Ag}^+$  ( $100 \mu\text{g L}^{-1}$ ) showing moderate ROS production on the shell. (10X, scale bar:  $50 \mu\text{m}$ ).

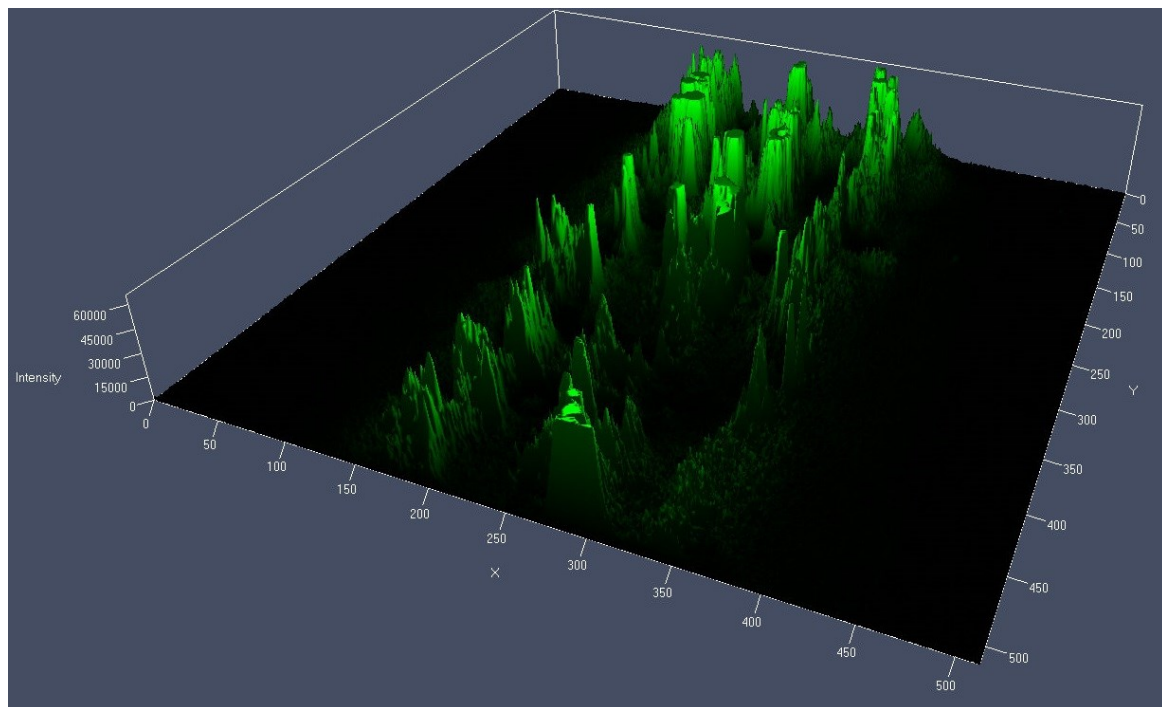


Figure I: 3D laser scanning of immune cells (amoebocytes) in induced state (12-24h) on sea urchin spine after  $\text{Ag}^+$ /100  $\mu\text{g/L}$  acute exposures (confocal microscopy). Few amoebocyte-type cells were detected inside injured area (on the top).

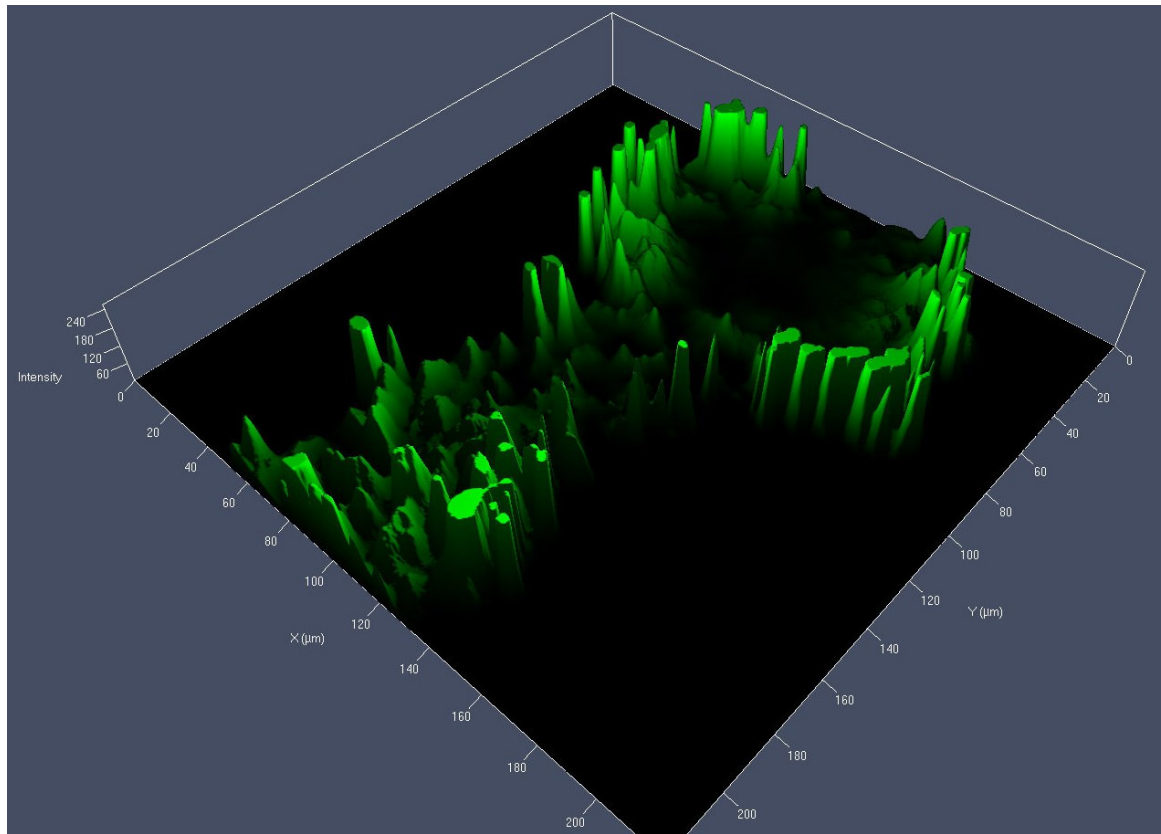


Figure J: 3D laser scanning of immune cells (amoebocytes) in agglomeration state (48-72h) on sea urchin spine after  $\text{Ag}^+/100 \mu\text{g/L}$  acute exposures (confocal microscopy). No cells were detected inside tumefied area (on the top).

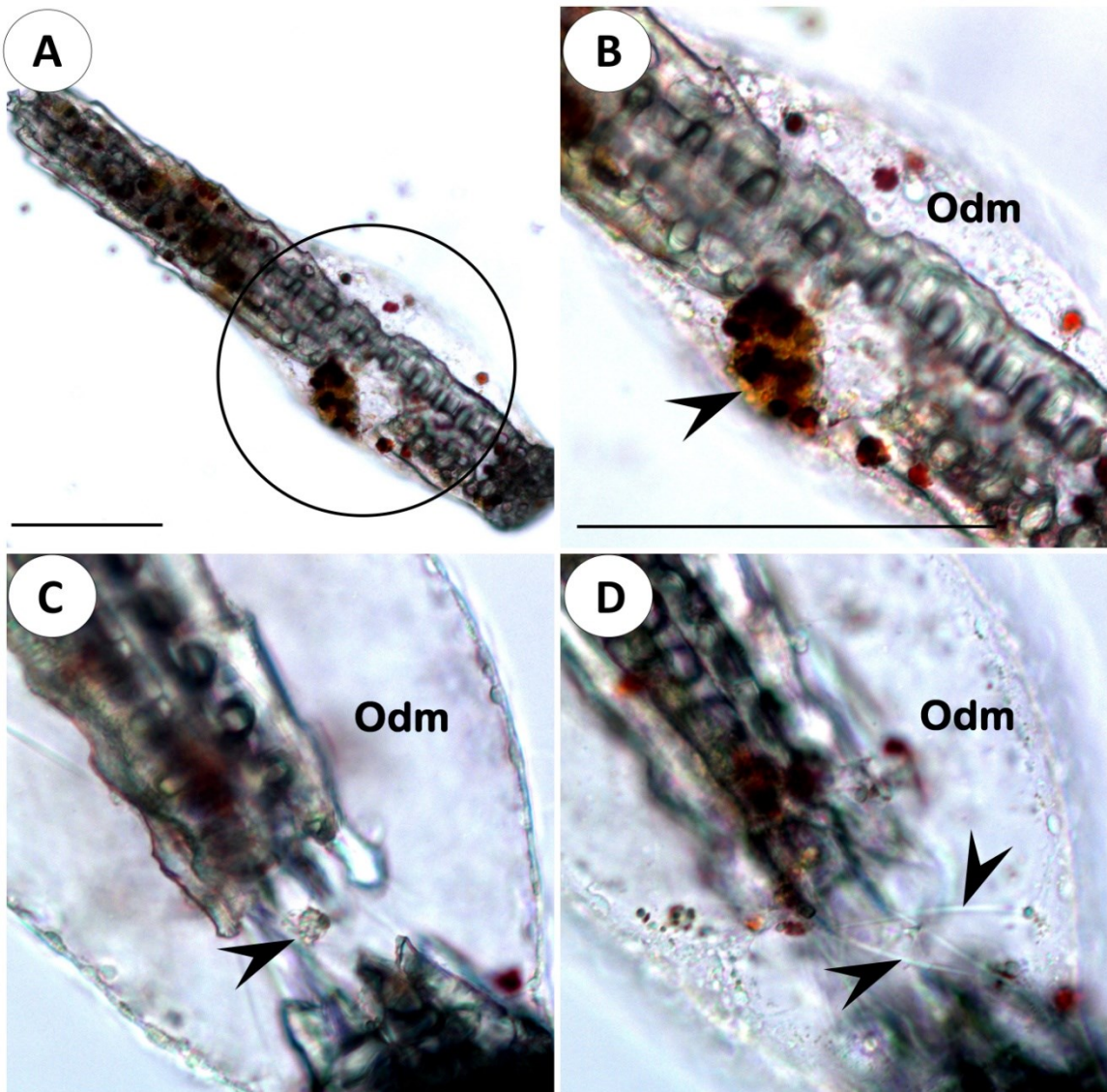


Figure K: Cooperation of amoebocyte-type cells and red spherule cells in healing processes in cohort 6 during recovery. A, B: Oedema post-chemical stress with a group of spherule cells close to a damaged area. C, D: Filopodial extensions of amoebocyte cells connected to oedema walls and skeleton; the presence of red spherule cells suggests interactions between both during regeneration processes. (A: 10X, scale bar: 50  $\mu$ m; B-D: 40X, scale bar: 50  $\mu$ m in light microscopy).

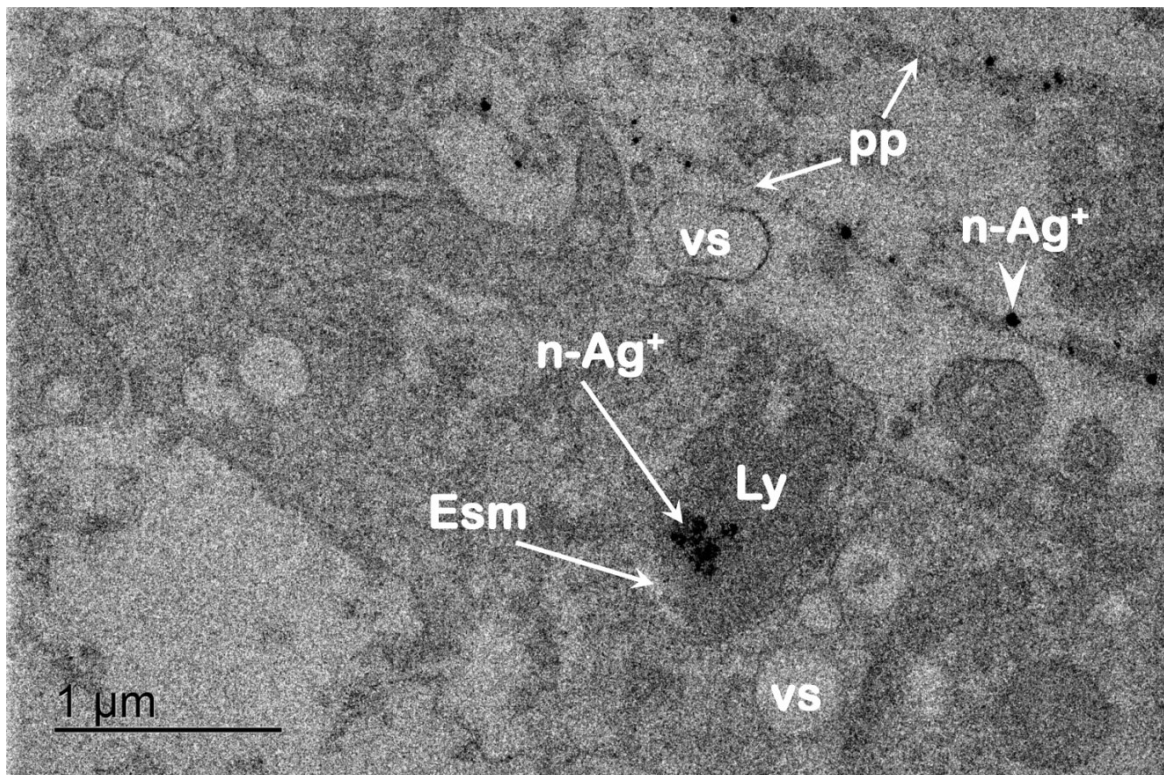


Figure L: TEM photomicrograph of nanoAg internalization by a peritoneocyte cell (non-phagocytic pathway) (non-contrasted sample). The same cell is indicated in Figure 9 (mechanism 2). Abbreviations- Esm: endosome, Ly: lysosome, n-Ag<sup>+</sup>: nanosilver, pp: parietal peritoneum, vs: vesicle. More AgNPs can be observed in mesenteries.

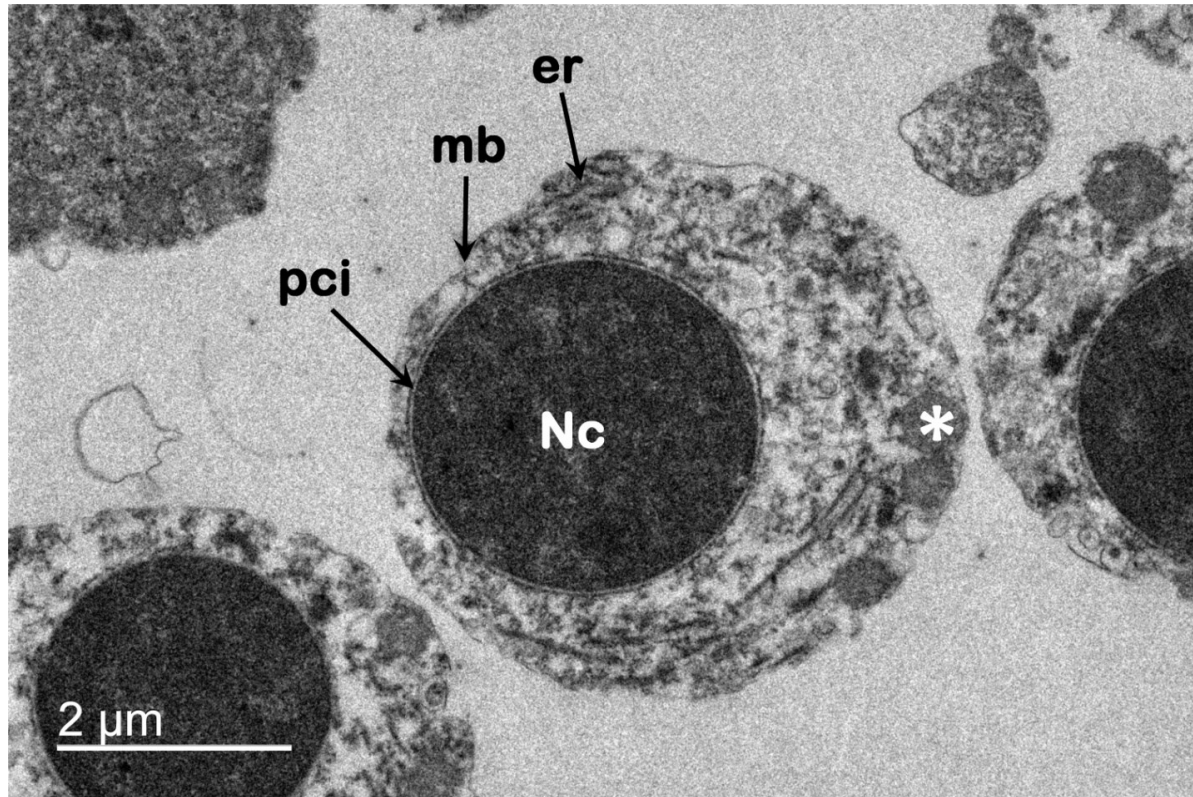


Figure M: TEM photomicrograph with coelomocytes from non-contaminated sea urchin (non-contrasted sample). No abnormality in cell morphology was detected. Abbreviations- er: endoplasmatic reticulum, Esm: endosome, mb: cell membrane, Nc: nucleus, pci: perinuclear cisternae. White asterisk indicate a lysosome.

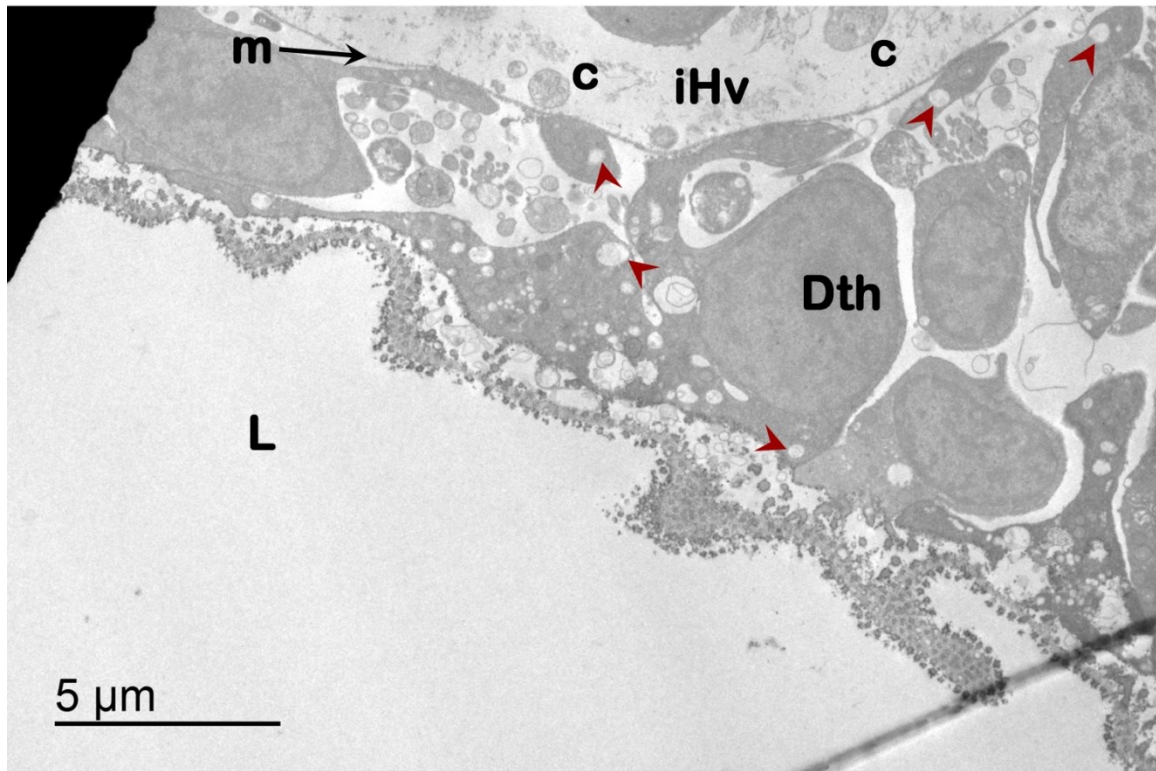


Figure N: TEM photomicrograph of digestive epithelium and internal haemal vessel from non-contaminated sea urchin (non-contrasted sample). Dark red arrowheads indicate clean vacuoles (without nanosilver). Abbreviations- c: coelomocyte, Dth: digestive epithelium, iHv: internal haemal vessel, L: lumen, m: mesentery.

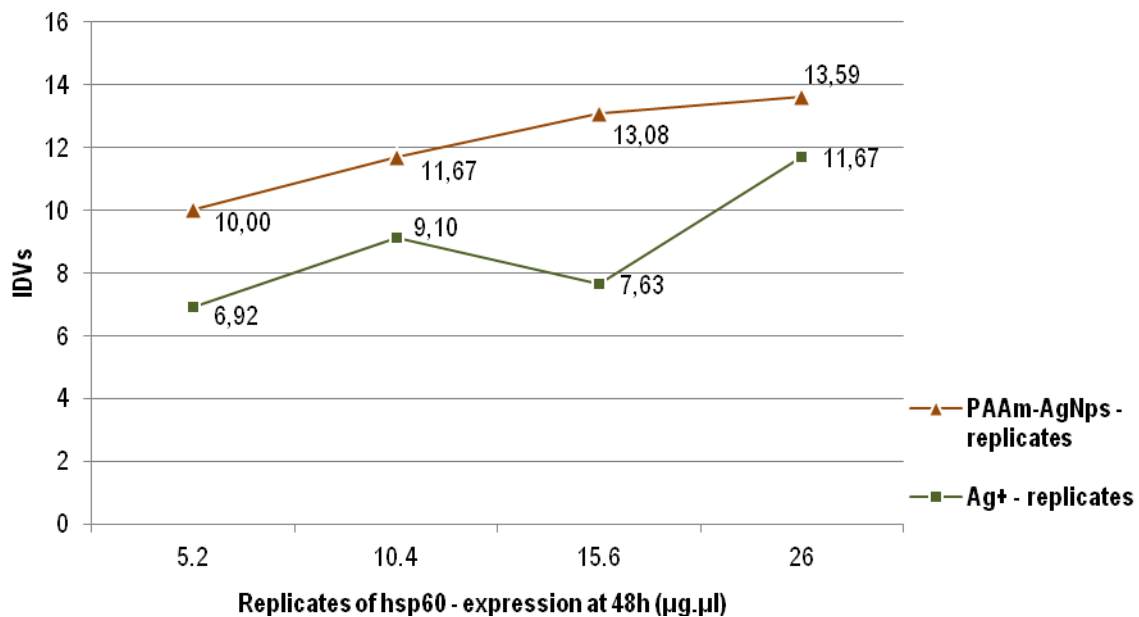


Figure O: Replicates of hsp60 expression at 48h for Ag<sup>+</sup> and PAAm-AgNPs treatments with different amounts of proteins probed at the same membrane ( $\mu\text{g}\cdot\mu\text{l}$ ) ( $p = 0.0242$ ).

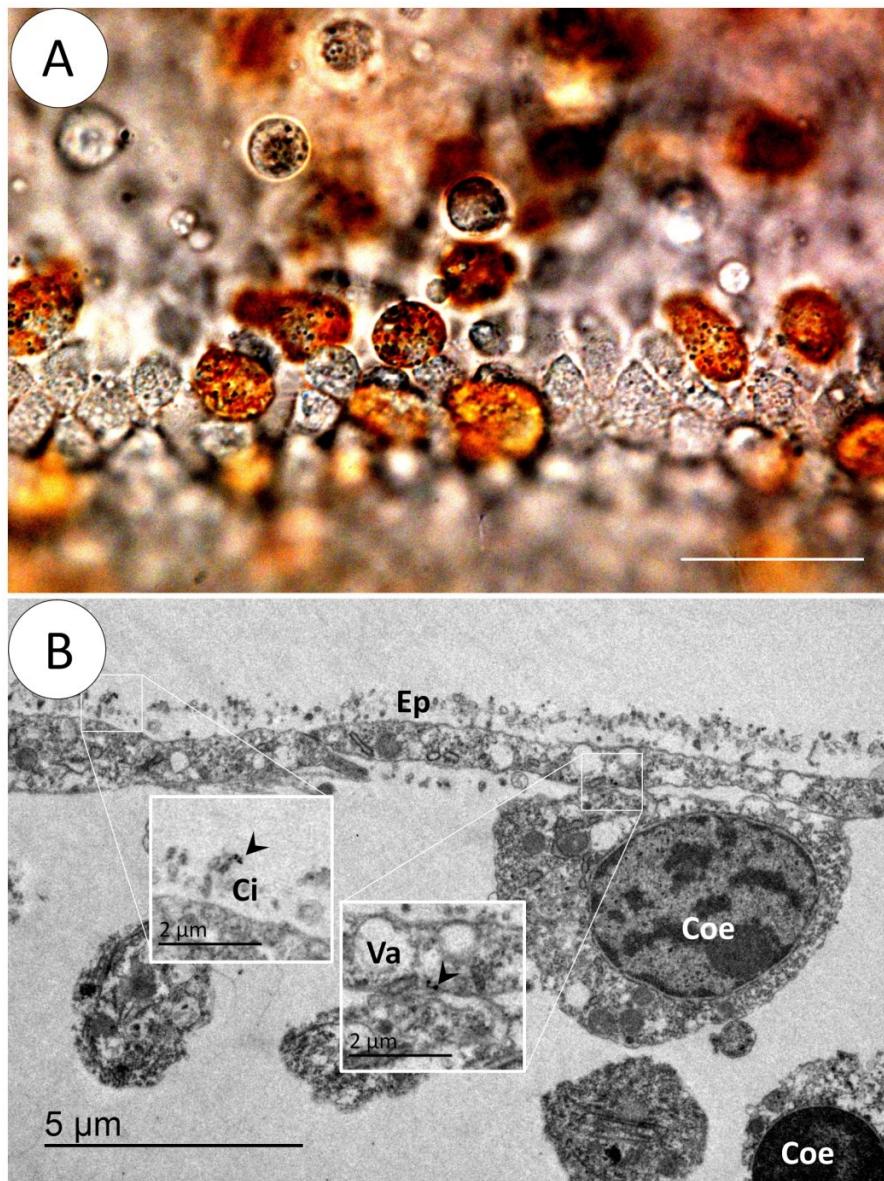
**APPENDICE 4: CONCLUSION GENERALE**


Figure 1: Illustration de l'épiderme des gastrules (*mid-to-late stage*) (A) et des larves échinoplateus métamorphiques L8<sub>2</sub> (B). (A) La différentiation des spherulocytes rouges devient un événement supplémentaire qui renforce la protection de l'épiderme (microscopie confocale). (B) Les AgNPs (8-16 nm) se lient aux cilles à l'extérieur de la larve; il y a peu d'internalisation cellulaire par les cellules épidermiques chez les larves L8<sub>2</sub> (micrographie TEM non-contrastée). Abréviations - Ci :

cilles, Coe : coelomocyte, Ep : épiderme, Va : vacuole. (A : 63x, barre d'échelle 15 µm en microscopie confocale).

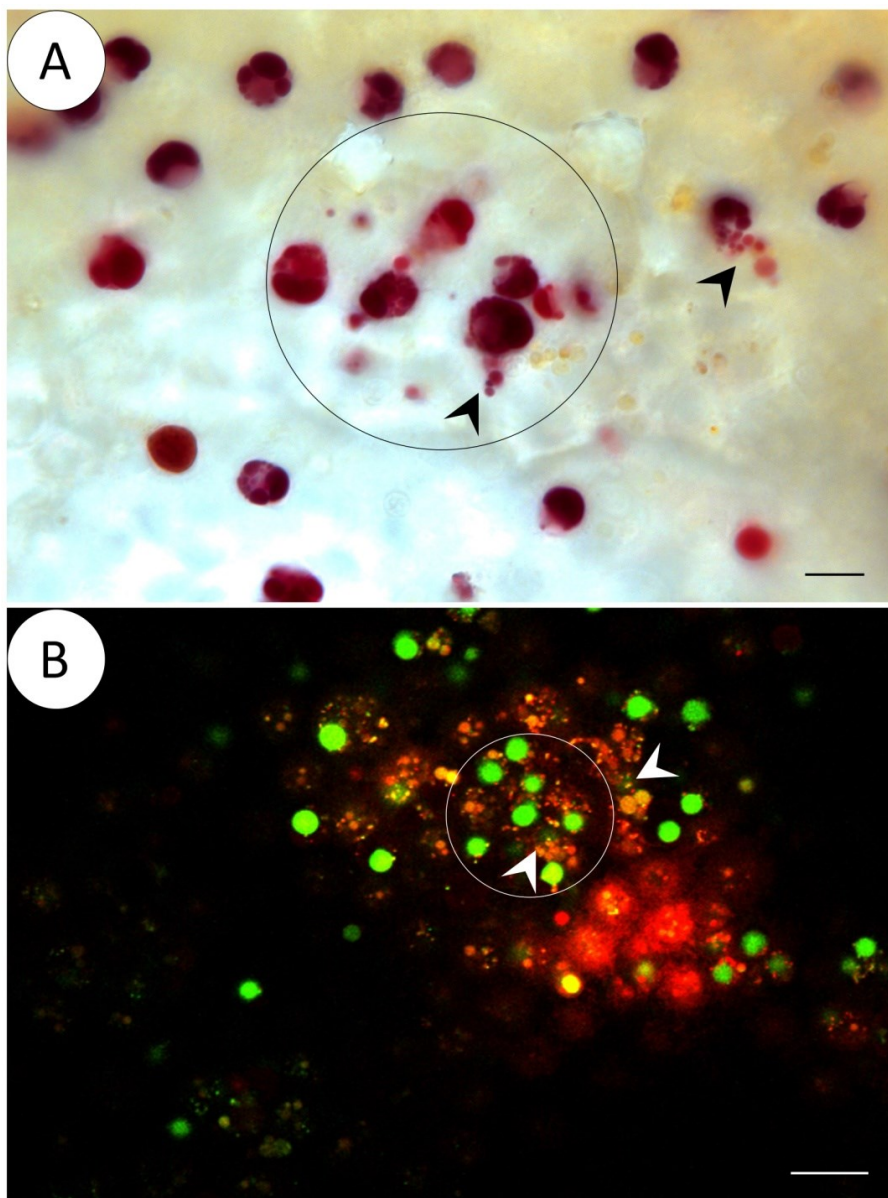


Figure 2: Dégranulation des spherulocytes contaminés avec les f-SWCNTs-PAAm-AgNPs (100 µg/L). (A) Tissu épidermique de la coquille d'oursin avec des spherulocytes en activité (cercle noir), les flèches noires indiquent des cellules en dégranulation. (B) Des spherulocytes et des amoebocytes translucides en stress oxydatif (cercle blanc), les spherulocytes rouges indiqués par les flèches

blanches semblent avoir moins de ROS. (A : 63x, barre d'échelle 15  $\mu\text{m}$  en microscopie photonique confocale, B : 63x, barre d'échelle 10  $\mu\text{m}$  en microscopie confocale à laser).

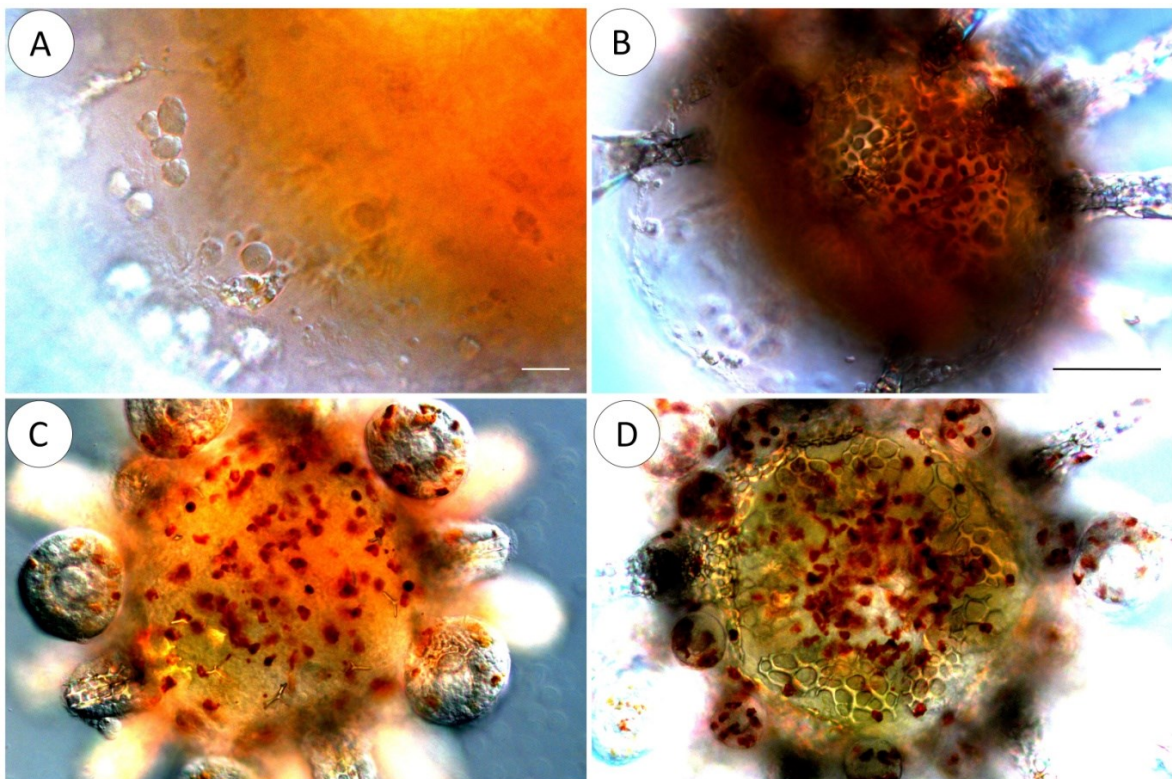


Figure 3: Illustration de l'épiderme des postlarves contaminées avec des ions  $\text{Ag}^+$  (100  $\mu\text{g L}^{-1}$ ). (A) Les cellules pigmentaires ne sont pas mobilisées vers les régions normalement endommagées (surface abactinale); quelques cellules minéralisatrices et des coelomocytes occupent la surface abactinale. (B) Réabsorption des tissus larvaires sur la surface abactinal vue en détail en (A). (C-D) La transformation de la postlarve en juvénile : une forte présence des spherulocytes dans la surface actinale est justifié par la formation des ossicules et de la bouche.

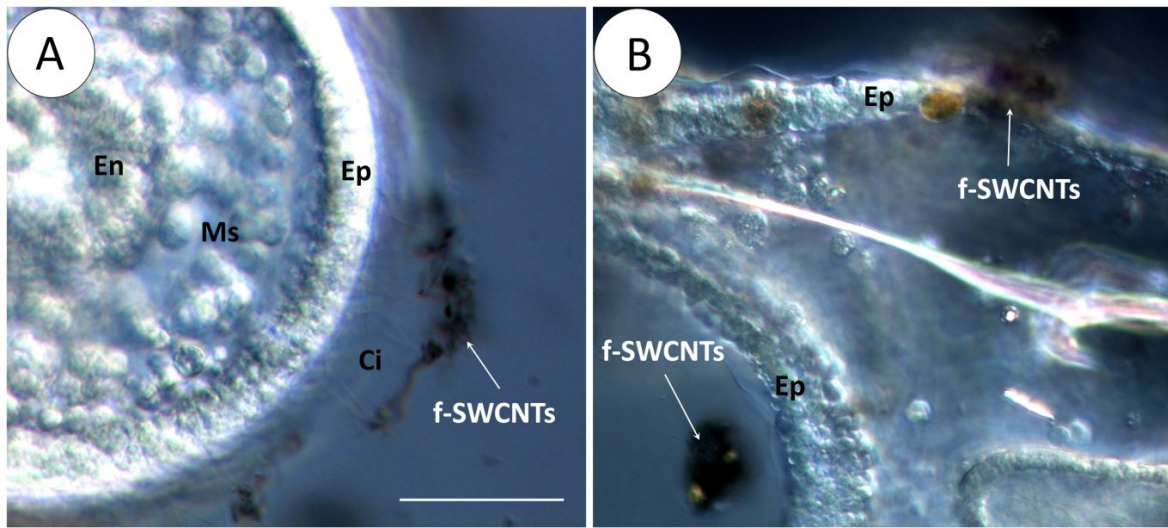


Figure 4: Effets des f-SWCNTs sur la flottabilité des embryons et des larves. (A) Le mouvement des cilles des embryons affecté par les f-SWCNTs. (B) L'adsorption des f-SWCNTs sur l'épiderme de la larve optimise le transfert de l'argent ionique. Abréviations - Ci : cilles, Ep : épiderme, En : endoderme, Ms : mésoderme.

## RÉFÉRENCES BIBLIOGRAPHIQUES

- ADAMS, N. W. H.; Kramer, J. R. 1999. Determination of silver speciation in wastewater and receiving waters by competitive ligand equilibration/solvent extraction. *Environmental Toxicology and Chemistry* 18(12): 2674–80.
- ADELEYE, A.; Keller, A. A. 2014. Long-term colloidal stability and metal leaching of single wall carbon nanotubes: Effect of temperature and extracellular polymeric substances. *Water Research* (49): 236–50.
- ADOMAKO-ANKOMAH, A.; Ettensohn, C. A. 2014. Growth factors and early mesoderm morphogenesis: insights from the sea urchin embryo. *Genesis* 52(3):158-72.
- AHEARN, G. A. et al. 2004. Mechanisms of heavy-metal sequestration and detoxification in crustaceans: A review. *Journal of Comparative Physiology B* 174(6): 439–52.
- ALLEN, W. V. 1974. Interorgan transport of lipids in the purple sea urchin, *Strongylocentrotus purpuratus*. *Comparative Biochemistry Physiology* 47A: 1297-1311.
- AL-SID-CHEIKH, M. et al. 2011. Synthesis and characterization of [110 mAg] nanoparticles with application to whole-body autoradiography of aquatic organisms. *Applied Radiation and Isotopes* 69 (10), 1415–1421.
- ANGEL, B. M. et al. 2013. The impact of size on the fate and toxicity of nanoparticulate silver in aquatic systems. *Chemosphere* 93(2): 359–65.
- ANGERER, L.; Angerer, R. 2003. Patterning the sea urchin embryo: gene, regulatory networks, signaling pathways, and cellular interactions. *Current Topics in Developmental Biology* (53):159-98.
- ANNUNZIATA, R. et al. 2014. Pattern and process during sea urchin gut morphogenesis: the regulatory landscape. *Genesis* 52(3): 251–68.
- ANTONOPOLOU, E. et al. 2013. Starvation and re-feeding affect Hsp expression, MAPK activation and antioxidant enzymes activity of European sea bass (*Dicentrarchus labrax*). *Comparative Biochemistry and Physiology - A Molecular and Integrative Physiology* 165 (1): 79–88.
- ARIZZA, V. et al. 2007. Cell cooperation in coelomocyte cytotoxic activity of *Paracentrotus lividus* coelomocytes. *Comparative Biochemistry and Physiology - A Molecular and Integrative Physiology* 147(2): 389–94.

- ARORA, S. et al. 2008. Cellular responses induced by silver nanoparticles: in vitro studies. *Toxicology Letters* 179 (2): 93–100.
- ARTS, M. J. et al. 2004. Stress proteins (Hsp70, Hsp60) induced in isopods and nematodes by field exposure to metals in a gradient near Avonmouth, UK. *Ecotoxicology* 13 (8): 739–55.
- ASTM, E1563-98 (2004). Standard guide for conducting acute toxicity tests with echinoid embryos, ASTM International, West Conshohocken.
- BALVAN, J. et al. 2015. Multimodal holographic microscopy: distinction between apoptosis and oncosis. *Plos One* 10 (3): 1–16.
- BANFALVI, G. 2014. Apoptotic agents inducing genotoxicity-specific chromatin changes. *Apoptosis* 19 (9): 1301–16.
- BAUN, A. et al. 2008. Ecotoxicity of engineered nanoparticles to aquatic invertebrates: A brief review and recommendations for future toxicity testing. *Ecotoxicology* (London, England) 17(5): 387–95.
- BAURAND, P.-E. et al. 2015. Differential expression of metallothionein isoforms in terrestrial snail embryos reflects early life stage adaptation to metal stress. *Plos One* 10(2): e0116004.
- BELL, R.; Kramer, J. R. 1999. Structural chemistry and geochemistry of silver-sulfur compounds: critical review. *Environmental Toxicology and Chemistry* 18(1): 9–22.
- BENN, T. et al. 2010. The release of nanosilver from consumer products used in the home. *Journal of Environmental Quality* 39(6): 1875–1882.
- BERDJEB, L. et al. 2013. Contrasting responses of marine bacterial strains exposed to carboxylated single-walled carbon nanotubes. *Aquatic Toxicology* 144–145: 230–41.
- BIANCHINI, A. et al. 2005. Mechanism of acute silver toxicity in marine invertebrates. *Aquatic Toxicology* 72 (1-2): 67–82.
- BIANCHINI, A. et al. 2007. Short-term silver accumulation in tissues of three marine invertebrates: shrimp *Penaeus duorarum*, sea hare *Aplysia californica*, and sea urchin *Diadema antillarum*. *Aquatic Toxicology* 84 (2 spec.iss.): 182–89.
- BIELMYER, G. K. et al. 2005. The effects of metals on embryo-larval and adult life stages of the sea urchin, *Diadema antillarum*. *Aquatic Toxicology* 74(3): 254–63.

- BIELMYER-FRASER, G. K. et al. 2014. Cellular partitioning of nanoparticulate versus dissolved metals in marine phytoplankton. *Environmental Science and Technology* 48 (22): 13443–50.
- BISHOP, C. D.; Brandhorst, B. P. 2007. Development of nitric oxide synthase-defined neurons in the sea urchin larval ciliary band and evidence for a chemosensory function during metamorphosis. *Developmental Dynamics* 236(6): 1535–46.
- BLAMOWSKA, M. et al. 2012. Biogenesis of the mitochondrial Hsp70 chaperone. *Journal of Cell Biology* 199 (1): 125–35.
- BOELSTERLI, U. A. 2003. Mechanistic toxicology. Cellular transport and selective accumulation of potentially toxic xenobiotics, in: The molecular basis of how chemicals disrupt biological targets. Taylor & Francis, London and New York, pp. 30-49.
- BOOLOOTIAN, R.; Campbell, J. L. 1964. A Primitive heart in the echinoid *Strongylocentrotus purpuratus*. *Science* 145(3628): 173–75.
- BORGES, J. C. et al. 2002. Phagocytosis *in vitro* and *in vivo* in the Antarctic sea urchin *Sterechinus neumayeri* at 0°C. *Polar Biology* 25: 891-897.
- BÖTTINGER, L. et al. 2015. Mitochondrial heat shock protein Hsp70 and Hsp10 cooperate in the formation of Hsp60 complexes. *Journal of Biological Chemistry* 290 (18): 11611–22.
- BRIX, K. V. et al. 2012. The effects of dietary silver on larval growth in the echinoderm *Lytechinus variegatus*. *Archives of Environmental Contamination and Toxicology* 63(1): 95–100.
- BROWNE, C. L. et al. 2007. Extracellular heat shock protein 70 has novel functional effects on sea urchin eggs and coelomocytes. *Journal Experimental Biology* 210, 1275–1287.
- BRUSCA, R. C. et al. 2016. *Invertebrates*. Sinauer Associates, Inc.
- BUFFET, P.-E. et al. 2014. A marine mesocosm study on the environmental fate of silver nanoparticles and toxicity effects on two endobenthic species: The ragworm *Hediste diversicolor* and the bivalve mollusc *Scrobicularia plana*. *The Science of the total environment* 470-471: 1151–59.

- BURIĆ, P. et al. 2015. Effect of silver nanoparticles on Mediterranean sea urchin embryonal development is species specific and depends on moment of first exposure. *Marine Environmental Research* 111: 50-59.
- BURKE, R. D. 1981. Structure of the digestive tract of the pluteus larva of *Dendraster excentricus* (Echinodermata: Echinoidea). *Zoomorphology* 98: 209-225.
- BURY, N. R.; Wood, C. M., 1999. Mechanism of branchial apical silver uptake by rainbow trout is via the proton-coupled Na (+) channel. *American Journal of Physiology*. 277, R1385–R1391.
- BYRNE, M. 2012. Global change ecotoxicology: Identification of early life history bottlenecks in marine invertebrates, variable species responses and variable experimental approaches. *Marine Environmental Research* 76: 3–15.
- CAMPBELL, P. G. C., Couillard, Y. 2004. Prise en charge et détoxicification des métaux chez les organismes aquatiques, in: Pelletier, E., Campbell, P. G. C., Denizeau, F. Écotoxicologie Moléculaire. Principes fondamentaux et perspectives de développement. Presses de l'Université du Québec, Québec, pp. 10-61.
- CANESI, L.; Corsi, I. 2016. Effects of Nanomaterials on Marine Invertebrates. *Science of The Total Environment*: 1–8.
- CANESI, L.; Procházková, P. 2014. The invertebrate immune system as a model for investigating the environmental impact of nanoparticles (Chapter 7). In: Boraschi, D.; Duschi, A. Nanoparticles and the Immune System. p. 91-112. Copyright Elsevier Inc.
- CANICATTI, C.; Farina-Lipari, E. 1990. Dynamic and morphological aspects of coelomocyte clotting in *Holothuria polii*. *Journal of Invertebrate Pathology* 56: 63-69.
- CHAN, C. Y. S.; Chiu, J. M. Y. 2015. Chronic effects of coated silver nanoparticles on marine invertebrate larvae: A proof of concept study. *Plos One* 10 (7): 0132457.
- CHORESH, O. et al. 2004. The Mitochondrial 60-kDa heat shock protein in marine invertebrates: biochemical purification and molecular characterization. *Cell stress & chaperones* 9 (1): 38–48.
- CLARK, K.R. et al. 2014. Change in marine communities : An approach to statistical analysis and interpretation. 3th (ed). Plymouth Marine Laboratory, Primer-E Ltd.

- CLAYTON, M. E. et al. 2000. Different expression patterns of heat shock proteins Hsp60 and Hsp70 in zebra mussels (*Dreissena polymorpha*) exposed to copper and tributyltin. *Aquatic Toxicology* 47, 213–226.
- COFFARO, K. A.; Hinegardner, R. T. 2016. Immune response in the sea urchin *Lytechinus pictus*. *Science* 197 (4311): 1389–90.
- COMFORT, K. K. et al. 2014. Less is more : Long-term *in vitro* exposure to low levels of silver nanoparticles provides new insights for nanomaterial evaluation. *ACS Nano* (4): 3260–71.
- CONG, Y. et al. 2014. Toxicity and bioaccumulation of sediment-associated silver nanoparticles in the estuarine polychaete, *Nereis (Hediste) diversicolor*. *Aquatic Toxicology* 156: 106–15.
- COTEUR, G. et al. 2003. Field Contamination of the starfish *Asterias rubens* by metals. Part 1: Short- and long-term accumulation along a pollution gradient. *Environmental Toxicology and Chemistry* 22 (9): 2136–44.
- CRAWFORD, K. 2003. Lithium chloride inhibits development along the animal vegetal axis and anterior midline of the squid embryo. *The Biological bulletin* 205(2): 181–82.
- CUNLIFFE, M. et al. 2012. Review: Sea surface microlayers - A unified physicochemical and biological perspective of the air-ocean interface. *Progress in Oceanography* 109: 104-116.
- DAUVIN, J. C. 2008. Effects of heavy metal contamination on the macrobenthic fauna in estuaries: The case of Seine estuary. *Marine Pollution Bulletin* 57: 160-69.
- DE MATTEIS, V. et al. 2015. Negligible particle-specific toxicity mechanism of silver nanoparticles: The role of Ag<sup>+</sup> ion release in the cytosol. *Nanomedicine: Nanotechnology, Biology and Medicine* 11 (3): 731–39.
- DE RIDDER, C.; Jangoux, M. 1982. Chapter 10: Digestive systems: Echinoidea. In: Jangoux, M.; Lawrence, J. M. *Echinoderm Nutrition*. pp. 225-227. A. A. Balkema, Rotterdam.
- DEPLEDGE, M. H. 1998. The ecotoxicological significance of genotoxicity in marine invertebrates. *Mutation Research*, 399, 109–122.

- DHEILLY, N. et al. 2011. Ultrastructural localization of highly variable 185/333 immune response proteins in the coelomocytes of the sea urchin, *Heliocidaris erythrogramma*. *Immunology and cell biology* 89(8): 861–69.
- DUBOC, V. et al. 2010. Nodal and BMP2/4 Pattern the mesoderm and endoderm during development of the sea urchin embryo. *Development* 137(2): 223–35.
- ECKELMAN, M. J.; Graedel, T. E. 2007. Silver emissions and their environmental impacts: a multilevel assessment. *Environmental science and Technology* 41(17): 6283–89.
- ELSAESSER, A.; Howard, C. V. 2012. Toxicology of nanoparticles. *Advanced Drug Delivery Reviews* 64 (2): 129–37.
- EMILY-FENOUIL, F. et al. 1998. GSK3beta/shaggy Mediates patterning along the animal-vegetal axis of the sea urchin embryo. *Development* 125(13): 2489–98.
- EOM, H.-J.; Choi, J. 2010. p38 MAPK activation, DNA damage, cell cycle arrest and apoptosis as mechanisms of toxicity of silver nanoparticles in Jurkat T Cells. *Environmental science & technology* 44(21): 8337–42.
- EZHOOVA, O. V. 2014. The morphology of the axial complex and associated structures in Asterozoa (Asteroidea, Echinoidea, Ophiuroidea). *Russian Journal of Marine Biology* 40 (3): 153–64.
- FABREGA, J. et al. 2011. Silver Nanoparticles: Behaviour and Effects in the Aquatic Environment. *Environment international* 37(2): 517–31.
- FALUGI, C et al. 2012. Toxicity of metal oxide nanoparticles in immune cells of the sea urchin. *Marine Environmental Research* 76: 114–21.
- FEI, L.; Perrett, S. 2009. Effect of nanoparticles on protein folding and fibrillogenesis. *International Journal of Molecular Sciences* 10(2): 646–55.
- FERGUSON, J. C. 1984. Translocative functions of the enigmatic organs of starfish - the axial organ, haemal vessels, Tiedemann's bodies, and rectal Caeca: An Autoradiographic Study. *Biological Bulletin* 166 (November 1983): 140–55.
- FERGUSON, P. L. et al. 2008. Influence of sediment-amendment with single-walled Carbon Nanotubes and Diesel Soot on Bioaccumulation of Hydrophobic Organic Contaminants by Benthic Invertebrates. *Environmental science and Technology* 42(10): 3879–85.

- FROLOV, A. et al. 2010. Ion interactions with the carbon nanotubes surface in aqueous solutions: understanding the molecular mechanisms. *Chemphyschem: a European Journal of Chemical Physics and Physical Chemistry* 11 (12): 2612-2616.
- FURUKAWA, R. et al. 2009. Defense system by mesenchyme cells in bipinnaria larvae of the starfish, *Asterina pectinifera*. *Developmental and comparative immunology* 33(2): 205–15.
- GALLON, C.; Flegal, A. R. 2015. Sources, fluxes and biogeochemical cycling of silver in the oceans. In: Whitacre, D. M. (ed.), *Reviews of Environmental Contamination and Toxicology*, v. 235.
- GALLOWAY, T. et al. 2010. Sublethal toxicity of nano-titanium dioxide and carbon nanotubes in a sediment dwelling marine polychaete. *Environmental Pollution* 158(5): 1748–55.
- GAMBARDELLA, C. et al. 2014. Toxicity and transfer of metal oxide nanoparticles from microalgae to sea urchin larvae. *Chemistry and Ecology* 30(4): 308–16.
- GARCÍA, C. P. et al. 2014. Detection of silver nanoparticles inside marine diatom *Thalassiosira pseudonana* by electron microscopy and focused ion beam. *Plos One* 9(5): 96078.
- GARCÍA-ALONSO, J. et al. 2011. Cellular internalization of silver nanoparticles in gut epithelia of the estuarine polychaete *Nereis diversicolor*. *Environmental science & technology* 45(10): 4630–36.
- GARCÍA-ALONSO, J. et al. 2014. Toxicity and accumulation of silver nanoparticles during development of the marine polychaete *Platynereis dumerilii*. *Science of the Total Environment* 476-477: 688–95.
- GARG, S. et al. 2016. Oxidative dissolution of silver nanoparticles by chlorine: implications to silver nanoparticle fate and toxicity. *Environmental Science & technology*: acs.est.6b00037.
- GARNER, K. L.; Keller, A. A. 2014. Emerging patterns for engineered nanomaterials in the environment: A review of fate and toxicity studies. *Journal of Nanoparticle Research* 16 (8).
- GERANIO, L. et al. 2009. The behavior of silver nanotextiles during washing. *Environmental Science and Technology* 43(21): 8113–18.

- GHOSH, J. et al. 2010. Sp185/333: A novel family of genes and proteins involved in the purple sea urchin immune response. *Developmental and comparative immunology* 34(3): 235–45.
- GILLES, K. W.; Pearse, J. S. 1985. Disease in sea urchins *Strongylocentrotus purpuratus*: Experimental infection and bacterial virulence. *Diseases of Aquatic Organisms* 1(1934): 105–14.
- GOSSELIN, L. A.; Qian, P. Y. 1997. Juvenile mortality in benthic marine invertebrates. *Marine Ecology Progress Series* 146(1-3): 265–82.
- GOSSELIN, P.; Jangoux, M. 1998. From competent larva to exotrophic juvenile: A morphofunctional study of the perimetamorphic period of *Paracentrotus Lividus* (Echinodermata, Echinoida). *Zoomorphology* 118(1): 31–43.
- GROSS, P. S. et al. 1999. Echinoderm immunity and the evolution of the complement system. *Developmental and comparative immunology* 23(4-5): 429–42.
- GUNAWAN, C. et al. 2014. Nanoparticle-protein corona complexes govern the biological fates and functions of nanoparticles. *Journal of Materials Chemistry B* 2(15): 2060–83.
- HALLIWELL, B., Gutteridge, J.M.C. 1989. Free radicals in biology and medicine. 2nd (ed). Clarendon Press, Oxford, UK.
- HAND, D. et al. 2012. Starvation reduces the heat shock protein response in white sturgeon larvae. *Environmental Biology of Fishes* 93: 333–342.
- HANDY, R. et al. The ecotoxicology of nanoparticles and nanomaterials : current status, knowledge gaps, challenges, and future needs. *Ecotoxicology*. 315–325 (2008).
- HARDIN, J. C. et al. 1992. Commitment along the dorsoventral axis of the sea urchin embryo is altered in response to  $\text{NiCl}_2$ . *Development* 116(3): 671–85.
- HODOR, P. G., Ettensohn, C. 1998. The dynamics and regulation of mesenchymal cell fusion in the sea urchin embryo. *Developmental biology* 199(1): 111–24.
- HOLDEN, P. et al. 2013. Ecological nanotoxicology: integrating nanomaterial hazard considerations across the subcellular, population, community, and ecosystems levels. *Accounts of Chemical Research* 46(3): 813–22.
- HOSSAIN, Z.; Huq, F. 2002. Studies on the interaction between  $\text{Ag}^+$  and DNA. *Journal of Inorganic Biochemistry* 91(2): 398–404.

- HOWE, P. D.; Dobson, S. 2002. Concise international chemical assessment document 44: silver and silver compounds: environmental aspects. *IPCS Concise International Chemical Assessment Documents* (44).
- HSIAO, I. L. et al. 2015. Trojan-horse mechanism in the cellular uptake of silver nanoparticles verified by direct intra- and extracellular silver speciation analysis. *Environmental Science and Technology* 49 (6): 3813–21.
- HUANG, R. et al. 2014. Effects of surface compositional and structural heterogeneity on nanoparticle and protein interactions : different protein configurations. *ACS Nano*. (6): 5402–12.
- HULL, M. S. et al. 2009. Release of metal impurities from carbon nanomaterials influences aquatic toxicity. *Environmental Science and Technology* 43(11): 4169–74.
- HYLLAND, K., 2006. Polycyclic aromatic hydrocarbon (PAH) ecotoxicology in marine eco- systems. *Journal of Toxicology and Environmental Health Part A* 69, 109–123.
- ITOH, H. et al. 2002. Mammalian HSP60 is quickly sorted into the mitochondria under conditions of dehydration. *European Journal of Biochemistry* 269 (23): 5931–38.
- JANGOUX, M. 1982. Digestive systems: General considerations (Chapter 7). In: Jangoux, M. and Lawrence, J. M. (ed). Echinoderm Nutrition. Balkema/Rotterdam, 654 p.
- JANGOUX, M. 1982. Excretion (Chapter 19). In: Jangoux, M.; Lawrence, J. M. (ed). Echinoderm Nutrition. Balkema/Rotterdam, 654 p.
- JEAN, S. et al. 2004. Chaetognaths: a useful model for studying heat shock proteins. Effect of wound healing. *Journal of Experimental Marine Biology and Ecology* 312: 319–332.
- JIANG, W. et al. 2008. Nanoparticle-mediated cellular response is size-dependent. *Nature nanotechnology* 3 (3): 145–50.
- JIMÉNEZ-ROJO, N. et al. 2015. Lipidic nanovesicles stabilize suspensions of metal oxide nanoparticles. *Chemistry and Physics of Lipids* 191:84-90.
- KAEGI, R. 2011. Behavior of silver nanoparticles in a pilot wastewater treatment plant SI. *Environmental science & technology* 45(21): 9113–14.
- KAEGI, R. et al. 2013. Fate and transformation of silver nanoparticles in urban wastewater systems. *Water Research* 47(12): 3866–77.

- KAEGI, R. et al. 2015. Transformation of AgCl nanoparticles in a sewer system — A Field Study. *Science of the Total Environment* 535: 20–27.
- KALMAR, B.; Greensmith, L. 2009. Induction of heat shock proteins for protection against oxidative stress. *Advanced Drug Delivery Reviews* 61 (4): 310–18.
- KARLSSON, H. L. et al. 2013. Cell membrane damage and protein interaction induced by copper containing nanoparticles — Importance of the metal release process. *Toxicology* 313(1): 59–69.
- KIM, S.; Ryu, D. Y. 2013. Silver nanoparticle-induced oxidative stress, genotoxicity and apoptosis in cultured cells and animal tissues. *Journal of Applied Toxicology* 33 (2): 78–89.
- KLAINE, S. J. et al. 2008. Nanomaterials in the environment: behavior, fate, bioavailability and effects. *Environmental Toxicology and Chemistry* 27, 1825–1851.
- KOBAYASHI, N.; Okamura, H. 2005. Effects of heavy metals on sea urchin embryo development. Part 2. *Interactive toxic effects of heavy metals in synthetic mine effluents*. *Chemosphere* 61(8): 1198–1203.
- KOMINAMI, T. et al. 2001. Behavior of pigment cells in gastrula-stage embryos of *Hemicentrotus pulcherrimus* and *Scaphechinus mirabilis*. *Development Growth and Differentiation* 43(6): 699–707.
- KOMINAMI, T. Takata, H. 2004. Gastrulation in the sea urchin embryo: a model system for analyzing the morphogenesis of a monolayered epithelium. *Development, growth and differentiation* 46(4): 309–26.
- KROEMER, G. et al. 2007. Mitochondrial membrane permeabilization in cell death. *Physiology Review*: 99–163.
- KROEMER, G. et al. 2009. Classification of cell death: recommendations of the Nomenclature Committee on cell death 2009. *Cell Death and Differentiation* 16(1): 3–11.
- KUNHIKRISHNAN A. et al. 2015. Sources, distribution, environmental fate, and ecological effects of nanomaterials in wastewater streams. *Critical Review of Environmental Science and Technology* 45: 277-318.
- KWOK, K. W. H. et al. 2012. Uptake of silver nanoparticles and toxicity to early life stages of Japanese Medaka (*Oryzias latipes*): effect of coating materials. *Aquatic Toxicology* 120-121: 59–66.

- LANCELEUR, L. et al. 2011. Long-term records of cadmium and silver contamination in sediments and oysters from the Gironde fluvial-estuarine continuum - Evidence of changing silver sources. *Chemosphere* 85(8): 1299–1305.
- LANONE, S.; Boczkowski, J. 2010. Les sources de nanoparticules. *Revue Française d'Allergologie*. 50, 211–213.
- LAPRESTA-FERNÁNDEZ, A., et al. 2012. Nanoecotoxicity effects of engineered silver and gold nanoparticles in aquatic organisms. *Trends in Analytical Chemistry* 32(797): 40–59.
- LAWRENCE, J. M.; Lane, J. M. 1982. The utilization of nutrients by post-metamorphic echinoderms (Chapter 15). p.331-371. In: Jangoux, M.; Lawrence, J. M. Echinoderm Nutrition. A. A. Balkema-Rotterdam.
- LECLERC, S.; Wilkinson, K. J. 2014. Bioaccumulation of nanosilver by *Chlamydomonas reinhardtii* - Nanoparticle or the free ion? *Environmental Science and Technology* 48(1): 358–64.
- LEROUEIL, P. R. et al. 2007. Nanoparticle interaction with biological membranes: does nanotechnology present a janus face? *Accounts of chemical research* 40(5): 335-342.
- LEVARD, C. et al. 2012. Environmental transformations of silver nanoparticles: impact on stability and toxicity. *Environmental Science and Toxicology* 46: 6900-6914.
- LI, X. et al. 2012. Aggregation kinetics and dissolution of coated silver nanoparticles. *Langmuir* 28, 1095-1104.
- LIU, P. 2013. Modification strategies for carbon nanotubes as a drug delivery system. *Industrial and Engineering Chemistry Research* 52(38): 13517–27.
- LOGAN, C. Y. et al. 1999. Nuclear  $\beta$ -catenin is required to specify vegetal cell fates in the sea urchin embryo. *Development* 126(2): 345–57.
- LUOMA, S. N. et al. 1995. Fate, bioavailability and toxicity of silver in estuarine environments. *Marine Pollution Bulletin* 31(1-3): 44–54.
- LUOMA, S. N.; Phillips, D. J. H. 1988. Distribution, variability and impacts of trace elements in San Francisco Bay. *Marine Pollution Bulletin*. 19, 413-425.
- LYNCH, I.; Dawson, K. 2008. Protein-nanoparticle interactions. *Nano Today* 3(1-2): 40–47.

- MA, H. et al. 2013. Ecotoxicity of manufactured ZnO nanoparticles - A Review. *Environmental Pollution* 172: 76–85.
- MAAN, K. H.; Lazier, J. R. N. 2006. Dynamics of marine ecosystems. 3th (ed.). Blackwell Publishing.
- MAGESKY, A. et al. 2016. Physiological effects and cellular responses of metamorphic larvae and juveniles of sea urchin exposed to ionic and nanoparticulate silver. *Aquatic toxicology* 174, 208-227.
- MAGESKY, A.; Pelletier, É. 2014. Silver nanoparticles as chemical stress triggers: different immune response capacities in early life of sea urchin. 41st Aquatic Toxicity Workshop (Ottawa).
- MAGESKY, A.; Pelletier, É. 2015. Toxicity mechanisms of ionic silver and polymer-coated silver nanoparticles with interactions of functionalized carbon nanotubes on early development of sea urchin. *Aquatic toxicology* 167, 106-23.
- MAGESKY, A; Pelletier, É. 2015. Interactions multiples des nanotubes de carbone avec l'argent libre et les nanoparticules d'argent au cours du développement embryonnaire de l'oursin vert 83e du Congrès de l'Acfas. Présence, persistance, devenir et effets des nanomatériaux dans l'environnement, Rimouski.
- MAGESKY, A; Pelletier, É. 2015. Utilisation des techniques de microscopie pour l'étude de l'assimilation et de l'internalisation des nanoparticules chez les premiers stades de développement des invertébrés marins. 83e du Congrès de l'Acfas. Colloque 210 - Présence, persistance, devenir et effets des nanomatériaux dans l'environnement.
- MARCHESANO, V. et al. 2013. Imaging inward and outward trafficking of gold nanoparticles in whole Animals. *ACS Nano* 7(3): 2431–42.
- MARIGÓMEZ, I. et al. 2002. Cellular and subcellular distribution of metals in molluscs. *Microscopy Research and Technique* 56(5): 358–92.
- MASHANOV, V. S.; Doimatov, Y. 2001. Ultrastructural features of gut regeneration in five-month-old pentactulae of the holothurian *Eupentacta fraudatrix*. *Russian Journal of Marine Biology* 27(6): 376–82.
- MAY, R. M. 1994. Conceptual aspects of the quantification of the extent of biological diversity. *Philosophical transactions of the Royal Society of London. Series B, Biological sciences*. Jul 29; 345(1311):13-20.

- MAYER, M. P. 2013. Hsp70 chaperone dynamics and molecular mechanism. *Trends in Biochemical Sciences* 38 (10): 507–14.
- MCEDWARD, L. R.; Miner, B. G. 2001. Larval and life-cycle patterns in echinoderms. *Canadian Journal of Zoology*. 79, 1125–1170.
- MCSHAN, D. et al. 2014. Molecular toxicity mechanism of nanosilver. *Journal of Food and Drug Analysis* 22(1): 116–27.
- METAXAS, A., Young, C. M. 1998. Behaviour of echinoid larvae around sharp haloclines: effects of the salinity gradient and dietary conditioning. *Marine Biology* 131(3): 443–59.
- MIAO, A. J. et al. 2009. The algal toxicity of silver engineered nanoparticles and detoxification by exopolymeric substances. *Environmental Pollution* 157(11): 3034–41.
- MIETHLING-GRAFF, R. et al. 2014. Exposure to silver nanoparticles induces size- and dose-dependent oxidative stress and cytotoxicity in human colon carcinoma cells. *Toxicology in Vitro* 28 (7): 1280–89.
- MILLER, J. R., McClay, D.R. 1997. Changes in the pattern of adherens junction-associated  $\beta$ -catenin accompany morphogenesis in the sea urchin embryo. *Developmental Biology* 192 (2): 310-22.
- MITRANO, D. et al. 2015. Review of nanomaterial aging and transformations through the life cycle of nano-enhanced products. *Environment International* 77: 132-147.
- MOORE, M. N. 1985. Cellular responses to pollutants. *Marine Pollution Bulletin* 16(4): 134-139.
- MORALES, A. E. et al. 2012. Starvation, energetic and antioxidant defenses. In: Abele, D. et al. Oxidative stress in aquatic ecosystems. pp. 281-294. Wiley-Blackwell.
- MORENO-GARRIDO, I. et al. 2015. Toxicity of silver and gold nanoparticles on marine microalgae. *Marine Environmental Research* 111: 60–73.
- MUKHOPADHYAY, S. M. 2003. Sample preparation for microscopic and spectroscopic characterization of solid surfaces and films in sample preparation techniques in analytical chemistry, v.162, John Wiley & Sons, Inc., USA.
- NDUNGU, K. 2011. Dissolved silver in the baltic sea. *Environmental Research* 111(1): 45–49.

- NEMER, M. et al. 1984. Developmental regulation, induction, and embryonic tissues specificity of sea urchin metallothionein gene expression. *Developmental biology* 102 (2): 471-82.
- NEWMAN, M. C. 2016. Fundamentals of Ecotoxicology: The Science of Pollution. 4th (ed.). CRC Press Taylor & Francis Group.
- NIYOGI, S. et al. 2002. Chemistry of single-walled carbon nanotubes. *Accounts of Chemical Research* (35):1105–13.
- NOWACK, B. et al. 2012. Potential scenarios for nanomaterial release and subsequent alteration in the environment. *Environmental Toxicology and Chemistry* 31(1): 50-59.
- NOWACK, B.; Bucheli, T. D. 2007. Occurrence, behavior and effects of nanoparticles in the environment. *Environmental pollution (Barking, Essex : 1987)* 150(1): 5–22.
- PAGLIARA, P.; Stabili, L. 2012. Zinc effect on the sea urchin *Paracentrotus lividus* immunological competence. *Chemosphere* 89 (5): 563–68.
- PANDURANGAN, M.; Kim, D. H. 2015. In vitro toxicity of zinc oxide nanoparticles: A Review. *Journal of Nanoparticle Research* 17(3).
- PARK, E. J. et al. 2010. Silver nanoparticles induce cytotoxicity by a Trojan-horse type mechanism. *Toxicology in vitro* 24(3): 872–78.
- PECHENIK, J. A. et al. 1998. Metamorphosis is not a new beginning: Larval experience reduces rates of postlarval growth, development, and survival in marine invertebrates. *Bioscience*. 48:901-910.
- PEDRINI-MARTHA, V. et al. 2016. Physiological, diurnal and stress-related variability of cadmium-metallothionein gene expression in land snails. *Plos One* 11(3): e0150442.
- PELLETIER, E. et al. 2014. The fate of nanomaterials at the river/ocean frontier using large mesocosms: the case story of silver nanoparticles. 35th Annual meeting of SETAC North America, Vancouver (BC), Canada.
- PILLAI, M. C., et al. 2003. Polycyclic aromatic hydrocarbons disrupt axial development in sea urchin embryos through a  $\beta$ -catenin dependent pathway. *Toxicology* 186(1-2): 93–108.
- PINSINO, A. et al. 2010. Sea Urchin Embryos as an *in vivo* model for the assessment of manganese toxicity: developmental and stress response effects. *Ecotoxicology* 19 (3): 555–62.

- PINSINO, A. et al. 2011. Manganese interferes with calcium, perturbs ERK signaling, and produces embryos with no skeleton. *Toxicological Sciences* 123(1): 217–30.
- PINSINO, A. et al. 2015. Titanium dioxide nanoparticles stimulate sea urchin immune cell phagocytic activity involving TLR/p38 MAPK-mediated signaling pathway. *Scientific Reports* 5(August): 14492.
- PINSINO, A.; Matranga, V. 2015. Sea urchin immune cells as sentinels of environmental stress. *Developmental & Comparative Immunology* 49 (1): 198–205.
- PITICHAROENPHUN, S. et al. 2012. Agglomeration of silver nanoparticles in sea urchin. *International Journal of Environmental Pollution and Remediation*. 1(1): 44-50.
- PROSIE, F. et al. 2008. Nanoparticles: structures, utilizations and health impacts. *Presse médicale* (Paris, France : 1983) 37, 1431–7.
- PURCELL, T. W.; Peters, J. J. 1998. Sources of silver in the environment. *Environmental Toxicology and Chemistry* 17(4): 539–46.
- QUADROS, M. E. et al. 2011. Silver nanoparticles and total aerosols emitted by nanotechnology-related consumer spray products. *Environmental Science and Technology* 45(24): 10713–19.
- QUIK, J.T.K. et al. 2014. Heteroaggregation and sedimentation rates for nanomaterials in natural waters. *Water Research* 48: 269-279.
- RANCE, G. et al. 2010. van Der Waals interactions between nanostructures. *ACS Nano* 4(8): 4920–28.
- RAND, G. M. et al. 1995. *Fundamentals of Aquatic Toxicology*. G. M. Rand (ed.); Taylor and Francis, Washington, DC.
- RANVILLE, M. A.; Flegal, A. R. 2005. Silver in the North Pacific Ocean. *Geochemistry Geophysics Geosystems* 6, Q03M01.
- RAO, G. P. et al. 2007. Sorption of divalent metal ions from aqueous solution by carbon nanotubes: a Review. *Separation and Purification Technology* 58(1): 224–31.
- REIDY, B. et al. 2013. Mechanisms of silver nanoparticle release, transformation and toxicity: A critical review of current knowledge and recommendations for future studies and applications. *Materials* 6(6): 2295–2350.

- RICHTER, K. et al. 2010. The heat shock response: life on the verge of death. *Molecular Cell* 40 (2): 253–66.
- RINGWOOD, A. et al. 2010. The effects of silver nanoparticles on oyster embryos. *Marine Environmental Research* 69 Suppl: S49–51.
- RIOS-ARANA, J. V. et al. 2005. Heat shock protein 60 (HSP60) response of *Platynus patulus* (Rotifera: Monogononta) to combined exposures of arsenic and heavy metals. *Hydrobiologia* 546 (1): 577–85.
- RIVERA-GIL, P. et al. 2013. The challenge to relate the physicochemical properties of colloidal nanoparticles to their. *Accounts Chemical Research* 46(3): 743–49.
- ROBERTS, C.M.; Hawkins, J.P. 1999. Extinction risk in the sea. *Trends in Ecology and Evolution*. 14: 241–246.
- ROITER, Y. O. et al. 2008. Interaction of nanoparticles with lipid membrane. *Nano Letters* 8, 941–944.
- RÖTTINGER, E. et al. 2008. FGF signals guide migration of mesenchymal cells, control skeletal morphogenesis and regulate gastrulation during sea urchin development. *Development* 135, 353–365.
- RUPPERT, E. E.; Barnes, R. D. 1994. Invertebrate Zoology, 6th (ed.). Saunders College Publishing, Harcourt Brace and Company, Orlando, Florida. 1100 p.
- RYBERG, E.; Lundgren, B. 1979. Some aspects on pigment cell distribution and function in the developing echinopluteus of *Psammechinus miliaris*. *Development, Growth & Differentiation* 21: 129–140.
- RYDER, K. et al. 2004. Avoidance of crude-oil contaminated sediment by the Australian seastar, *Patiriella exigua* (Echinodermata: Asteroidea). *Marine Pollution Bulletin* 49: 11-12, p.900-909.
- SAKHTIANCHI, R. et al. 2013. Exocytosis of nanoparticles from cells: role in cellular retention and toxicity. *Advances in Colloid and Interface Science* 201-202: 18–29.
- SAMEOTO, J. A. et al. 2010. The effect of flow on larval vertical distribution of the sea urchin, *Strongylocentrotus droebachiensis*. *Journal of Experimental Marine Biology and Ecology* 383(2): 156–63.

- SATO, Y. et al. 2006. Larval arm resorption proceeds concomitantly with programmed cell death during metamorphosis of the sea urchin *Hemicentrotus pulcherrimus*. *Cell and Tissue Research* 326(3): 851–60.
- SCHAEUBLIN, N. M. et al. 2011. Surface charge of gold nanoparticles mediates mechanism of toxicity. *Nanoscale* 3(2): 410–20.
- SCHEIBLING, R. E.; Hatcher, B. G. 2013. Chapter 26: *Strongylocentrotus droebachiensis*. In: Sea urchins: Biology and Ecology. V.38. John Lawrence, Elsevier.
- SCHULZ, A. G. et al. 2014. Aquatic toxicity of manufactured nanomaterials: challenges and recommendations for future toxicity testing. *Environmental Chemistry* 11: 207–226.
- SCOTT, F. C. 1955. The food canal of the sea urchin *Echinus esculentus* L. and its functions. *Proceedings of the Zoological Society of London* 125: 63–86.
- SHARMA, V. K. et al. 2014. Organic-coated silver nanoparticles in biological and environmental conditions: fate, stability and toxicity. *Advances in Colloid and Interface Science* 204: 15–34.
- SHERWOOD, D. R.; McClay, D. R. 1999. LvNotch signaling mediates secondary mesenchyme specification in the sea urchin embryo. *Development* 126(8): 1703-13.
- SHEMETOV, A. A. et al. 2012. Molecular interaction of proteins and peptides with nanoparticles. *ACS Nano* 6 (6): 4585-4602.
- SIKES, C. S. et al. 1981. Respiratory CO<sub>2</sub> and the supply of inorganic carbon for calcification of sea urchin embryos. *Comparative Biochemical Physiology - Part A* 70(3): 285–291.
- ŠILLER, L. et al. 2013. Silver nanoparticle toxicity in sea urchin *Paracentrotus lividus*. *Environmental pollution*. 178: 498–502.
- SILVA, J. R. 2000. The onset of phagocytosis and identity in the embryo of *Lytechinus variegatus*. *Developmental and comparative immunology* 24(8): 733–39.
- SILVA, J. R. M. C. 2013. Immunology in Sea Urchin (chapter 13). In: Sea Urchins - Biology and Ecology. 3th (ed.), Elsevier.
- SINGER, C. et al. 2005. Induction of heat shock proteins (Hsp70) in the zebra mussel (*Dreissena polymorpha*) following exposure to platinum group metals (platinum,

- palladium and rhodium): Comparison with lead and cadmium exposures. *Aquatic Toxicology* 75 (1): 65–75.
- SIRIPATTANAKUL-Ratpukdi, S.; Fürhacker, M. 2014. Review: Issues of silver nanoparticles in engineered environmental treatment systems. *Water, Air, and Soil Pollution* 225(4): 1–18.
- SMITH, G. J.; Flegal, A. R. 1993. Silver in San Francisco Bay estuarine waters. *Estuaries* 16, 547-558
- SNELGROVE, P. V. R. 1999. Getting to the bottom of marine biodiversity: sedimentary habitats. *Bioscience* 49, 129–138.
- SODERGREN, E. et al. 2006. Shedding genomic light on Aristotle's lantern. *Developmental Biology* 300(1): 2–8.
- SOHAEBUDDIN, S. K. et al. 2010. Nanomaterial cytotoxicity is composition, size, and cell type dependent. *Particle and Fibre Toxicology* 7: 22.
- SOKOLOVA, I. M. et al. 2012. Energy homeostasis as an integrative tool for assessing limits of environmental stress tolerance in aquatic invertebrates. *Marine environmental research* 79: 1–15.
- SOLOVIEV, A; Lukas, R. 2014. The near-surface layer of ocean: structure, dynamics and applications. Springer.
- SPERLING, R.; Parak, W. J. 2010. Surface modification, functionalization and bioconjugation of colloidal inorganic nanoparticles. *Philosophical transactions. Series A, Mathematical, physical, and engineering sciences* 368(1915): 1333–83.
- STERN, S. T. et al. 2012. Autophagy and lysosomal dysfunction as emerging mechanisms of nanomaterial toxicity. *Particle and Fibre Toxicology* 9:20.
- STRATHMANN, R. 1971. The feeding behavior of planktotrophic echinoderm larvae: Mechanisms, regulation, and rates of suspension feeding. *Journal of Experimental Marine Biology and Ecology* 6 (2): 109-160.
- STUMPP, M. et al. 2012. Acidified seawater impacts sea urchin larvae pH regulatory systems relevant for calcification. *PNAS* 109 (44): 18192-18197.
- SU, Y. et al. 2013. Risks of single-walled carbon nanotubes acting as contaminants-carriers: potential release of phenanthrene in Japanese Medaka (*Oryzias latipes*). *Environmental Science and Technology* 47(9): 4704–10.

- SUCHANEK, T. H. 1993. Oil impacts on marine invertebrate populations and communities. *Amer. Zool.* 33(6): 510–523.
- SUN, Y. P. et al. 2002. Functionalized carbon nanotubes: properties and applications. *Accounts of chemical research* 35(12): 1096–1104.
- SUTHERBY, J. et al. 2012. Histamine is a modulator of metamorphic competence in *Strongylocentrotus purpuratus* (Echinodermata: Echinoidea). *BMC Developmental Biology* 12(1): 14.
- SUTHERLAND, W. J. et al. 2010. A horizon scan of global conservation issues for 2010. *Trends in ecology & evolution* 25(1): 1–7.
- SUWA, R. et al. 2014. Effects of silver nanocolloids on early life stages of the scleractinian coral *Acropora japonica*. *Marine Environmental Research* 99: 198–203.
- SWEET, H. C. et al. 2002. LvDelta is a mesoderm-inducing signal in the sea urchin embryo and can endow blastomeres with organizer-like properties. *Development* 129(8): 1945–55.
- TAJIMA, K. et al. 2007. Disease in sea urchins. In: Edible Sea Urchins: Biology and Ecology. Developments in Aquaculture and Fisheries Science. 2nd (ed.). v.37, p. 167–182.
- TALLURY, P. et al. 2009. Ultra-small water-dispersible fluorescent chitosan nanoparticles: synthesis, characterization and specific targeting. *Chemical communications* 17: 2347–49.
- TAPPIN, A. D. et al. 2010. Dissolved silver in European estuarine and coastal waters. *Water Research* 44(14): 4204–16.
- TEMEREVA, E. N. 2010. The digestive tract of actinotroch larvae (Lophotrochozoa, Phoronida): anatomy, ultrastructure, innervations, and some observations of metamorphosis. *Canadian Journal of Zoology* 88(12): 1149–68.
- TEMPLETON, R. C. et al. 2006. Life-cycle effects of single-walled carbon nanotubes (SWNTs) on an estuarine meiobenthic copepod. *Environmental Science and Technology* 40(23): 7387–93.
- THALMANN, B. et al. 2015. Effect of ozone on nano-sized silver sulfide in wastewater effluent. *Environmental Science and Technology* 49: 10911–10919.

- TOKUOKA, M. et al. 2002. Specification and differentiation processes of secondary mesenchyme-derived cells in embryos of the sea urchin *Hemicentrotus pulcherrimus*. *Development Growth and Differentiation* 44(3): 239–50.
- TOMANKOVA, K. et al. 2015. Cytotoxicity, cell uptake and microscopic analysis of titanium dioxide and silver nanoparticles *in vitro*. *Food and Chemical Toxicology* 85: 20–30.
- TREUEL, L. et al. 2013. New views on cellular uptake and trafficking of manufactured nanoparticles. *The Journal of the Royal Society Interface* 10(82):20120939.
- TRUMP, B. F. et al. 1997. The pathways of cell death: oncosis, apoptosis and necrosis. *Toxicology Pathology* 25:1.
- TUCKER, R. P. 1986. The role of glycosaminoglycans in anuran pigment cell migration. *Journal of embryology and experimental morphology* 92: 145–64.
- TURNER, A. 2010. Marine Pollution from Antifouling Paint Particles. *Marine pollution bulletin* 60(2): 159–71.
- UNFRIED, K. et al. 2007. Cellular Responses to Nanoparticles: Target Structures and Mechanisms. *Nanotoxicology* 1(1): 52–71.
- VAN STRAALEN, N. M.; Hoffmann, A. A. 2000. Review of experimental evidence for physiological costs of tolerance to toxicants. In: Kammega, J. E.; Laskowski, R., Demography in Ecotoxicology. John Wiley/Chichester, U.K., pp.115-124.
- VANCE, M. E. et al. 2015. Nanotechnology in the real world: Redeveloping the nanomaterial consumer products inventory. *Beilstein Journal of Nanotechnology* 6(1): 1769–80.
- VAZZANA, M. et al. 2015. Cellular responses and HSP70 expression during wound healing in *Holothuria tubulosa* (Gmelin, 1788). *Fish and Shellfish Immunology* 42 (2): 306–15.
- VENTURA, C. R. R. et al. 2006. In: Helena Passeri Lavrado & Bárbara Lage Ignacio. (Org.). Biodiversidade bentônica da região central da Zona Econômica Exclusiva brasileira. 1th (ed.). Rio de Janeiro, v. 18, p. 339-389.
- VIDAVSKY, N. et al. 2014. Initial stages of calcium uptake and mineral deposition in sea urchin embryos. *Proceedings of the National Academy of Sciences of the United States of America* 111(1): 39–44.

- WANG, F. et al. 2013. The biomolecular corona is retained during nanoparticle uptake and protects the cells from the damage induced by cationic nanoparticles until degraded in the lysosomes. *Nanomedicine: Nanotechnology, Biology, and Medicine* 9(8): 1159–68.
- WANG, H. et al. 2014. Stability and aggregation of silver and titanium dioxide nanoparticles in seawater: Role of salinity and dissolved organic carbon. *Environmental Toxicology and Chemistry* 33 (5):1023 –1029.
- WANG, H. et al. 2014. Toxicity, bioaccumulation, and biotransformation of silver nanoparticles in marine organisms. *Environmental Science & Technology* 48(23): 13711–17.
- WANG, W. X. 2001. Comparison of metal uptake rate and absorption efficiency in marine bivalves. *Environmental Toxicology and Chemistry* 20, 1367–1373.
- WANG, Y. et al. 2015. An overview on nanotoxicity and nanomedicine research: principles, progress and implications on cancer therapy. *Journal of Materials Chemistry B* 3: 7153–72.
- WEIS, J. S. 2014. Physiological, developmental and behavioral effects of marine pollution. Springer Dordrecht Heidelberg, New York, London.
- WERNER, I.; Nagel, R. 1997. Stress proteins HSP60 and HSP70 in three species of amphipods exposed to cadmium, diazinon, dieldrin and fluoranthene. *Environmental Toxicology and Chemistry* 16 (11): 2393–2403.
- WIDDICOMBE, S. 2008. Predicting the impact of ocean acidification on benthic biodiversity: What can physiology tell us? *Journal of Experimental Marine Biology and Ecology* 366, 187-197.
- WURL, O.; Obbard, J. P. 2004. A review of pollutants in the sea-surface microlayer (SML): a unique habitat for marine organisms. *Marine Pollution Bulletin* 48 (11-12): 1016-30.
- YAMEEN, B. et al. 2014. Insight into nanoparticle cellular uptake and intracellular targeting. *Journal of Controlled Release* 190: 485–99.
- YARON, P. N. et al. 2011. Single wall carbon nanotubes enter cells by endocytosis and not membrane penetration. *Journal of Nanobiotechnology* 9(1): 45.
- YETISEN, A. K. et al. 2016. Nanotechnology in textiles. *ACS Nano*: 5b08176.

- YOUNG, J. C. 2010. Mechanisms of the Hsp70 chaperone system. *Biochemistry and Cell Biology* (88): 291-300.
- YU, Z. G., Wang, W. X. 2013. Influences of ambient carbon nanotubes on toxic metals accumulation in *Daphnia magna*. *Water Research* 47(12): 4179–87.
- YUE, T.; Xianren Z. 2012. Cooperative effect in receptor-mediated endocytosis of multiple nanoparticles. *ACS Nano* (4): 3196–3205.
- YUNG, S.; Chan, T. M. 2007. Mesothelial cells. *Peritoneal dialysis international : journal of the International Society for Peritoneal Dialysis* 27 Suppl 2: S110–15.
- ZHANG, S. et al. 2009. Size-dependent endocytosis of nanoparticles. *Advanced Materials* 21: 419-424.
- ZHU, M. et al. 2012a. Physicochemical properties determine nanomaterial cellular uptake, transport and fate. *Accounts of Chemical Research* 46(3): 622–31.
- ZHU, M. et al. 2012b. Exosomes as extrapulmonary signaling conveyors for nanoparticle-induced systemic immune activation. *Small* 8: 404–412.
- ZHU, X. et al. 2011. The toxicity and oxidative stress of TiO<sub>2</sub> nanoparticles in marine abalone (*Haliotis diversicolor supertexta*). *Marine pollution bulletin* 63(5-12): 334–38.
- ZIEGLER, A. et al. 2008. Systematic comparison and reconstruction of sea urchin (Echinoidea) internal anatomy: a novel approach using magnetic resonance imaging. *BMC Biology* 6(1): 33.
- ZOTO, G. A., Robinson, W. E. 1985. The toxicity of one-hour silver exposures to early-life stages of the surf clam *Spisula solidissima* (Dillwyn). *Marine Environmental Research* 16(1): 61–75.
- ZUPANC, J. et al. 2010. A new approach to analyze effects of nanoparticles on lipid vesicles. *International Journal of Biomedical Nanoscience and Nanotechnology* 1(1): 34–51.



